Light controlled active and passive motion of colloidal particles

Institute of Physics and Astronomy, 9th November 2020

by

Pooja Arya

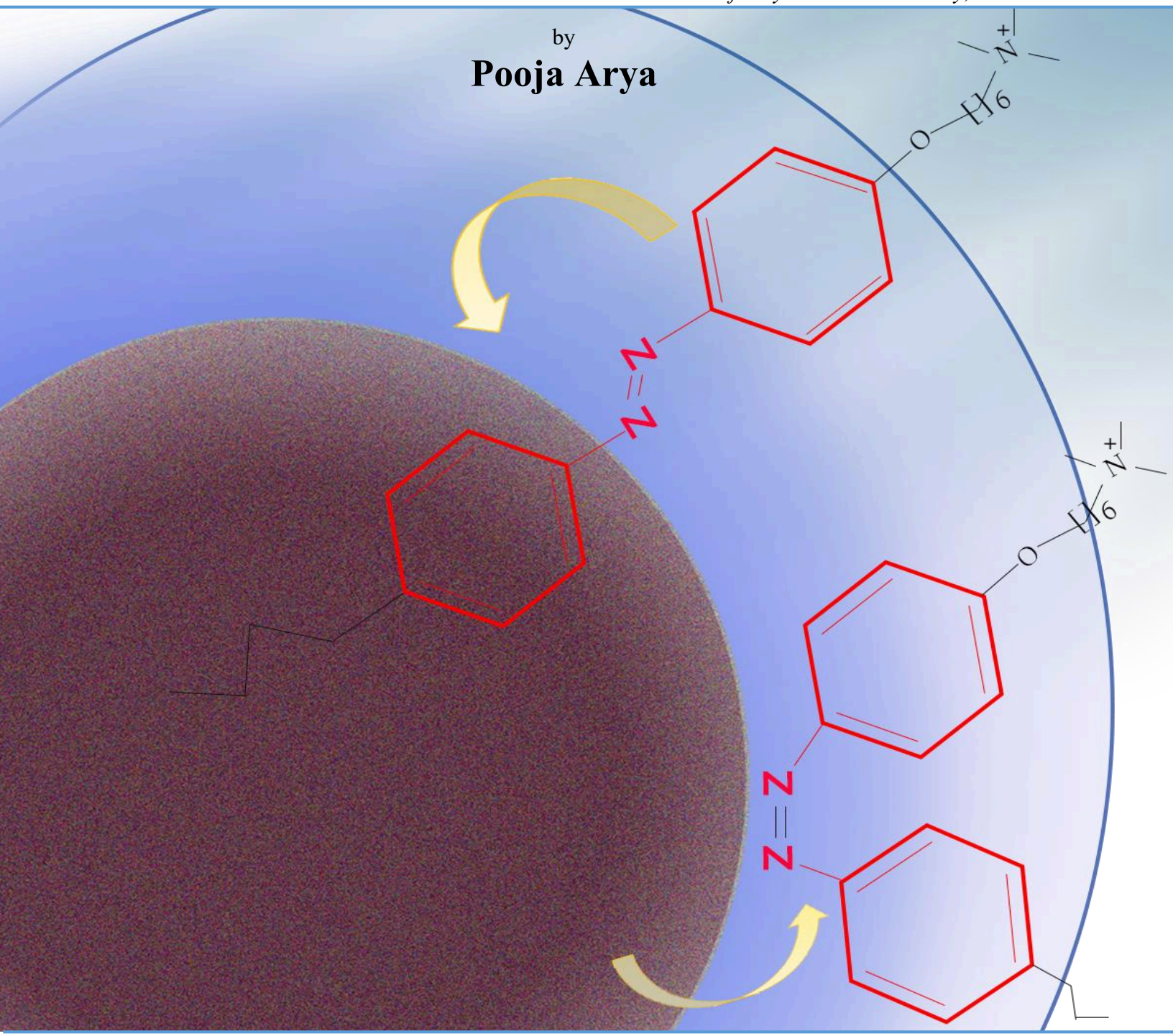

A cumulative dissertation for the degree
"Doctor of rerum naturalium"
(Dr. rer. Nat.)
in Experimental Physics

Submitted to
The Faculty of Mathematics and Natural Sciences
University of Potsdam

The studies described in this dissertation were conducted from 1 February, 2017 to May, 2020 at the University of Potsdam under the supervision of Prof. Dr. Svetlana Santer.

Referees:

Prof. Dr. Svetlana Santer
Experimental physics
Institute for Physics and Astronomy, University of Potsdam, Germany

Prof. Dr. Carsten Beta
Biological Physics
Institute for Physics and Astronomy, University of Potsdam, Germany

Prof. Dr. Holger Stark
RG Statistical Physics of Soft Matter and Biological Systems
Institute for theoretical Physics, Technical University of Berlin, Germany

Published online on the
Publication Server of the University of Potsdam:
https://doi.org/10.25932/publishup-48388
https://nbn-resolving.org/urn:nbn:de:kobv:517-opus4-483880

"When you change the way you look at things; the things you look at change"

(**Max Plank**)

Acknowledgements

The best part about writing a thesis is recalling the efforts of people who made it possible. While my work is based on complex phenomena of light-driven diffusioosmosis, the experimental work is also analogous to the various important system of human connections that made this thesis possible. Foremost, I take this opportunity to express my heartfelt indebtedness to my PhD supervisor, Professor Svetlana Santer, who convincingly guided and encouraged me to be professional and motivated me to do the right things when required. I am glad that I met such a selfless and caring person who combined intellectual inspiration with warmth and steered deeply stimulating discussions which led to further explorations.

My special thanks goes to my project advisor Dr. David Feldmann, for all the intellectual discussions we had. I am indebted to him for all his kindness and for being a constant moral and academic support.

I would like to thank Prof. Carsten Beta and his group for giving me access to work on their optical microscopes especially the TIRF setup which gave a different dimension to my project and allowed me to think deeper in my project.

I also extend my sincere thanks to Dr. Nino Lomadze for the synthesis of photoactive surfactant and Dr. Alexey Kopyshev for REM measurements and for preparing the schemes of the mechanisms/processes we wanted to present in publications. His expertise in softwares like blender, python, and image J also motivated me to learn these tools.

I express my gratitude to Prof. Olga I. Vinogradova and Dr. Taras Y. Molotilin for their fruitful collaboration and help in understanding the mechanism of l-LDDO flow from theoretical point of view.

I am deeply indebted to University of Potsdam and International Max-Plank Research School (IMPRS) on multiscale bio systems for financing my research. Especially, I would like to thank my second supervisor Dr. Mark Santer (Max Planck Institute of Colloids and Interfaces) for making it a smooth ride and for his valuable comments when required. Also, I extend my gratitude to Dr. Angelo Valleriani (Max Planck Institute of Colloids and Interfaces) for keeping me updated with all the workshop and soft skill courses. I thank him for giving me advice when required**.**

My deepest thanks goes to my collogue/best friend Joachim Jelken for being there for me always in good times as well as in bad timings of my thesis. I learnt a lot from him counting from optics, physics, microscopy, writing, humor, team spirit and the list goes on... Working with him was always fun and very intellectual. Jennifer (my bike) is also thanking his efforts for taking care of her. Along with my degree, one thing which I am sure is our friendship which will go along throughout my life.

I also thank my other fellow group members and PhD buddies for their constant feedback and corporations. Sarah Loebner (for having deep discussions about animals, plants, and other interesting things), Maren Umlandt (for discussion regarding work and experiments, family, and other creative approaches), Selina Schimka (for helping me in spectroscopy technique and for letting me be the part of the most important moment of her life), Dr. Marek Bekir (For giving me an insight of physical chemistry once again), and Olga Gritsai (helping me in preparation of Janus particles). I would Like to recognize all the invaluable assistance that you all provided during my PhD span. I thank these guys for teaching me special deutsche Schimpfwörter (Z.B. sturmfrei, halt die Klappe, paar aufs Maul) which I might have not learnt in my German class.

I also thank Manuel Schulze for helping us in preparation of Janus particles by coating porous colloids from gold layer using electron beam evaporator.

I thank the organization staff of the University of Potsdam Frau Elke Derlig, Herr. Andreas Horka and Frau Dagmar Stabenaw for helping me in all the administration and technical issues. I also thank to Frau Susanne at IMPRS of multiscale biosystem for keeping me updated with all the activities which took place in my graduate school. My special gratitude goes to Dipl. Ing. Andreas Pucher for sharing the recipe of his special coffee which also became one of my favorite beverage during this time.

To my friends who held me up and encouraged me throughout this journey, you value more to me than I can express in words. It is difficult to name them all, but some need special mention. I owe special thanks to my PhD confidants, Ankit Agarwal (for his continuous guidance and support), Manaswita Kar (for late night chats and coffee breaks), Sohini Bhattacharjee, Samudrajeet Thappa, Rupam Shukla, Saurabh Gupta, and Vittoria Sposini who were always there for me with a listening ear and a word of inspiration. Your support and friendship made me feel this place like home, miles away from India.

I am also thankful to my friends who are living thousand kilometers away: Abha Goyal, Chinmay Saraf, Santosh Chaudhary, Pragati Dugar, Sahitya Movva , Saloni Garg, Tanya Singhal. These guys are more than a family who kept motivating me always and never let the distance come in between.

My greatest thanks goes to Aman Kejriwal, my partner, for his constant encouragement and for being always available to listen to my jokes, complaints, and my crying over phone. He has been most understanding and compassionate all the time. I thank him for believing in me, even in times when I didn’t believe in myself.

Finally, my deep and sincere gratitude to my family for their unconditional care and love. I am grateful to my brothers Vivek Arya and Gaurav Garg and my sister Vandana Arya for always being there for me in every situation. I am forever indebted to my parents Keshav Dev Arya and Bharti Arya for giving me all the opportunities and experiences that have made me who I am today.

Abstract

In this dissertation we introduce a concept of light driven active and passive manipulation of colloids trapped at the solid/liquid interface. The motion is induced due to the generation of light driven diffusioosmotic flow (LDDO) upon irradiation with light of appropriate wavelength. The origin of the flow is due to the osmotic pressure gradient resulting from a concentration gradient at the solid/liquid interface of the photosensitive surfactant present in colloidal dispersion. The photosensitive surfactant consists of a cationic head group and a hydrophobic tail in which azobenzene group is integrated in. The azobenzene is known to undergo reversible photo-isomerization from a stable *trans* to a metastable *cis* state under irradiation with UV light. Exposure to light of larger wavelength results in back photo-isomerization from *cis* to *trans* state. The two isomers have different molecular properties, for instance, *trans* isomer has a rod like structure and low polarity (0 dipole moment), whereas *cis* one is bent and has a dipole moment of ~3 Debye. Being integrated in the hydrophobic tail of the surfactant molecule, the azobenzene state determines the hydrophobicity of the whole molecule: in the *trans* state the surfactant is more hydrophobic than in the *cis*-state. In this way, many properties of the surfactant such as the CMC, solubility, and the interaction potential with a solid surface can be altered by light. When the solution containing such a surfactant is irradiated with focused light, a concentration gradient of different isomers is formed near the boundary of the irradiated area near the solid surface resulting in osmotic pressure gradient. The generated diffusioosmotic (DO) flow carries the particles passively along.

The local-LDDO flow can be generated around and by each particle when mesoporous silica colloids are dispersed in the surfactant solution. This is because porous particles act as a sink/source which absorbs azobenzene molecule in *trans* state and expels it when it is in the *cis* state. The DO flows generated at each particle interact resulting in aggregation or separation depending upon the initial state of surfactant molecules. The kinetics of aggregation and separation can be controlled and manipulated by altering the parameters such as the wavelength and intensity of the applied light, as well as surfactant and particle concentration. Using two wavelengths simultaneously allow for dynamic gathering and separation creating fascinating patterns like 2D disk of well separated particles or establishing collective complex behavior of particle ensemble as described in this thesis.

The mechanism of l-LDDO is also used to generate self-propelled motion. This is possible when half of the porous particle is covered by metal layer, basically blocking the pores on one side. The LDDO flow generated on the uncapped side pushes the particle forward resulting in a super diffusive motion. The system of porous particle and azobenzene containing surfactant molecule can be utilized for various application such as drug delivery, cargo transportation, self-assembling, micro motors/ machines or micropatterning.

Zusammenfassung

In dieser Doktorarbeit führen wir das Konzept der lichtinduzierten Diffusioosmose (LDDO) zur licht-kontrollierten passiven und aktiven Bewegung von Kolloiden an der fest-flüssig Grenzfläche ein. Bei diesem neuartigen Phänomen wird ein Grenzflächenfluss mittels Lichtes bestimmter Wellenlänge erzeugt. Ein lichtempfindliches Tensid wirkt hierbei als Quelle der Diffusioosmose: Durch Einstrahlung von Licht wird ein Konzentrationsgradient an der Oberfläche erzeugt, der wiederum ein Ungleichgewicht im lateralen osmotischen Druck verursacht. Dieser Druckunterschied führt dann zu einem grenzflächennahen diffusioosmotischen Fluss. Das lichtaktive Molekül besteht aus einer kationischen Kopfgruppe und einer hydrophoben Kohlenstoffkette, in die die Azobenzolgruppe eingebettet ist. Azobenzol fungiert hier als Lichtschalter, da es mit Licht zwischen einem stabilen *trans* und einem metastabilen *cis* Zustand hin- und hergeschaltet werden kann. Nahes UV Licht führt hier zur *trans*-*cis* und sichtbares Licht zur *cis*-*trans* Isomerisation. Das *trans* Isomer unterscheidet sich in einigen Eigenschaften vom *cis* Isomer. So ist z.B. das *trans*-Isomer langgestreckt und besitzt eine geringe Polarität (verschwindendes Dipolmoment), währenddessen das *cis* Isomer gebogen ist und ein deutliches Dipolmoment von ca. 3 Debye besitzt. Durch die Integration der Azobenzolgruppe in die hydrophobe Kette des Tensids, bestimmt der Isomerisationszustand des Tensids die Hydrophobizität des gesamten Moleküls: Der *trans* Zustand ist deutlich hydrophober als der *cis* Zustand. Dieser Unterschied zeigt sich in den Löslichkeitseigenschaften des Moleküls, der kritischen Mizellenkonzentration sowie des Wechselwirkungspotentials zwischen Molekül und Grenzfläche. Dies kann genutzt werden, um diese Eigenschaften mittels Lichtbestrahlung zu ändern. Wird das Molekül in Wasser gelöst und mit fokussiertem Licht bestrahlt, kann ein isomerer Konzentrationsgradient im Bestrahlungsbereich an der fest-flüssig Grenzfläche erzeugt werden, der wiederum in einem osmotischen Druckgunterschied resultiert. Die daraus resultierende Diffusioosmose (DO), welche an der Grenzfläche erzeugt wird, ist in der Lage Kolloide, die sich an der Grenzfläche befinden, transportieren (passiv).

Im Unterschied dazu kann ein sogenannter lokaler diffusioosmotischer Fluss (l-LDDO) um jedes einzelne Kolloid erzeugt werden, sobald es sich um meso-poröse Kolloide handelt. Hierbei agiert jedes Kolloid selbst als Konzentrationsquelle- bzw. –senke (ähnlich dem fokussiertem Licht im oberen Fall). Je nach Isomerisationszustand lagert sich das Molekül eher im Kolloid an oder bevorzugt die Umgebung des Wassers. Befindet sich das Molekül im *trans* Zustand lagert es sich im Kolloid an, während es im *cis* Zustand eher die Umgebung des Wassers sucht. Der diffusioosmotische Fluss wird um jedes einzelne Kolloid erzeugt, wodurch eine Wechselwirkung zwischen allen Kolloiden zustande kommt, die entweder anziehend oder abstoßend sein kann. Das hängt vom Isomerisationszustand der Tensidmoleküle vor der Bestrahlung ab. Durch die Änderung der folgenden Parameter kann die Bewegung der Kolloide kontrolliert werden: Lichtwellaen-ge

Lichtintensität, Tensidkonzentration, Kolloidkonzentration. Durch die gleichzeitige verw-Verwendung zweier verschiedener Lichtquellen (mit unterschiedlichen Wellenlängen), ist es möglich eine interessante Dynamik in der Anziehung und Abstoßung der Kolloide zu erzeugen, die faszinierende Kolloidformationen entstehen lassen wie sie in dieser Arbeit näher beschrieben werden.

Das Phänomen der lokalen Diffusioosmose kann auch zu selbst-getriebener Bewegung führen, nämlich wenn eine Hälfte des Kolloids bedeckt wird (z.B. mit einer Metallschicht) und somit für Tensidmoleküle undurchlässig macht. Der diffusioosmotische Fluss, der auf der unbedeckten Seite des Kolloids erzeugt wird, bewegt das Kolloid in eine Richtung fort und führt so durch Überlagerung zur thermischen Bewegung zu super-diffusivem Verhalten. Das System, bestehend aus porösen Kolloiden und azobenzolhaltigem Tensidmolekül kann sinnführend genutzt werden, z.B. für folgende Anwendungen: gezieltem Medikamententransport, Mikrofrachttransport, Selbstassemblierung, Mikromotoren/-maschinen oder Mikrostrukturierung.

Contents

List of frequently used abbreviations

LDDO	Light driven diffusioosmosis
CMC	Critical micelle concentration
MSP	Mesoporous silica particle
l-LDDO	Local-Light driven diffusioosmosis
EDL	Electrostatic double layer
DO	Diffusioosmosis
2D	2 Dimensional
MSD	Mean square displacement
NPD	Nearest particle distance
PSD	Particle surface density
ACS	Azobenzene containing surfactant
Azo-C6	Azobenzene containing surfactant with a spacer of 6CH_2 groups
AzoCn	Azobenzene containing surfactant with a spacer of nCH_2 groups
SRG	Surface relief grating

1. Introduction

"Life at low Reynolds number"

Propulsion and transportation of micro-organisms in fluids have become an important aspect of current research. For instance, many mechanical separations or self-assembly processes involve the movement of colloids or micro/nano organisms through one or the other fluid system. However, at micro scale, motion occurs at low Reynolds number, where fluid friction and its viscosity dominates over inertia.[1] Locomotion at this scale requires a continuous expenditure of work, which can be generated by converting external forces into kinetic energy of particles. In the microorganism, propulsion is possible either due to rotation or beating of flagella or its cilia.[2–4] For artificial microswimmers, alternative concepts of harvesting environmental energy into kinetic energy is taken into account to generate active Brownian motion that drives them out of the equilibrium process of directed motion.[5–7]

In the current era, researchers have developed their interest in investigating different systems of artificial micro swimmers as it can be used for numerous applications from both fundamental and applied point of views. For instance, it is possible to understand the flow mechanism or collective behavior of pool of bacteria in the certain environment by mimicking them with active artificial swimmers.[8–15] Even at a macro scale, particle dynamics has prompted researchers to describe pedestrian dynamics as they say that human crowds can also show striking resemblance to interacting particle systems.[16] Other examples where particle dynamics is utilized include a flock of birds, insects or other microorganism in water like fishes, which synchronizes their motion with their neighbors in order to translocate from one place to another.[17] One can also perform different tasks at microscale such as micropumps, micro/nano machine could help to tackle many challenges in industries dealing with different technologies like health care, food, or medicines.[18–27] For instance, micromotors can be a good source for transporting medicines to specific places for the controlled release of drugs.[28]

The increasing importance of fabricating and designing new systems of synthetic micro/nano-machines is now evident and considerable efforts have been employed for the preparation of smart and efficient nano-/micro motors which can be propelled by different external stimuli.[29,30] Most of the propulsion mechanisms reported are the response of the generation of local gradient of

chemicals,[31,32] ionic charges,[33] temperature,[34,35] or concentration gradient of solute molecules.[36] Different forms of energy like electric, magnetic, optical, gravitational, thermal, or acoustic can be used to generate such local gradients.[37–45] Among all these forms of energy, optical energy is most promising and has been reported as one of the powerful and commonly used external stimuli for decades in a vast range of applications. Also, it is one of the best accessible sources discovered which can be molded according to the requirements, transforming optical energy into multiple other forms of energy depending on the systems where motion can be induced either due to bubble propulsion,[46] diffusiophoresis,[47] due to electro or diffusioosmosis,[48,49] catalytic motion,[50,51] or by optical trapping.[52–55] For decades, most commonly reported systems used photocatalytic materials like AgCl or TiO_2 or photoactive solutions like H_2O_2 where the motion of micro swimmer was controlled by light of appropriate wavelength.[56–60] For instance, J. Simmchen and co-workers recently reported the directional motion of metal capped TiO_2 particle present in H_2O_2 solution where particles were driven upon UV or visible light illumination.[61,62] Another interesting approach for manipulating the motion of micro swimmers includes the use of photoactive surfactant solutions such as Azobenzene Containing Surfactant (ACS). The use of ACS for controlling and monitoring the motion of colloids is currently taking pace due to its robust, flexible and completely reversible nature.[63–65]

Motivated by diverse light driven approaches of particle motion, in this dissertation, we discuss a mechanism for the propulsion of porous/non-porous silica particles dispersed in the aqueous solution of azobenzene containing surfactant using the appropriate wavelength of light. The mechanism of light driven diffusioosmotic (LDDO) flow is taken into account in order to drive particles at solid/ liquid interface. The basic principle of LDDO flow has been recently introduced by members of our group and discussed in detail in **Section 2.3.2**. The flow is induced due to the concentration gradient of the photosensitive surfactant at the solid/liquid interface which is generated upon irradiation with light of appropriate wavelength. The azobenzene incorporated into the hydrophobic tail of the cationic surfactant undergoes reversible photo isomerization between stable *trans* state to metastable *cis* state under irradiation of UV and visible light.[66] The *trans* and *cis* isomers of azobenzene unit have different molecular properties, for instance *trans* molecule is symmetrical with zero dipole moment and thus hydrophobic, whereas the *cis* state has higher dipole moment and thus more hydrophilic. This means, the surface properties of surfactant molecules are also different for the *cis* and the *trans* states and can be easily triggered by light.[67,68] For instance, critical micelles concentration (CMC) of certain surfactants (Azo-C6) is 4 to 8 times larger in the *cis*

form as compared to trans form.[69] The remote triggering of the surfactant's hydrophobicity can make many oppositely charged soft matter systems photo-responsive by simply utilizing the electrostatic interactions. In this way one can make microgels photo-responsive and change their size by two times within seconds by applying light of different wavelengths.[70] Another example is light controlled compaction/de-compaction of the DNA molecules in the presence of the photo-sensitive surfactant.[71,72] It is also possible to make polymer brushes photo-responsive by preparing super molecular complexes using azobenzene containing surfactants.[73–75]

In this dissertation, we focus on the interaction of photo-active surfactant with mesoporous silica particles (MSPs) exposed to irradiation with light of different wavelengths. MSPs are negatively charged with a pore size of 6 nm and porosity of 850 m^2/mg. When surfactant molecule is in *trans* state it enters into the pores and forms micelles depending upon surfactant concentration, in contrast, in *cis* state, it prefers to stay in bulk solution due to higher hydrophilicity of *cis* molecules. This different interaction potential generates diffusioosmotic flows around each particle causing either repulsion or attraction between porous colloids. Separation or aggregation of particles can be controlled and manipulated just by controlling irradiation wavelength of light. Here we discuss motion under blue and UV light irradiation. The combined effect of two wavelengths on particle motion is also discussed. Using the same system, it is also possible to generate self-propelled motion which requires very less energy and is perpetual without any external changes.

This thesis is based on five papers in which we describe in detail the effects mentioned above. The motivation of this work is to develop light controlled mechanism for passive and active particle motion. The aim is achieved by varying two main components: wavelength of light and nature of colloidal particles.

The first paper[76] (**Arya, P.; Jelken, J.; Lomadze, N.; Santer, S.; Bekir, M; Kinetics of photo-isomerization of azobenzene containing surfactants, *J. Chem. Phys*., 152, 024904 , 2020**) deals with the kinetics of photo-isomerization of azobenzene containing surfactant (Azo-Cn) in aqueous solution. The surfactant photo-isomerization kinetics is approximated by a kinetic model of a pseudo first-order reaction approaching equilibrium. It is also demonstrated that amount of *trans* and *cis* isomers at photo-stationary state depends upon irradiation wavelength, intensity of the applied light, and concentration of the surfactant.

The second paper[77] (**Feldmann, D.; Arya, P.; Molotilin, TY.; Lomadze, N.; Kopyshev, A.; Vinogradova, OI.; Santer, S., Extremely long-range light-driven repulsion of porous microparticles, *Langmuir*, DOI: 10.1021/acs.langmuir.9b03270 , 2020**) is concerned about the mechanism of local-light driven diffusioosmosis (l-LDDO) flow induced around porous silica particles. Under blue light irradiation and with suitable particle concentrations l-LDDO results in formation of stable 2D crystal-like patterns. The strength of repulsion depends upon intensity of light and concentration of particles. The range of the flow is measured using tracer non-porous particles.

In 3rd paper[78] (**Arya, P.; Jelken, J.; Feldmann, D.; Lomadze, N. and Santer, S., Light driven diffusioosmotic repulsion and attraction of colloidal particles, *J. Chem. Phys.*, in printing, 2020**), the effect of global UV light irradiation on collective motion of mesoporous colloidal particles is reported. UV light isomerizes most of *trans* molecules to *cis* which generates l-LDDO flow initially resulting in particle separation up to distances of 10 times larger than the particle diameter. However, separation does not sustain longer because flow vanishes after photo stationary state is achieved. Moreover, in this paper we show that the direction of the l-LDDO flow can be changed spontaneously from the outward (out of the particles) to inwards for certain set of parameters (Intensity of UV irradiation, surfactant and particle concentrations). In this way we introduce a phenomenon of extremely long range diffusioosmotic repulsion and attraction.

In the fourth paper[79] (**Arya, P.; Feldmann, D.; Kopyshev, A.; Lomadze, N. and Santer, S. ; Light driven guided and self-organized motion of mesoporous colloidal particles, *Soft Matter*, 16 , 1148, 2020**) we investigate the dynamic self-organization of porous colloids using simultaneous irradiation of blue (λ = 455nm) and UV light (λ = 365nm) lights of different spot sizes (UV global irradiation and blue focused). The combined effect of passive and active motion of colloidal particles trapped at solid/liquid interface results in a well ordered 2D crystalline-like pattern of silica porous particles which are trapped inside the blue spot by global LDDO flow. The parameters controlling the organization of particles are discussed in **Appendix B**.

The fifth paper[80] (**Feldmann, D.; Arya, P.; Lomadze, N.; Kopyshev, A.; Santer, S.; Light-driven motion of self-propelled porous Janus particles, *Applied Physics Letters,* 115 , 263701, 2019**) deals with light driven self-propelled motion of porous-Janus particles. The mechanism is based on generation of local light driven diffusioosmotic flow around the porous particles under blue light. Motion can be achieved by covering half hemisphere of porous silica particles with a metal layer (gold/platinum) which results in generation of the flow only at the uncapped side (i.e. porous side)

resulting in self- propelled motion of the Janus particle in the direction of the gold cap. The motion of dimer particles around cyclic trajectories is discussed with respect to gold cap orientation.

This cumulative dissertation is organized in 6 chapters. The next chapter (Chapter 2) describes the theoretical and experimental basis of the thesis. Chapter 3 consists of the summary of the publications emerging out of this thesis. The reprints of the published papers with supporting information are presented in Chapter 4. Chapter 5 contains the discussion and conclusion of the obtained results. At the end, the Appendices complement the details on different aspects reported in the publications.

2. Theoretical and experimental basis

2.1. Introduction to azobenzene

Azobenzene is an aryl azo compound composed of two phenyl rings linked by N=N double bond. Due to presence of diazene's group, the azobenzene compounds absorb light from ultraviolet to visible region and changes its conformations from *trans*- and *cis*-state.[81,82] *Trans* form of azobenzene is planar, whereas *cis* azobenzene is nonplanar with dihedral angle of 173.5° (see structure scheme in **Figure 2.1**).

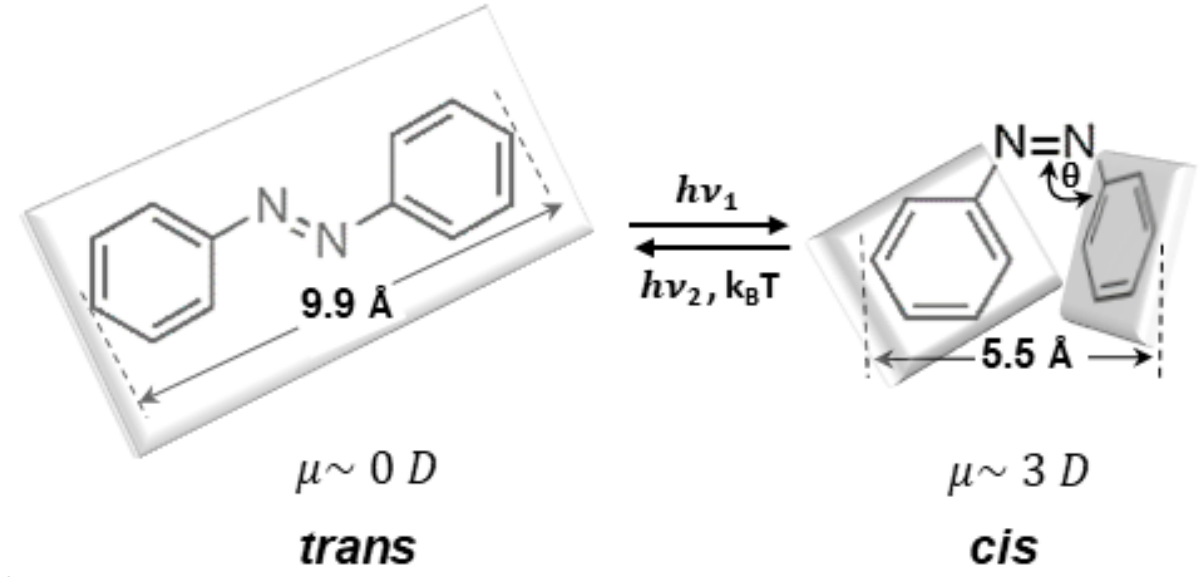

Figure 2.1. Chemical structure of *trans*- and *cis*- isomers of azobenzene molecule. *Trans*- isomer is planer whereas *cis*- isomer is non planer with dihedral angle of $\theta = 173.5^0$.

The photo isomerization of azobenzene is completely reversible and occurs in pico-second time scale.[66,83,84] The energy barrier to *cis* state is overcome by photo-excitation of *trans* molecules with appropriate wavelength of light (**Figure 2.2a**). For instance, under irradiation with UV light the stable *trans* state isomerizes to meta stable *cis* state, which can be reconverted by applying light of longer wavelength or by thermal relaxation.[85] The energy barrier for back (*cis* to *trans*) isomerization is ca.

1.1 eV (105 kJ/mol).[86] The *trans* state has a characteristic absorption band (π-π* transition) with a maximum at 351 nm and *cis* isomer is characterized by two absorption bands with maxima at 313 nm (π-π* transition) and at 437 nm (n-π* transition).[87] The characteristic absorption spectra of *trans* and cis azobenzene are shown in **Figure 2.2b**. *Trans* isomer is non-polar with a dipole moment of 0D, while *cis* molecule is polar with a dipole moment of 3 Debye.

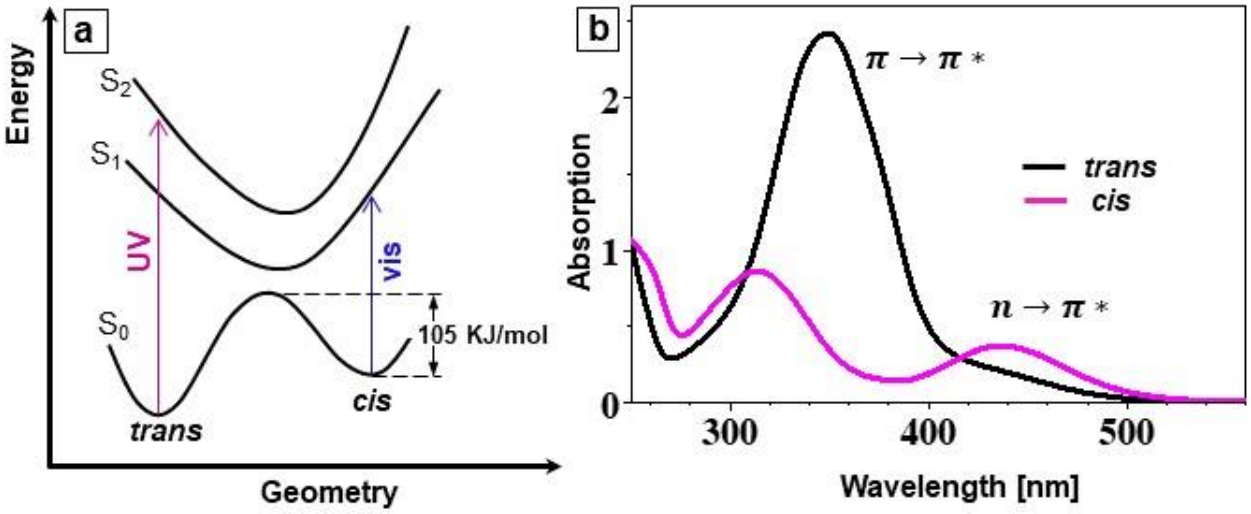

Figure 2.2. (a) Schematic energy diagram of single azobenzene molecule. *Trans*-isomer has lowest energy level. *Trans*- or *cis*- state is excited by UV and visible light respectively and isomerizes back to ground state by inversion or rotation of molecules in to *cis*- or *trans*- state. *Trans*- to *cis*- isomerization requires high energy whereas *cis* to *trans* isomerization can take place either by irradiation with longer wavelength or by thermal relaxation crossing the energy barrier of 105 kJ/mol. (b) Characteristic UV-vis absorption spectra of azobenzene molecule in *trans* (black line) and in *cis*- (magenta line) state.

Azobenzene molecule is used as a parent molecule for broad class of aromatic azo compounds and is utilized as a photo switch in variety of polymer materials and molecules. Some of its applications are: as molecular machines[88], in probing protein[89], as metal ion chelators or indicators[90], in hologram recording devices[91–93], industrial dyes[94,95] and as photo active surfactants.[96–98]

2.2. Azobenzene containing surfactant

Photoactive surfactants are nowadays receiving theoretical and experimental attention due to their ability to change surface properties remotely. One of the most efficient ways to make surfactant molecules photo active is by the integration of azobenzene unit, as the photo-isomerization of the

azobenzene is one of the cleanest photo-reaction known (i.e. free of side product).[99] In recent years azobenzene containing surfactants are widely used to manipulate small objects at water/air interface using simple light sources without the need for extra additives.[100–102] For instance, one can make control delivery of a droplet consisting of cargos (drugs or other chemical materials) using photoactive surfactant solution. The droplet moves due to change in surface tension under different wavelengths of light (surface tension decreases when surfactant is in *cis*- form). This phenomenon is well explained with the help of well-known Marangoni flow which is generation of fluid flow at liquid/air interface due to gradient of surface tension.[103,104]. This Marangoni-type effect is intensively utilized and demonstrated in several systems consisting of light-driven photo fluidics.[105–109]

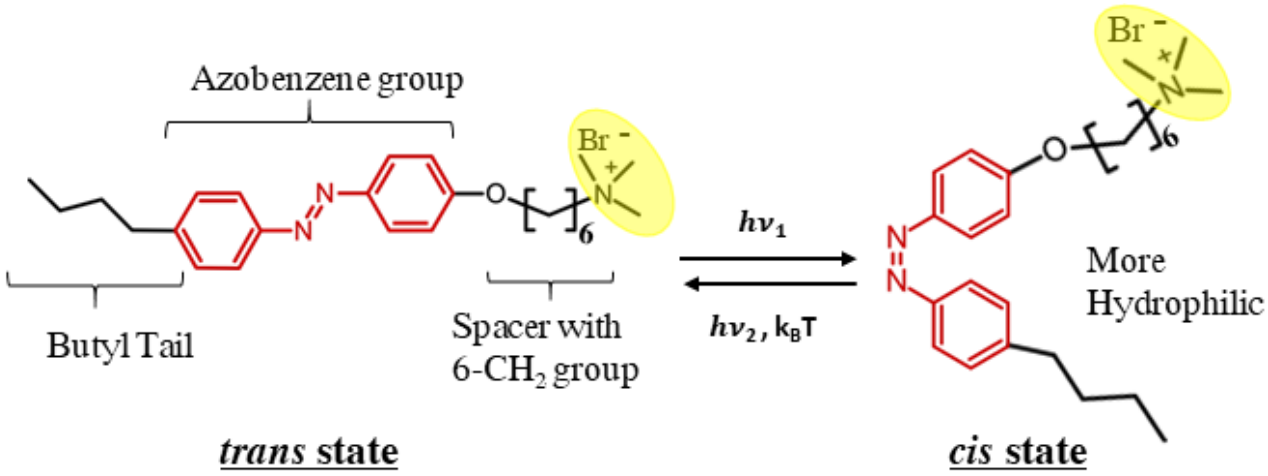

Figure 2.3. Azobenzene containing surfactant molecule with cationic head group (marked in yellow) and azobenzene unit incorporated between spacer of 6 methyl group and one butyl tail. Surfactant molecule undergoes reversible photo isomerization from *trans*- state (left) to *cis*- state (right) when exposed to photon of high energy.

In this dissertation, azobenzene containing surfactant is utilized to manipulate collective motion of colloidal particles at solid/liquid interface under appropriate wavelength of light. The azobenzene containing surfactant used in this work is cationic surfactant consisting of a positively charged trimethylammonium bromide head group, and a hydrophobic tail where azobenzene unit is incorporated between 6 CH_2 groups and a butyl tail at the para position (Azo-C6). Indeed, due to the presence of azobenzene unit, the surfactant molecules also undergo reversible photo isomerization from stable *trans* state to meta stable *cis* state under UV light irradiation.[110,111] **Figure 2.3** shows the corresponding *trans* and *cis* states of the surfactant molecule used. The photo-isomerization of

azobenzene unit also tailors the molecular properties of surfactant molecules,[112,113] i.e. in *trans* state it is hydrophobic whereas in *cis*- state it is hydrophilic. This means, the tail of the same molecule can either be tuned as non-polar (*trans*) or polar *(cis*) under different wavelengths of light. Also, surface properties of surfactant such as surface tension[114] and also CMC shifts from 0.5 mM to 4 mM in *cis* state (**Figure 2.4a**).[115] Photo isomerization also changes its solubility and interaction with the other molecules or materials. The typical UV-Vis absorption spectra of surfactant molecules in *trans* state (in dark) and in *cis* state (after UV irradiation) is shown in **Figure 2.4b**. *Cis* isomers can undergo thermal back isomerization to stable *trans* state where the lifetime of *cis* isomer in the dark at room temperature is measured to be ca. 40 hours.[76]

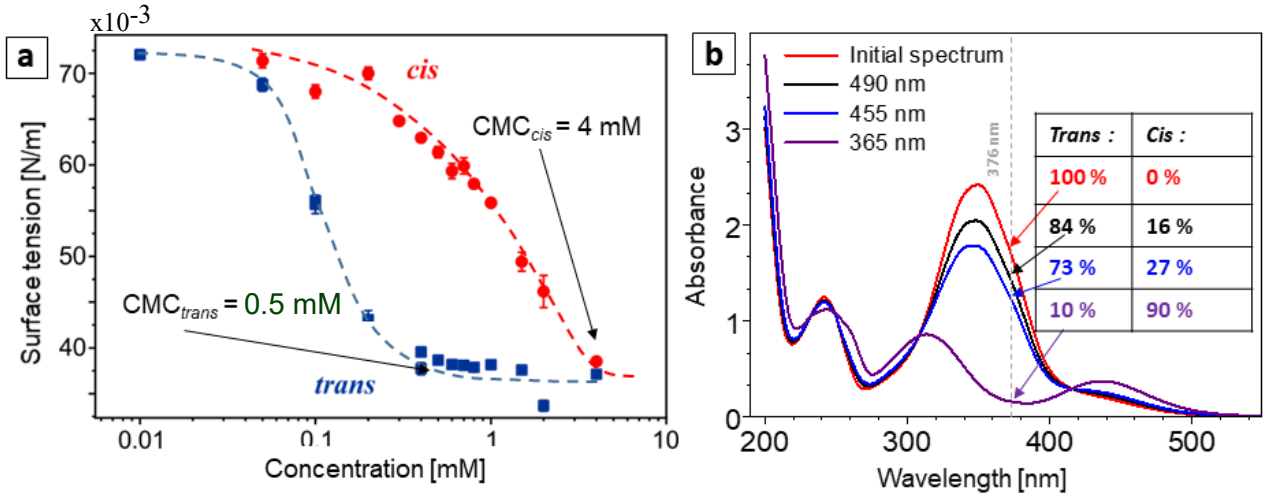

Figure 2.4. (a) Surface tension measurements as a function of surfactant concentration for Azo-C6 in *trans* state (in dark all molecules are in *trans* state) and in *cis* state (achieved after 10 min of UV irradiation). (b) Absorption spectra of 1mM Azo-C6 at photo-stationary state achieved after irradiation of different wavelength λ = 490 nm (black line), λ = 455 nm (blue line), λ = 365 nm (Violet line). Red line represents spectra without irradiation (in dark maximum molecules are in *trans*- state). Table represent fraction of *trans* and *cis* molecules at photo stationary state for different irradiation wavelength.

The ratio of *trans* and *cis* isomers at equilibrium, i.e. after photo stationary state is reached, depends on the wavelength of light and is measured for UV (λ = 365 nm), blue (λ = 455 nm and λ = 490 nm), and green (λ = 530 nm) light as shown in table in **Figure 2.4b**. Photo stationary state also depends on different surfactant concentrations above CMC. The time taken to reach photo stationary state depends on the intensity of irradiation, while the amount of *trans* and *cis* isomers are independent of intensity of particular wavelength used. The photo kinetics of the Azo-C6 under blue and UV irradiation is reported in **Chapter 4, Publication 1**.[76] It is also shown that the ratio of *trans* and *cis*

isomers can be altered using multiple wavelength of light simultaneously and can be manipulated by different ratio of intensities.

2.3. Osmosis to Light Driven Diffusioosmosis

2.3.1. Introduction to osmosis and diffusioosmosis

Osmosis is a universal phenomenon occurring in vast varieties of systems and processes. From etymological point of view, the word osmosis means a push and is related to the notion of force and pressure. It was first described by Jean- Antoine Nollet in 17th century. He observed swelling of a cylindrical vial filled with alcohol placed into a bowl full of water. Conventionally, osmosis is diffusion of water molecules across a semipermeable membrane: membrane which blocks the passage of solute molecules but allows solvent molecules to pass through.[116–118] The movement of solvent is due to the difference between the concentrations of the solutes on both the sides of the membrane. For instance, if two solutions of liquids with different solute concentrations are put into a chamber and are separated by a semipermeable membrane, the solvent from lower solute concentration moves towards the higher solute concentration due to the gradient of chemical potential. A pressure has to be applied in order to prevent the motion of solvent through the membrane to stop the flow, which is commonly referred as osmotic pressure and can be written according to Van't Hoff relation[119] as.

$$\Delta\pi = k_B T \Delta c_S \qquad \textbf{(1)}$$

Where k_B is the Boltzmann constant, T the temperature and Δc_s the concentration gradient of the solute. On the microscopic level, osmosis is an example of diffusion where only solvent molecules are allowed to move through the nano-channels of semipermeable membrane, but not solute molecules. Difference between osmosis and pure diffusion is shown in **Figure 2.5**.

The physical force driving the osmosis is not only the interaction of solute with the membrane but also the existence of differential forces acting separately on the solvent and solute molecules. This means that osmosis is also possible without the semipermeable membrane where forces acting on solvent and solutes occur at interface. The most common osmotic flows without membrane, but with solid interfaces are: electroosmosis and diffusioosmosis.[120]

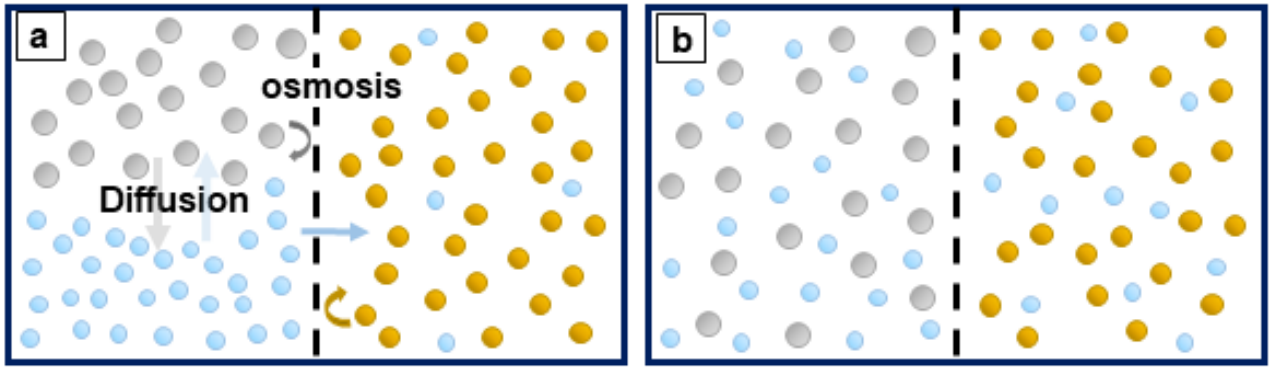

Figure 2.5. Osmosis versus diffusion. Grey and yellow molecules cannot pass through membrane whereas blue molecules are allowing to cross membrane. (a) Situation before any diffusion and osmosis. (b) Equilibrium achieved after diffusion and osmosis.

Electroosmosis (EO) is the outcome of net electric forces due to applied electric field along the solid interface.[121] It can be viewed as a force balance between electrostatic forces in electrostatic double layer (EDL) and viscous frictional forces at the interface. Net electric forces induce the motion of ions in EDL which move the fluid (**Figure 2.6a**). It is commonly used in microfluidic devices which has ample applications in the field of medicine such as drug delivery, for soil and chemical analyses, and for particle assembly.[122–126]

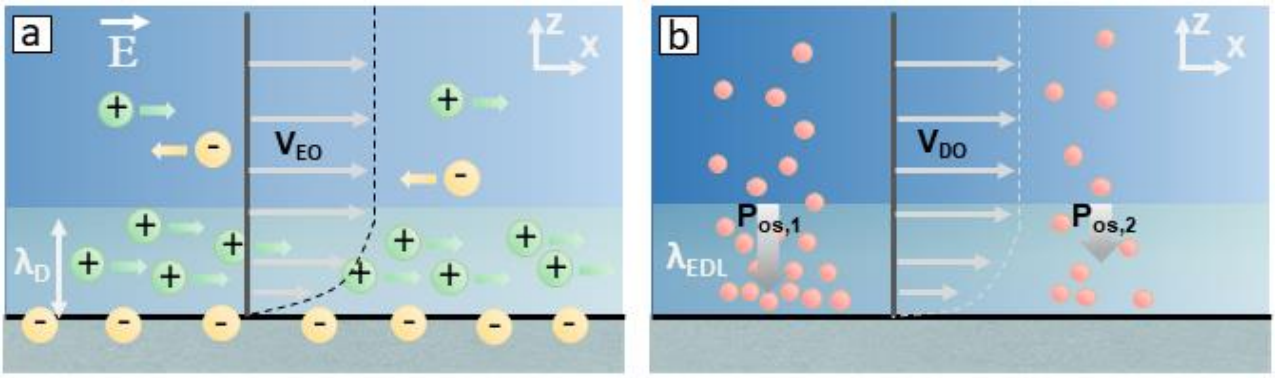

Figure 2.6. Scheme of osmotic flows at the solid/liquid interface (membrane free systems). (a) Electroosmosis: a net electric force is developed in the electrostatic double layer under the applied electric filed which drives the solvent parallel to the solid/liquid interface. (b) Diffusioosmosis: gradient of solute at the interface induces a flow due to varying interaction potential along x direction. Solute interaction with the surface induces a pressure which is higher towards the higher concentration of solute driving the fluid towards the lower concentration.

Diffusioosmosis (DO) originates due to gradient of solute concentration at a solid/liquid interface.[127] It is basically an interface driven flow which occurs due to differences in solute concentrations with within the EDL layer (a thin layer- few nanometres close to the surface) where solute interaction

potential to surface provokes pressure gradient (**Figure 2.6b**). In various reports diffusioosmosis has been advised as a suitable tool for diversity of applications including particle delivery,[128,129] micro/ nano- fluidic,[130] and many others.[49,131] DO process has a complex mechanism because of its subtle and less intuitive behavior. The theoretical basis of DO is reported in few publications[120,127,132–135] but still there are less experimental evidence for the process. One can conclude two important components for introducing Diffusioosmosis flow:

1. A solute gradient along x (parallel to interface) direction should be generated
2. The interaction potential $\Phi(z)$ of the solute at solid interface introduces an osmotic pressure gradient pushing the fluid against the wall which induces flow along the surface.

Keeping in mind above mentioned points, a novel light actuated phenomenon is recently introduced where Diffusioosmotic flows are generated by light of different wavelengths. This phenomenon is named as light driven diffusioosmosis (LDDO) [49] and explained in detail in the next section.

2.3.2. Light Driven Diffusioosmosis (LDDO)

In the previous section it is shown that azobenzene containing surfactant undergoes conformational changes under specific wavelength of light, for instance, *trans*- to *cis*- state under UV light and *cis*- to *trans*- state when longer wavelength of light is used. These isomers have different interaction potentials to the surface due to differences in their molecular properties (dipole moment) which means *trans*- and *cis*- isomers can be treated as two different solute molecules whose concentrations can be altered by different light irradiation. This optical control on concentration of *trans* and *cis* isomers make azobenzene containing surfactant a unique electrolyte to generate light driven diffusioosmotic flows.

Let us consider a fluid containing a solute (azobenzene containing surfactant) with concentration c_s, filled into a closed chamber. Because surfactant molecule is positively charged and is in *trans* state, it will interact with the glass surface (z= 0) *via* electrostatic forces leading to Electrostatic Double Layer (EDL) at the solid/liquid interface.[135,136] At thermal equilibrium, the concentration in the EDL follows the Boltzmann distribution[137] and can be written as**:**

$$c_s(x,z) \approx c_\infty \exp\left(\frac{-\Phi(z)}{k_B T}\right) \qquad \textbf{(2)}$$

Here c_∞ is the bulk concentration, $\Phi(z)$ the interaction potential of surfactant molecules with a solid surface, $k_B\ the$ Boltzmann constant, and T the temperature of the system. The thickness of EDL can be referred as Debye length and is calculated as $\lambda_D = 10\ nm$ for c_s = 1 mM.[49]

Upon focused UV irradiation, *trans* molecules isomerize to *cis* molecules at the irradiated area. This results in a boundary which divides the fluid into two spaces either with excess *cis* (inside irradiation spot) isomers or excess *trans* isomers (outside the spot). Due to different chemical potential of *cis*- and *trans*- isomers, osmotic pressure gradient along the surface occurs which drives the fluid from higher concentration of *cis* isomers to lower concentration (scheme of the process is shown in **Figure 2.7**). The pressure gradient between two spaces can be written using coupled Stokes and Smoluchowski equation as[120]:

$$p(x,z) - p_\infty = k_B T[c_+(x,z) + c_-(x,z) - 2c_0(x)] \qquad \textbf{(3)}$$

where p_∞ is the osmotic pressure in bulk, $c_\pm(x,z)$ the concentrations of ions (both salt and surfactant) in EDL, and $c_0(x)$ the bulk concentration of the solute. This pressure difference can be seen as osmotic pressure equilibrate at the diffuse layer.[138] The pressure difference is compensated by a hydrodynamic flow where the flow field satisfies Stokes equation:

$$\eta\nabla^2 v = \nabla p, \quad \nabla \cdot v = 0 \qquad \textbf{(4)}$$

Where, η is the viscosity of surfactant solution and v the fluid velocity. The velocity increases through the interface to finite and constant value V_{LDDO} (light driven diffusioosmotic velocity) in bulk and can be obtained by solving equation **(3)** and **(4)**:

$$V_{LDDO} \propto -\frac{k_B T}{\eta}\left(\frac{\partial(\Gamma_{EDL}\lambda_d)}{\partial c_t}\nabla c_t(x) + \frac{\partial(\Gamma_{EDL}\lambda_d)}{\partial c_c}\nabla c_c(x)\right) \qquad \textbf{(5)}$$

where c_t and c_c are concentration of *trans* and *cis* isomers, respectively. The terms $\frac{\partial(\Gamma_{EDL}\lambda_d)}{\partial c_{t/c}}$ represent the adsorption isotherm of surfactant molecules in *trans* and *cis* states at solid /liquid interface (in EDL). Γ_{EDL} is the surface excess of surfactant and depends upon the individual concentration of *cis* and *trans*, and can be related to the interaction potential by Boltzmann distribution[139] shown in **Equation (2)** as,

$$\Gamma_{EDL}(x) \sim (c_+(0) + c_-(0) - 2c_0)\lambda_d \sim\ c_0\lambda_d\left(\frac{e\Phi_0}{k_B T}\right)^2 \qquad \textbf{(6)}$$

From equation **(5)** and **(6)**, and calculating diffusioosmotic slip velocity for concentrations above CMC (0.5 mM) with respect to *cis* molecules gives an expression for velocity:

$$V_{LDDO} = \frac{\lambda_d^2}{\eta} \cdot \frac{RTc_0}{L} \cdot \left(\frac{e\Phi_0}{k_B T}\right)^2 \qquad \textbf{(7)}$$

in which L is the diameter of the laser spot[49]. In the specific case (focused UV), the LDDO flow generated points away from the irradiated area. The streamline of the flow is shown in **Figure 2.7.** Considering certain parameters' values in agreement with the experimental data, L = 60 μm λ_d = 10

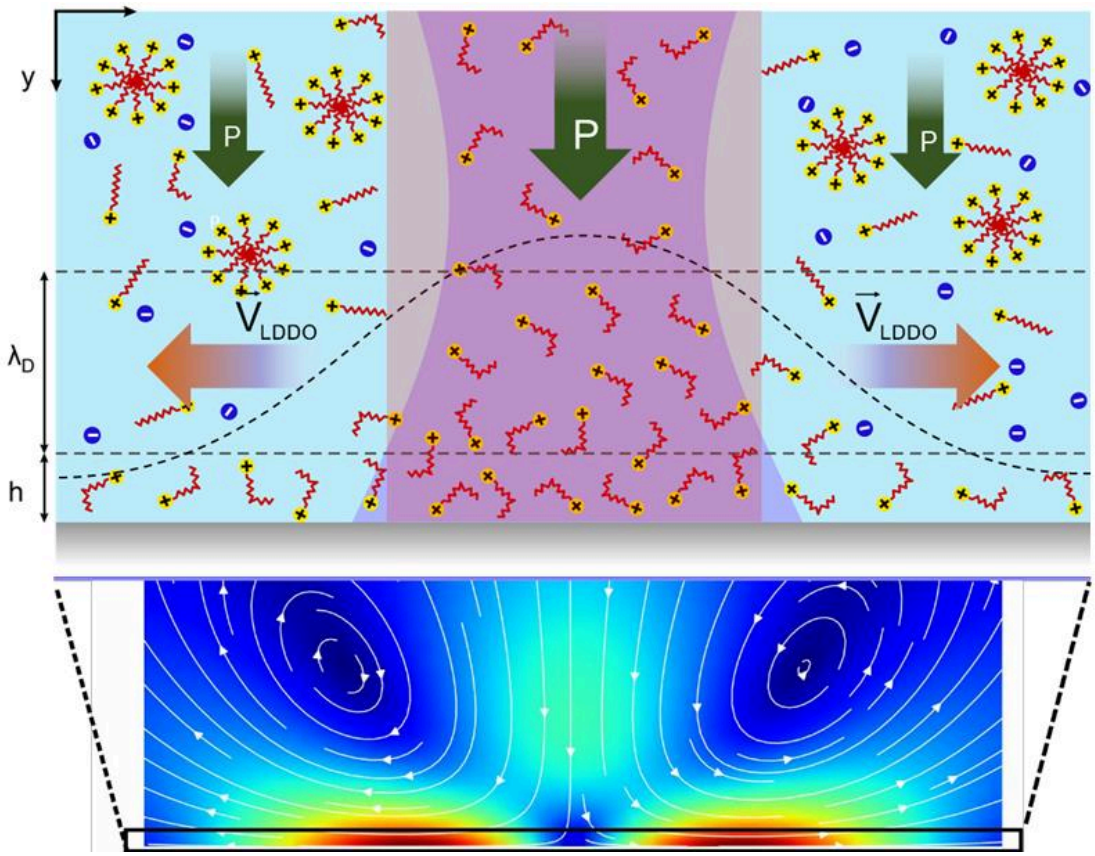

Figure 2.7. Scheme of light-driven diffusioosmotic flow. Focused UV light is exposed in the center resulting in photo-isomerization of *trans* to *cis* isomers. Red arrows show the direction of the flow pointing away from the irradiation spot. Schematic streamlines of liquid flow are presented at the bottom. Different colors represent regions with different absolute value of the liquid velocity being at maximum in red. Scheme of the streamlines is taken from *Scientific Report* 6, 36443 (2016).[49]

nm at C_0 = 1mM, η = 1 mPa·s, T = 20°C and for the surface potential Φ_0 = 70mV (taken from Surface zeta potential (SZP) measurements for C_0 = 1mM) the diffusion osmotic velocity yields $V_{LDDO} \approx 7\mu m/s$.

The direction of LDDO flow can be reverse (towards the irradiated spot) using focused light of longer wavelength (blue or green). To induce the flow initially most of the *trans*- isomers are converted into *cis* isomers using global UV irradiation until photo-stationary state (90 % *cis*) is reached. Afterwards, irradiations of focused green laser re-isomerizes *cis*- state to *trans*- state in the green irradiated area which contributes back to micelles (for concentrations above CMC) and decreases the concentration of *cis*- molecules near the solid/liquid interface resulting in osmotic pressure which generates the flow towards the laser spot.

Considering what has been discussed above, one can sum up the phenomena of light driven diffusioosmotic flow as shown in **Figure 2.8**.

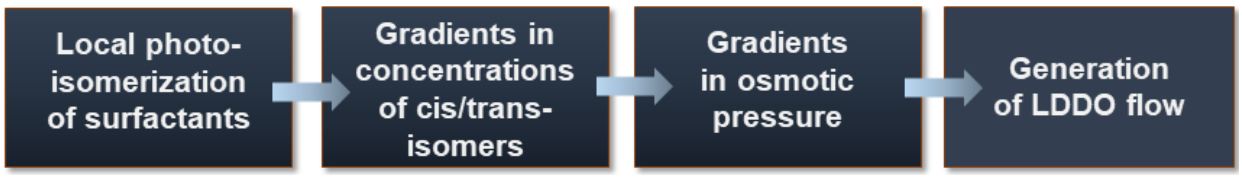

Figure 2.8. Flow diagram of mechanism of light driven diffusioosmotic flow.

2.4. LDDO flow as a tool of particle motion

Light driven diffusioosmosis (LDDO) flow generated due to focused irradiation with UV or visible light, can be used to drive colloids and other micro-organism present at the solid/liquid interface. One can visualize it as passive motion of particles, induced due to generated osmotic flows at interface, which can carry the particles along it. The particle speed depends upon the slip velocity of the flow. LDDO is a special case because of contactless control on concentration of solute molecules at the solid surface. The other advantage of LDDO is the possibility of manipulating the direction of motion, just by changing the wavelength of light.

In case of focused UV light, flow is generated radially away from the spot resulting in cleaning of ensemble layer(s) of silica particles from the solid/liquid interface. **Figure 2.9a** shows the time dependent optical micrographs of silica particles which are dispersed in 1 mM azobenzene containing

surfactant on a glass surface. When focused UV light of 20 µm laser spot size is applied, particles immediately go away from the irradiated spot leaving behind a clean surface.

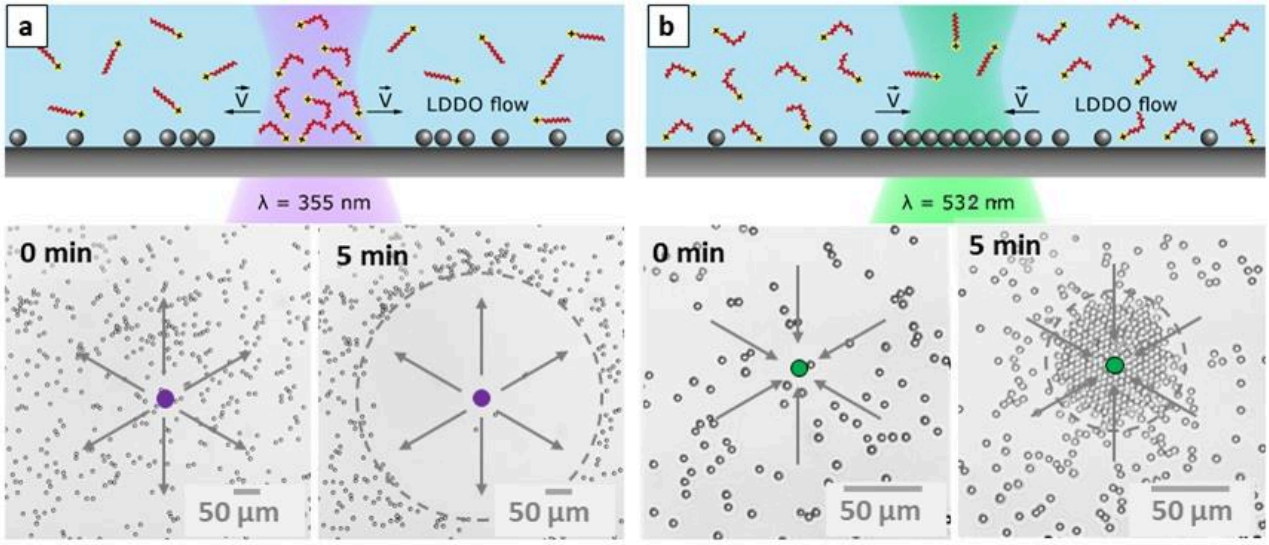

Figure 2.9. Scheme of light driven diffusioosmosis flow. (a) Under focused UV laser direction of flow points away from the irradiated spot resulting in cleaning of the surface. (b) Flow direction is reverse using focused green light (particles gather towards the spot). Sample is exposed to global UV light for complete conversion of *trans* into *cis* isomers. Shown below are the optical micrographs of 4 µm silica particles in 1mM Azo-C6 at time scale t= 0min and t= 5 min. Corresponding videos are provided as **Figure S2.9** in Appendix D.

It is also possible to change the direction of particle motion. To achieve this, first we have to irradiate whole sample with global UV light which converts most of *trans* to *cis* molecules. Now applying irradiation with focused green light, will convert *cis* isomers back to *trans* isomers due to which osmotic pressure in green light irradiated area decreases. Now this gradient of pressure develops a flow towards the laser spot which will swipe the particles along with it and result in gathering a pool of particles at the center of the spot (**Figure 2.9b**).

One can analyze the flow velocity by calculating the velocities of particles with respect to the center of irradiation spot. It has been observed that the particles nearest to the laser spots are faster than which are away of the laser spot. The particle velocity varies with surfactant concentrations and intensity of light. The maximum velocity is observed for 1 mM surfactant concentration; this is because at concentrations above CMC (0.5 mM) after UV irradiation more amount of *cis* molecules

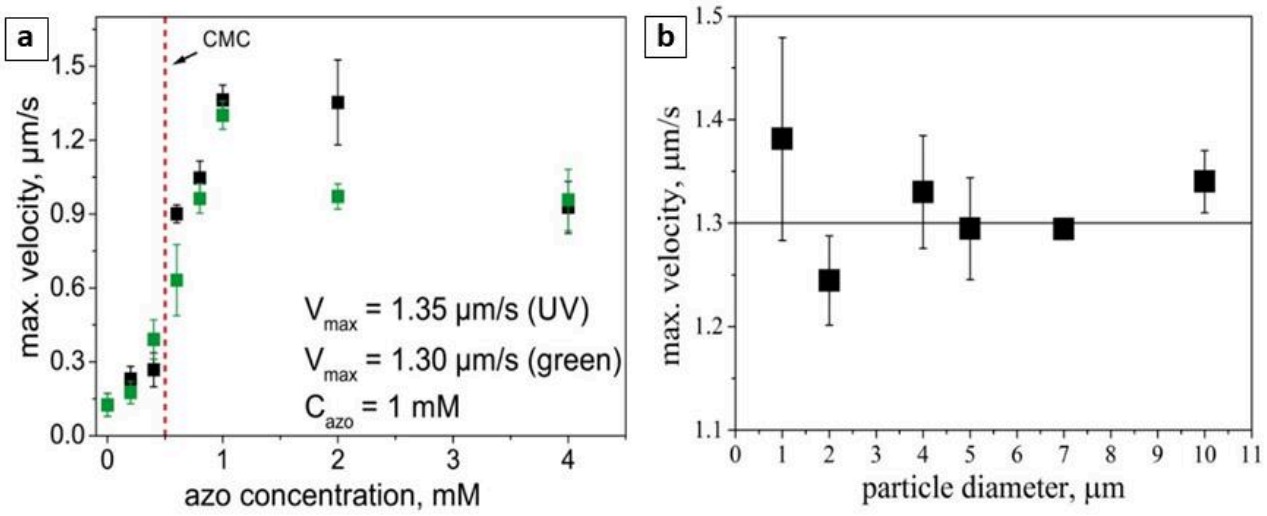

Figure 2.10. (a) Maximum velocity of 2 µm particles for different surfactant concentration under focused UV and green irradiation. (b) Maximum velocity of particles dispersed in 1mM Azo-C6 plotted as a function of particle diameter. It is observed that velocity is independent of particle size. Above figure is taken from *Scientific Report* 6, 36443 (2016).[49]

forms due to presence of micelles as compared to lower concentrations (upon UV exposure micelles are decomposed to single *cis* specimens) which results in higher gradient of concentration and hence the slip velocity of the flow. **Figure 2.10a** shows the maximum velocity plot with respect to the concentration of surfactant under UV and green light irradiation. This behavior was also observed for another surfactant molecules which differs in spacer length of CH_2 groups in between azobenzene and the head group of surfactant molecule **(Figure 2.11**).

It has been reported that the velocities of particles are independent of particle size, shape and orientation at least up to tens of µm of particle diameter (**Figure 2.10b**). The range and stability of the flow depends on different parameters such as surfactant concentration, laser spot size, and intensity of UV/green light or initial state of solution (initial ratio of *cis* and *trans* isomers in the solution). These dependencies are discussed in detail in **Appendix A**.

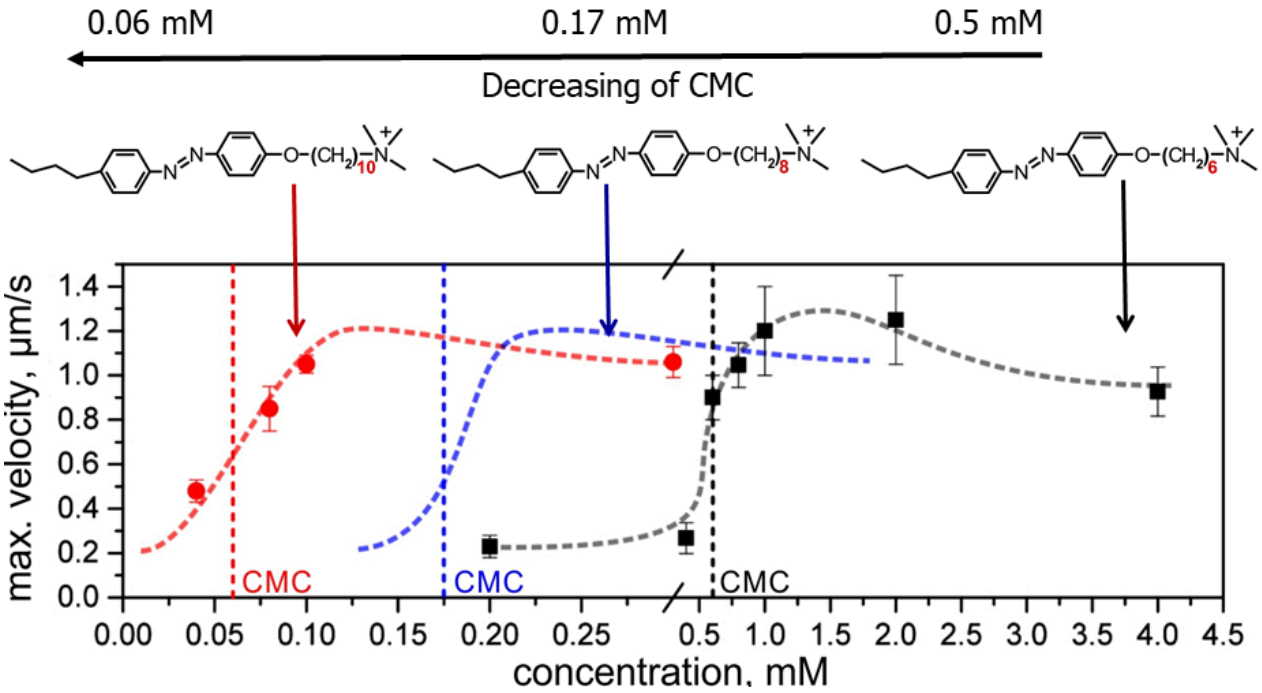

Figure 2.11. Maximum velocity of particles plotted as a function of different surfactant concentrations and for different surfactant molecules differing in spacer length as: n = 10 (CMC = 0.06 mM), n = 8 (CMC = 0.17 mM), and n=6 (CMC =0.5 mM). Figure is taken from the data obtained from PhD dissertation of Dr. D. Feldmann.

2.5. Passive motion to active motion of colloids

In the previous sections we discussed about the concept and the mechanism of light driven diffusioosmosis. It is shown that the focused irradiation of light can induce LDDO flow which drives colloidal particles passively either towards or away from irradiated area. In this section, we will discuss about the generation of active motion of colloids at solids surfaces utilizing the principal mechanism of LDDO flow. Active motion is achieved when mesoporous silica particles (MSPs) are dispersed in photoactive surfactant solution. The local-LDDO (l-LDDO) flow around each porous particle is generated upon irradiation of appropriate wavelength of light, resulting in repulsion between the particles. The phenomena of local-LDDO flow is well described in **Chapter 3**, **Publication 2**. In brief, the flow is basically originated due to different interaction potential of *trans*- and *cis*- isomers with mesoporous silica particles. MSPs are negatively charged particles with zeta potential of -26 mV measured in water. The zeta potential becomes positive under photoactive surfactant solution and increases with concentration of surfactant (-26 mV to +50mV) as shown in **Figure 2.12b**. It also varies for different wavelength of light due to different

interactions of *trans*- and *cis*- isomers with the silica particle. In *trans*- state surfactant molecules diffuse into the pores where as in *cis* state it is more likely to stay in bulk solution due to higher hydrophilicity. Upon irradiation, fraction of *trans* and *cis* molecules in the solution, as well as in the pores of particle (because particle is transparent) changes resulting in desorption of *cis*- and adsorption of *trans*- isomers from the pores of MSP. This causes a concentration gradient of *cis/trans* isomers around the particle inducing a radial flow outwards/inward the particle depending upon initial conditions and wavelength of light. The isomerization dependent adsorption and release of solutes into mesoporous silica particles has been also reported few times earlier for different systems for applications in drug delivery. [140] The SEM image and scheme of porous particles and its interaction with surfactant molecules in both *trans*- and *cis*- isomers are shown in **Figure 2.12 a,c,d**. In an ensemble of MSPs on glass surface, each particle's individual flow interacts with each other resulting in separation of particles and collectively forms a 2D crystalline pattern.

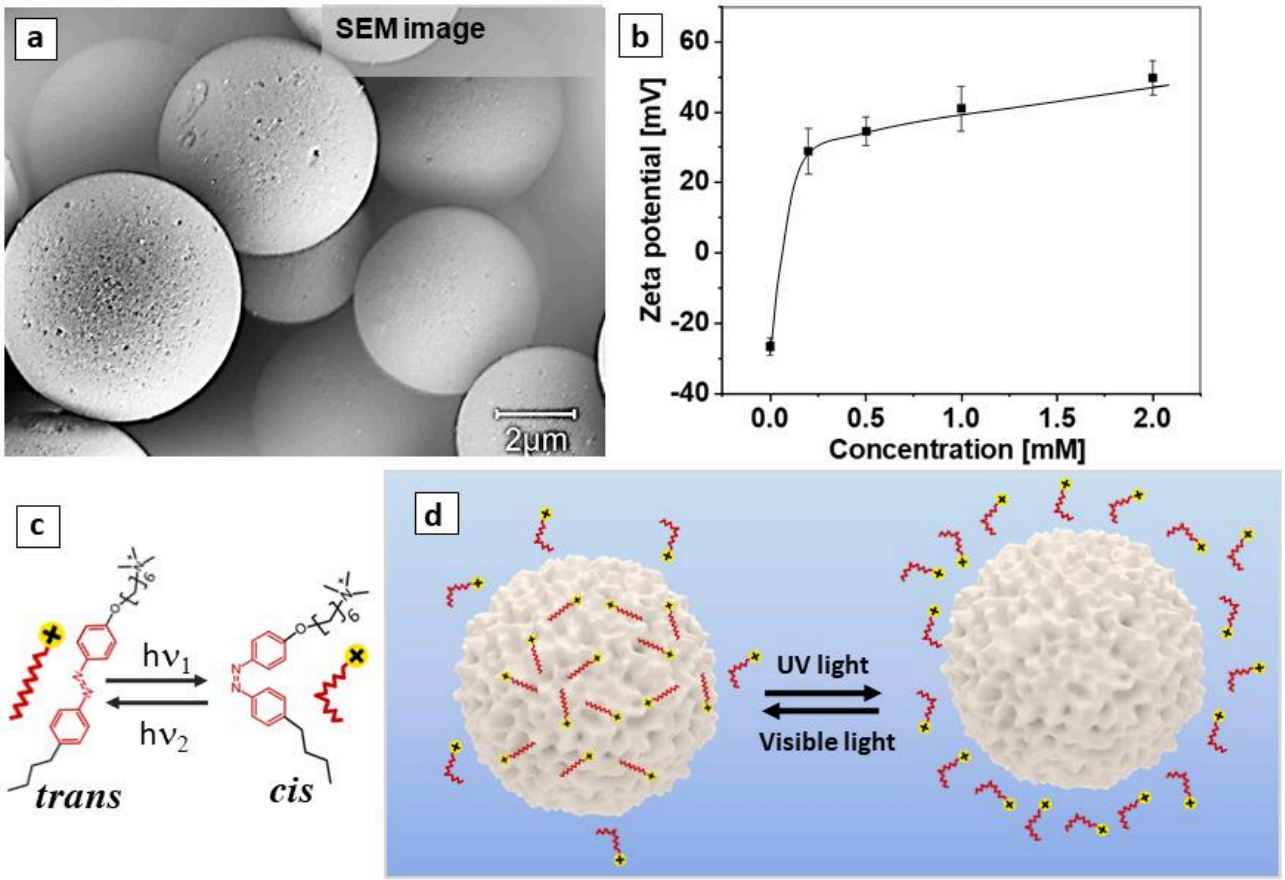

Figure 2.12. (a) SEM image of porous particle. (b) Zetapotnetial of MSPs in different concentrations of azobenzene containing surfactant solution. (c,d) Scheme of porous silica particles dispersed in Azo-C6. Molecules which are in *trans* state diffuse into the pores. Upon exposure to UV (365 nm)

light *cis* molecules are forms which expelled outside the particles. When light of higher wavelength is applied isomerized *trans* molecules enter again into the pores of the particle.

The range of separation and stability of the pattern depends upon the consistency of the flow which is highly dependent on the wavelength (that is upon fraction of *trans* and *cis* isomer at the photo-stationary state) and the intensity of irradiation and described in details in **Publication 2** (effect under blue light irradiation) and **Publication 3** (effect under UV light irradiation). The collective motion of particles under simultaneous irradiation of blue and UV light is further discussed **publication 4**. The diffusion of *trans* and *cis* isomers inside and outside porous particles are visualized using fluorescence dye and explained in more detail in **Appendix B.8**.

The system of porous particles with photoactive surfactant can be a powerful tool for generating self-propelled motion which is discussed in **Publication 4**. This is achieved by preparing Janus particles by covering half hemisphere of porous particles with gold metal layer. The basic idea behind, is to block the pores of one side of the particle, so that the flow induced on the other side (where pores are open) pushes the particle forward. With this approach in mind it is also possible to transport non-porous rods or particles (act as a cargo) to any specific locations. The methodology and dependency of different parameters are well discussed in **Appendix C**.

3. Summary of publications

3.1. Publication 1. Kinetics of photo-isomerization of azobenzene containing surfactants[76]

Here we report on photo-isomerization kinetics of azobenzene containing surfactants. The surfactants differ in their hydrophobicity, i.e. the length of spacer connecting azobenzene group and charged head group varies from $6CH_2$, $8CH_2$, to $10CH_2$. The photo-isomerization is studied depending upon the wavelength of applied irradiation (365 nm, 455 nm, 490 nm and 532 nm, and their combinations), on intensity of irradiation, as well as on the surfactant concentration. These results are important for understanding the generation of local-LDDO flow since it is shown to be a function of the photo-isomerization kinetics and isomers fractions at a photo-stationary state.[79] We have shown that at fixed intensity, the rate of *trans* to *cis* isomerization (K_{TC}) is larger for shorter wavelength whereas it is smaller for longer wavelength. The rate of back isomerization (K_{CT}), i.e. (*cis* to *trans* isomerization) is higher at longer wavelength. The overall rate of isomerization increases with increasing intensity while fraction of *trans* and *cis* isomers at equilibrium remains unchanged. The isomerization kinetics also depends upon surfactant concentration. We observe that below CMC, kinetics is independent of concentration, while above CMC, it decreases with concentration. It is explained by steric hindrance generated due to micelles above CMC. Decrease in kinetics also influences the fraction of *trans* and *cis* isomers at photo isomerization state above CMC. The effect of combination of two wavelengths on photo isomerization kinetics and photo stationary state is also reported for UV and blue light. Surfactant photo-isomerization is completely reversible and is discussed for multiple cycles of UV and blue light irradiation in sequence. Kinetic model is also expanded for simultaneous irradiation of two wavelengths. It was shown that one can also manipulate the fractions of *trans* and *cis* isomers at photo stationary state by combining two wavelengths and with fine tuning of intensities.

We have also shown that thermal back-isomerization of *cis* to *trans* molecules is relatively slow and can be neglected for higher intensities. Activation energy required for back-isomerization is experimentally calculated as 79 kJ mol^{-1} for AZO-C6.

3.2. Publication 2. Extremely long-range light-driven repulsion of porous micro particles[77]

In this work, we report on the phenomena of local light driven diffusioosmotic (l-LDDO) flow which results in formation of 2D crystal-like pattern of an ensemble of mesoporous silica particles (MSPs). Collective behavior of porous silica particles dispersed in aqueous solution of azobenzene containing surfactant at the solid/water interface is reported under global irradiation with blue (λ=455 nm) light. Different molecular properties of two isomers of surfactant molecules, i.e. *trans*- and *cis*-, play key role in generation of l-LDDO flow. More hydrophobic *trans* molecules are absorbed into the pores of porous particles, while *cis* molecules prefer to stay in the aqueous solution due to their hydrophilic nature. Combination of porous particles and Azo-C6 under constant global blue irradiation induces localized-LDDO flow around each particle. And when two particles are nearby each other, their flows interact instigating repulsion between particles. The strength of repulsion and stability of l-LDDO flow depend on the wavelength of applied light.

In the first part, we discuss the effect of blue (λ=455 nm) irradiation on particle motion. We have shown that induced l-LDDO flow is continuous and stable under blue irradiation while it stops when UV light is used. It has been observed that blue light is absorbed by both *trans* and *cis* isomers causing continuous isomerization of both conformers which maintains a fraction of *trans* and *cis* as 73% and 27% respectively at photo stationary state (see **Publication 1**). This means when *cis* molecules are expelled out of the particles, *trans* molecules present in solution diffuses in to the pores of the particles. This cycle of absorbing and desorbing surfactant molecules keeps going as long as the sample is exposed to blue irradiation. This continuous diffusion of *cis*- isomers out of the particles and *trans*- isomers into the pores of particle results in a continuous flow around each single MSP which keeps the separation between them stable forming a 2D crystalline pattern. When irradiation is switched off, flow stops and particles aggregate. However, they can be reproduced by switching blue light again. Nearest particle distance (NPD) is used to characterize aggregation and separation of particles. NPD increases during separation and stays constant until the blue light is on, as shown in **Figure 3.1**.

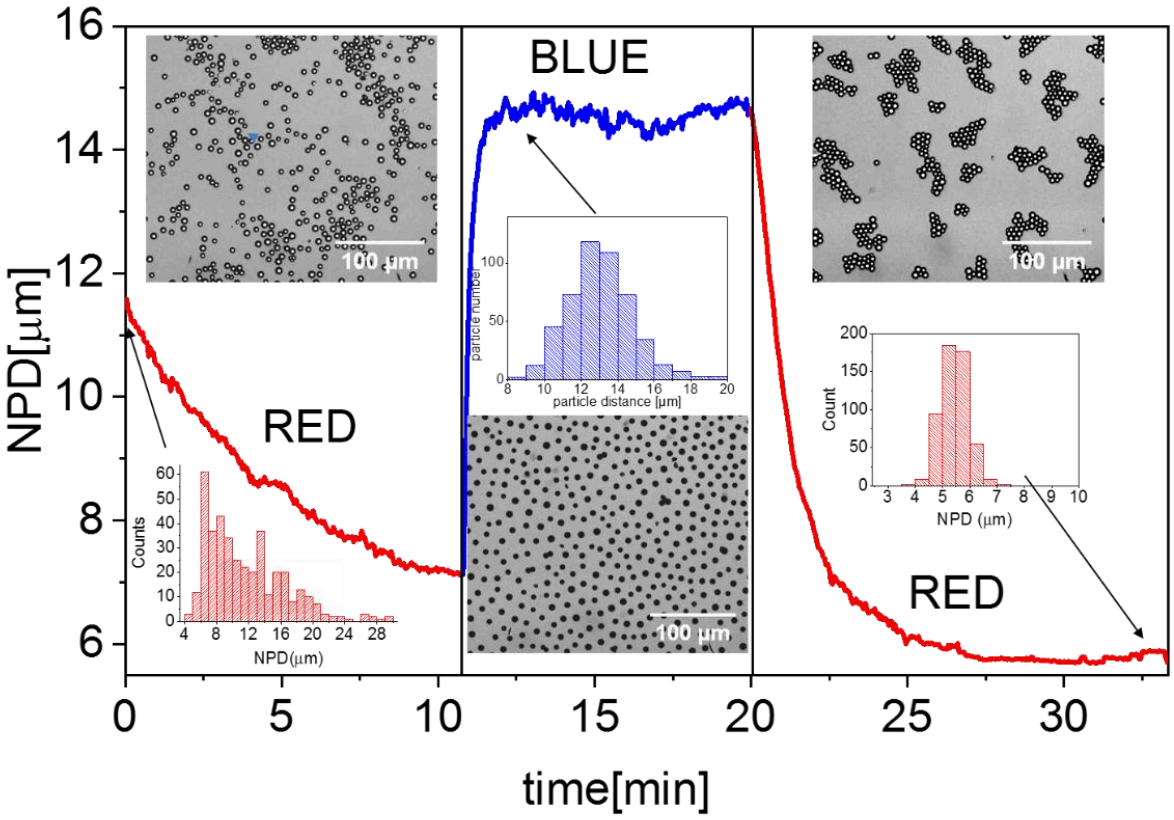

Figure 3.1. Average nearest particle distance of ensemble of porous silica particle in 1 mM Azo-C6. Without irradiation particles are randomly distributed (image at t = 0 min. When exposed to global blue light, immediate separation of particle occurs (optical micrograph at t = 12 min), NPD increases and becomes constant. At t= 20 min, blue light is switched off resulting in aggregation of particles (image at t = 37 min).

It is shown that the repulsion between the particles is long range. The extent of the flow is measured using binary mixture of porous and non-porous particles. Porous particles act as a source of l-LDDO flow (active particle) and non-porous particles move radially away with the flow (passive motion). In simple terms, porous particles act as a micro pump. It is demonstrated that the distance between particles at the time of equilibrium reduces with increase in particle density and the strength of repulsion also depends on different surfactant concentrations and their maxima at CMC (0.5 mM). The addition of an electrolyte decreases the flow strength which reduces velocity of separation process infect it has been witnessed that particle motion completely stops at salt (NaBr) concentration of 10 mM.

3.3. Publication 3. Light driven diffusioosmotic repulsion and attraction of colloidal particles[78]

In this article, we presented the effect of global UV light irradiation on collective behavior of mesoporous colloidal particles dispersed in azobenzene containing surfactant. Upon irradiation with UV light almost 90% of *trans* molecules isomerize to *cis* state (**Publication 1**). The more hydrophilic *cis* molecules are expelled out of the particles, this creates a concentration gradient of *cis* molecules around the particles, which results in local light driven diffusioosmotic flow. In contrast to irradiation with blue light, the l-LDDO flow lasts only for a short time, ca. 10 minutes. The reason for this is that within this period of time almost all *trans*- molecules are converted to *cis*-one, and, therefore, there is no supply of *trans*– isomers which can refill the particle pores. The process appears as following: when the UV light is switched on, the particles start to repel each other due to generation of l-LDDO flow, but with time, the flow stops and the particles start to move freely undergoing thermal motion. Now the particles are empty of surfactant and move within the surfactant solution in *cis*-state.

It is also found that the strength and the sign of the l-LDDO flow depend strongly on the intensity of irradiation and surfactant concentration. For lower intensities of UV light, the particles first aggregate to small clusters followed by strong mutual repulsion. During further irradiation, the flow strength decreases, and the particles start to move thermally (**Figure 3.2**). With an increase in intensity, the initial aggregation time decreases, and for intensities above 1.4 mW/cm^2 direct separation is observed when 1mM surfactant concentration is used. Similar behavior is observed for different surfactant concentrations. Increasing the concentration results in initial aggregation which is followed by separation and thermal motion. In contrast to UV light, blue light does not show such behavior and has direct dependence on the motion, i.e. upon increasing intensity the strength of flow increases which also corresponds to the particle velocity.

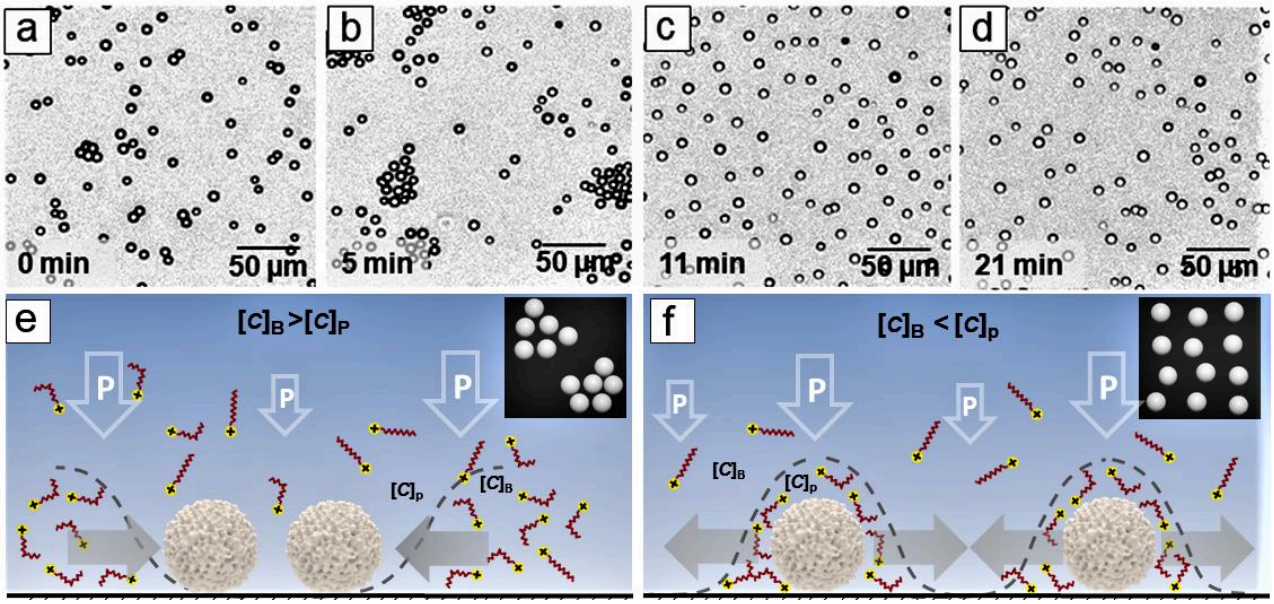

Figure 3.2. Motion of 5 µm porous silica particles in 1 mM Azo-C6 under global UV light irradiation. (a→d) Time scale optical micrographs of the process at t=0 min (showing random thermal motion), t= 5 min (aggregation phase), t= 11 min (separation phase), and t= 21 min (thermal aggregation). (e) Scheme of the process of aggregation. (f) Scheme of the separation process.

This phenomenon is attributed to local light driven diffusioosmotic flow where the direction of the flow depends on the concentration gradient of *cis*/*trans* molecules around the particles and in the bulk. This means that particles experience diffusioosmotic attraction, when *cis*-isomer concentration in bulk $[C]_B$ is larger than that nearer to particle $[C]_p$. DO repulsion sets on when the concentration nearer to the particle is larger. When exposed to lower intensity of UV light, it is stated that due to slow photo-isomerization within the particle, increase of *cis* isomer at the vicinity of particle is delayed causing inversion of *cis* gradient which reverses the flow direction of induced l-LDDO flow.

3.4. Publication 4: Light driven guided and self-organized motion of mesoporous colloidal particles[79]

In this article, we report on combination of passive and active motion of colloidal particles which is the outcome from simultaneous irradiation with global UV and focused blue light. The combination of global UV light and blue light induces continuous LDDO flow towards the blue laser. The phenomena are explained as described in **Section 2.3.2**. The generated LDDO flow passively moves

the MSPs into the blue zone. After reaching the blue irradiation spot (diameter > 70 µm) almost empty particles are now exposed to *trans* molecules, which immediately diffuses from bulk solution to the pores of the particles. At the beginning this results in the depletion of *trans* molecules around each particles and thus the small island of tight clusters are formed. With time, due to generation of local-LDDO flow, clusters start to fall apart and due to mutual repulsion, particles arrange into 2D well separated crystalline pattern in confinement due to laser spot (**Figure 3.3**). The separation distance is a function of particle density, size of the blue laser, intensity of light and surfactant concentration. For instance, in case of 0.5 mM surfactant concentration,there is no significant motion of particles towards the spot and particles which are already present inside the spot aggregates into small clusters and coarsen and then slowly separate with time. However, at a larger concentration of 1.5 mM, after entering to blue zone, direct separation is witnessed. It has been observed that the maximum velocity is achieved at the irradiation boundary. These dependencies on surfactant and particles concentrations, irradiation time, spot size, and intensity of irradiation is explained in detail in **Appendix B**.

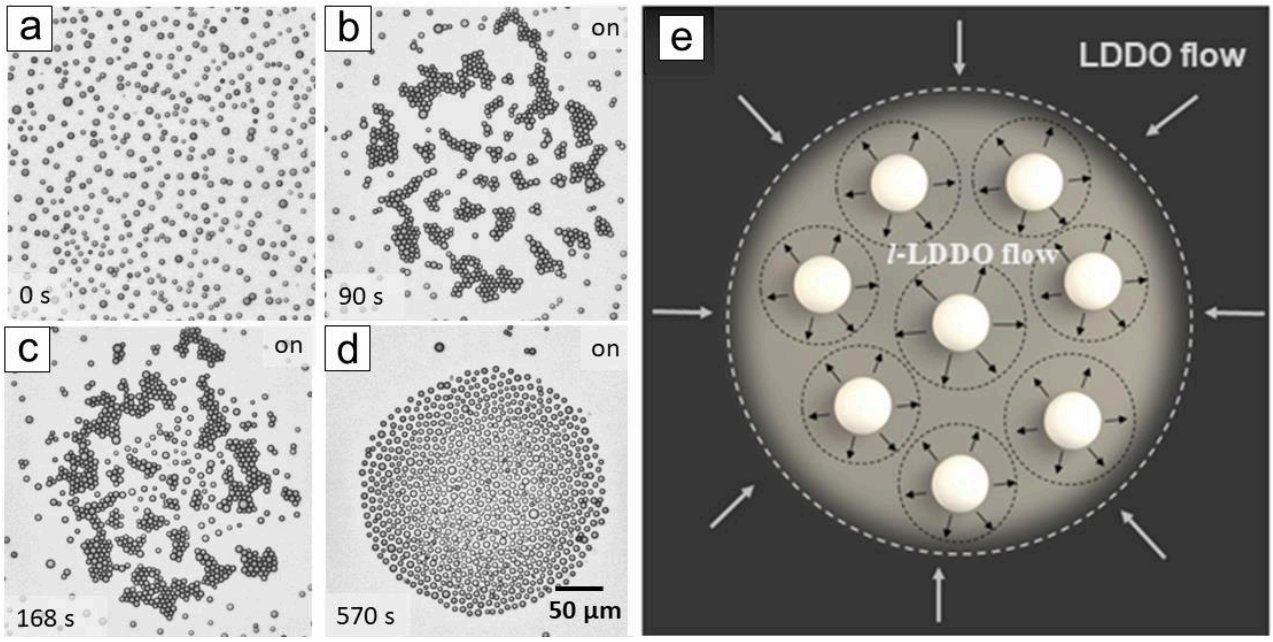

Figure 3.3. Effect of simultaneous irradiation of two wavelengths (focused blue and global UV light) on the collective motion of porous silica particle dispersed in 1 mM Azo-C6 at glass surface. (a-d) Optical micrographs of the process at different time scale; t= 0s (loosely separated particle), t = 90s (particles move towards the irradiated spot and aggregate), at t= 168 s (repulsion between particles started due to generation of local LDDO flow around each colloid), and at t=570s (complete separation: stable 2D pattern). Global UV irradiation is started 10 min before the focused blue laser is switched on. (e) Scheme of the process. White arrows show the direction of the flow induced by global LDDO. Black arrows around the particles represent the direction of local –LDDO flow.

One can say that the interplay between the two modes global and local LDDO flow leads to fascinating possibilities of dynamical organization and manipulation of colloidal ensembles adsorbed at solid–liquid interfaces. While the passive mode can be thought of to allow for a coarse structuring of a cloud of colloids, the inter-particle mode may be used to impose a fine structure on a 2D particle grid.

3.5. Publication 5. Light-driven motion of self-propelled porous Janus particles[80]

In this article, we discussed self-propelled motion of Janus colloids using the mechanism of l-LDDO. The l-LDDO flow is radially symmetric and points outside the particle. If half of the particle is covered by metal layer (gold), it breaks the symmetry of the local flow, leading to self-propelled motion. The random walk of prepared Janus particles is characterized by the mean square displacement (MSD) plots. When the logarithmic slope of MSD is greater than 1, the motion falls into the category of super-diffusion. In case of dimers, the motion depends on the orientation of gold cap. When the gold caps are opposite to each other, dimer rotates with respect to the intersection point of the particles. Whereas if both caps are on the same side of the particles, the dimer follows helical trajectories: a combination of rotational as well as translational displacements. It has been shown that using a substrate with microchannel, one can maintain the direction of motion over larger distances. The uniqueness of this process of self-propelled motion is that, the particle moves for indefinite time due to continuous l-LDDO flow (under irradiation with blue light) and stops only when blue light is switched off.

The above-discussed phenomenon of self-propulsion gives rise to more interesting possibilities. For instance, a porous particle can be used as a carrier for non-porous colloidal swimmers when pores of one side of particles are blocked by the cargo material itself (interesting results are shown in **Appendix C**).

4. Reprints

The Journal of Chemical Physics

Kinetics of photo-isomerization of azobenzene containing surfactants

Cite as: J. Chem. Phys. **152**, 024904 (2020); https://doi.org/10.1063/1.5135913
Submitted: 08 November 2019 . Accepted: 19 December 2019 . Published Online: 10 January 2020

Pooja Arya, Joachim Jelken, Nino Lomadze, Svetlana Santer, and Marek Bekir

AIP Publishing

The Journal of Chemical Physics ARTICLE scitation.org/journal/jcp

Kinetics of photo-isomerization of azobenzene containing surfactants

Cite as: J. Chem. Phys. 152, 024904 (2020); doi: 10.1063/1.5135913
Submitted: 8 November 2019 • Accepted: 19 December 2019 •
Published Online: 10 January 2020

Pooja Arya, Joachim Jelken, Nino Lomadze, Svetlana Santer,[a] and Marek Bekir

AFFILIATIONS

Institute of Physics and Astronomy, University of Potsdam, 14476 Potsdam, Germany

[a]Email: santer@uni-potsdam.de

ABSTRACT

We report on photoisomerization kinetics of azobenzene containing surfactants in aqueous solution. The surfactant molecule consists of a positively charged trimethylammonium bromide head group, a hydrophobic spacer connecting via 6 to 10 CH_2 groups to the azobenzene unit, and the hydrophobic tail of 1 and 3CH_2 groups. Under exposure to light, the azobenzene photoisomerizes from more stable *trans*- to metastable *cis*-state, which can be switched back either thermally in dark or by illumination with light of a longer wavelength. The surfactant isomerization is described by a kinetic model of a pseudo first order reaction approaching equilibrium, where the intensity controls the rate of isomerization until the equilibrated state. The rate constants of the *trans-cis* and *cis-trans* photoisomerization are calculated as a function of several parameters such as wavelength and intensity of light, the surfactant concentration, and the length of the hydrophobic tail. The thermal relaxation rate from *cis*- to *trans*-state is studied as well. The surfactant isomerization shows a different kinetic below and above the critical micellar concentration of the *trans* isomer due to steric hindrance within the densely packed micelle but does not depend on the spacer length.

I. INTRODUCTION

Photosensitive surfactants consisting of a charged head and a hydrophobic tail modified with an azobenzene group have attracted extensive experimental and theoretical attention in recent years.[1–6] The broad interest in these substances is stimulated by their intriguing phenomenology. For instance, azobenzene containing surfactants allow for rendering of any type of charged photosensitive object without the need for (irreversible) chemical conjugation to a photoresponsive substance. Thus, one can make polyelectrolytes[7–18] and microgels[19–22] photosensitive by preparing supramolecular complexes with azobenzene containing surfactants or change plasmonic properties of gold nanoparticles[23,24] in the presence of either *trans*- or *cis*-isomers of the surfactant. It is also possible to make polyelectrolyte brushes photoresponsive by loading them with oppositely charged photosensitive surfactants,[25–31] which allows for a structuring of the brush by optical stimuli. It was also reported that irradiation of a solution of photosensitive surfactants with focused light results in the generation of local diffusio-osmotic flow at solid/liquid interfaces, thereby moving and relocating particles trapped at the interface.[32,33] At the water/air or liquid/liquid interface, the illumination with light results in a Marangoni-type effect intensively utilized in light-driven photofluidics.[34–46] The key mechanism inherent to all of these rather diverse applications is the reversible photoisomerization process of azobenzene molecules from a stable *trans*- to a metastable *cis*-state under illumination with light of appropriate wavelength. The two isomers differ, e.g., in polarity, the *trans*-state being nonpolar (with a dipole moment of ~0 D provided that there are no exceptional ring substituents), while the *cis*-isomer is highly polar (a dipole moment of ~3 D). The presence of an azobenzene group in the hydrophobic tail of a surfactant molecule thus permits changing its hydrophobicity upon triggering photoisomerization. Hence, in applying simple optical stimuli, the solubility, critical micellar concentration (CMC), interfacial energy, and the strength of interactions of the surfactant with other substances can be toggled.[47–52]

Understanding the isomerization kinetics of photosensitive surfactants plays an important role when describing the dynamic response of conjugated soft objects upon illumination. The nature and extent of this response depend sensitively on the kinetics of photoswitching and the relative concentration of *trans*- and *cis*-isomers

at a photostationary state, light driven fluid flow, and changes in surface tension being two prominent examples.[53–55] Depending on the physicochemical system at hand, azobenzene photoisomerization within the surfactant molecule may have a multitude of other effects, fine-tuned by additional parameters such as intensity and wavelength of the irradiation applied, the surfactant concentration, and the hydrophobicity of the surfactant molecule as a whole.

In this work, we report on the photoisomerization kinetics of azobenzene containing surfactants in aqueous solution. The surfactant consists of a positively charged triamino bromide head group, a hydrophobic spacer of 4–10 CH_2 groups connecting to the azobenzene unit, and a hydrophobic tail of either 1 or 3 CH_2 groups. The surfactant isomerization is approximated by a kinetic model of a pseudo first order reaction describing the approach to equilibrium.

II. EXPERIMENTAL PART

A. Materials

Light responsive surfactant: The azobenzene containing trimethyl-ammonium bromide surfactants (C_{m+1}-Azo-OC_nTMAB) with m = 1 or 3 and n = 6, 8, and 10 are synthesized as described elsewhere [Fig. 1(a)].[56] A stock solution of the surfactant is adjusted to the concentration of 10 mM and diluted to the required concentrations ranging from 0.05 mM to 2 mM.

B. Methods

Time resolved UV-Vis measurements are performed with a commercial Cary 5000 UV-Vis-near-infrared (NIR) spectrophotometer instrument (Agilent Technologies, USA). A rectangle quartz cuvette (commercial cuvette from Helma Analytics, transparent in all directions), of either 1 cm in thickness for the surfactant concentration of up to 0.5 mM or of a thickness 0.1 cm for larger concentrations, is filled with 2 ml or 0.6 ml of aqueous solution and closed in order to keep the concentration constant. A light source of a different wavelength is placed perpendicular near the sample holder, with the illumination path faced toward the sample holder. The light-emitting diode (LED) lamp irradiates the total volume of the sample holder. The data are recorded for the set of different intensities for each fixed wavelength, i.e., λ = 365 nm, λ = 455 nm, λ = 490 nm, and λ = 530 nm. The intensity of light is directly measured at the sample position prior to each measurement with a commercial S170C power meter (Thorlabs). The light from the LED lamp is filtered by a commercial lowpass filter (10SWF-400-B, cutoff from 400 nm to higher, see Fig. S1) of the company Newport Corporation placed in between the sample holder and detector in the monitoring beam path.

Measurements are performed by a continuous acquiring of absorbance at λ = 376 nm (I = 0.02 mW/cm^2) until reaching the stationary state. To exclude the effect of the recording beam, the isomerization kinetics is measured over 30 min without the blue light irradiation [Fig. 2(a)].

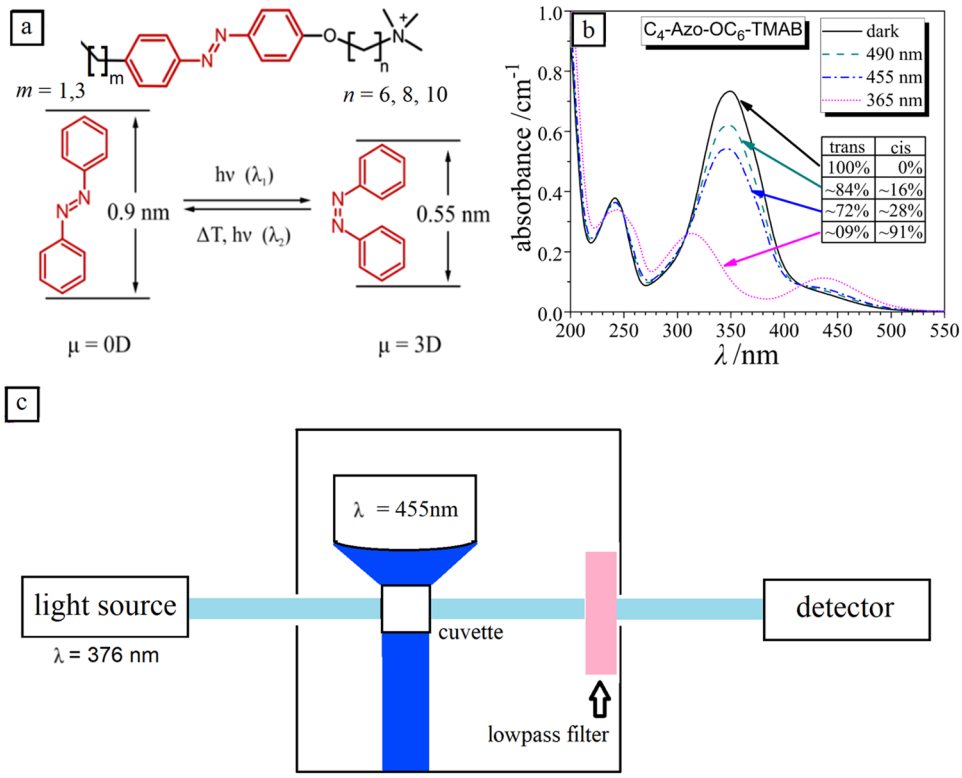

FIG. 1. (a) Chemical structure of the azobenzene containing cationic surfactant (C_{m+1}-azo-OC_nTMAB). Shown below is a scheme of azobenzene photoisomerization. (b) UV-Vis spectra of C_4-azo-OC_6TMAB in different photostationary states: dark (black line), after illumination with UV light of λ = 365 nm (magenta dotted line) and blue light of λ = 455 nm (blue dashed dotted line) and λ = 490 nm (turquoise dashed line) at 1 mM concentration. (c) Scheme of the setup: continuous monochromatic light (λ = 376 nm) passing through the quartz cuvette and is recorded at the detector as a function of time. Scheme shows an example for blue light with λ = 455 nm.

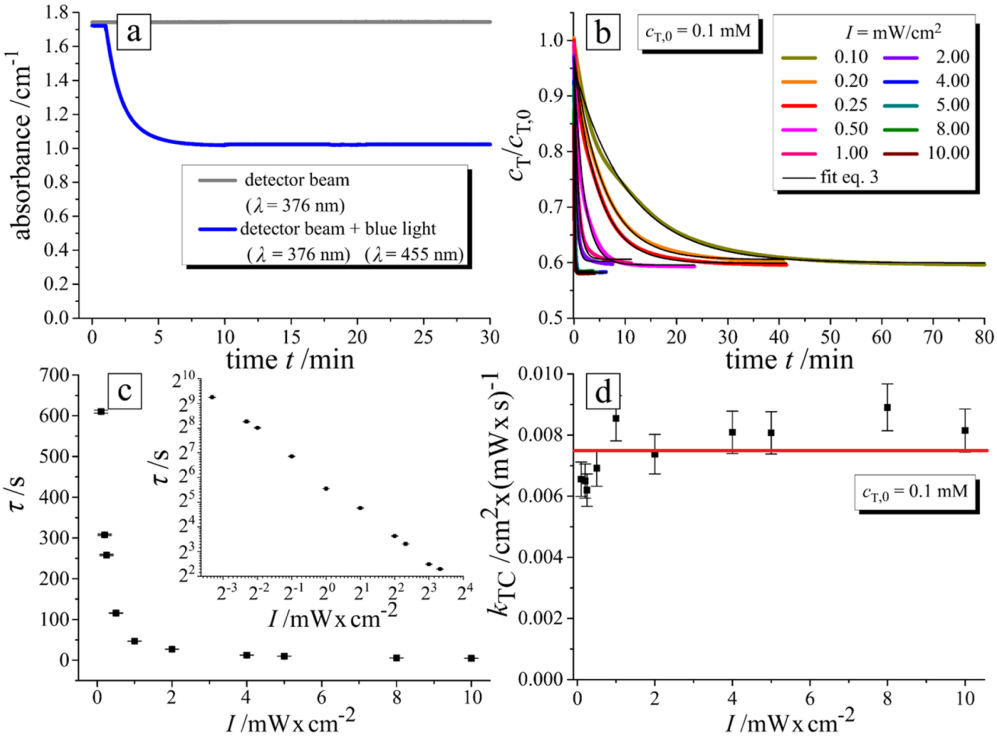

FIG. 2. (a) Representative plot of a change of the absorption coefficient of the *trans* isomer ($c_{T,0}$ = 0.1 mM) measured at 376 nm as a function of irradiation time. The blue curve depicts the values under irradiation with blue light (λ_B = 455 nm) acquired with a detector beam (λ = 376 nm). The gray line illustrates absorption of the surfactant aqueous solution without irradiation but exposed to the detector beam. (b) The change in the concentration of the *trans* isomer as a function of time for different irradiation intensities ranging from 0.1 mW/cm^2 to 10 mW/cm^2. (c) The decay time, τ, obtained by fitting the results from (b) using Eq. (7). With increasing light intensity, the decay time decreases exponentially as also illustrated by the log-log plot (see inset). (d) The isomerization constant [obtained using Eq. (8)] is plotted as a function of irradiation intensity. Red line illustrates the average value of k_{TC}. Surfactant spacer parameters are m = 3 and n = 6. All measurements are performed at T = 20 °C.

The concentration of the surfactant molecule is calculated from the initial value of transmission based on the knowledge of the adjusted concentration from a stock solution. At the initial time of irradiation with different light sources, we assume that the total surfactant concentration is equal to *trans* isomer concentration, $c_S = c_{T,0}$. The absorbance at 376 nm (exactly between the absorption peaks of the *cis*-form) of the dark state spectrum, where the absorption of the *cis*-isomer is assumed to be minimal, is used to estimate the amount of *trans* isomers in solution after the isomerization process,[62]

$$c_T(t) = \frac{\text{abs}}{\text{abs}_0} \cdot c_{T,0}, \tag{1}$$

where abs is the absorbance at 376 nm at any time and before irradiation, abs_0.

III. RESULTS AND DISCUSSION

Figure 1 shows the chemical structure and the UV-Vis absorption spectra of azobenzene containing surfactant. The *trans* isomer has a characteristic absorption band (π–π^* transition) with a maximum at 351 nm [Fig. 1(b)]. The spectrum of the *cis* isomer is characterized by two absorption bands with maxima at 313 nm (π–π^* transition) and 437 nm (n-π^* transition). The lifetime of the *cis* isomer in the dark or under illumination with a red light of λ = 600 nm is ~40 h at 20 °C, while the photoisomerization from *cis*- to *trans*-state under irradiation with blue light (λ = 455 nm) takes place at a much shorter time. The photostationary state with a fraction of *trans* and *cis* isomers of 72% and 28%, respectively [Fig. 1(b)], is reached after a certain time of irradiation being light intensity dependent. Under UV illumination (λ = 365 nm) at the photostationary state, the surfactant molecules are predominantly in *cis* state with a fraction of 91%.

A. Kinetic model and data interpretation

The kinetics of the photoisomerization is first studied under irradiation with blue light (λ = 455 nm) by time-resolved absorbance measurements with a monitoring light of 376 nm wavelength [Fig. 1(c)]. The monitoring beam results in photoisomerization of the surfactant; however, the intensity of the beam is several orders of magnitude lower (I = 0.02 mW/cm^2) than the used intensity in the range between 0.1 and 10 mW/cm^2. Thus, the isomerization kinetics with respect to the monitoring intensity may be neglected, as observed in Fig. 2(a).

As a first step, we shortly discuss the outcome for the expected time resolved experiments. We state that the probability of photoisomerization reaction correlates with reaction rate constants k_{TC} (*trans* → *cis*) and k_{CT} (*cis* → *trans*) described as a second order reaction,

$$trans \rightarrow cis: \quad \frac{dc_T}{dt} = -k_{TC} \cdot I \cdot c_T, \tag{2}$$

where the term on the left describes the time dependent change in the *trans*–isomer concentration under irradiation with light intensity I, c_T is the concentration of *trans* isomers, and k_{TC} is the photoisomerization rate constant from *trans* to *cis*-state.

The reverse photoisomerization from *cis* to *trans*-state is described in the same way,

$$cis \rightarrow trans: \quad \frac{dc_T}{dt} = k_{CT} \cdot I \cdot c_C, \tag{3}$$

and the thermal relaxation,

$$cis \rightarrow trans: \quad \frac{dc_T}{dt} = k_T \cdot c_C. \tag{4}$$

The concentration of *trans* isomers is reduced by the forward reaction, but it is increased by all reverse reactions. Thus, the isomerization rate is described as[57]

$$\frac{dc_T}{dt} = -\frac{dc_C}{dt} = -k_{TC} \cdot I \cdot c_T + (k_{CT} \cdot I + k_T) \cdot c_C. \tag{5}$$

Since in our experiments the intensity of light, I, is constant over irradiation, the photoisomerization reactions can be considered as a pseudo first order reaction. Furthermore, the thermal relaxation is very slow with the rate constant of $k_T = 6.99 \cdot 10^{-6}$ s^{-1} and can be neglected in Eq. (5). Then, we approximate the reaction approaching equilibrium by the kinetics of pseudo first order with respect to forward and reverse photoisomerization reactions. The concentration of *trans* isomers, c_T, at any time t is[53,57]

$$c_T = \frac{k_{CT} + k_{TC} \cdot \exp(-[k_{TC} + k_{CT}] \cdot I \cdot t)}{k_{CT} + k_{TC}} \cdot c_{T,0}, \tag{6}$$

where $c_{T,0}$ is the initial concentration, which is equal to the surfactant concentration, $c_{T,0} = c_S$. The derivation of Eq. (6) from Eq. (5) is provided in Sec. 1 of the supplementary material.

Exposing the surfactant solution to light leads to the concentration fraction of *trans* and *cis* isomers in equilibrium, where both rates are equal, i.e., $dc_T/dt = -dc_C/dt$, and results in a rate constant ratio X between k_{TC} and k_{CT}, $X \cdot k_{TC} = k_{CT}$. Then, Eq. (6) can be transformed into (for details, see Secs. 2 and 3 of the supplementary material)

$$c_T = c_{T,eq} \cdot \left(1 - \exp\left(-\frac{t}{\tau}\right)\right) + c_{T,0} \cdot \exp\left(-\frac{t}{\tau}\right), \tag{7}$$

with characteristic time τ,

$$\tau = \frac{1}{(1+X) \cdot k_{TC} \cdot I}, \text{ with } X = \frac{c_{T,eq}}{c_{T,0}} \Big/ \left(1 - \frac{c_{T,eq}}{c_{T,0}}\right) \text{ or } \frac{1}{X} = K_{eq}, \tag{8}$$

where $c_{T,0}$ and $c_{T,eq}$ are the concentrations of *trans* isomers in the initial and at a photostationary state, respectively. For example, at the photostationary state for blue light (λ = 455 nm) and for surfactant concentrations below CMC_{trans}, the concentration fraction of *trans* and *cis* isomers is 0.6:0.4; thus, X = 1.5. From the time resolved change of the absorption coefficient of the *trans* isomer at 376 nm, we calculate the change in concentration, c_T, as a function of irradiation time [Fig. 2(b)]. Fitting the data using Eqs. (7) and (8), the decay time τ [Fig. 2(c)] and the rate constant k_{TC} [Fig. 2(d)] are calculated for different irradiation intensities. Figure 2 depicts the results obtained for the surfactant with n = 6 CH_2 groups in the spacer and $c_{T,0}$ = 0.1 mM.

From Fig. 2(c), one can see that the decay time of *trans* to *cis* isomerization decreases exponentially with increasing intensity. The photoisomerization constant, k_{TC}, could be considered not to depend on the intensity [Fig. 2(d)] with an average value of k_{TC} (λ = 455 nm) = (7.53 ± 0.90) · 10^{-3} cm^2/mW s. With known k_{TC}, we calculate k_{CT} (λ =455 nm) = 1.50 ± 0.53 × 10^{-2} cm^2/mW s.

B. Effect of surfactant concentration

Here, we investigate how the photoisomerization rate and the decay time, τ, vary with surfactant concentration with other parameters fixed, i.e., T = 20 °C, I = 7.5 mW/cm^2, and λ = 455 nm (Fig. 3). One can see that τ does not depend on surfactant concentration below the CMC, while above the CMC, it increases with concentration [Fig. 3(b)].

Calculating k_{TC} using Eqs. (7) and (8) [black squares, Fig. 3(d)], we have found that below the critical micellar concentration (CMC), k_{TC} is constant, but decreases with increasing concentration above the CMC. The rate constants for *cis-trans* isomerization, k_{CT}, remain constant at any concentration [red circles in Fig. 3(d)]. The same tendency is found under irradiation with UV light (λ = 365 nm, see Fig. S2). This could be explained by a steric hindrance of the molecules confined in micelles and different effective dielectric constants around the surfactant in the solvent and the micelle (Scheme 1(a)).[58] To calculate the rate constant of the *trans* isomer in the micelles, $k_{TC,M}$, we suggest that above the critical micelle concentration, the k_{TC} is a fractional mean value of single molecules $k_{TC,S}$ and molecules aggregated in micelles, $k_{TC,M}$,

$$k_{TC} = \frac{c_{CMC}}{c_T} \cdot k_{TC,S} + \frac{c_T - c_{CMC}}{c_T} \cdot k_{TC,M}, \tag{9}$$

where the value $k_{TC,S}$=(8.49 ± 0.17) · 10^{-3} cm^2/(mW s) is obtained from measurements below the CMC. More details related to Eq. (9) are provided in Sec. 3.1 of the supplementary material. The calculated values of $k_{TC,M}$ are plotted as a function of surfactant concentration in Fig. 3(d) (green triangles). One can see that the isomerization rate is approximately 80% slower in micelles compared to single molecules.

C. Effect of different wavelengths

Here, we investigate how the photoisomerization rate depends on different irradiation wavelengths, λ = 365 nm, 455 nm, 490 nm, and 530 nm (Fig. 4). The surfactant concentration is fixed to $c_{T,0}$ = 0.1 mM, and irradiation intensity is kept constant at 1 mW/cm^2 for all wavelengths. The fraction of *trans* and *cis* isomers at a photostationary state differs for each wavelength with

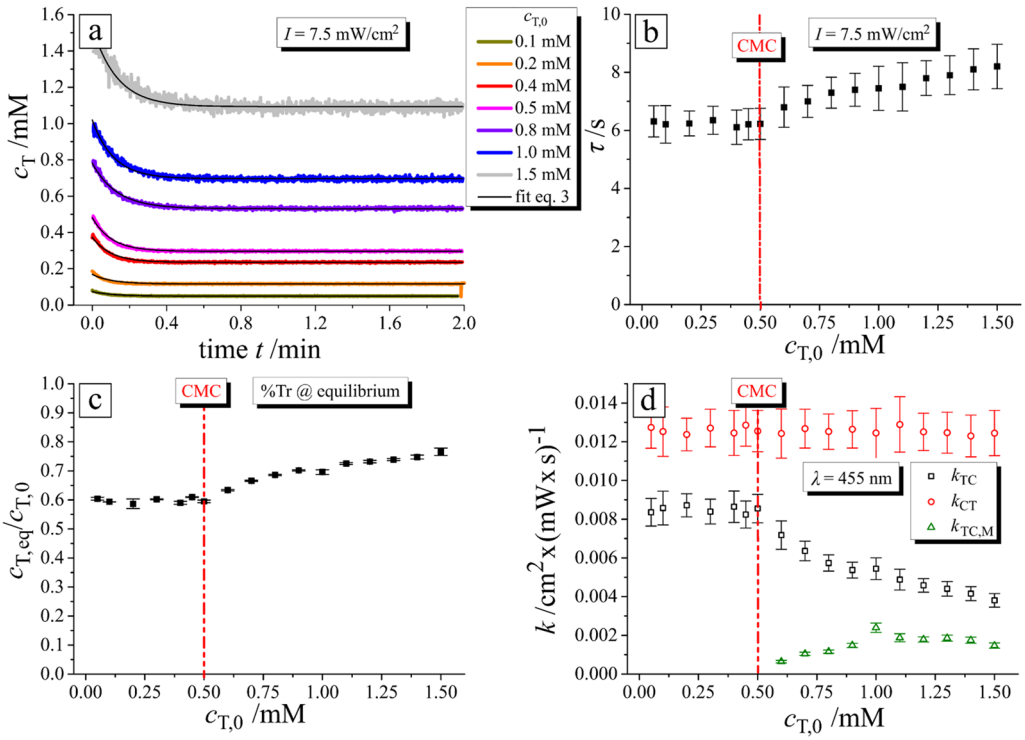

FIG. 3. (a) Dependence of *trans*-isomer concentration, c_T, on irradiation time (λ = 455 nm and I = 7.5 mW/cm^2) for different initial surfactant concentrations, $c_{T,0}$. (b) Dependence of the decay time, τ, on a surfactant concentration. Red dashed line indicates the CMC of the *trans* isomer, c_{CMC} = 0.5 mM. (c) The concentration fraction of c_T isomers at a photostationary state as a function of surfactant concentration. (d) Dependence of the rate constants on surfactant concentration for forward reaction k_{TC} (black squares), reverse reaction k_{CT} (red circles), and forward reaction of molecules in micelle $k_{TC,M}$ (green triangles).

a large value of *trans*-isomers at a longer wavelength [Fig. 4(a)]. The photoisomerization time, τ, to reach a photostationary state increases with the wavelength as well from ~1 s at λ = 365 nm to ~15 s at λ = 530 nm [Fig. 4(b)]. The photoisomerization rate

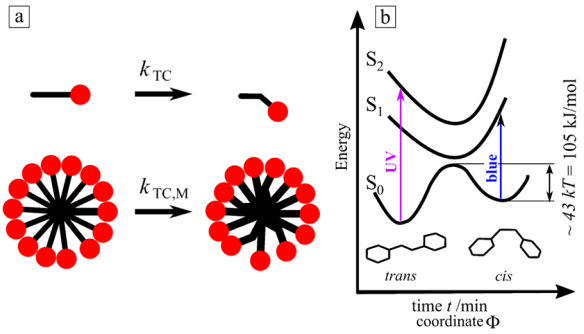

SCHEME 1. (a) Cartoon of *trans* to *cis* photoisomerization for a single molecule and those in a micelle. (b) Schematic view of the lowest potential energy surfaces of azobenzene, namely, S_0 and S_1 and the ground-state barrier for the back *cis* to *trans* isomerization. The *trans* and *cis* isomers are shown with excitations for photoisomerizations under UV light of the *trans* isomer and blue light of the *cis* isomer.[59].

constants, k_{TC} and k_{CT} [Fig. 4(c)], as well as their ratio $K_{eq} = k_{TC}/k_{CT}$ [Fig. 4(d)], decrease from UV to green light. At λ = 365 nm, k_{TC} is larger compared to k_{CT}, while at larger wavelengths, it is reversed. Under irradiation with UV light, the k_{TC} is 25 times faster than k_{CT}, implying large value of K_{eq}. Thus, under UV light (λ = 365 nm) at a photostationary state, the fraction of *cis* isomers is ~96.3% with negligible *cis-trans* back photoisomerization. The reduction of k_{TC} with increasing wavelength is related to a probability of photoexcitation. The *trans* isomer corresponds to the lower energy minimum on the ground state potential energy surface in comparison to the *cis*-isomer [Scheme 1(b)]. Since larger energy is needed to excite the *trans*- compared to the *cis*-isomer, the photoisomerization *trans-cis* is more probable at the wavelength close to 353 nm (main adsorption).[60,61]

The isomerization of the surfactant is reversible, where the switch from UV to blue and vice versa adjusts to the new equilibrium with respect to the wavelength of k_{TC}/k_{CT} (Fig. 5). The photostationary state is reached after ~4 min in both cases of UV and blue irradiation.

D. Effect of combined wavelengths

As discussed earlier, depending on the illumination wavelength, one gets different fractions of *trans* and *cis* isomers at a

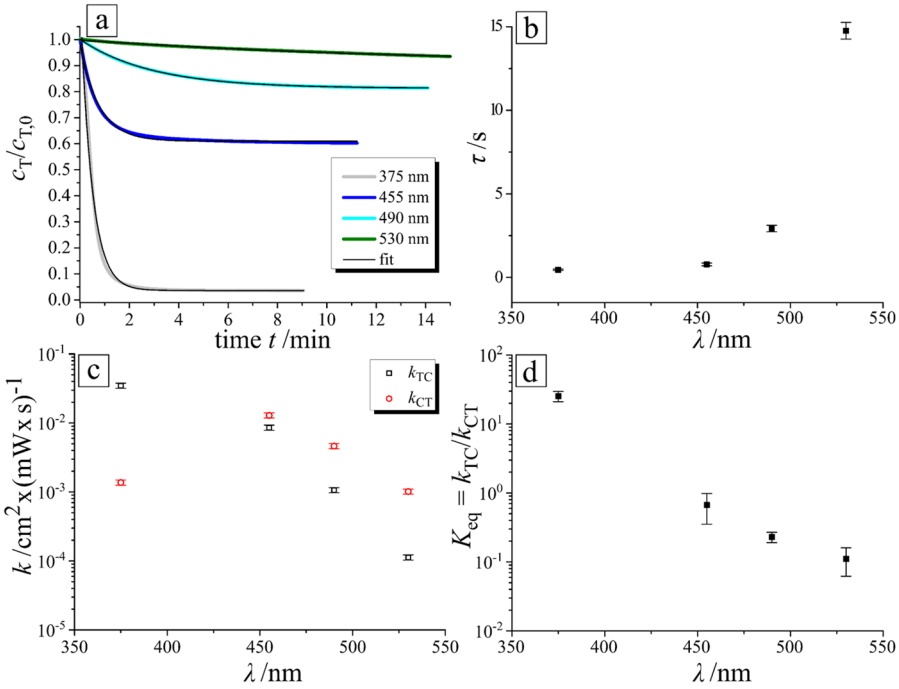

FIG. 4. (a) The change of c_T as a function of irradiation time at different wavelengths λ = 365 nm (gray curve), 455 nm (blue curve), 490 nm (azure curve), and 530 nm (green curve). The initial surfactant concentration, $c_{T,0}$ = 0.1 mM, is kept constant for all measurements. (b) The decay time, τ, as a function of irradiation wavelength. (c) Rate constants of photoisomerization: forward, k_{TC}, (black squares) and reverse photoisomerization, k_{CT}, (red circles) and (d) their ratio $K_{eq} = k_{TC}/k_{CT}$ as a function of irradiation wavelength.

photostationary state. In order to have a mean for an accurate control over the equilibrium fractions of isomers, we apply a combination of two wavelengths. Here, the equilibrium isomer fraction (at a photostationary state) is expressed as follows:

$$c_{T,eq} = c_{T,0} \cdot \frac{k_{CT_1} + k_{CT_2} \cdot R}{(k_{CT_1} + k_{TC1}) + (k_{CT_2} + k_{TC_2}) \cdot R}, \qquad (10)$$

where $k_{TC,1}$ and $k_{TC,2}$ are the forward rate constants, $k_{CT,1}$ and $k_{CT,2}$ are the reverse rate constants of the first and the second wavelengths, and R is the ratio between the intensity of both wavelengths,

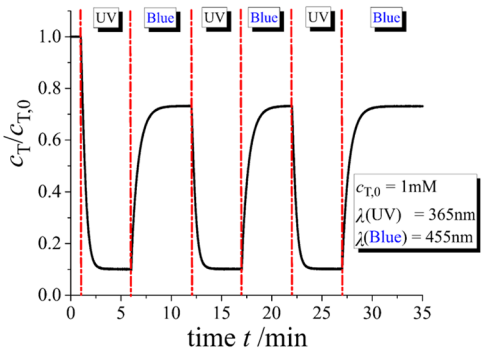

FIG. 5. Concentration of *trans*-isomers normalized over initial concentration as a function of irradiation wavelength. Red dashed-dotted lines indicate the change of the wavelength between UV (λ = 365 nm) and blue (λ = 455 nm) light. Intensity is set to 1.25 mW/cm^2.

$R = I_2/I_1$. Equation (10) is derived from Eq. S6 as described in detail in Sec. 4 (supplementary material). Applying Eq. (10) and utilizing values for the rate constants presented in Fig. 4, we estimate the variation of the concentration fraction of *trans*- and *cis*-isomers as a function of irradiation with combined wavelengths [Fig. 6(a)]. First, the surfactant solution ($c_{T,0}$ = 0.1 mM) is exposed to illumination with UV light (I = 1 mW/cm^2) for 5 min to get a photostationary state (96.3% of *cis*-isomers), followed by switching on the blue light (λ =455 nm) [Fig. 6(a)]. Different intensities of the blue light, i.e., 0.25 mW/cm^2, 1 mW/cm^2, 2 mW/cm^2, and 3 mW/cm^2, are used to measure the fraction of isomers at the equilibrated state after 10 min of irradiation [Fig. 6(a)]. Figure 6(b) (see also Fig. S4 of the supplementary material) depicts the comparison of experimentally and theoretically calculated values [using Eq. (10)] of the equilibrated isomer fractions for three combinations of different wavelengths: 455 nm/365 nm [blue color, values from Fig. 6(a)], 490 nm/365 nm (azure color, values from Fig. S3b), and 530 nm/365 nm (green color, values from Fig. S3c). As one can see from Fig. 6(b), the calculated and measured values are in good agreement, with a deviation of ~10% for $c_{T,0}$ = 0.1 mM and 16% for $c_{T,0}$ = 1 mM. The results for the surfactant concentration 1 mM are presented in Figs. 6(c) and 6(d). Figure 6(d) shows as well the kinetic of the change of the *trans* and *cis* isomers fraction when UV and blue light are applied to a surfactant in a *trans* state, i.e., without preirradiation with UV light. The values of the equilibrium ratio of *trans* and *cis* isomers are the same for both procedures of irradiation, i.e., first, UV is switched on followed by additional blue light irradiation [Fig. 6(c)] and immediate irradiation with UV and blue light [Fig. 6(d)]. The larger deviation between theoretical and experimental values for a concentration of 1 mM is explained by the

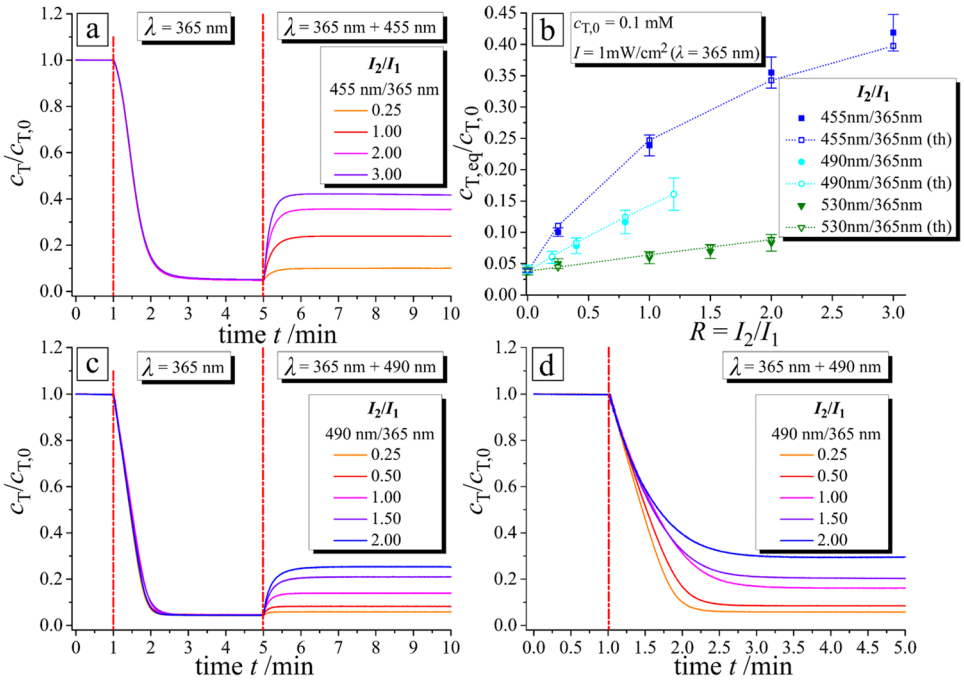

FIG. 6. Irradiation with two combined wavelengths. (a) Concentration of *trans* isomers as a function of irradiation time. The sample is first exposed to UV light (I_1 = 1 mW/cm^2) for 5 min followed by switching on the blue light (λ = 455 nm). The intensity of the blue light (second wavelength) is varied to get different ratios $R = I_2/I_1$ as indicated in the plot. (b) $c_{T,eq}/c_{T,0}$ as a function of R for different combinations of the wavelength: 455 nm/365 nm (blue color), 490 nm/365 nm (azure color), and 530 nm/365 nm (green color). Theoretical values obtained using Eq. (10) are shown as open symbols, while the experimental results are shown with filled symbols. Surfactant concentration is 0.1 mM, and temperature is set to 20 °C. (c) and (d) *Trans* concentration as a function of the time with illumination of the sample with two light sources UV (λ_1 = 365 nm) and blue (λ_2 = 490 nm). (c) First, UV is switched on at minute 1 and then blue light at minute 5. (d) The irradiation with UV and blue light starts when most of the surfactant is in *trans*-state.

fact that the rate constants for different wavelengths are taken for concentrations below the CMC, resulting in underestimation of the k_{TC} as explained in Fig. 3(d) for λ = 455 nm.

E. Effect of spacer length

In Sec. III B, we report on decrease in the isomerization rate with increasing surfactant concentration above the CMC. We suggest that due to the steric hindrance, the isomerization rate of the molecule located in a micelle is smaller than that in a solution. Here, we study the effect of the hydrophobicity of the surfactant tail with respect to isomerization kinetics. Four surfactants are investigated with the ethyl tail with 4 CH_2 spacers and butyl tail with nCH_2 spacers, n = 6, 8, 10 [Fig. 1(a)]. The increase in the spacer length connecting the charged head group and the azobenzene as well as in the tail length results in a shift of the CMC toward smaller concentration.[62] The CMC of the studied surfactant is 4 mM (m = 1 and n = 4), 0.5 mM (m = 3 and n = 6), 0.17 mM (m = 3 and n = 8), and 0.06 mM (m = 3 and n = 10).[1] According to these data, we choose the concentration of 0.05 mM for all surfactants in order to avoid the influence of the hindered photoisomerization in micelles. As one can see from Fig. 7, there is no dependence of the isomerization kinetics on the spacer length below the CMC, i.e., the reaction constants for the forward, k_{TC}, and reverse reaction, k_{CT}, have similar values.

F. Thermal relaxation of *cis* isomer

The rate law of thermal relaxation is, per definition, a first order reaction and leads to the simple exponential decay for the *cis* concentration,

$$c_C = c_{C,0} \cdot \exp(-k_T \cdot t), \text{ and } k_T = \frac{1}{\tau}, \tag{11}$$

where k_T is the rate constant of thermal relaxation and τ is the decay time. The decay time τ and the corresponding k_T are measured for a total temperature range from 20 to 60 °C [Fig. 8(a)] and yield an activation energy of 79 kJ/mol for thermal relaxation, which is in good agreement with the reported value in the literature.[59] The decay time τ for a temperature of 20 °C has a value of ~40 h and correspond to ~ $k_T = 6.99 \cdot 10^{-6}$ s^{-1}.

The true rate law of photoisomerization must include the thermal relaxation, where the forward photoisomerization reaction is

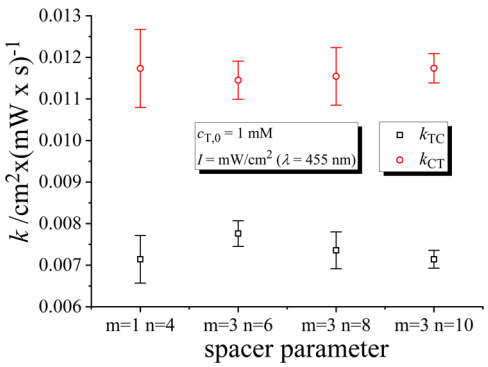

FIG. 7. Photoisomerization rate constants for the forward reaction, k_{TC}, (black squares) and back reaction, k_{CT}, (red circles) as a function of the spacer parameter. The surfactant concentration is 0.05 mM in all measurements.

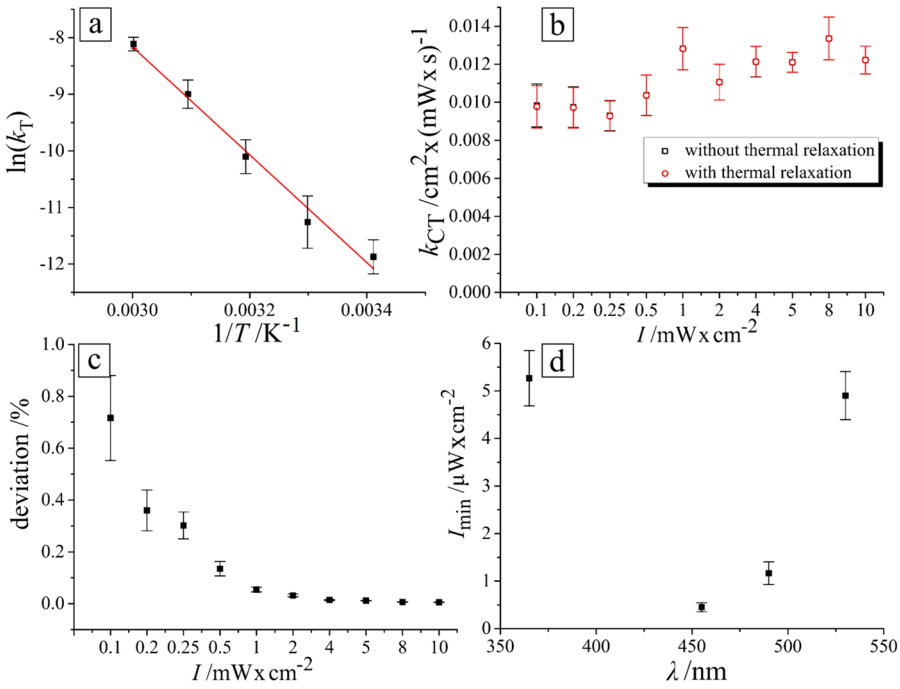

FIG. 8. (a) Arrhenius plot of thermal relaxation of $n = 6$ for a temperature range from 20 to 60 °C. (b) k_{CT} as a function of light intensity calculated without including thermal isomerization [black squares, Eq. (8)] and with additional thermal *cis-trans* isomerization [red circles, Eq. (13)] at a surfactant concentration of 0.1 mM, a temperature of 20 °C, and different irradiation intensities ranging from 0.1 mW/cm^2 to 10 mW/cm^2. (c) Deviation of the data presented in (b) as a function of light intensity. (d) Minimal light intensity where thermal relaxation is comparable to *cis-trans* photoisomerization.

equalized by the reverse photoisomerization and thermal relaxation, and after integration, the *trans* concentration is calculated as

$$c_T = c_{T,0} \cdot \frac{k_{CT} \cdot I + k_T + k_{TC} \cdot I \cdot \exp(-([k_{TC} + k_{CT}] \cdot I + k_T) \cdot t)}{(k_{CT} + k_{TC}) \cdot I + k_T}. \tag{12}$$

The derivation of Eq. (12) from Eq. (5) is provided in Sec. 6 of the supplementary material. To include the contribution of thermal relaxation to back isomerization, i.e., *cis* to *trans* conversion, we write

$$k_{TC} \cdot X - \frac{k_T}{I} = k_{CT}, \tag{13}$$

where $k_{TC} \cdot X$ is reduced by the ratio of thermal relaxation and the light intensity, k_T/I. Note that the rate constants of photoisomerization [units = cm^2/(mW s)] result from a formal second relation with respect to the forward and reverse isomerization and that of the thermal relaxation of a first order reaction (units = 1/s). To equalize their units, k_T is divided by the light intensity. To compare values for k_{CT} describing only the photoisomerization with values of photoisomerization plus thermal relaxation calculated using Eqs. (7) and (8) [Fig. 8(a)], we use Eqs. (7) and (13) (see Sec. 6 of the supplementary material) with $X = 1.5$ corresponding to the equilibrium for $\lambda = 455$ nm [Fig. 2(c)]. Both values for k_{CT} differ slightly, where those including thermal relaxation are, in generally, smaller due to the sum of the thermal relaxation and photoinduced *cis* to *trans* isomerization, $k_{CT} \cdot I + k_T$. The difference is small because thermal relaxation is much slower compared to the photoisomerization but becomes more pronounced with decreasing light intensity [Figs. 8(b) and 8(c)]. At critical light intensity (calculations are presented in Sec. 7 of the supplementary material), the reverse photoisomerization reaction becomes equal probable to thermal relaxation and is, for the different wavelengths, in the range of μW/cm^2 [Fig. 8(d)].

IV. CONCLUSIONS

We report on isomerization kinetics of light responsive azobenzene containing surfactants as a function of surfactant concentration, irradiation intensity, wavelength, and surfactant hydrophobicity. Moreover, we have studied how the combination of different wavelengths influences the photoisomerization kinetics and concentration fraction of *trans* and *cis*-isomers at a photostationary state. The photoisomerization has been studied by the time resolved UV-Vis spectroscopy, where the irradiation of the samples with different wavelengths and intensities is introduced *in situ* during simultaneous recording of the absorbance. We have demonstrated that photoisomerization of the surfactant can be described by a kinetics model of pseudo first order reactions approaching equilibrium. Our experiments show that the *trans-cis* photoisomerization kinetics strongly depends on the light intensity, where an increase in the intensity decreases the isomerization time (the decay time, τ), while the concentration fraction of the *trans* and *cis*-isomers at equilibrium is not altered. Depending on the surfactant concentration, we recognize two regimes: below the CMC, where the isomerization kinetic is independent of the surfactant concentration, and above the critical micelle concentration, where the isomerization kinetics decreases with increasing concentration. The latter, with an ~80% slower rate constant of *trans-cis*

photoisomerization compared to the free molecule, is explained by steric hindrance of the surfactant in the micelle. Thus, the concentration fraction of the *trans* and *cis* isomers at the photostationary state increases with concentration above the CMC.

Additionally, the fraction of *trans* and *cis* isomers at a photostationary state strongly depends on the wavelength of applied irradiation with the shift toward the higher *cis* fraction at a smaller wavelength. Furthermore, the concentration fraction of the isomers can be controlled by a simultaneous illumination with two different wavelengths of different intensities. In contrast, the increase in the hydrophobicity of the surfactant by adding more methyl groups either in the spacer between the azobenzene and the charged head group or in the tail shows a minor influence on the photoisomerization kinetics. We have also shown that the thermal *cis-trans* isomerization is quite slow and can be neglected as long as the light intensity is above a critical value.

SUPPLEMENTARY MATERIAL

See the supplementary material for all derivations of equations, kinetics of isomerization for different concentrations above the CMC for UV light, *trans* concentration as function of time for the combination of different wavelengths, and time concentration of trans as a function of time for different spacer lengths and adsorption spectra.

ACKNOWLEDGMENTS

This research was supported by the Priority Program 1726 "Microswimmers-From Single Particle Motion to Collective Behaviour," Germany; DFG (Grant No. SA1657/8-1); and the International Max Planck Research School (IMPRS) on Multiscale Bio-Systems, Potsdam, Germany.

The authors declare no competing financial interests.

REFERENCES

[1] S. Santer, J. Phys. D: Appl. Phys. **51**, 013002 (2017).
[2] J. Eastoe and A. Vesperinas, Soft Matter **1**, 338 (2005).
[3] P. Brown, C. P. Butts, and J. Eastoe, Soft Matter **9**, 2365 (2013).
[4] M. Sollogoub, S. Guieu, M. Geoffroy, A. Yamada, A. Estévez-Torres, K. Yoshikawa, and D. Baigl, ChemBioChem **9**, 1201 (2008).
[5] A. A. Zinchenko, M. Tanahashi, and S. Murata, ChemBioChem **13**, 105 (2012).
[6] S. Rudiuk, K. Yoshikawa, and D. Baigl, Soft Matter **7**, 5854 (2011).
[7] Y. Zakrevskyy, P. Cywinski, M. Cywinska, J. Paasche, N. Lomadze, O. Reich, H.-G. Löhmannsröben, and S. Santer, J. Chem. Phys. **140**, 044907 (2014).
[8] S. Schimka, S. Santer, N. M. Mujkic-Ninnemann, D. Bleger, L. Hartmann, M. Wehle, R. Lipowsky, and M. Santer, Biomacromolecules **17**, 1959–1968 (2016).
[9] A. Zinchenko, Adv. Colloid Interface Sci. **232**, 70 (2016).
[10] A.-L. M. Le Ny and C. Lee, J. Am. Chem. Soc. **128**, 6400 (2006).
[11] A.-L. Le Ny and C. Lee, Biophys. Chem. **142**, 76 (2009).
[12] M. Geoffroy, D. Faure, R. Oda, D. Bassani, and D. Baigl, ChemBioChem **9**, 2382 (2008).
[13] A. Diguet, N. K. Mani, M. Geoffroy, M. Sollogoub, and D. Baigl, Chem. Eur. J. **16**, 11890 (2010).
[14] M. Deiana, Z. Pokladek, K. Matczyszyn, P. Mlynarz, M. Bucklec, and M. Samoca, J. Mater. Chem. B **5**, 1028 (2017).
[15] M. Deiana, Z. Pokladek, J. Olesiak-Banska, P. Mlynarz, M. Samoc, and K. Matczyszyn, Sci. Rep. **6**, 28605 (2016).
[16] Y. Li, J. Gao, C. Zhang, Z. Cao, D. Cheng, J. Liu, and X. Shuai, Top. Curr. Chem. Z **375**, 27 (2017).
[17] S. Yadava, S. R. Dekaa, D. Jhab, H. K. Gautam, and A. K. Sharma, Colloids Surf. B **148**, 481 (2016).
[18] A. S. Lubbe, W. Szymanski, and B. L. Feringa, Chem. Soc. Rev. **46**, 1052 (2017).
[19] S. Schimka, N. Lomadze, M. Rabe, A. Kopyshev, M. Lehmann, R. von Klitzing, A. M. Rumyantsev, E. Y. Kramarenko, and S. Santer, Phys. Chem. Chem. Phys. **19**, 108 (2017).
[20] A. M. Rumyantsev, S. Santer, and E. Y. Kramarenko, Macromolecules **47**, 5388–5399 (2014).
[21] Y. Zakrevskyy, M. Richter, S. Zakrevska, N. Lomadze, R. von Klitzing, and S. Santer, Adv. Funct. Mater. **22**, 5000 (2012).
[22] S. Schimka, Y. D. Gordievskaya, N. Lomadze, M. Lehmann, R. von Klitzing, A. M. Rumyantsev, E. Kramarenko, and S. Santer, J. Chem. Phys. **147**, 031101 (2017).
[23] T. Bian, Z. Chu, and R. Klajn, Adv. Mater. **31**, 1905866 (2019).
[24] L. Lysyakova, N. Lomadze, D. Neher, K. Maximova, A. V. Kabashin, and S. Santer, J. Phys. Chem. C **119**, 3762 (2015).
[25] H. Kollarigowda, C. Fedele, C. Rianna, A. Calabuig, A. C. Manikas, V. Pagliarulo, P. Ferraro, S. Cavalli, and P. A. Netti, Polym. Chem. **8**, 3271 (2017).
[26] S. Minko, J. Macromol. Sci., Part C: Polym. Rev. **46**, 397 (2006).
[27] A. Kopyshev, K. Kanevche, N. Lomadze, E. Pfitzner, S. Loebner, R. R. Patil, J. Genzer, J. Heberle, and S. Santer, ACS Appl. Polym. Mater. **1**, 3017 (2019).
[28] A. Kopyshev, N. Lomadze, D. Feldmann, J. Genzer, and S. Santer, Polymer **79**, 65 (2015).
[29] A. Kopyshev, C. J. R. R. Galvin, R. R. Patil, J. Genzer, N. Lomadze, D. Feldmann, J. Zakrevski, and S. Santer, ACS Appl. Mater. Interfaces **8**, 19175 (2016).
[30] A. Kopyshev, C. J. Galvin, J. Genzer, N. Lomadze, and S. Santer, Polymer **98**, 421 (2016).
[31] N. Lomadze, A. Kopyshev, M. Bargheer, M. Wollgarten, and S. Santer, Sci. Rep. **7**, 8506 (2017).
[32] D. Feldmann, S. R. Maduar, M. Santer, N. Lomadze, O. I. Vinogradova, and S. Santer, Sci. Rep. **6**, 36443 (2016).
[33] P. Arya, D. Feldmann, A. Kopyshev, N. Lomadze, and S. Santer, "Light driven guided and self-organized motion of mesoporous colloidal particles," Soft Matter (published online 2019).
[34] D. Baigl, Lab Chip **12**, 3637 (2012).
[35] A. Diguet, R.-M. Guillermic, N. Magome, A. Saint-Jalmes, Y. Chen, K. Yoshikawa, and D. Baigl, Angew. Chem., Int. Ed. **48**, 9281 (2009).
[36] S. N. Varanakkottu, S. D. George, T. Baier, S. Hardt, M. Ewald, and M. Biesalski, Angew. Chem., Int. Ed. **52**, 7291 (2013).
[37] L. Nurdin, A. Venancio-Marques, S. Rudiuk, M. Morel, and D. Baigl, C. R. Chim. **19**, 199–206 (2016).
[38] I. Lagzi, S. Soh, P. J. Wesson, K. P. Browne, and B. J. Grzybowski, Am. Chem. Soc. **132**, 1198 (2010).
[39] H. Kitahata, R. Aihara, N. Magome, and K. Yoshikawa, J. Chem. Phys. **116**, 5666 (2002).
[40] M. M. Hanczyc, T. Toyota, T. Ikegami, N. Packard, and T. Sugawara, J. Am. Chem. Soc. **129**, 9386 (2007).
[41] E. F. Greco and R. O. Grigoriev, Phys. Fluids **21**, 042105 (2009).
[42] K. T. Kotz, K. A. Noble, and G. W. Faris, Appl. Phys. Lett. **85**, 2658 (2004).
[43] S. N. Varanakkottu, M. Anyfantakis, M. Morel, S. Rudiuk, and D. Baigl, Nano Lett. **16**, 644 (2016).
[44] N. Kavokine, M. Anyfantakis, M. Morel, S. Rudiuk, T. Bickel, and D. Baigl, Angew. Chem., Int. Ed. **55**, 11183 (2016).
[45] M. Schmitt and H. Stark, Phys. Fluids **28**, 012106 (2016).
[46] R. Deleurence, C. Parneix, and C. Monteux, Soft Matter **10**, 7088 (2014).
[47] H. Rau, "Photoisomerization of azobenzens," in *Photochemistry and Photophysics*, edited by J. Rebek (CRC Press, Boca Raton, FL, 1990), p. 110.
[48] D. Feldmann, P. Arya, N. Lomadze, A. Kopyshev, and S. Santer, Appl. Phys. Lett. **115**, 263701 (2019).
[49] M. Montagna and O. Guskova, Langmuir **34**, 311 (2018).

[50]A. Mamane, E. Chevallier, L. Olanier, F. Lequeux, and C. Monteux, Soft Matter **13**, 1299 (2017).
[51]S. Chen, C. Wang, Y. Yin, and K. Chen, RSC Adv. **6**, 60138 (2016).
[52]T. Hayashita, T. Kurosawa, T. Miyata, K. Tanaka, and M. Igawa, Colloid Polym. Sci. **272**, 1611 (1994).
[53]T. Shang, K. A. Smith, and T. A. Hatton, Langmuir **19**, 10764 (2003).
[54]E. Chevallier, A. Mamane, H. A. Stone, C. Tribet, F. Lequeuxa, and C. Monteux, Soft Matter **7**, 7866 (2011).
[55]A. Venancio-Marques, F. Barbaud, and D. Baigl, J. Am. Chem. Soc. **135**, 3218 (2013).
[56]D. Dumont, T. Galstian, S. Senkow, and A. Ritcey, Mol. Cryst. Liq. Cryst. **375**, 341 (2002).
[57]P. Atkins and J. de Paula, *Atkins' Physical Chemistry*, 8th ed. (Oxford University Press, 2006).
[58]C. Gahl, R. Schmidt, D. Brete, E. R. McNellis, W. Freyer, R. Carley, K. Reuter, and M. Weinelt, J. Am. Chem. Soc. **132**, 1831 (2010).
[59]E. Titov, Ph.D. thesis, Univesity of Potsdam, 2016, http://nbn-resolving.de/urn:nbn:de:kobv:517-opus4-394610.
[60]H. M. D. Bandara and S. C. Burdette, Chem. Soc. Rev. **41**, 1809 (2012).
[61]C. Ciminelli, G. Granucci, and M. Persico, Chem. Eur. J. **10**, 2327 (2004).
[62]Y. Zakrevskyy, J. Roxlau, G. Brezesinski, N. Lomadze, and S. Santer, J. Chem. Phys. **140**, 044906 (2014).

Supplementary Material

Kinetics of Photo-Isomerization of Azobenzene Containing Surfactants

Pooja Arya, Joachim Jelken, Nino Lomadze, Svetlana Santer,* Marek Bekir

Institute of Physics and Astronomy, University of Potsdam, 14476 Potsdam, Germany

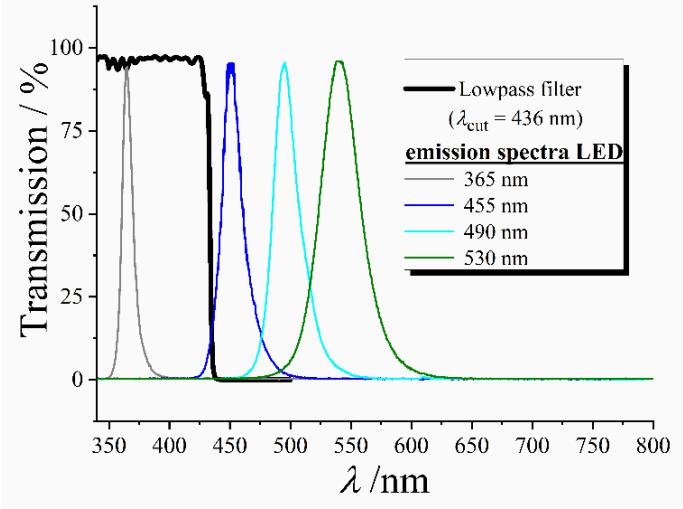

Figure S1. Transmission spectrum of the used lowpass filter, emission spectra of LED (UV, λ_{UV} = 365 nm), (blue, λ_B = 455 nm), (turquoise, λ_T = 490 nm), (green, λ_G = 530 nm).

1 Derivation of the equilibrium reaction

The reaction with respect to the forward and all reverse reaction can be written as:

$$\frac{dc_T}{dt} = -k_{TC} \cdot I \cdot c_T + k_{CT} \cdot I \cdot c_C + k_T \cdot c_C \quad \text{(S1)}$$

$$\frac{dc_T}{dt} = -k_{TC} \cdot I \cdot c_T + (k_{CT} \cdot I + k_T) \cdot c_C \quad \text{(5)}$$

If the value of k_T is neglectable due to thermal relaxation is very slow the rate of trans isomers is:

$$\frac{dc_T}{dt} = -k_{TC} \cdot I \cdot c_T + k_{CT} \cdot I \cdot c_C \quad \text{(S2)}$$

If initial concentration of *trans* is $c_{T,0}$ and no c_C is present, then at all times:

$$c_T + c_C = c_{T,0}, \quad \text{(S3)}$$

Inserting the expression of c_C from **Eq. S3** in **Eq. S2**:

$$\frac{dc_T}{dt} = -k_{TC} \cdot I \cdot c_T + k_{CT} \cdot I \cdot (c_{T,0} - c_T) \quad \text{(S4)}$$

$$\frac{dc_T}{dt} = -(k_{TC} + k_{CT}) \cdot I \cdot c_T + k_{CT} \cdot I \cdot c_{T,0} \quad \text{(S5)}$$

Further under assumption, that the light intensity not changing during the measurement $k_{TC} \cdot I$ or $k_{CT} \cdot I$ can be assumed as constant, i.e. approximating the second order reaction with respect to *trans* to *cis* isomerization and vice versa as pseudo first order reaction.

Then the integration of equation S4 is reported in the literature in detailed fashion in reference 57 and leads to the expression of:

$$c_T = c_{T,0} \cdot \frac{k_{CT} \cdot I + k_{TC} \cdot I \cdot \exp(-[k_{TC} + k_{CT}] \cdot I \cdot t)}{(k_{CT} + k_{TC}) \cdot I} \quad \text{(S6)}$$

$$c_{\mathrm{T}} = c_{\mathrm{T},0} \cdot \frac{k_{\mathrm{CT}} + k_{\mathrm{TC}} \cdot \exp(-[k_{\mathrm{TC}} + k_{\mathrm{CT}}] \cdot I \cdot t)}{(k_{\mathrm{CT}} + k_{\mathrm{TC}})} \quad (6)$$

2 Dependency between k_{TC} and k_{CT}

At equilibrium the concentration changes per time of c_{T} and c_{C} isomers is equal:

$$\frac{dc_{\mathrm{T}}}{dt} = \frac{dc_{\mathrm{C}}}{dt} \quad (S7)$$

$$-k_{\mathrm{TC}} \cdot I \cdot c_{\mathrm{T,eq}} = -k_{\mathrm{CT}} \cdot I \cdot c_{\mathrm{C,eq}} \quad (S8)$$

$$k_{\mathrm{TC}} \cdot c_{\mathrm{T,eq}} = k_{\mathrm{CT}} \cdot c_{\mathrm{C,eq}} \quad (S9)$$

Using $c_{\mathrm{T,eq}} + c_{\mathrm{C,eq}} = c_{\mathrm{T,0}}$,**Eq. S9** can be written as :

$$k_{\mathrm{TC}} \cdot c_{\mathrm{T,eq}} = k_{\mathrm{CT}} \cdot (c_{\mathrm{T,0}} - c_{\mathrm{T,eq}}) \quad (S10)$$

$$k_{\mathrm{TC}} \cdot \frac{c_{\mathrm{T,eq}}}{c_{\mathrm{T,0}}} / \left(1 - \frac{c_{\mathrm{T,eq}}}{c_{\mathrm{T,0}}}\right) = k_{\mathrm{CT}} \quad (S11)$$

with:

$$X = \frac{\%\mathrm{Tr}_{\mathrm{eq}}}{\%\mathrm{Cis}_{\mathrm{eq}}} = \frac{c_{\mathrm{T,eq}}}{c_{\mathrm{T,0}}} / \left(1 - \frac{c_{\mathrm{T,eq}}}{c_{\mathrm{T,0}}}\right). \quad (S12)$$

$$k_{\mathrm{TC}} \cdot X = k_{\mathrm{CT}} \quad (S13)$$

Apparently, X is here defined as the rate constant ratio between k_{TC} and k_{CT}. Also one can say that X is the ratio of trans to cis isomer at photo stationary state. Values for the equilibrium concentration $c_{\mathrm{T,eq}}$ can be read after approaching the equilibrium, where values for the initial concentration $c_{\mathrm{T,0}}$ are known. For sample concentration below the CMC measured values are reported in table 1. For blue light of wavelength 455 nm X = 1.5 was used.

Table S1. Equilibrium ratio of *trans*- $c_{T,eq}/c_{T,0}$ and *cis*- isomers, 1-($c_{T,eq}/c_{T,0}$), and rate constant ratio X at different irradiation wavelength.

λ	$\frac{c_{T,eq}}{c_{T,0}}$	$\left(1-\frac{c_{T,eq}}{c_{T,0}}\right)$	X
nm		min	
375	0.036	0.964	0.04
455	0.600	0.400	1.50
490	0.810	0.019	4.35
530	0.900	0.010	9.00

3 Derivation of the fitting equation.

Substituting k_{CT} from **Eq. S13** into with **Eq**. **6** yields:

$$c_T = c_{T,0} \cdot \frac{k_{TC} \cdot X + k_{TC} \cdot \exp(-[k_{TC} + k_{TC} \cdot X] \cdot I \cdot t)}{(k_{TC} \cdot X + k_{TC})} \quad \text{(S14)}$$

$$c_T = c_{T,0} \cdot \frac{k_{TC} \cdot [X + \cdot \exp(-[(1+X) \cdot k_{TC}] \cdot I \cdot t)]}{k_{TC} \cdot (1+X)} \quad \text{(S15)}$$

$$c_T = c_{T,0} \cdot \frac{X}{(1+X)} + c_{T,0} \cdot \frac{1}{(1+X)} \cdot \exp(-[(1+X) \cdot k_{TC}] \cdot I \cdot t) \quad \text{(S16)}$$

The exponential term may be written into the simpler form of $\exp\left(-\frac{t}{\tau}\right)$,which mean from **Eq. S16** we can write:

$$\tau = \frac{1}{(1+X) \cdot k_{TC} \cdot I} \text{ and } X = \frac{c_{T,eq}}{c_{T,0}} / \left(1 - \frac{c_{T,eq}}{c_{T,0}}\right) \text{ or } \quad \frac{1}{X} = K_{eq}, \quad (15)$$

then **Eq**. **S16** is:

$$c_T = c_{T,0} \cdot \frac{X}{(1+X)} + c_{T,0} \cdot \frac{1}{(1+X)} \cdot \exp\left(-\frac{t}{\tau}\right) \quad \text{(S17)}$$

The term $\frac{X}{(1+X)}$ and $\frac{1}{(1+X)}$ is equal to $\%Tr_{eq}$ and $\%Cis_{eq}$, thus:

$$\%Tr_{eq} = \frac{X}{(1+X)} \quad \text{(S18)}$$

$$\%Cis_{eq} = \frac{1}{(1+X)}, \quad \text{(S2)}$$

and substituting both **Eq**. **S18** and **S19** into **Eq**. **17**:

$$c_T = \%\mathrm{Tr}_{eq} \cdot c_{T,0} + \%\mathrm{Cis}_{eq} \cdot c_{T,0} \cdot \exp\left(-\frac{t}{\tau}\right) \quad \text{(S20)}$$

Further, $\%\mathrm{Cis}_{eq}$ may be rewritten into expression considering $\%\mathrm{Tr}_{eq}$:

$$c_T = \%\mathrm{Tr}_{eq} \cdot c_{T,0} + (1 - \%\mathrm{Tr}_{eq}) \cdot c_{T,0} \cdot \exp\left(-\frac{t}{\tau}\right) \quad \text{(S21)}$$

$$c_T = \frac{c_{T,eq}}{c_{T,0}} \cdot c_{T,0} + \left(1 - \frac{c_{T,eq}}{c_{T,0}}\right) \cdot c_{T,0} \cdot \exp\left(-\frac{t}{\tau}\right), \quad \text{(S22)}$$

$$c_T = c_{T,eq} \cdot \left(1 - \exp\left(-\frac{t}{\tau}\right)\right) + c_{T,0} \cdot \exp\left(-\frac{t}{\tau}\right) \quad (7)$$

with $c_{T,0}$ as initial *trans* concentration with the value of 0.1 mM and $c_{T,eq}$ as the equilibrium concentration, which can be read from the data.

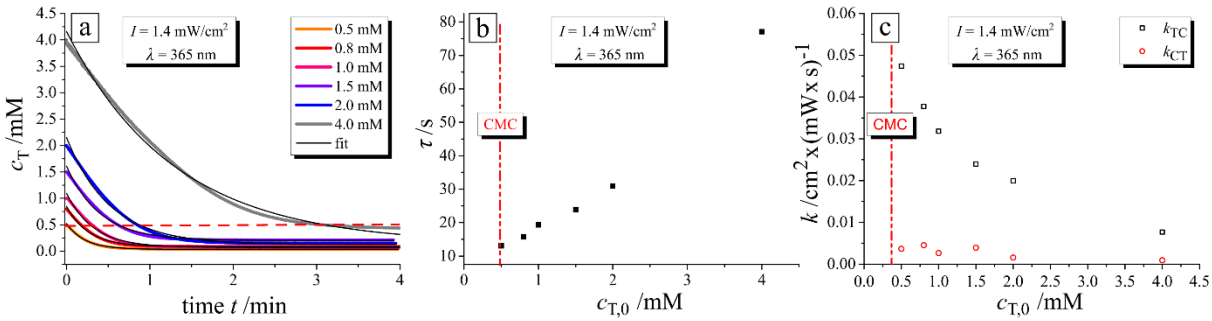

Figure S2. Dependence pf the photo-isomerization kinetic on surfactant concentration under irradiation with UV light (λ = 365 nm, I=1.4 mW/cm^2). (a) *trans* isomer concentration as a function of irradiation time, (b) decay time, fitting function is **Eq. 9** and **10**. (c) Rate constant as a function of surfactant concentration.

3.1 Details of $k_{TC,M}$ calculation.

Above the CMC we observe a peculiar phenomenon that the measured k_{TC} decreases with increasing concentration. Now the measured average value of k_{TC} is a fractional mean value of single molecules $k_{TC,S}$ and molecules aggregated in micelles, $k_{TC,M}$:

$$k_{TC} = \frac{c_{T,S}}{c_T} \cdot k_{TC,S} + \frac{c_{T,M}}{c_T} \cdot k_{TC,M}, \quad \text{(S23)}$$

where $c_{T,S}$ and $c_{T,M}$ are the concentration of *trans* isomers as single molecules and in micelles, plus to maintain the fractional mean relation, it must be normalized by the total concentration of *trans* isomers

c_T. We know, that the molecules can be considered as single molecules as long the CMC is not reached, thus the concentration of *trans* isomers as single molecules is equal to the cmc, $c_{T,S} = c_{cmc}$. In contrast $c_{T,M}$ is the excess concentration of total *trans* isomers subtracted from the cmc, $c_{T,M} = c_T - c_{cmc}$. Substituting both relations into **Eq**. **S23** following equation can be obtained:

$$k_{TC} = \frac{c_{cmc}}{c_T} \cdot k_{TC,S} + \frac{c_T - c_{cmc}}{c_T} \cdot k_{TC,M}. \quad (11)$$

Value of $k_{TC,S}=(8.49 \pm 0.17)\cdot 10^{-3} cm^2/(mW\cdot s)$ is the average value obtained from measurements before reaching cmc. k_{TC} is the calculated from the decay reported in **Figure 3d**.

Table S2. Fitting values for **Figure 3**: c_T concentration, equilibrium ratio from *trans* isomer concentration $c_{T,eq}/c_{T,0}$, decay time τ, rate constant of *trans* to *cis* isomerization (measured) k_{TC}, rate constant of *cis* to *trans* isomerization (measured) k_{CT}, rate constant of *trans* to *cis* isomerization for micelles (calculated) $k_{TC,M}$

c_T	τ	$c_{T,eq}/c_{T,0}$	k_{TC}	k_{CT}	$k_{TC,M}$
mM	s		$cm^2/mW\cdot s$	$cm^2/mW\cdot s$	$cm^2/mW\cdot s$
0.05	6.2	0.60	$8.36\cdot10^{-3}$	$1.27\cdot10^{-2}$	–
0.1	6.3	0.59	$8.57\cdot10^{-3}$	$1.25\cdot10^{-2}$	–
0.2	6.2	0.59	$8.72\cdot10^{-3}$	$1.24\cdot10^{-2}$	–
0.3	6.4	0.60	$8.39\cdot10^{-3}$	$1.27\cdot10^{-2}$	–
0.4	6.2	0.59	$8.65\cdot10^{-3}$	$1.25\cdot10^{-2}$	–
0.45	6.3	0.61	$8.24\cdot10^{-3}$	$1.29\cdot10^{-2}$	–
0.5	6.3	0.59	$8.55\cdot10^{-3}$	$1.26\cdot10^{-2}$	–
0.6	6.8	0.63	$7.18\cdot10^{-3}$	$1.24\cdot10^{-2}$	$6.40\cdot10^{-4}$
0.7	7.0	0.67	$6.36\cdot10^{-3}$	$1.27\cdot10^{-2}$	$1.05\cdot10^{-3}$
0.8	7.3	0.69	$5.74\cdot10^{-3}$	$1.25\cdot10^{-2}$	$1.15\cdot10^{-3}$
0.9	7.4	0.70	$5.37\cdot10^{-3}$	$1.26\cdot10^{-2}$	$1.48\cdot10^{-3}$
1.0	7.5	0.70	$5.44\cdot10^{-3}$	$1.25\cdot10^{-2}$	$2.40\cdot10^{-3}$
1.1	7.5	0.73	$4.88\cdot10^{-3}$	$1.29\cdot10^{-2}$	$1.87\cdot10^{-3}$
1.2	7.8	0.73	$4.58\cdot10^{-3}$	$1.25\cdot10^{-2}$	$1.79\cdot10^{-3}$
1.3	7.9	0.74	$4.41\cdot10^{-3}$	$1.25\cdot10^{-2}$	$1.85\cdot10^{-3}$
1.4	8.1	0.75	$4.16\cdot10^{-3}$	$1.23\cdot10^{-2}$	$1.75\cdot10^{-3}$
1.5	8.2	0.77	$3.81\cdot10^{-3}$	$1.25\cdot10^{-2}$	$1.47\cdot10^{-3}$

Table S3. Fitting values for **Figure 4**: wavelength λ, equilibrium ratio from *trans* isomer concentration $c_{T,eq}/c_{T,0}$, decay time τ, rate constant ratio X, equilibrium constant K_{eq}

λ	$\frac{c_{T,eq}}{c_{T,0}}$	τ	X	$K_{eq} = k_{TC}/k_{CT}$
nm		min		
365	0.036	0.46	0.04	25.39
455	0.600	0.78	1.50	0.67
490	0.810	2.93	4.35	0.23
530	0.900	14.76	9.00	0.11

4 Irradiation with combined wavelengths.

For calculating the equilibrium for irradiation with combined wavelengths the expression of:

$$k_{TC} \cdot I = k_{TC,1} \cdot I_1 + k_{TC,2} \cdot I_2 \quad \text{(S24)}$$

and:

$$k_{CT} \cdot I = k_{CT,1} \cdot I_1 + k_{CT,2} \cdot I_2 \quad \text{(S25)}$$

must be substituted into **Eq. S6**:

$$c_T = c_{T,0} \cdot \frac{k_{CT,1} \cdot I_1 + k_{CT,2} \cdot I_2 + (k_{TC,1} \cdot I_1 + k_{TC,2} \cdot I_2) \cdot U}{k_{CT,1} \cdot I_1 + k_{CT,2} \cdot I_2 + k_{TC,1} \cdot I_1 + k_{TC,2} \cdot I_2},$$

$$U = \exp(-[k_{TC,1} \cdot I_1 + k_{TC,2} \cdot I_2 + k_{CT,1} \cdot I_1 + k_{CT,2} \cdot I_2] \cdot t), \quad \text{(S26)}$$

where $c_{T,0}$ as the *trans* isomer concentration at the initial time, $k_{TC,1}$ and $k_{CT,1}$ are the rate constants for the forward and reverse reaction for the light flux of the first wavelength I_1, $k_{TC,2}$ and $k_{CT,2}$ are the rate constant for the forward and reverse reaction for the light intensity of the second wavelength I_2.

Now the intensity of the second wavelength I_2 has a certain fraction R of the first intensity I_1, thus:

$$I_2 = R \cdot I_1, \quad \text{(S27)}$$

and substituting **Eq**. **S27** into **Eq**. **S26**:

$$c_T = c_{T,0} \cdot \frac{k_{CT,1} \cdot I_1 + k_{CT,2} \cdot R \cdot I_1 + (k_{TC,1} \cdot I_1 + k_{TC,2} \cdot R \cdot I_1) \cdot U}{k_{CT,1} \cdot I_1 + k_{CT,2} \cdot R \cdot I_1 + k_{TC,1} \cdot I_1 + k_{TC,2} \cdot R \cdot I_1},$$

$$U = \exp(-[k_{TC,1} \cdot I_1 + k_{TC,2} \cdot R \cdot I_1 + k_{CT,1} \cdot I_1 + k_{CT,2} \cdot R \cdot I_1] \cdot t), \quad \text{(S28)}$$

$$c_T = c_{T,0} \cdot \frac{(k_{CT,1} + k_{CT,2} \cdot R) \cdot I_1 + (k_{TC,1} + k_{TC,2} \cdot R) \cdot I_1 \cdot U}{(k_{CT,1} + k_{CT,2} \cdot R + k_{TC,1} + k_{TC,2} \cdot R) \cdot I_1},$$

$$U = \exp(-[k_{TC,1} + k_{TC,2} \cdot R + k_{CT,1} + k_{CT,2} \cdot R] \cdot I_1 \cdot t), \quad \text{(S29)}$$

$$c_{\mathrm{T}} = c_{\mathrm{T},0} \cdot \frac{k_{\mathrm{CT}_1} + k_{\mathrm{CT}_2} \cdot R + (k_{\mathrm{TC}_1} + k_{\mathrm{TC}_2} \cdot R) \cdot \mathrm{U}}{(k_{\mathrm{CT}_1} + k_{\mathrm{TC}_1}) + (k_{\mathrm{CT}_2} + k_{\mathrm{TC}_2}) \cdot R}$$

$$U = \exp(-[k_{\mathrm{TC},1} + k_{\mathrm{CT},1} + (k_{\mathrm{TC},2} + k_{\mathrm{CT},2}) \cdot R] \cdot I_1 \cdot t), \qquad \text{(S30)}$$

In equilibrium ($\lim_{t\to\infty}$) the term $U = 0$

$$c_{\mathrm{T,eq}} = c_{\mathrm{T},0} \cdot \frac{k_{\mathrm{CT}_1} + k_{\mathrm{CT}_2} \cdot R}{(k_{\mathrm{CT}_1} + k_{\mathrm{TC}_1}) + (k_{\mathrm{CT}_2} + k_{\mathrm{TC}_2}) \cdot R} \qquad (10)$$

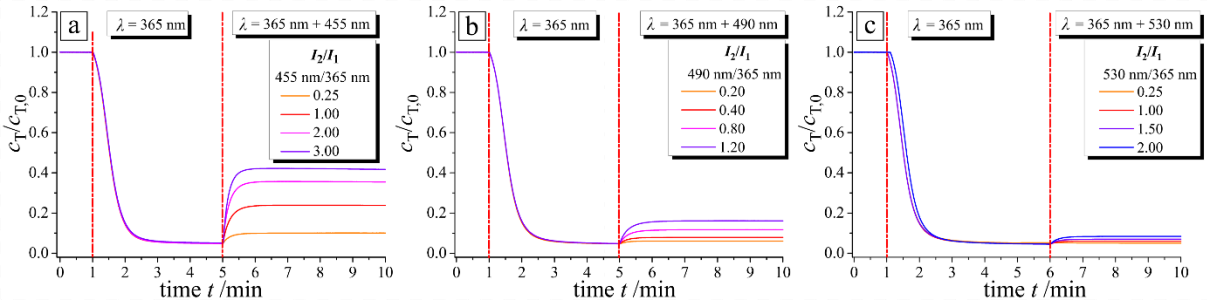

Figure S3. *Trans* isomers concentration as a function of the time with illuminating the sample with two light sources UV and (a) 455 nm, (b) 490nm, (c) 530nm at different intensity ratios *R*. Sample concentration is set to 0.1 mM and temperature is set to 20 °C.

Table S4. Values for **Figure 5c**: wavelength λ of second light, ratio of both light intensities $R=I_2/I_1$, equilibrium ratio from *trans* isomer concentration $c_{\mathrm{T,eq}}/c_{\mathrm{T},0}$ (theoretical and measured), deviation of theoretical and measured value.

λ	***R***	$\frac{c_{\mathrm{T,eq}}}{c_{\mathrm{T},0}}$	$\frac{c_{\mathrm{T,eq}}}{c_{\mathrm{T},0}}$	**Theo/measured**
		theoretical	measured	
nm			min	%
455	0.00	0.0038	0.0036	5.0
455	0.25	0.0110	0.0100	9.2
455	1.00	0.0247	0.0239	3.4
455	2.00	0.0343	0.0355	3.6
455	3.00	0.0398	0.0419	5.3
490	0.00	0.0038	0.0039	2.9
490	0.20	0.0061	0.0060	2.4
490	0.40	0.0084	0.0079	6.2
490	0.80	0.0124	0.0117	6.3

490	1.20	0.0161	0.0161	0.2
530	0.00	0.0038	0.0036	5.0
530	0.25	0.0045	0.0050	12.2
530	1.00	0.0064	0.0060	6.8
530	1.50	0.0076	0.0070	8.9
530	2.00	0.0088	0.0083	5.8

I(UV, λ=365nm) =1mW/cm^2

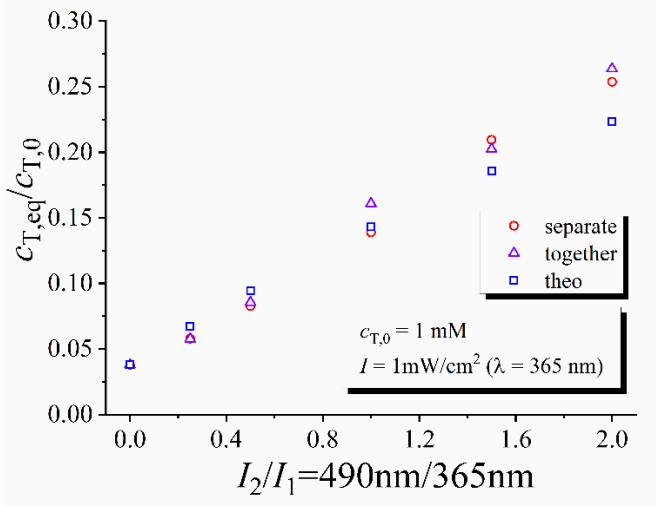

Figure S4. Comparison between measured and calculated %Tr$_{eq}$=$c_{T,eq}/c_{T,0}$ as a function of R=I_2/I_1 data. Surfactant concentration is set to 1 mM and temprature is set to 20 °C.

Table S5. Values for **Figure S4**: wavelength λ of second light, ratio of both light intensities $R=I_2/I_1$, equilibrium ratio from *trans* isomer concentration $c_{T,eq}/c_{T,0}$ (theoretical and measured), deviation of theoretical and measured value.

λ	***R***	$\frac{c_{T,eq}}{c_{T,0}}$	$\frac{c_{T,eq}}{c_{T,0}}$	**Theo/measured**	$\frac{c_{T,eq}}{c_{T,0}}$	**Theo/measured**
		theoretical	measured separated	separated	measured simultaneously	simultaneously
nm				%		%
490	0.00	0.0379	0.0379	0.0	0.0379	0.0
490	0.25	0.0672	0.0578	16.2	0.0577	16.4
490	0.50	0.0943	0.0827	14.1	0.0856	10.2
490	1.00	0.1431	0.1389	3.0	0.1610	11.1
490	1.50	0.1857	0.2095	11.4	0.2025	8.3
490	2.00	0.2231	0.2537	12.0	0.2637	15.4

Intensity of first wavelength (UV, λ = 365 nm) I =1mW/cm^2

5 Spacer length

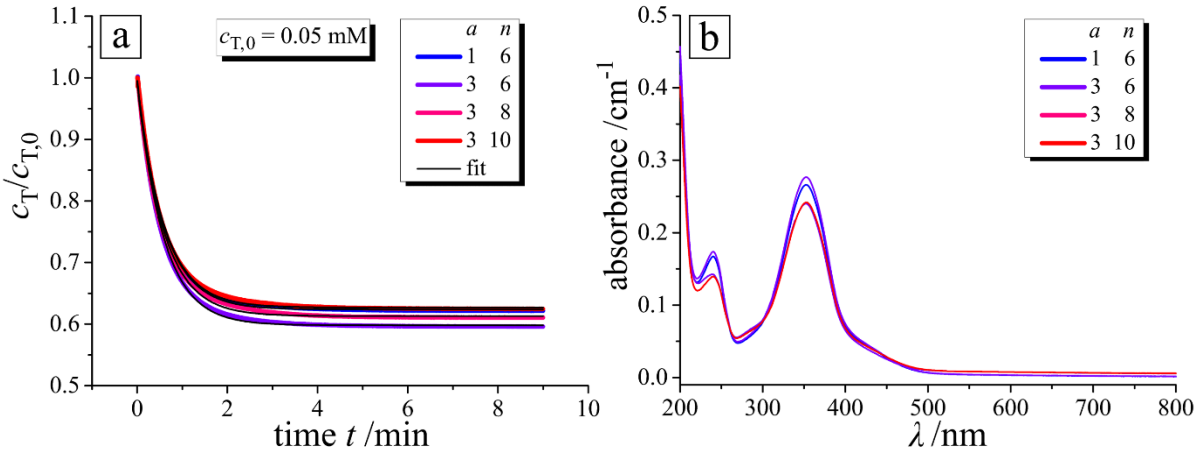

Figure S5. (a) *Trans* isomer concentration as a function of the time for surfactant of different spacer lengths. (b) Adsorption spectra.

Table 4. Fitting values for figure 7: tail length *m*, spacer length *n* equilibrium ratio from *trans* isomer concentration $c_{T,eq}/c_{T,0}$, decay time τ, equilibrium ratio *X*, rate constant of forward and reverse reaction k_{TC} and k_{CT}

m	*n*	$\frac{c_{T,eq}}{c_{T,0}}$	τ	*X*	k_{TC}	k_{CT}
			min		$cm^2/(mW \cdot s)$	$cm^2/(mW \cdot s)$
1	6	0.62	0.59	1.64	$7.14 \cdot 10^{-3}$	$1.17 \cdot 10^{-2}$
3	6	0.60	0.58	1.48	$7.76 \cdot 10^{-3}$	$1.15 \cdot 10^{-2}$
3	8	0.61	0.59	1.57	$7.36 \cdot 10^{-3}$	$1.15 \cdot 10^{-2}$
3	10	0.62	0.59	1.64	$7.14 \cdot 10^{-3}$	$1.17 \cdot 10^{-2}$

I =1mW/cm^2

6 Photo-isomerization and thermal relaxation

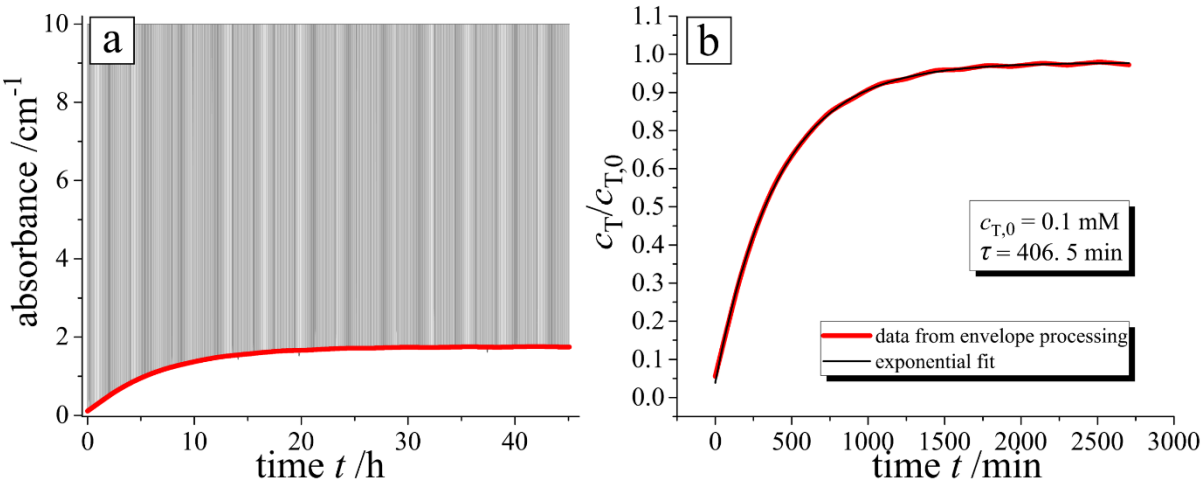

Figure S6. (a) Absorbance (at λ=376nm) as a function of time for m=3 and n=6 initially in *cis* state. To minimize the influence of the monitoring beam, it is switched on for only 2 seconds every 5 minutes. To obtain the information about concentration of *trans* isomer, the lower border (red line) in (a) is processed by an envelope procedure. (b) Fitting the data with a simple exponential decay yields the relaxation time τ.

Thermal relaxation

The rate law of thermal relaxation is per definition a first order reaction:

$$\frac{dc_T}{dt} = -\frac{dc_C}{dt} = k_T \cdot c_C, \qquad \text{(S31)}$$

where c_T and c_C are the concentrations of *trans* and *cis* isomers and k_T the rate constant for the thermal relaxation. The integration of **Eq. S26** leads to the simple expression for the *cis* concentration:

$$c_C = c_{C,0} \cdot \exp(-k_T \cdot t), \text{ and } k_T = \frac{1}{\tau} \quad (11)$$

where τ is the decay time. The decay time τ and corresponding k_T are measured for a total temperature range from 20 till 50°C.

Photo-isomerization and thermal relaxation

To include now the thermal relaxation k_T in **Eq**. **5** is now not to be assumed as zero. The generation of trans isomers includes now the rate constant of photo induced *trans-cis* and *cis-trans* isomerization. Under same assumption as discussed in **Section 1** the integration of **Eq**. **5** is reported in the literature in detailed fashion[57] and leads to the expression of:

$$c_T = c_0 \cdot \frac{k_{CT} \cdot I + k_T + k_{TC} \cdot I \cdot \exp(-[k_{TC} \cdot I + k_{CT} \cdot I + k_T] \cdot t)}{k_{CT} \cdot I + k_T + k_{TC} \cdot I} \quad (S32)$$

$$c_T = c_0 \cdot \frac{k_{CT} \cdot I + k_T + k_{TC} \cdot I \cdot \exp(-[(k_{TC} + k_{CT}) \cdot I + k_T] \cdot t)}{(k_{CT} + k_{TC}) \cdot I + k_T} \quad (12)$$

Relation between k_{TC} and $k_{CT}+k_T$

At equilibrium the concentration change per time of dc_T/dt and dc_C/dt isomers, **Eq**. **S10**, is equal:

$$k_{TC} \cdot I \cdot c_{T,eq} = (k_{CT} \cdot I + k_T) \cdot c_{C,eq} \quad (S33)$$

Using $c_{T,eq} + c_{C,eq} = c_{T,0}$, **Eq. S33** can be written in simplified form as :

$$k_{TC} \cdot I \cdot c_{T,eq} = (k_{CT} \cdot I + k_T) \cdot (c_{T,0} + c_{T,eq}) \quad (S34)$$

$$k_{TC} \cdot I \cdot \frac{c_{T,eq}}{c_{T,0}} / \left(1 - \frac{c_{T,eq}}{c_{T,0}}\right) = (k_{CT} \cdot I + k_T) \quad (S35)$$

Substituting the term in left from **Eq**. **S12** into **Eq**. **S35** yields:

$$k_{TC} \cdot I \cdot X = k_{CT} \cdot I + k_T \quad (S36)$$

$$k_{TC} \cdot I \cdot X - k_T = k_{CT} \cdot I \quad (S37)$$

For a surfactant concentration of 0.1 mM and blue light (λ = 455 nm) the ratio $\frac{c_{T,eq}}{c_{T,0}} = 0.6$ and X = 1.5.

Only consideration of the exponential decay from **Eq**. **12**:

$$\exp(-[k_{TC} \cdot I + k_{CT} \cdot I + k_T] \cdot t) \quad (S38)$$

now substituting $k_{CT} \cdot I$ with **Eq**. **S37**:

$$\exp(-[k_{\mathrm{TC}} \cdot I + k_{\mathrm{TC}} \cdot I \cdot X - k_{\mathrm{T}} + k_{\mathrm{T}}] \cdot t) \quad \text{(S39)}$$

$$\exp(-[(k_{\mathrm{TC}} + k_{\mathrm{TC}} \cdot X) \cdot I] \cdot t) \quad \text{(S40)}$$

Eq. S40 leads to same expression in the exponential term as presented in **Eq**. **S15**.

The relation between reaction constants of the slowed forward reaction $k_{\mathrm{TC}} \cdot I$ from thermal relaxation k_{T} and *cis* to *trans* isomerization $k_{\mathrm{CT}} \cdot \Phi$ can be calculated via:

$$k_{\mathrm{TC}} \cdot I \cdot X - k_{\mathrm{T}} = k_{\mathrm{CT}} \cdot I \quad \text{(S41)}$$

$$k_{\mathrm{TC}} \cdot X - \frac{k_{\mathrm{T}}}{I} = k_{\mathrm{CT}} \quad \text{(S42)}$$

$X = 1.5$ for blue of λ = 455 nm

7 Calculation of the minimal light intensity to equalize the rate of thermal relaxation

To get the minimal light concentration, where *trans* to *cis* isomerization will be equalized by the thermal relaxation will be obtained if the rate of *trans* to *cis* isomerization from photoisomerization is equal to that of the thermal relaxation in equilibrium.

$$k_{\mathrm{TC}} \cdot I \cdot c_{\mathrm{T}} = k_{\mathrm{T}} \cdot c_{\mathrm{C}} \quad \text{(S43)}$$

Inserting for the c_{T} and c_{C} concentration the expression in S9 and S10 for the equilibrium concentration as a function of initial concentration, one get:

$$k_{\mathrm{TC}} \cdot I \cdot \frac{c_{\mathrm{T,eq}}}{c_{\mathrm{T,0}}} = k_{\mathrm{T}} \cdot \left(1 - \frac{c_{\mathrm{T,eq}}}{c_{\mathrm{T,0}}}\right) \quad \text{(S44)}$$

$$k_{\mathrm{TC}} \cdot I \cdot \frac{c_{\mathrm{T,eq}}}{c_{\mathrm{T,0}}} \Big/ \left(1 - \frac{c_{\mathrm{T,eq}}}{c_{\mathrm{T,0}}}\right) = k_{\mathrm{T}} \quad \text{(S45)}$$

Substituting the left term with **Eq**. **S12**:

$$k_{\mathrm{TC}} \cdot I \cdot X = k_{\mathrm{T}} \quad \text{(S46)}$$

$$I = \frac{k_{\mathrm{T}}}{k_{\mathrm{TC}} \cdot X}, \quad \text{(S47)}$$

or with the relation from **Eq**. **S13**:

$$I = \frac{k_{\mathrm{T}}}{k_{\mathrm{CT}}} \quad \text{(S48)}$$

The same relation presented in **Eq**. **S48** will be obtained if the thermal relaxation is equal probable to the photo induce *cis* to *trans* isomerization:

$$k_{\mathrm{CT}} \cdot I \cdot c_{\mathrm{C}} = k_{\mathrm{T}} \cdot I \quad \text{(S49)}$$

LANGMUIR

Publication 2

pubs.acs.org/Langmuir Article

Extremely Long-Range Light-Driven Repulsion of Porous Microparticles

David Feldmann, Pooja Arya, Taras Y. Molotilin, Nino Lomadze, Alexey Kopyshev, Olga I. Vinogradova,* and Svetlana A. Santer*

Cite This: https://dx.doi.org/10.1021/acs.langmuir.9b03270 Read Online

ACCESS | Metrics & More | Article Recommendations | Supporting Information

ABSTRACT: The repulsive surface forces, such as electrostatic or steric, acting between particles explain why they remain well separated in aqueous electrolyte solutions and are responsible for the stability of colloidal dispersions. However, the effective range of these interactions is always well below hundreds of nanometers and typically can be controlled by advanced manipulations such as tuning the electrolyte concentration or modifying the particle surface or, in some more specific cases, via subjecting the suspension to an external electric or magnetic field. Here we employ solutions with small additives of a photosensitive ionic surfactant to investigate if a repulsive interaction of microsized particles sedimented at the solid surface can be remotely controlled simply by illuminating it with an appropriate wavelength. We show that interactions of conventional impermeable particles remain practically unaffected by light, but, in contrast, for porous particles, we observe a long-range repulsion, several orders of magnitude longer than any conceivable equilibrium surface force. This repulsion emerges due to the diffusio-osmotic flow generated near the porous particles that in this scenario are playing a role of micropumps. The diffusio-osmotic repulsion of porous particles can be used for a remote control of their two-dimensional assemblies at the solid wall, and in particular, we demonstrate that by simply using two different illumination wavelengths it is possible to reversibly switch the state of porous particle dispersion from densely packed surface aggregates to a periodic lattice of particles separated by distances on the order of tens of micrometers.

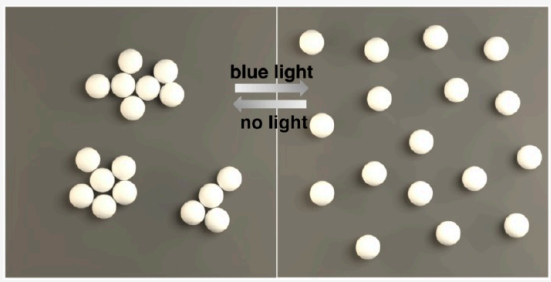

INTRODUCTION

Understanding the mutual interaction of colloidal particles is the key issue controlling a broad spectrum of scientific, technological, and industrial processes related to biological fluids, applications in the chemical and pharmaceutical fields, products of food industry, paintings, and coatings.[1−3] Beyond the wide range of product-related applications, quasi two-dimensional ensembles of colloids are probably the most important model systems to study and understand a plethora of phenomena in biology, physical chemistry, and statistical physics such as collective motion and swarming of micro-swimmers, motion in crowded environments, or the novel nonequilibrium phase separation behavior of ensembles of self-propelled particles.[4−11] Boiled down to quasi two-dimensional systems, colloidal ensembles are both, convenient to handle in theoretical or computational investigations, and relatively simple to study in experiments with optical microscopy especially when adhering to solid−liquid interfaces. However, whereas in the numerical modeling the interparticle interactions can be adjusted easily,[12] in the experiment the mutual interactions are difficult to modify on demand as this usually involves irreversible changes of the system mediated via salt concentration, polymers, surfactants, or other agents.[13] Here we report an approach allowing one to induce extremely long-range interactions in an ensemble of colloids. The strength and possibly the sign of the interaction can be tuned dynamically and reversibly by applying simple optical stimuli.

To achieve this, we exploit a physical mechanism related to the recently introduced phenomenon of light driven diffusio-osmosis (LDDO): local flows can be generated at a solid liquid interface by irradiation with a weak focused laser beam if the liquid phase consists of a suitable azobenzene-containing surfactant solution.[14] Under irradiation a spatial gradient of *trans* and *cis* species of the surfactant is generated, which, in turn, leads to a flow that is strong enough to push away colloids in the vicinity of the spot area (Figure 1a). Similar phenomena could also be induced by an individual porous particle illuminated with homogeneous irradiation. In this case, the radial concentration gradient would be generated by the particle itself. As a consequence, nearby colloids will interact

Special Issue: Advances in Active Materials

Received: October 21, 2019
Revised: February 18, 2020
Published: February 19, 2020

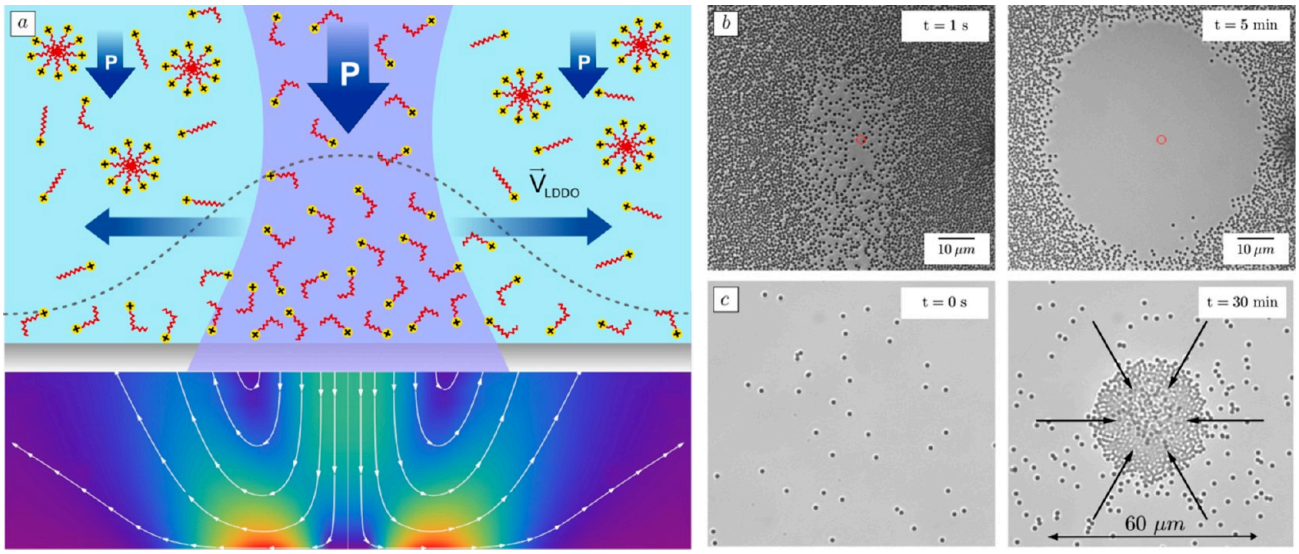

Figure 1. (a) Schematic representation of generation of light-driven diffusio-osmotic (LDDO) flow. (below) Schematic streamlines of bulk liquid flow (far from the surface) as calculated in ref 11. (b) Optical micrographs of the motion of colloids (d = 2 μm) under irradiation with UV light (λ = 355 nm, P = 1.5 μW). (c) Particle displacement under irradiation with green light (λ = 532 nm, P = 30 μW). The particles are dispersed in aqueous solution containing photosensitive surfactant (c_{azo} = 1 mM, the chemical structure is shown in Figure 2b).

through the diffusio-osmotic flows induced by themselves, leading to an effective long-range repulsive force. In the following, we shall first review the mechanism of LDDO generated flow and then explain in detail how single colloids are able to mimic this phenomenology. One remarkable feature is that the strength of repulsion can be tuned almost arbitrarily and on demand, i.e. on and off with high spatiotemporal precision by simple control of illumination parameters. It might thus be considered as a variable component in the interaction of colloids where the attractive part is fixed. Before presenting our results on ensembles, we shall first review the generation of LDDO driven flows in some detail.

LDDO: From an Optical Sweep to Interparticle Interactions. LDDO becomes possible due to a photosensitive surfactant bearing an azobenzene group in its hydrophobic tail.[15,16] The azobenzene group undergoes a reversible photoisomerization reaction from a more stable *trans* to a metastable *cis* conformation during irradiation with light of different wavelengths.[17] Photoisomerization toggled by alternating illumination with UV and blue/green light can thus alter the hydrophobicity/hydrophilicity of the surfactant as a whole and hence its solubility, the critical micelle concentration (CMC), the interfacial energy, and strength of interaction with other substances.[18,19] For instance, since the *trans* state of the surfactant molecule is more hydrophobic than the *cis* state, the CMC of the surfactant may rise by an order of magnitude when going from *trans* to *cis*.[20] When irradiation with a focused UV laser beam is applied at a solid/liquid interface, it triggers a photoisomerization of the surfactant molecules from *trans* to *cis*, generating a majority of *cis* isomers in the vicinity of the irradiated area and near the surface (Figure 1a).[14] The attractive interaction potential of the more hydrophilic *cis* isomers with the charged glass surface generates a local excess concentration of the *cis* isomers near the surface at the irradiated area, leading to an increase in osmotic pressure developing in normal direction within the range of the interaction potential between surfactant and solid/liquid interface. The lateral gradient in *cis* concentration generated during illumination (Figure 1a) induces a corresponding osmotic pressure *gradient*, leading to a *lateral* diffusio-osmotic flow directed outward with characteristic velocity of the order of several micrometers per second. When colloidal particles are trapped at the surface within the irradiated region, the local light driven diffusio-osmotic (LDDO) flow drives them along leaving behind a clean surface (Figure 1b). The direction of the flow can be adjusted by the irradiation wavelength. This is achieved by first bringing all surfactants in a *cis* state by global irradiation with UV light and then illuminating locally with green light that triggers the return to *trans* state resulting in the generation of reversed concentration gradients. This leads to a correspondingly reversed LDDO flow in the direction toward the irradiation spot and consequent gathering of the particles (Figure 1c).[14]

As discussed above, a local fluid flow is generated by illumination with focused laser light, capable of either removing or gathering particles from or within the illuminated area, i.e. all particles trapped at the irradiated solid/liquid interface are moved passively within the local LDDO flow. The natural question is whether the colloids could become the source of the flow, thus essentially playing the part of a micropump.

In the present work, we employ the light driven diffusio-osmosis (LDDO) to create a local flow around individual colloids that repel neighboring particles.

To achieve this we utilize particles having a large surface area, i.e. porous colloids. When these particles are immersed in water solution containing surfactants in the *trans* state, the surfactant molecules are absorbed by the particles. Under irradiation with UV light that promotes *trans*−*cis* isomerization, the more hydrophilic *cis* isomers are expelled from the particles leading to an effective out-flow. The emergence of a laterally inhomogeneous excess of *cis* species around the particle close to the solid−liquid interface leads to a local generation of LDDO flow effectively resulting in a micropump state. Since *cis* species are leaving the particles, the flow is directed away from them and leads to an effective repulsion of particles. Strength and duration of the process strongly depends on the irradiation wavelength (at fixed intensity).

https://dx.doi.org/10.1021/acs.langmuir.9b03270

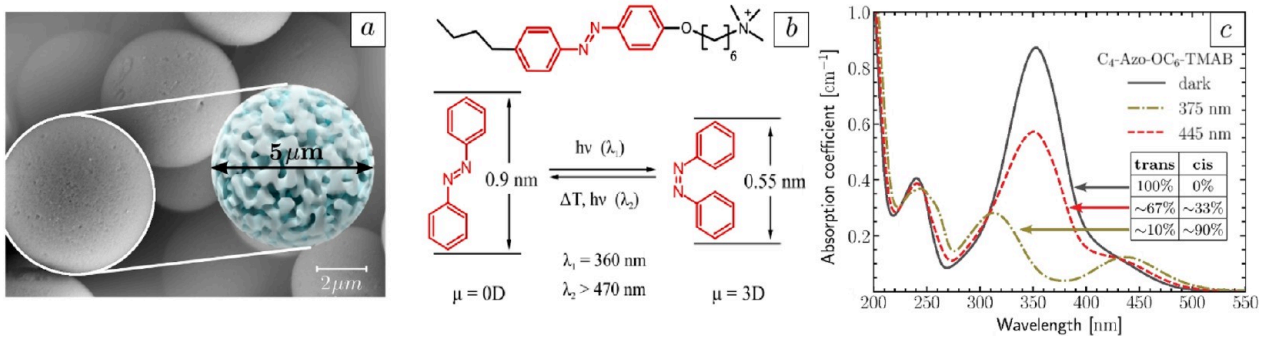

Figure 2. (a) SEM image and scheme of the porous particle of 5 μm in diameter and pore size of 6 nm. (b) Chemical structure of the azobenzene containing cationic surfactant (C_4-azo-OC_6TMAB). Shown below is a scheme of azobenzene photoisomerization. (c) UV−vis spectra of C_4-azo-OC_6TMAB in different photostationary states: dark (black line), after irradiation with UV light of λ = 375 nm (green dashed line), and blue light of λ = 445 nm (red dash-dotted line).

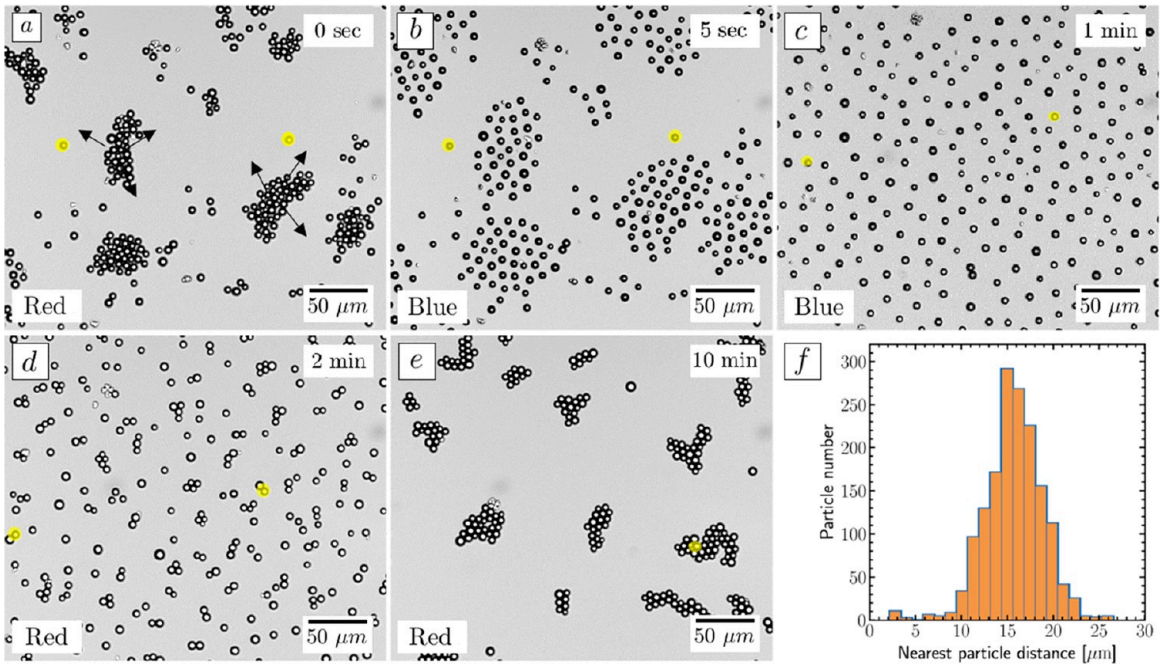

Figure 3. Optical micrographs of porous silica particles (d = 5 μm) trapped at a glass surface and immersed into aqueous solution of azobenzene containing surfactant (c_{azo} = 1 mM). (a) Before irradiation particles aggregate, (b) after switching on irradiation with blue light (λ = 450 nm, I = 1.5 mW/cm^2), the particles move apart and reach a stable state with a narrow, unimodal distribution of interparticle distances (c). The isolated particles (marked in yellow in all micrographs) do not move at the beginning of irradiation. (d−e) After switching off illumination, the particles reaggregate within minutes. (f) Nearest particle distance (NPD) distribution calculated from part c. In Figure S1 (Supporting Information) the corresponding video is provided.

When studying an ensemble of such particles at a solid surface, the local repulsion generated around each colloid (of 5 μm in diameter) results in 2-dimensional crystalline arrangement of particles with equalized interparticle distances varying between 7 and 85 μm depending on the particle surface density. A subsequent change to nonisomerizing red light eliminates local LDDO flow restoring the particle aggregates. The separation/aggregation process can be repeated indefinitely by periodically changing the wavelength of the applied irradiation. We note that particle separation is a result of a light driven diffusio-osmotic flow (LDDO) generated by every single particle on its own. The key to understanding the relevant processes is related to the role played by the pore walls, providing a large area to which surfactant molecules can adsorb. Effectively, porous particles act as sources and sinks of surfactants depending on the illumination wavelength, and this results in a concentration gradient of surfactants inside and outside of the particles. This technique's forté lies in the fact that long-range repulsion can be established and tuned in a spatiotemporal way.

EXPERIMENTAL SECTION

Materials. Nanoporous silica microspheres of d = 5 μm in diameter are purchased from Micromod (Sicastar, prod. nr. 43-00-503, Germany). The particles have a porosity of 850 m^2/g (the diameter of the pores is ca. 6 nm) and are otherwise unmodified. The porous particles are dispersed in an aqueous solution at different concentrations ranging between 0.005 and 0.5 mg/mL. The nonporous particles of 1.5 μm in diameter are purchased from Micromod (Sicastar, Germany).

The azobenzene containing trimethylammonium bromide surfactant (C_4-Azo-OC_6TMAB) is synthesized as described before.[21] The surfactant (Figure 2b) consists of a spacer of 6 methylene groups

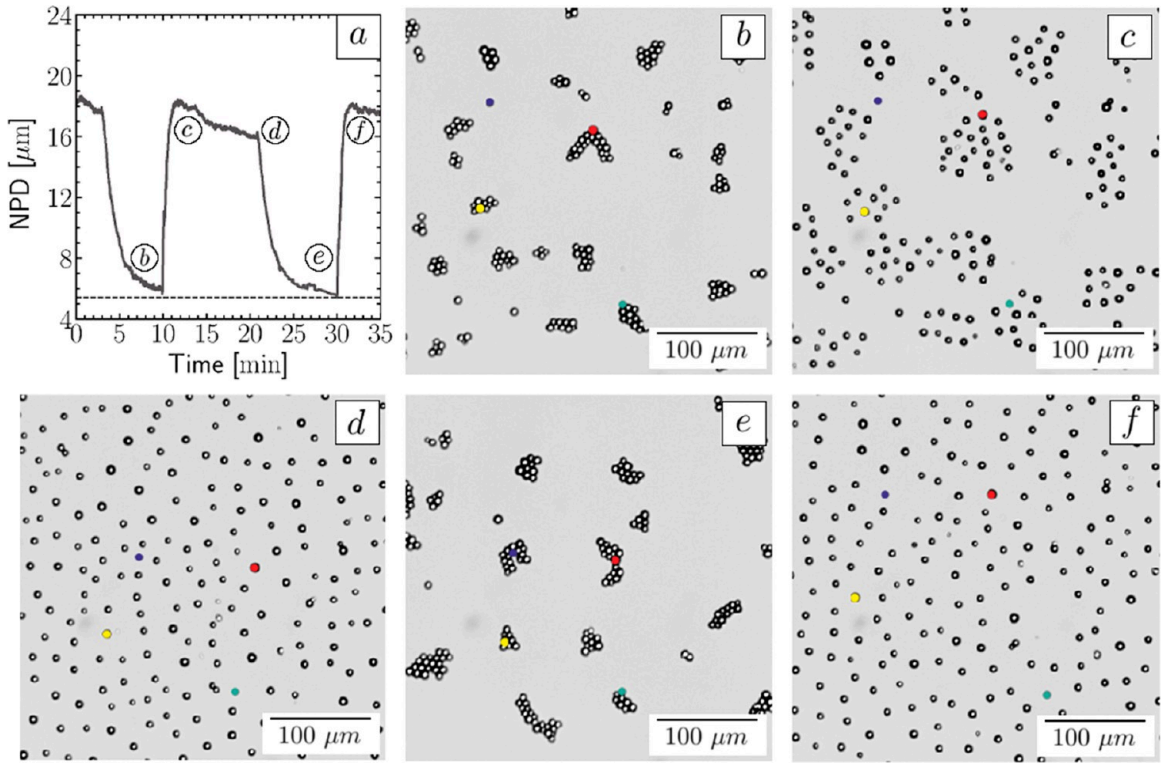

Figure 4. (a) Dependence of the nearest particle distance (NPD) on irradiation wavelength and time. Time t = 0 corresponds to the particle ensemble forming a periodic grid under irradiation with an average NPD of 17 μm. (b–f) Optical micrographs taken at irradiation steps marked in a: (b) at the end of particle aggregation under red illumination, (c) beginning of particle separation (second cycle) under blue light, (d) stable particle pattern under blue irradiation, (e) aggregated state, (f) separated particles during the third irradiation cycle. Single colored colloids (red, green, blue, and yellow) have been tracked to illustrate the extent of particle motion in the micrograph area. The corresponding video is provided in Figure S2, Supporting Information.

between the positively charged trimethylammonium bromide headgroup and the azobenzene unit with a bythyl tail attached. The surfactant is dissolved in Milli-Q water and diluted to the required concentrations ranging from 0.1 to 2 mM.

The aqueous dispersion of the silica particles is mixed with surfactant solution at different concentrations and kept at least 2 h for equilibration. A closed chamber (Gene Frames of size 1.5 × 1.5 cm^2 and height at 250 μm) with a volume of 65 μL is used in order to provide a closed environment, i.e. eliminate water/air interface. All samples are kept in the dark or in red light to prevent unwanted photoisomerization.

The photoisomerization behavior of the surfactant is described in detail in the previous publication.[22] The *trans* isomer has a characteristic absorption band (π–π* transition) with a maximum at 351 nm (Figure 2c). The spectrum of the *cis* isomer is characterized by two absorption bands with maxima at 313 nm (π–π* transition) and at 437 nm (n–π* transition). The lifetime of the *cis* isomer in the dark or under illumination with red light of λ = 600 nm is 48 h, while the photoisomerization from a *cis* to a *trans* state under irradiation with blue light (λ = 450 nm, I = 1.5 mW/cm^2) takes place within a few seconds, approaching a photostationary state after 10 min of irradiation at which a fraction of *trans* isomers of 66% is achieved. Under UV illumination (λ = 375 nm) at the photostationary state, the surfactant molecules are predominantly in a *cis* state with a fraction of 90%.

Methods. An inverted Olympus IX71 equipped with a tunable monochromatic light source (Polychrome V, FEI Munich GmbH) acts as illumination and lighting source. The illumination intensity is measured by an optical power meter 1918-R with sensor 918D-UV-OD3R (Newport Corporation, Irvine, CA, USA). Images are acquired with an Olympus XM10 monochrome camera at a speed of maximal 14 frames per second or a Hamamatsu Orca Flash 4.0 at 100fps. The setup is kept in dark to prevent uncontrolled isomerization. Motion of silica particles on a glass substrate is studied under illumination from the top with a monochromatic light of λ = 450 nm (blue, I = 1.5 mW/cm^2) and λ = 600 nm (red, I = 2 mW/cm^2) wavelengths. The intensity of irradiation is kept constant over the whole imaging area.

Particle motion is tracked using the Mosaic Single Particle Tracking plugin for ImageJ (Rasband, W.S., ImageJ, U.S. National Institutes of Health, Bethesda, Maryland, USA). The tracking algorithm is described by Koumoutsakos.[23] Motion analysis and calculation has been implemented in Matlab.

UV–vis spectroscopy (Cary 5000 UV-vis-NIR spectrophotometer, Agilent Technologies, USA) is used to measure the amount of surfactant absorbed by porous colloids.

A scanning electron microscope (Ultraplus 4061, Zeiss, Germany) is utilized to characterize colloidal particles.

RESULTS

The porous particles (d = 5 μm, pore size = 6 nm, Figure 2a) are dispersed in aqueous solution of photosensitive surfactants (c_{azo} = 1 mM) (Figure 2b) and their dispersion is placed in a closed chamber placed in the optical microscope as described in the Experimental Section.

Without illumination (the imaging is performed under red light which does not result in surfactant photoisomerization) the porous particles sediment to a solid surface (glass) and form different aggregates (Figure 3a). The image acquisition is performed under illumination with red light of λ = 600 nm, at which no photoisomerization of the azobenzene takes place. When blue light (λ = 450 nm) is switched on, the particles start to move, repel each other, and form a stable grid with a rather narrow distribution of interparticle distances (Figures

https://dx.doi.org/10.1021/acs.langmuir.9b03270

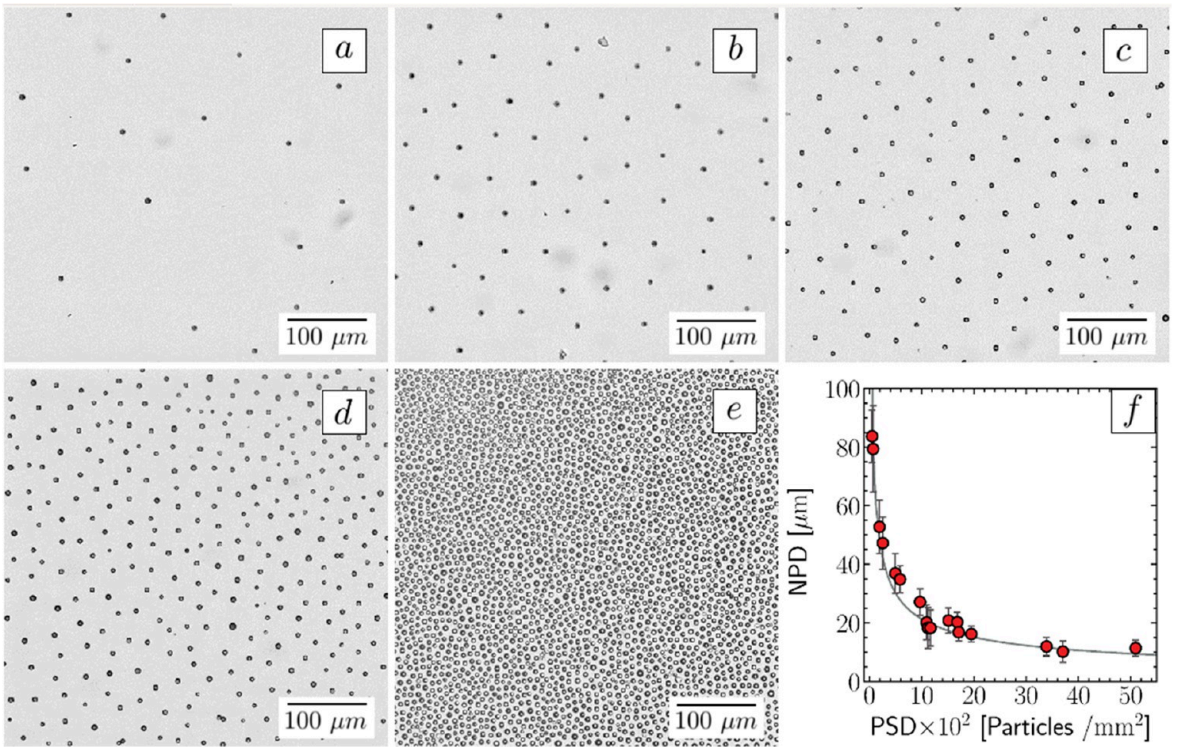

Figure 5. Optical micrographs of porous silica particles (d = 5 μm) in 1 mM azobenzene containing surfactant aqueous solution under blue illumination at different particle surface densities (PSD): (a) 0.8 × 10^2, (b) 3.4 × 10^2, (c) 5.5 × 10^2, (d) 1.6 × 10^3, and (e) 10^4 mm^{-2}. (f) Nearest particle distance (NPD) shown as a function of the particle surface density for surfactant concentration of 1 mM. The black line represents the exponential fit of the data.

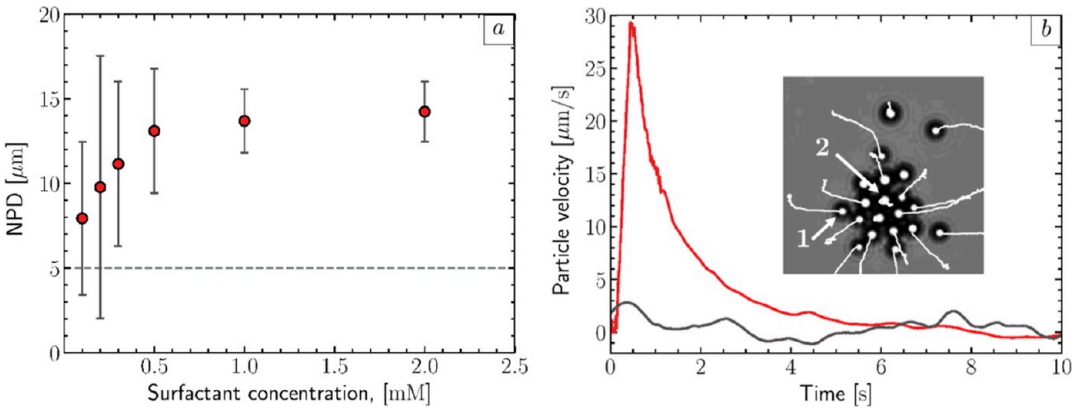

Figure 6. (a) Averaged nearest particle distance (NPD) as a function of surfactant concentration at fixed particle concentration (PSD = 3 × 10^3 mm^{-2}). The dashed gray line indicates the particle distance in the aggregated state. (b) Particle velocities as a function of time: red curve depicts the velocity variation of the outer particle (1), while the black line corresponds to the particle (2) in the center of the aggregate. The trajectories of the particles are marked by white lines on the inserted micrographs.

3b, c). For this particular example, the distance between the particles is measured to be of ca. 15 μm (Figure 3f).

The periodic lattice of distant particles is maintained throughout the whole irradiation time (at least during several hours). In this time scale, the particles are essentially trapped at the positions of lattice sites, with some fluctuations due to Brownian motion (see video in Figure S1, Supporting Information). As will be interpreted below, the long-range repulsion arises since porous particles become micropumps generating liquid flows. Isolated particles (for example the particles marked yellow in Figure 3) do not show displacement at the beginning of irradiation. But they start to repel strongly if they are initially located in the vicinity of each other. After switching off the external light source, the long-range repulsion ceases and the particles reaggregate within a few minutes (Figures 3d, e). This separation/aggregation cycle can be conducted many times just by applying the irradiation protocol repetitively with two different wavelengths, blue light (separation) and red light (aggregation) (Figure 4, and video in Figure S2, Supporting Information). To characterize the particle distribution, we introduce the so-called nearest particle distance (NPD) parameter, which is defined as the smallest average distance to a neighboring particle.

Figure 4a shows the dependence of the NPD on irradiation time and wavelength for the particle ensemble subjected to blue light (λ = 450 nm). The particles are separated every time

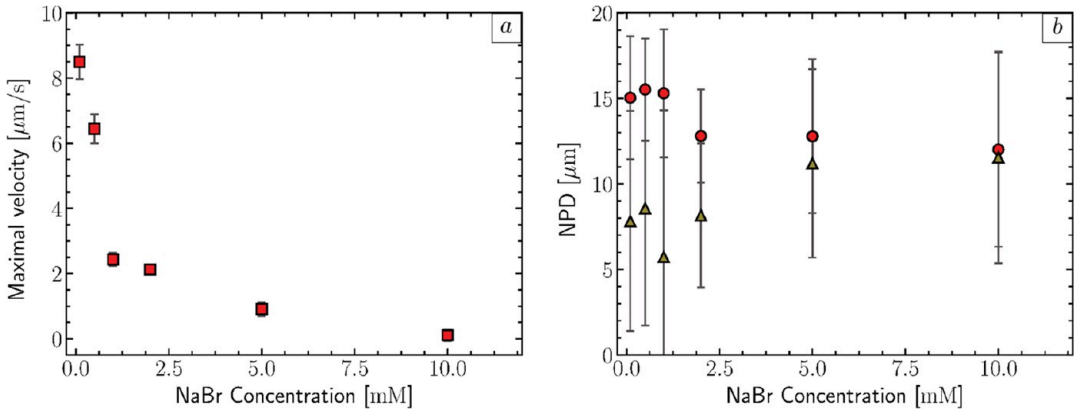

Figure 7. (a) Maximal velocity averaged over many particles under irradiation with blue light and (b) the NPD as a function of the NaBr concentration. Increasing the salt concentration reduces the effectiveness of particle separation under irradiation. Particle motion is completely suppressed at a concentration of 10 mM. Surfactant concentration is fixed to 1 mM and the PSD is $35 \times 10^2/\mathrm{mm}^2$ for all measurements. The red points indicate NPD during blue irradiation, while the gray triangles depict it under red light. Corresponding videos of particle repulsion are presented in Figure S4 in the Supporting Information.

when the blue light is switched on forming a pattern/grid with a well-defined NPD of 17 μm (Figures 4d, f). The separation takes place within the first seconds of irradiation (Figure 6b). When the blue light is switched off the NPD decreases down to 5 μm revealing ongoing aggregation and saturates after ca. 5 min (Figure 4a).

It was found that the greatest achievable distance between particles depends on their number density per unit area (at fixed surfactant concentration and irradiation intensity), i.e. the particle surface density (PSD). Figure 5 shows the dependence of this distance on the PSD during irradiation with blue light. ca. 85 μm (PSD of 80 particles/mm^2) (Figure 5a). Note that this is currently the minimum density detectable within our experimental setup, and it is likely that the repulsion can be observed at larger distances. With increasing the particle concentration, the distance between the particles decreases as shown in Figure 5f. The smallest measured NPD is about 7 μm for a PSD of $\sim 10^4$ particles/mm^2 (Figure 5e). At large surface densities, switching on blue light at the beginning of the particle separation process some of them "jump" off the surface followed by readsorption as soon as free areas are generated by repulsion (see videos in Figure S3, Supporting Information).

The extent of particle separation also depends on the surfactant concentration. With increasing surfactant concentration, the repulsive strength increases resulting in a larger NPD at fixed surface particle density (Figure 6a). Starting from ca. 0.5 mM (critical micelle concentration) the NPD saturates. The particle velocity during the separation process is shown in Figure 6b. Following particle trajectories recorded during the transition from the aggregated to the well-separated state reveals that most particles move away from the center of a cluster in radial direction except particles initially located at the center of the aggregate (Figure 6b, inset). These particles remain at their initial positions implying that the forces on these particles are balanced. The particles at the periphery of the aggregate lack neighbors; therefore, an effective force drives those outward. This observation would, for example, be consistent with a repulsive interaction between particles. The velocity of the particles under illumination with blue light increases to a maximal value within the first 0.5 s of irradiation and then slowly drops to zero within 10 s: the time it takes to reach the stationary lattice (Figure 6b shows a velocity of particles marked by 1 and 2). A similar trend in the variation in particle velocity is observed for all surfactant concentrations in the range between 0.2 and 2 mM. The absolute value of the maximum velocities, however, depends on many parameters such as surfactant concentration, particle surface density, and the position within the particle aggregate.

Particle repulsion is suppressed by increasing the ionic strength of the surfactant solution. Adding NaBr results in a decrease of the maximum particle velocity showing complete suppression of particle motion at 10 mM NaBr (Figure 7a). Furthermore, this effect can be observed analyzing the NPD as a function of salt concentration (Figure 7b). The difference in NPD in the dark and after 10 s of illumination with blue light decreases with salt concentration. In Figure S4 one can see the process of particle repulsion under blue light recorded for several salt concentrations. Up to 2 mM NaBr when the Debye length drops down to ca. 6 nm, the particle repulsion is still pronounced, while from 5 mM NaBr on, particle motion is suppressed.

Based on the results described above we can propose the following mechanism of the light-driven reversible particle repulsion/aggregation process. An explanation for an emerging flow can be obtained if we invoke LDDO. This diffusio-osmotic flow originates due to gradients of *trans* and *cis* isomer concentrations in the lateral direction induced by illumination, being driven by an electrostatic diffuse layer (EDL) of thickness of the order of Debye length of electrolyte solution, λ_D:[14]

$$v^{\mathrm{LDDO}} = -\frac{k_B T}{\eta}\left[\frac{\partial(\Gamma_{\mathrm{EDL}}\lambda_D)}{\partial c_c}\nabla c_c + \frac{\partial(\Gamma_{\mathrm{EDL}}\lambda_D)}{\partial c_t}\nabla c_t\right] \quad (1)$$

where $k_B T$ is the thermal energy, η is the dynamic viscosity of the solution, $\frac{\partial(\Gamma_{\mathrm{EDL}}\lambda_D)}{\partial c_{t,c}}$ are the characteristic adsorptions of *trans* and *cis* isomers to the surface, $\nabla c_{t,c}$ are gradients of the concentrations of corresponding isomers, and $c_{t,c}$ are concentrations of *trans* and *cis* isomers in the vicinity of the porous particle.

According to 1, the LDDO flow is generated due to the excess concentration of surfactant near the porous particle, which in turn causes the local excess near the surface and a large gradient of osmotic pressure. For this effect to occur, it is necessary to have a certain asymmetry in the system, otherwise

https://dx.doi.org/10.1021/acs.langmuir.9b03270

the opposing gradients of the two surfactant isomers will cancel each other. In our previous work[14] such an asymmetry emerges due to focused illumination (creating two distinct zones: inside and outside of the laser beam), different CMCs for *trans* and *cis* isomers (in our case CMCs for *trans* and *cis* differ significantly[24] (CMC for the *cis* isomer in our case is 8 times higher) and stronger interaction of the *cis* isomer with the surface. In this way one generates a stronger concentration gradient near the surface for the *cis* form. In the current work the illumination is global, but *trans* and *cis* forms have different absorption affinity into the porous particles.

Electrochemical potentials of *trans* and *cis* isomers follow the usual distribution that depends on their concentrations:

$$\mu_{c,t} = \mu_{0\,c,t} + k_B T \ln c_{t,c} + ze\Phi \tag{2}$$

where μ_0 is defined far from the particles, and c (surfactant concentration) and Φ (electrostatic potential) vary in inner and outer regions of the porous particle. This expression holds below the CMC for each type of isomer. However, for *trans* isomers, which are capable of forming aggregates both inside and outside the particle, we have to take those surfactant aggregates into account, so in equilibrium the chemical potentials outside and inside the particles yield:

$$k_B T \ln c_{0,t} = k_B T \ln \mathrm{CMC}_t + \frac{k_B T}{N} \ln \frac{C_t - \mathrm{CMC}_t}{N} + ze\Phi \tag{3}$$

where $c_{0\,t,s}$ is the bulk concentration of the *trans*-/*cis*-surfactants, CMC_t is the critical micelle concentration of the trans-isomer, N is the packing factor, that stands for the number of surfactant molecules per aggregate and can differ in the outside region (where aggregates are micelles) and inside the pores, and C_t is the total concentration of trans-isomers inside the porous particle. Assuming that CMC_t inside the pores is vanishing,[25] eq 3 reduces to

$$C_t \simeq N\left(\frac{c_{0,t}}{\mathrm{CMC}_t}\right)^N \exp\left(-\frac{Nze\Phi}{k_B T}\right) \tag{4}$$

Note that here Φ is a function of C_t, since the charge inside the pores is screened stronger for larger surfactant concentrations. For *cis* isomers, however, which have a substantially higher CMC, and thus are incapable of forming aggregates inside the pores, the equilibrium concentrations should follow a Boltzmann distribution:

$$c_c = c_{0,c} \exp\left(-\frac{ze\Phi}{k_B T}\right) \tag{5}$$

Experimental results support this model. Indeed, without irradiation, the surfactant molecules are mostly in their stable *trans* isomer and are absorbed in the particle pores. Due to high particle porosity, the amount of the absorbed surfactant is quite high and increases with surfactant concentration. For instance, at c_0 = 1 mM of initial surfactant concentration, only 0.3 mM is left in solution after dispersion of porous particles (Table S1, Supporting Information). It is plausible that such an efficient sorption of surfactants is due to a gain in free energy upon micellization in the particle interior.[25] This scenario is also supported by UV−vis absorption measurements where the hypsochromic shift from 353 to 348 nm is visible indicating formation of aggregates within the particles.[16] The absorption of the surfactant molecules results in a change of the ζ-potential of the particles from −20 ± 5 mV (without surfactant) to +26 ± 9, +33 ± 3, and +39 ± 5 mV for surfactant concentrations 0.3, 1, and 2 mM, respectively. Having now analyzed the distribution of isomers in- and outside of the porous particles in the dark, let us consider further the situation under illumination.

What happens, then, when the blue light is switched on? Since the porous particles are transparent to wavelengths of 450 nm, upon irradiation with blue light the photoisomerization of the surfactant takes place not only in solution but also within the particles. *Trans* isomers are converted to *cis* and, therefore, break the aggregates inside the pores, which leads to a drastic increase of inner surfactant concentration, exceeding the value given by eq 5 and prompting the accelerated escape of excess *cis* molecules. The excess inner concentration of *cis* isomer can be estimated from eqs 4−5:

$$\Delta C_c \simeq \frac{2}{3} N\left(\frac{c_{0,t}}{\mathrm{CMC}_t}\right)^N \exp\left(-\frac{Nze\Phi}{k_B T}\right) \tag{6}$$

where N can be found from the equilibrium measurements of surfactant uptake by porous particles (Table S1, Supporting Information): $N \sim 5-10$.

As soon as the illumination is turned on, there appears a nonequilibrium concentration distribution of *cis* molecules in the vicinity of a single porous particle. In other words, the *trans*−*cis* photoisomerization should result in a release of the *cis* isomer out of the pores (Figure 8). The release of the *cis* isomers is governed by two factors, an increased osmotic pressure within the particles (since the micelles formed within the particles by *trans* isomers are destroyed during photoisomerization), and the effect of the increased hydrophilicity of the *cis* isomer.[19] As a result, a concentration gradient of the isomers around the single particle is generated inducing a diffusio-osmotic flow pointing away of the particles (red arrows in Figure 8).

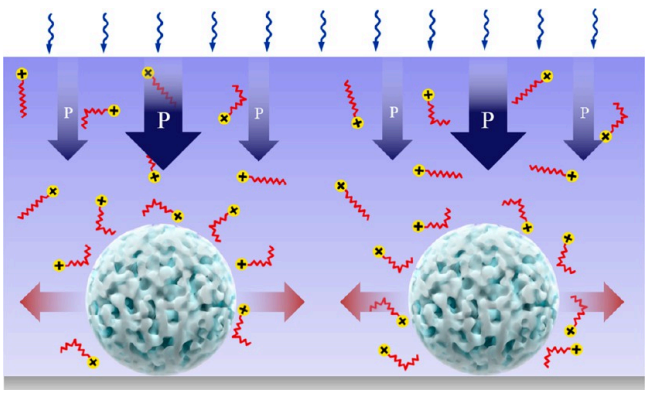

Figure 8. Scheme of light driven diffusio-osmotic flow generated at single porous particles under irradiation with blue light. The excess concentration of the *cis*-isomers around the particle is generated during desorption of the surfactant molecules out of the particle. The blue arrows indicate schematically the local distribution of osmotic pressure. The red arrows depict the direction of hydrodynamic flow pattern at the particle level.

This indicates that the particles act as an effective source of *cis*-isomers released out of the interior during irradiation. In this way, each single porous particle generates its own local radial flow, acting as a micropump. When two or more

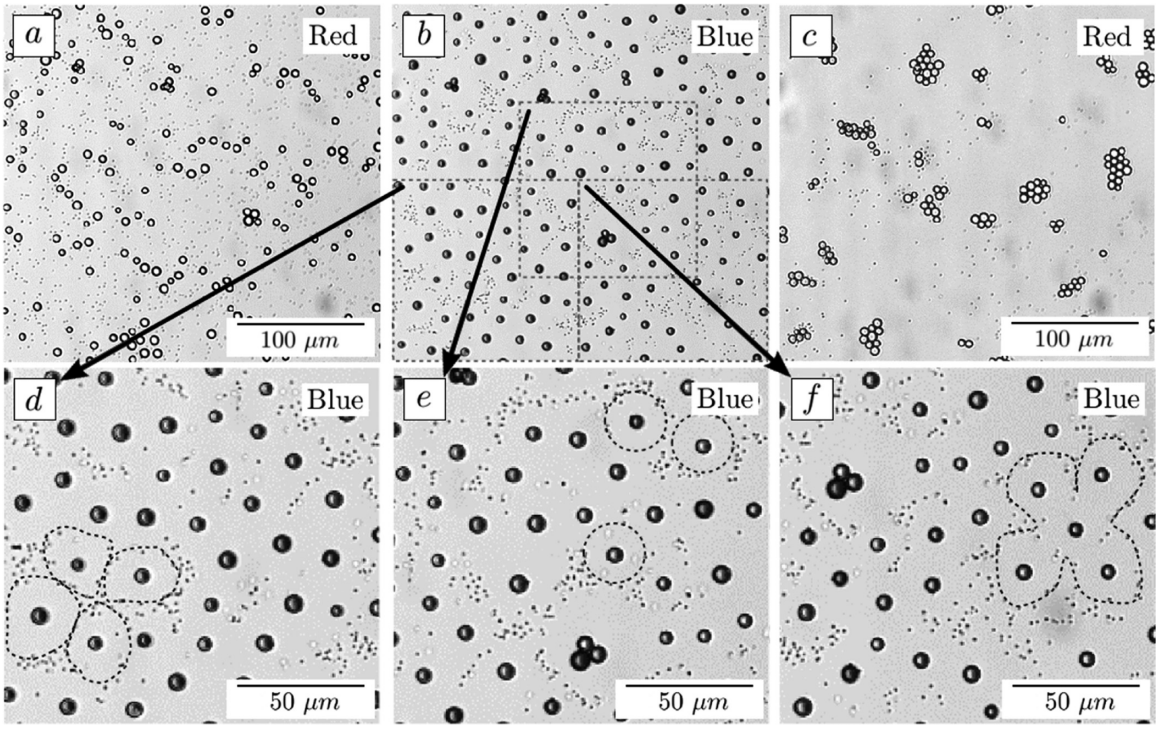

Figure 9. Optical micrographs showing the motion of porous (d = 5 μm) and nonporous (1.5 μm) silica particles dispersed in 1 mM surfactant solution and exposed to illumination with (a) red light, (b) blue light (450 nm), and subsequently (c) red light. (d–f) Enlargements of the selected areas in b. The corresponding movie is provided in Figure S5, Supporting Information.

particles are close to each other, these flows lead to a diffusio-osmotic repulsion resulting in a separation of particles.

In order to estimate the magnitude of the flow, we only take into account the gradient of the *cis* surfactant from eq 1:

$$v^{\mathrm{LDDO}} = -\frac{k_{\mathrm{B}}T}{\eta}\frac{\partial(\Gamma_{c\mathrm{EDL}}\lambda_{\mathrm{D}})}{\partial c_c}\nabla c_c \tag{7}$$

Approximating the surface excess of *cis* isomers in the EDL near the wall,

$$\Gamma_c = \int_0^\infty [c_+ + c_- - 2c_0]\,\mathrm{d}y \sim c_0\tilde{\phi}_0^2\lambda_{\mathrm{D}}$$

where c_0 is the combined bulk concentration of the surfactant, $c_\pm$ are the concentrations of ions (both salt and surfactant) within EDL, $\tilde{\phi}_0 = e\Phi/k_{\mathrm{B}}T$ is the dimensionless electrostatic potential of the wall, and the concentration gradient is $\nabla c \simeq \frac{\Delta c_c}{D/2}$, where D is the diameter of the particles and Δc_c is local excess of *cis* isomer concentration near the particle, we can estimate the speed of the diffusio-osmotic flow:

$$|v^{\mathrm{LDDO}}| \simeq \frac{\lambda_{\mathrm{D}}^2}{\eta}\frac{k_{\mathrm{B}}T\Delta c_c}{D/2}\left(\frac{e\phi_0}{k_{\mathrm{B}}T}\right)^2 \simeq \frac{k_{\mathrm{B}}T\tilde{\phi}_0^2}{4\pi\eta l_{\mathrm{B}}D}\frac{\Delta c_c}{I} \tag{8}$$

where l_{B} is the Bjerrum length and I is the ionic strength in the bulk.

According to eq 8, the initial velocity close to the particle can be rather high, up to hundreds of micrometers per second but depends strongly on the relative excess concentration $\frac{\Delta c_c}{I}$ and dimensionless electrostatic potential of the wall $\tilde{\phi}_0$. The values of $\frac{\Delta c_c}{I}$ and $\tilde{\phi}_0$ can be found from the experimental data. For the simplest case of $\tilde{\phi}_0 \simeq 1$ we can estimate $\frac{\Delta c_c}{I}$, knowing that $v_{\mathrm{max}}^{\mathrm{LDDO}} \simeq 30$ μm/s is 0.15. The disappearance of motion with increasing NaBr concentration (Figure 7a) can be explained by a decrease in Debye length.[14]

To explore a generated flow in more detail, we visualized the repulsion zone between particles by adding small nonporous colloids to the solution. A mixture of porous and nonporous silica particles of size 5 and 1.5 μm, respectively, is dispersed in 1 mM surfactant solution. The particles are initially distributed on the surface as shown in Figure 9a: porous and nonporous particles form small aggregates as well as single objects and undergo thermal motion near the glass surface. Under illumination with blue light, the porous particles start to repel and form a grid with average particle distance of ca. 14 μm (Figure 9b). At the same time, the small particles are pushed away from the porous colloids and are aligned at the stagnation zones of the local diffusio-osmotic flows (Figures 9b, d–f). This is a strong indication of the radial flows generated by each porous particle under illumination. Switching back to red light leads to vanishing of repulsive interactions, since the local flow around each porous particle stops (Figure 9c).

The wavelength of irradiation plays a key role in the long time stability of particle repulsion and separation. Indeed, a stationary state is attained under irradiation with blue light when the fraction of *trans* and *cis* surfactant molecules in solution shifts to 66% and 34%, respectively (Figure 2c), implying a continuous, steady state *trans*–*cis* and *cis*–*trans* isomerization processes: photogenerated *trans* isomers can continuously diffuse into the porous particle thereby replenishing its stock of *cis* species. Particle repulsion disappears completely when the light is switched off. The surfactant molecules in *trans* state diffuse into the pores of the particles, form aggregates inside and the system equilibrates. In

https://dx.doi.org/10.1021/acs.langmuir.9b03270

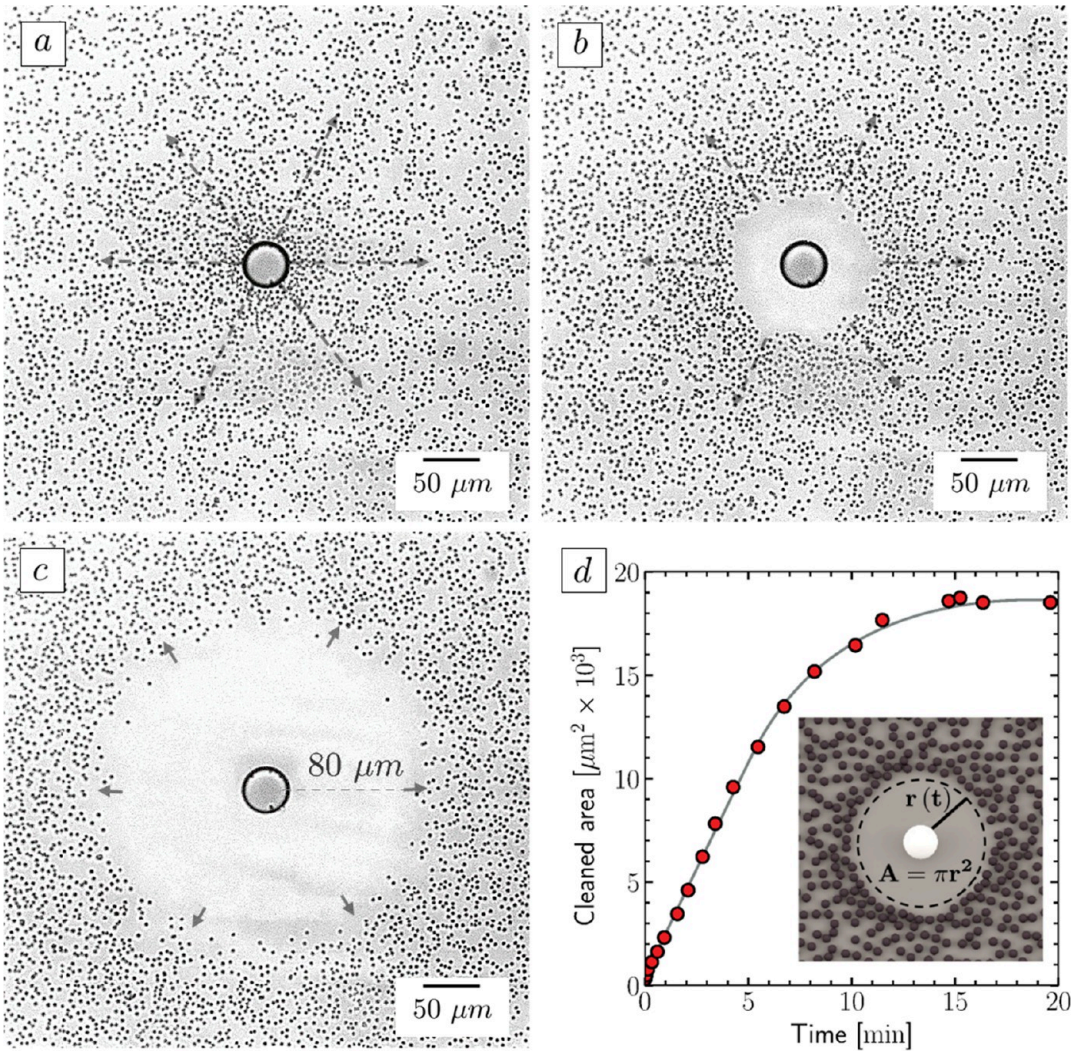

Figure 10. (a–c) Optical micrographs show the motion of small silica particles of 1.5 μm in diameter in the vicinity of a porous silica particle (d = 20 μm). The particles are immersed in aqueous solution of azobenzene containing surfactant (c = 1 mM). Before irradiation, the small particles move randomly and distribute randomly on the surface (see the video in Figure S7, Supporting Information). Under irradiation with blue light (λ = 455 nm, homogeneous intensity distribution), the local LDDO flow around the porous particle repels the small particles (b). Under continuous irradiation the "cleaned area" increases (c). (d) Particle-free area A as a function of irradiation time. The inset shows a scheme depicting the circular parameters. The black line depicts a fit of the data.

contrast, when irradiation is conducted with UV light, after 10 min of irradiation ca. 90% are switched to *cis* exhausting the amount of *trans* isomers, and the LDDO driven flow ceases, i.e. the time for which effective particle repulsion can be observed is much smaller (ca. 10 min). The weakening of repulsion can be observed by a more pronounced Brownian motion of the particles at the spots where they are trapped (Figure S6, Supporting Information).

The generation of the stationary flow under irradiation with blue light generated around the particle is supported by an additional independent experiment. Figure 10 shows the increase of the "cleaned area" around porous particle as a function of irradiation time. Here a single porous particle of 20 μm in diameter is attached to a surface and surrounded by many small nonporous silica colloids (1.5 μm in diameter). During the irradiation with blue light the locally generated LDDO flow around the porous micropump repels the passive small colloids. The cleaned area increases with time and saturates after ca. 10 min of irradiation (Figure 10b). The area stays free of small particles during further irradiation. We can evaluate the velocity of the flow at a given radial distance, r, from the particle of diameter D: $v^{\mathrm{LDDO}}(r) \leq v_0^{\mathrm{LDDO}}\frac{D}{2r}$, which is valid for a stationary flow. Now, in order to estimate how the area of a cleaned spot around the porous particle grows with time, we will consider the radius of the spot r, which satisfies the differential condition: $\mathrm{d}r = v^{\mathrm{LDDO}}\mathrm{d}t \simeq v_0^{\mathrm{LDDO}}\frac{D\,\mathrm{d}t}{2r}$. After integrating, we get $r^2(t) \simeq v_0^{\mathrm{LDDO}}Dt$ or, for the area $A(t) \simeq \pi v_0^{\mathrm{LDDO}}Dt$. This analysis, therefore, implies that a linear dependence of A on time might indicate the stationary DO flow at the surface of the porous particle, which, in turn, indicates a steady generation of the *cis* surfactant.

CONCLUSIONS

We report extremely long-range repulsion of porous microparticles induced by LDDO flow, with each particle serving as a micropump that efficiently pushes its neighbors away. We unraveled the mechanism responsible for this phenomenon to be comprised of several equally crucial factors. First, the micropumps are triggered by the conformational change in

photosensitive surfactant due to a *trans*−*cis* isomerization of the incorporated azobenzene group in its hydrophobic tail. Second, these surfactant molecules are absorbed in the pores of the microparticles due to the aggregates formed by surfactant molecules in *trans* conformation. We prove this to be an important step, since nonporous particles do not demonstrate the repulsive behavior. Third, after irradiation the newly formed *cis* molecules leave the pores, thus generating a significant excess concentration near the colloids' surfaces. This transition leads to the generation of an LDDO flow, rendered possible by the fourth factor: the presence of a charged wall, on which the colloids are sitting.

This combination of four factors was studied in detail, and the dependence of particle separation, initial drift velocity, meta-2D-crystallic state stability on factors such as particle, surfactant, and salt concentration, and irradiation wavelength is reported. We have also demonstrated how our system can be tuned in order to facilitate fast aggregation/separation of colloidal suspension with optical irradiation. This route opens a vast spectrum of possibilities for simplified particle manipulation, including but not limited to delicate surface cleaning, microfluidics and "lab-on-a-chip" applications, precise structures and pattern formations in colloid suspensions, and others.

■ ASSOCIATED CONTENT

Supporting Information

The Supporting Information is available free of charge at https://pubs.acs.org/doi/10.1021/acs.langmuir.9b03270.

Supplementary Videos Figure S1, Figure S2, Figure S3 (includes 5 videos), Figure S4 (includes 6 videos), Figure S5, Figure S6, and Figure S7 provide movies of particle motion under blue and UV irradiation (ZIP)

Supplementary Table S1 represents the amount of surfactant molecules absorbed in porous particles as a function of bulk surfactant concentration (PDF)

■ AUTHOR INFORMATION

Corresponding Authors

Svetlana A. Santer − *Institute of Physics and Astronomy, University of Potsdam, 14476 Potsdam, Germany;* orcid.org/0000-0002-5041-3650; Email: santer@uni-potsdam.de

Olga I. Vinogradova − *A.N. Frumkin Institute of Physical Chemistry and Electrochemistry, Russian Academy of Sciences, 119071 Moscow, Russia; DWI-Leibniz Institute for Interactive Materials, RWTH Aachen, 52056 Aachen, Germany;* orcid.org/0000-0002-3327-162X; Email: oivinograd@yahoo.com

Authors

David Feldmann − *Institute of Physics and Astronomy, University of Potsdam, 14476 Potsdam, Germany*

Pooja Arya − *Institute of Physics and Astronomy, University of Potsdam, 14476 Potsdam, Germany*

Taras Y. Molotilin − *A.N. Frumkin Institute of Physical Chemistry and Electrochemistry, Russian Academy of Sciences, 119071 Moscow, Russia*

Nino Lomadze − *Institute of Physics and Astronomy, University of Potsdam, 14476 Potsdam, Germany*

Alexey Kopyshev − *Institute of Physics and Astronomy, University of Potsdam, 14476 Potsdam, Germany*

Complete contact information is available at: https://pubs.acs.org/10.1021/acs.langmuir.9b03270

Author Contributions

S.A.S. and O.I.V. designed and supervised the project and wrote the manuscript. D.F., P.A., and A.K. performed the device fabrication, measurements, and analysis of the experimental data. N.L synthesized the photosensitive surfactant. T.Y.M. and O.I.V. developed the theory. All authors contributed to the final version of manuscript.

Notes

The authors declare no competing financial interest.

■ ACKNOWLEDGMENTS

This research is supported by the Priority Program 1726 "Microswimmers-From Single Particle Motion to Collective Behaviour", Germany; DFG (SA1657/9-2 and VI 243/4-2), Helmholtz Graduate School on Macromolecular Bioscience (Teltow, Germany), and the Russian Ministry of Education and Science. We thank C. Beta (University of Potsdam) for technical support during measurements with optical microscopy and fruitful discussions.

■ REFERENCES

(1) Li, B.; Zhou, D.; Han, Y. Assembly and phase transitions of colloidal crystals. *Nat. Rev. Mater.* **2016**, *1*, 15011.

(2) Wagner, N. J.; Brady, J. F. Shear thickening in colloidal dispersions. *Phys. Today* **2009**, *62*, 27−32.

(3) Liang, Y.; Hilal, N.; Langston, P.; Starov, V. Interaction forces between colloidal particles in liquid: Theory and experiment. *Adv. Colloid Interface Sci.* **2007**, *134*−*135*, 151−166.

(4) Anderson, V. J.; Lekkerkerker, H. N. W. Insights into phase transition kinetics from colloid science. *Nature* **2002**, *416*, 811−815.

(5) Padding, J. T.; Louis, A. A. Hydrodynamic interactions and Brownian forces in colloidal suspensions: Coarse-graining over time and length scales. *Phys. Rev. E* **2006**, *74*, 031402.

(6) Soyka, F.; Zvyagolskaya, O.; Hertlein, C.; Helden, L.; Bechinger, C. Critical Casimir Forces in Colloidal Suspensions on Chemically Patterned Surfaces. *Phys. Rev. Lett.* **2008**, *101*, 208301.

(7) Martínez-Pedrero, F.; Tierno, P. Advances in colloidal manipulation and transport via hydrodynamic interactions. *J. Colloid Interface Sci.* **2018**, *519*, 296−311.

(8) Schlesener, F.; Hanke, A.; Dietrich, S. Critical Casimir Forces in Colloidal Suspensions. *J. Stat. Phys.* **2003**, *110*, 981−1013.

(9) Poulin, P.; Cabuil, V.; Weitz, D. A. Direct Measurement of Colloidal Forces in an Anisotropic Solvent. *Phys. Rev. Lett.* **1997**, *79*, 4862−4865.

(10) Berner, J.; Müller, B.; Gomez-Solano, J. R.; Krüger, M.; Bechinger, C. Oscillating modes of driven colloids in overdamped systems. *Nat. Commun.* **2018**, *9*, 999.

(11) Ciliberto, S. Experiments in Stochastic Thermodynamics: Short History and Perspectives. *Phys. Rev. X* **2017**, *7*, 021051.

(12) Malescio, G.; Pellicane, G. Stripe phases from isotropic repulsive interactions. *Nat. Mater.* **2003**, *2*, 97−100.

(13) Quesada-Perez, M.; Moncho-Jorda, A.; Martınez-Lopez, F.; Hidalgo-Alvarez, R. Probing interaction forces in colloidal monolayers: Inversion of structural data. *J. Chem. Phys.* **2001**, *115*, 10897−10902.

(14) Feldmann, D.; Maduar, S. R.; Santer, M.; Lomadze, N.; Vinogradova, O. I.; Santer, S. Manipulation of small particles at solid liquid interface: light driven diffusioosmosis. *Sci. Rep.* **2016**, *6*, 36443.

(15) Eastoe, J.; Vesperinas, A. Self-assembly of light-sensitive surfactants. *Soft Matter* **2005**, *1*, 338−347.

(16) Zakrevskyy, Y.; Roxlau, J.; Brezesinski, G.; Lomadze, N.; Santer, S. Photosensitive surfactants: Micellization and interaction with DNA. *J. Chem. Phys.* **2014**, *140*, 044906.

(17) Rau, H. Photoisomerization of Azobenzenes. In *Photochemistry and Photophysics*; Rabek, J. F., Ed.; CRC Press, Inc., 1990; pp 119−142.
(18) Liu, X.; Abbott, N. L. Spatial and temporal control of surfactant systems. *J. Colloid Interface Sci.* **2009**, *339*, 1−18.
(19) Montagna, M.; Guskova, O. Photosensitive Cationic Azobenzene Surfactants: Thermodynamics of Hydration and the Complex Formation with Poly(methacrylic acid). *Langmuir* **2018**, *34*, 311−321.
(20) Santer, S. Remote control of soft nano-objects by light using azobenzene containing surfactants. *J. Phys. D: Appl. Phys.* **2018**, *51*, 013002.
(21) Zakrevskyy, Y.; Cywinski, P.; Cywinska, M.; Paasche, J.; Lomadze, N.; Reich, O.; Löhmannsröben, H.-G.; Santer, S. Interaction of photosensitive surfactant with DNA and poly acrylic acid. *J. Chem. Phys.* **2014**, *140*, 044907.
(22) Zakrevskyy, Y.; Richter, M.; Zakrevska, S.; Lomadze, N.; Klitzing, R.; Santer, S. Light-Controlled Reversible Manipulation of Microgel Particle Size Using Azobenzene-Containing Surfactant. *Adv. Funct. Mater.* **2012**, *22*, 5000−5009.
(23) Sbalzarini, I. F.; Koumoutsakos, P. Feature point tracking and trajectory analysis for video imaging in cell biology. *J. Struct. Biol.* **2005**, *151*, 182−195.
(24) Hayashita, T.; Kurosawa, T.; Miyata, T.; Tanaka, K.; Igawa, M. Effect of structural variation within cationic azo-surfactant upon photoresponsive function in aqueous solution. *Colloid Polym. Sci.* **1994**, *272*, 1611−1619.
(25) Rumyantsev, A. M.; Santer, S.; Kramarenko, E. Y. Theory of Collapse and Overcharging of a Polyelectrolyte Microgel Induced by an Oppositely Charged Surfactant. *Macromolecules* **2014**, *47*, 5388−5399.

Supporting Information

Extremely Long-Range Light-Driven Repulsion of Porous Microparticles

David Feldmann, Pooja Arya, Taras Y. Molotilin, Nino Lomadze, Alexey Kopyshev, Olga I. Vinogradova,* and Svetlana A. Santer*

Table S1: Dependence of the amount of adsorbed surfactant within the porous particles on bulk surfactant concentration. Amount of surfactant adsorbed per mg (second column) when 5µm porous particles with 6nm in pore size are added to the surfactant solution of different concentrations. Concentration of the surfactant left in the solution, $C_{residual}$, is in the last column. The adsorption is given in various units.

C_{azo}/mM	C_{azo} (µmol/mg)	Molecule/nm^2*	(Molecule/Particle)**	$C_{residual}$/mM
0.5	0.06	0.04	$0.5 \cdot 10^{10}$	0.29
1	0.21	0.14	$1.5 \cdot 10^{10}$	0.3
2	0.35	0.25	$2.5 \cdot 10^{10}$	0.8

* Adsorbed density of the surfactant in units of molecules per nm^2

** Number of surfactant molecules absorbed by one particle

Light driven diffusioosmotic repulsion and attraction of colloidal particles

Pooja Arya[1], Joachim Jelken[1], David Feldmann[1,2], Nino Lomadze[1], Svetlana Santer[1*]

[1]*Institute of Physics and Astronomy, University of Potsdam, 14476 Potsdam, Germany*
[2]*School of Mechanical Engineering, Tel-Aviv University, Tel-Aviv 6997801, Israel*

TITLE RUNNING HEAD: Light induced motion of particles, azobenzene containing surfactant, porous particles

KEYWORDS: azobenzene containing cationic surfactants, light induced motion of particles, light driven diffusioosmosis, porous colloids

ABSTRACT

In this paper we introduce the phenomenon of light driven diffusioosmotic long-range attraction and repulsion of porous particles under irradiation with UV light. The change in the inter-particle interaction potential is governed by flow patterns generated around single colloids and results in reversible aggregation or separation of the mesoporous silica particles that are trapped at a solid surface. The range of the interaction potential extends to several times the diameter of the particle and can be adjusted by varying the light intensity. The "fuel" of the process is a photosensitive surfactant undergoing photo-isomerization from a more hydrophobic *trans*- to a rather hydrophilic *cis*-state. The surfactant has different adsorption affinities to the particles depending on the isomerization state. The *trans*-isomer for example tends to accumulate in the negatively charged pores of the particles while the *cis*-isomer prefers to remain in solution. This implies that when under UV irradiation *cis*-isomers are being formed within the pores they tend to diffuse out readily and generate an excess concentration near the colloids outer surface, ultimately resulting in the initiation of diffusioosmotic flow. The direction of the flow depends strongly on the dynamic redistribution of the fraction of *trans*- and *cis*-isomers near the colloids due to different kinetics of photo-isomerization within the pores as compared to the bulk. The unique feature of the mechanism discussed in the paper is that the long range mutual repulsion but also the attraction can be tuned by convenient external optical stimuli such as intensity so that a broad variety of experimental situations for manipulation of a particle ensemble can be realized.

Introduction

For manipulation of a colloidal ensemble at a solid-liquid interface, the diffusioosmosis phenomenon has recently attracted much attention.[1,2] The central point in this remarkable membrane-free osmotic transport approach is the generation of fluid flow close to a solid surface where the colloids are trapped. The colloids can then be moved either passively following the diffusioosmotic (DO) flow pattern or even undergo self-propelled (diffusiophoretic) motion in case the flow results from an asymmetrically shaped particle.[3,4,5,6,7] The DO flow is driven by an osmotic pressure gradient resulting from a gradient of a solute close to the solid surface.[8,9,10,11,12,13] The osmotic pressure squeezes the fluid against the wall, its lateral gradient generates fluid flow along the interface. The direction of the DO flow generated within the diffuse layer defined by the

range of solute/surface interactions (typically within the first few nanometers) can point towards or out the area of maximum solute concentration depending on the interaction potential of the solute with the surface and the differential solvent−solute near-wall mobility.[14] It is reported that in a simple case of non-ionic interactions, the attractive potential results in the solvent flow towards the area of low concentration, while repulsive interactions might result in a DO flow towards the larger concentration of the solute.[1] Experimental observations of diffusioosmotic flow have been reported for several systems subjected to a gradient of solutes such as salt, ethanol-water mixtures or neutral polymers.[15,16,17,18] The challenging task of establishing gradients of solutes that are strong enough to drive a measurable DO flow is managed by constructing a line of microfluidic channels connected to pressurizing reservoirs containing solute, solvent and tracer particles.[19] The construction of such devices requires elaborate knowledge of microfabrication techniques and is a science of its own. Therefore, the key task of using DO flow as reliable and convenient tool for particle manipulation is the ability to generate solute concentration gradients with spatio-temporal control, in a reversible manner and at an arbitrary surface.

Recently we have introduced the phenomenology of light driven diffusioosmotic (LDDO) flow, where photo-sensitive surfactant molecules are used to generate solute gradients.[20] The cationic surfactant contains an azobenzene group integrated in a hydrophobic tail.[21] Under photo-isomerization, the azobenzene switches from a *trans* to a *cis* state differing significantly in polarity, where the *cis*-conformation is the more polar one.[22] The decoration of the surfactant with this photo-responsive group allows for reversible switching of the hydrophobicity of the whole molecule upon illumination with light of appropriate wavelength.[23] For instance, the exposure to UV-light results in generation of a majority of *cis*-population in solution, while illumination with longer wavelength (blue and green light) results in larger amounts of *trans*-isomers (more hydrophobic).[24] As a result, one can easily change the solubility, the critical micelle concentration (CMC), the interfacial energy, and the strength of interaction with other substances just by applying light. [20,25] We have found that when the surfactant solution is irradiated with focused light, an osmotic pressure gradient is developed at the solid/liquid interface near the laser spot resulting in a light driven diffusioosmotic (LDDO) flow along the solid surface.[20] Depending on the irradiation wavelength one can establish the radially directed DO flow pointing either out of or into the area of the laser spot. Under exposure to focused UV light, the attractive interaction potential of the *cis*-isomers with the charged glass surface generates a local excess concentration near the surface at the UV irradiated area. This, in turn, causes the

osmotic pressure at the irradiated area to increase and together with the lateral gradient in *cis*-concentration a corresponding osmotic pressure gradient develops, leading to a lateral LDDO flow directed outwards. Irradiation with a longer wavelength generates LDDO flow directed inwards, i.e. towards the laser spot. Here, first all surfactants are converted to the *cis* state by global irradiation with UV light and subsequent illumination with focused green light triggers local photo-isomerization to the *trans*-state resulting in the generation of reversed concentration and osmotic pressure gradients and thus a reversed LDDO flow.[20] This flow is capable of either removing or gathering colloids from or within the illuminated area, where the particles passively follow the local streamlines. Utilizing a similar mechanism, one can also generate LDDO flow at single porous particles, while globally irradiating with non-focused light. [26] The driving force behind this effect is based on a reversible accumulation of cationic surfactant within the negatively charged pores of the colloids,[27,28,29] where the *trans*-isomer preferentially stays within the pores, while the more hydrophilic *cis*-isomer seek the bulk solution. This allows the porous particles to act as a "micro-pump" generating a diffusion of *cis*-isomers out and *trans*-isomers into the particle when exposed to light.[30] The direction, strength and the duration of the flow depends on the wavelength of the applied irradiation, since it defines the ratio of *trans*- and *cis*-isomers (given an overall absolute surfactant concentration). For instance, when a porous particle immersed in a solution of *cis*-isomers is illuminated with green light (converting from *cis*- to *trans*), the diffusion of *trans*-isomers into the particles generates a depletion zone near the colloid surface resulting in aggregation of colloids due to attractive diffusioosmotic interactions.[30] On the other hand, under irradiation with blue light, a steady state DO flow is established around the particles leading to stable long-time repulsive DO interactions.[26] The generation of the different DO flows at the porous particles renders them active in the sense that the inter-particle interactions can be adjusted. In this paper we show that under irradiation with UV light, the direction and the strength of the local light driven diffusioosmotic (*l*-LDDO) flow changes spontaneously enforcing either long range attraction or repulsion. We explain this by the dynamic redistribution of the fraction of *trans*- and *cis*-isomers near the colloids, induced by the difference in pore and bulkkinetics of photo-isomerization.

Experimental Setup

Materials

Mesoporous silica microspheres of 5 μm in diameter with BET (specific surface area) value of 850m^2/g and pore diameter of 6 nm are purchased from Micromod (Sicastar, Prod. Nr. 43-00-503, Germany).

Azobenzene containing trimethyl-ammonium bromide surfactant (C4-Azo-OC6TMAB) is synthesized as described elsewhere.[31] The surfactant is dissolved in milli-Q water and diluted to the required concentrations ranging from 0.1 mM to 2 mM. The CMC of surfactant in *trans* state is 0.5 mM.[23]

The aqueous dispersion of the silica particles is mixed with surfactant solution so that the particle concentration is 0.1mg/ml, while the surfactant concentration is adjusted on demand. The dispersion is kept for equilibration at least 1 hour. A sealed chamber of 920 μm in height and a sample volume of 40 μl is used to exclude effects originating from a water/air interface (marangoni flows). All samples are kept in the dark or in red light to prevent unwanted photo-isomerization.

Photo-isomerization of azobenzene surfactant. The molecules undergo photo-isomerization from the *trans*- to the *cis*-state under irradiation with UV light (λ = 365 nm).[24] The photo-stationary state with 90% of *cis* isomers is achieved within several minutes (intensity dependent) of irradiation. UV-Vis absorption spectra recorded in dark (*trans* state) and during UV illumination at the photo-stationary state (*cis* isomers) are presented in **Figure 1f**. Under illumination with longer wavelengths, the photo-isomerization from the *cis*- to the *trans*- state takes place within seconds, while thermal back relaxation in the dark takes more than 48 hours.[24] The red light (λ = 625 nm) illumination does not affect photo-isomerization of the surfactant.

Methods

An inverted microscope Olympus IX73 equipped with a light source of different wavelengths is used for all measurements. A UV LED (M365L2-C1) purchased from Thorlabs Gmbh (Lübeck, Germany) is used to achieve a homogeneous, global irradiation (guaranteeing a constant intensity all across the sample). The illumination power is measured by an optical power meter PM100D with sensor S170C (Thorlabs Gmbh, Germany). Micrographs are acquired with a Hamamatsu ORCA-Flash4.0 LT (C11440) at rate of 1 frame per sec. The setup is kept in the dark to prevent the uncontrolled isomerization. When required, red light (M625L1- C1, Thorlabs Gmbh) is used

for imaging in dark as it does not affect the photo-isomerization, i.e. the azobenzene molecules do not change their isomerization state. The motion of particles under UV light irradiation is studied for different surfactant concentration and intensity of UV light ranging from 42 μW/cm^2 to 1.8 mW/cm^2.

Particle trajectories are acquired using the Mosaic Single Particle Tracking plugin for ImageJ (Rasband, W.S., ImageJ, U. S. NIH, Bethesda, Maryland, USA). The tracking algorithm is described by Koumoutsakos.[32] Motion analysis and calculation are done using a custom Matlab script.

UV-Vis spectroscopy (Cary 5000 UV-Vis-NIR spectrophotometer, Agilent Technologies, USA) is used to measure the kinetics of *trans-cis* photo-isomerization at different surfactant concentrations and UV light intensities. The amount of surfactant adsorbed by the porous colloids is calculated exploiting the UV-Vis spectroscopy data.

Results

Generation of local-light driven diffusioosmotic flow (l-LDDO) under irradiation with UV light.

Mesoporous silica particles (d = 5 μm, pore size ~ 6 nm) are dispersed in 1 mM aqueous solution of photosensitive surfactant and placed on a glass substrate in a sealed chamber of 0.92 mm in height and 40 μl in volume as described in the **Experimental Part**. After sedimentation, particles are randomly distributed on the surface and undergo thermal motion (**Figure 1a**). The analysis of the mean square displacement (MSD) as a function of time is shown in **Figure S1** (**Supplementary Material**). Under red light irradiation (for imaging), the surfactant molecules, being in *trans*-state, diffuse into the pores and are deposited within the particles. The amount of absorbed surfactant is measured with UV-Vis spectrometry by determining the surfactant concentration in solution with and without particles. For a particle and surfactant concentration of 0.1 mg/ml and 1 mM, respectively, a total amount of 10% is removed from solution due to the adsorption within the particles. When UV light (λ = 365 nm, I = 1.8 mW/cm^2) is switched on, the particles start repelling each other (**Figures 1b, c**). This process takes place within the first seconds of irradiation followed by a formation of a regularly spaced grid with colloids trapped by their nearest neighbors at

constant separation of 20 μm (4x particle diameter). The velocity distribution of the particles as a function of irradiation time is shown in **Figure S2** (**Supplementary Material**). The distance between the colloids under separation is mainly determined by the particle concentration, and can be tuned from small (1 μm) to separations exceeding the particle diameter by a factor of 5 (**Figure S3**, **Supplementary Material**). After a while, the repulsion strength decreases again and colloids resume purely thermal motion (**Figure 1d**).

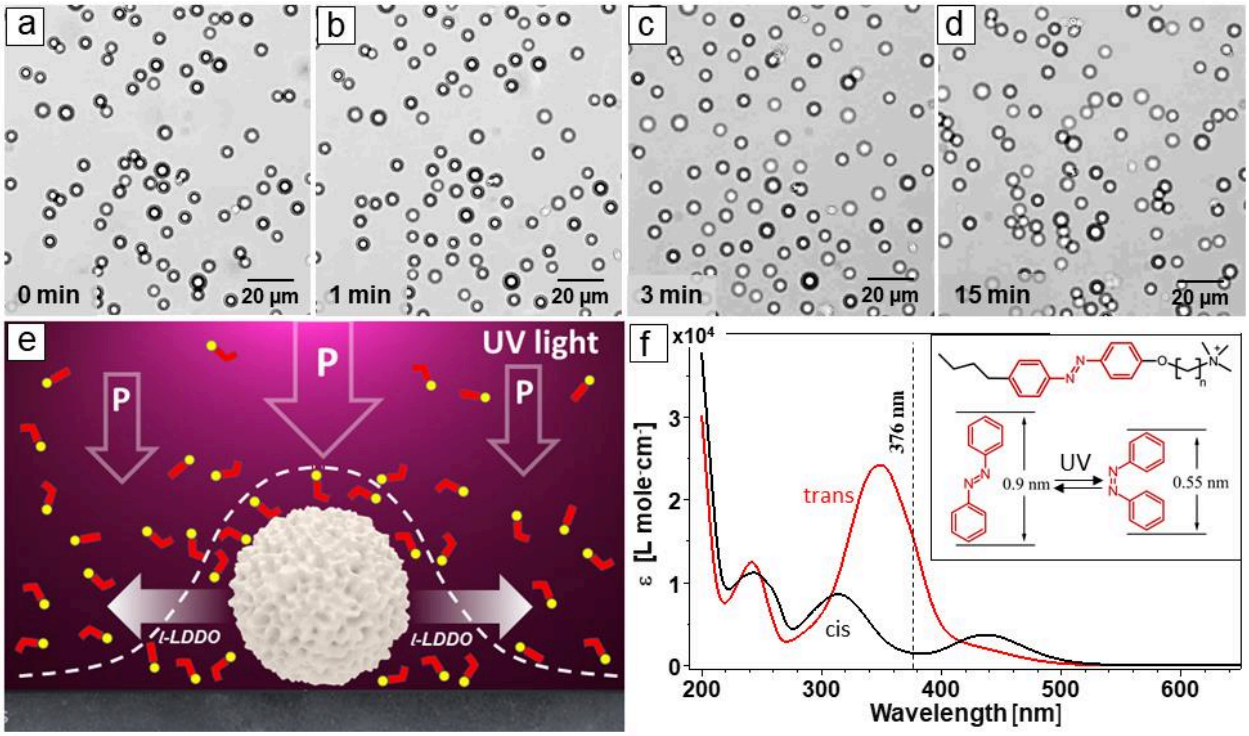

Figure 1. (a-d) Optical micrographs of mesoporous silica particles (d = 5μm) at a glass surface immersed in aqueous solution of 1mM surfactant under UV irradiation (λ = 365 nm, I= 1.8mW/cm^2) at different irradiation time: (a) before irradiation, (b) 1 min, (c) 3 min, and (d) 15 min. (e) Scheme of the local-light driven diffusioosmotic flow (*l*-LDDO) generated at each single colloid. "P" indicates osmotic pressure, the surfactant is shown in yellow and red, the white dashed line depicts concentration gradients of *cis*-isomers around the colloid, white arrows show the direction of the *l*-LDDO flow. (f) UV-Vis absorption spectra of the surfactant in *trans* state (red curve) and after UV irradiation (black curve). The inset depicts the chemical structure of the surfactant molecule, below a scheme of azobenzene photo-isomerization is shown.

The process of particle repulsion under exposure to UV-Vis light is attributed to *local* light driven diffusioosmotic flow (*l*-LDDO) around each colloid.[20,30] The photo-isomerization from *trans*- to *cis*- takes place not only in solution, but also within the particle pores as the silica particles are

transparent for the wavelength used in this work. During photo-isomerization of the *trans*-isomers stored in the colloid, the generated *cis*-molecules diffuse out of the pores forming an excess concentration of *cis*-isomers, $[\mathbf{c}]_p$, in the vicinity of the particle leading to a concentration gradient (see scheme in **Figure 1e**), inducing a local gradient in osmotic pressure. Consequently, a diffusioosmotic flow pointing radially away from the particle is generated. Nearby situated particles experience diffusioosmotic repulsion, which can extend over large distances (in this work distances as large as 25 μm have been observed, i.e. 5 times larger than the particle diameter, **Figure S3**, **Supplementary Material**). Following the initially strong particle repulsion, the *l*-LDDO flow eventually decays because under UV light the amount of surfactant molecules in the particle decreases during continuous irradiation. In the photo-stationary state achieved after ca. 2 minutes at an intensity of 1.8 mW/cm^2 almost all surfactant molecules have been switched to the *cis*-state implying molecular depletion within the particles. As a result, the almost empty porous particles move now thermally in the aqueous solution containing mostly surfactant molecules in their *cis*-state (see **Figure S4**, **Supplementary Material**).

However, the particle motion strongly depends on the wavelength of applied light. Under irradiation with blue light (λ = 455 nm), for instance, mutual particle repulsion is sustained as irradiation goes on continuously by far exceeding the time needed to reach a photo-stationary state.[26] The reason for this continuous flow is that under irradiation with blue light at a photo-stationary state there are both isomers present in solution, i.e. 28% of *cis*- and 72% of *trans*- (**Figure S5**, **Supplementary Material**). This means that when a *cis* molecule diffuses out of the particle, a *trans*- molecule present in solution can enter the pore, occupying its space. Thus, a continuous diffusion of *cis* isomers out of and *trans* isomers into the particles can be established. In fact, under blue light, continuous supply of the "fuel" for the *l*-LDDO flow takes place, which is not the case for UV light irradiation.[30]

With these two examples of dependence of *l*-LDDO flow on different wavelength, we demonstrate that the relative fraction of the *trans* and *cis* isomers at a photo-stationary state is an important parameter governing the extent of local diffusioosmotic flow. In the following, we show that under irradiation with only one wavelength, i.e. UV light, one can trigger the strength and even the direction of the *l*-LDDO flow and enforce either long range DO repulsion or attraction.

Dependence of the l-LDDO on intensity of UV light

Let's first consider how the generation of *l*-LDDO flow depends on irradiation intensity with remaining parameters kept fixed, i.e. $\lambda = 365$ nm, $c_{particles} = 0.1$ mg/ml and $c_{azo} = 1$ mM. When the irradiation intensity is low ($I = 163$ μW/cm^2), particle motion exhibits a rather complex behavior. During the first two minutes of irradiation, the colloids appear unaffected and move freely; during the following 3 minutes they start aggregating moving with a maximum velocity of about 1 μm/s, exhibiting pronounced attractive interactions (**Figure 2b**).

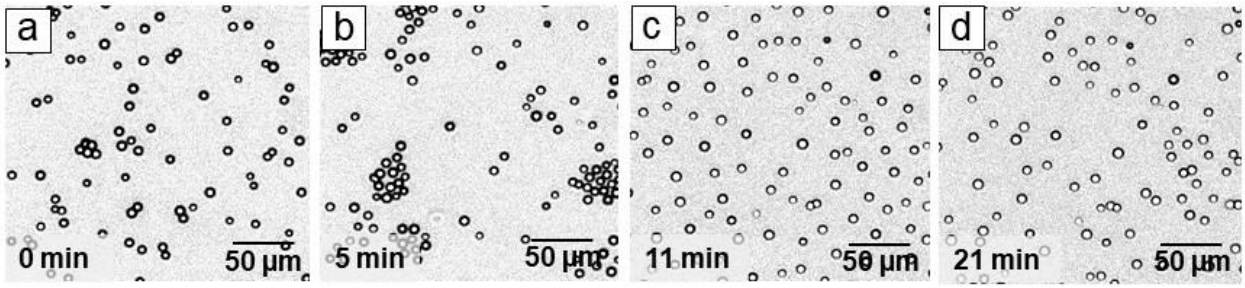

Figure 2. Optical micrographs of an ensemble of porous colloids immersed into an aqueous solution of surfactant ($c_{azo} = 1$ mM) and exposed to irradiation with UV light ($\lambda = 365$ nm, $I = 163$ μW/cm^2) for different irradiation times: (a) t = 0 min, just before UV irradiation starts; (b) t = 5 min exhibiting maximum aggregation; (c) t = 11 min, maximum separation and (d) t = 21 min, thermal motion.

Only after 11 minutes of irradiation the particles are completely separated (**Figure 2c**) due to *l*-LDDO repulsion as described above (see **Figure 1)**. Repulsion settles only after ca. 21min of exposure to UV light (**Figure 2d**).

The intensity of the UV irradiation is varied within a broad range, from 42 μW/cm^2 to 1.8 mW/cm^2 and yet a common behavior emerges: for lower intensities particles tend to aggregate initially and disperse in the long run. To characterize the particle distribution, we track the average nearest particle distance (NPD), which is defined as the ensemble average over the particle centered distances of nearest neighbors. **Figure 3g** shows the dependence of the NPD on UV irradiation intensities. For the lowest intensity of 42 μW/cm^2, aggregation starts only after 4 minutes with an initial maximum velocity of 1 μm/s and saturates only after 8 min (**Figure 3b**). The inter-colloid distance decreases by approximately 90 μm in average corresponding to ca. 18 times their diameter. As a follow up, diffusioosmotic repulsion sets in for about 8.5 minutes (black curve in **Figure 3g**). The time spend in between aggregation and separation decreases with increasing

irradiation intensity (**Figure 3h**). For the highest intensity used in our work, 1.8 mW/cm^2 (pink line in **Figure 3g**), only particle separation without initial aggregation has been observed.

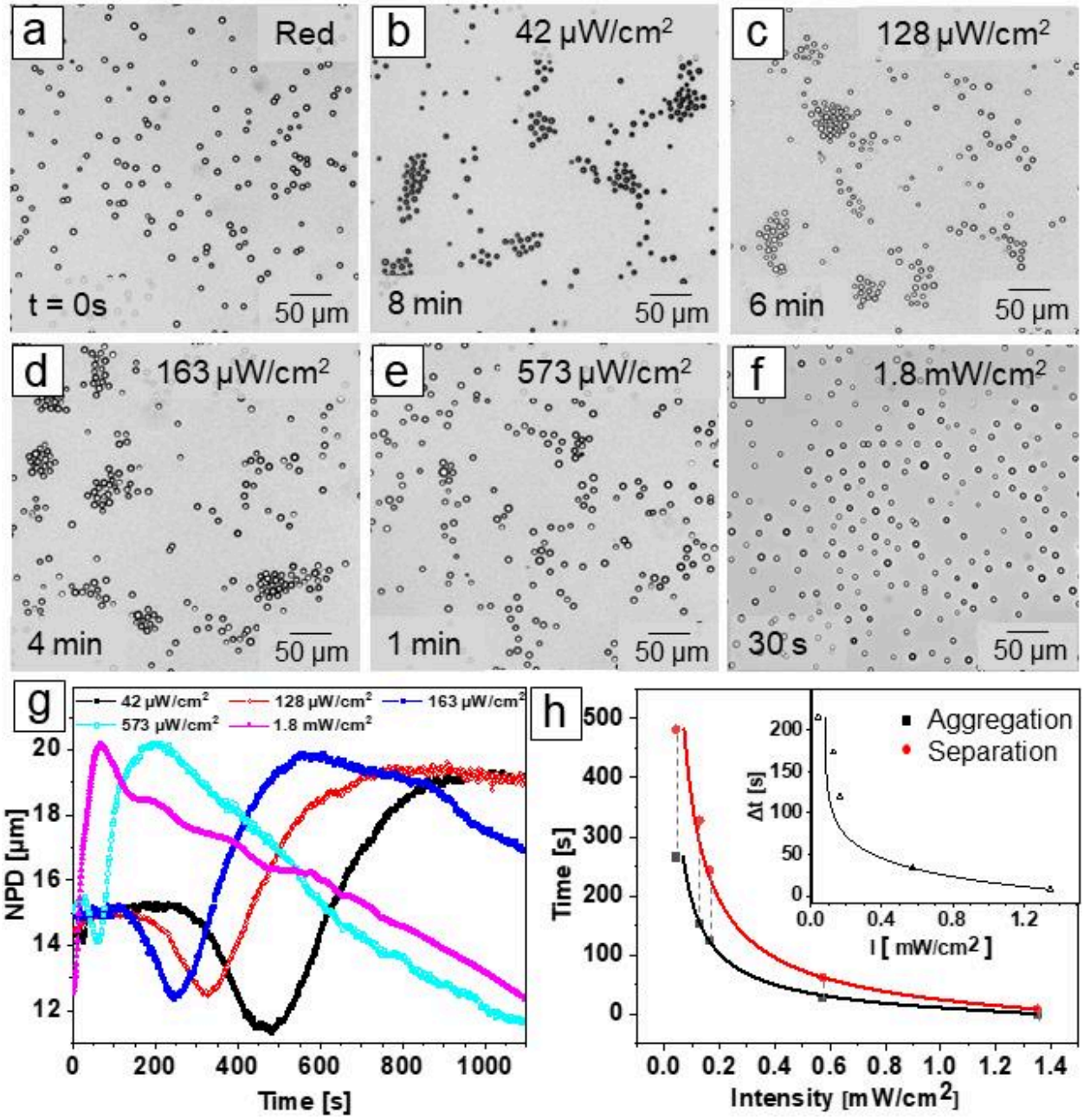

Figure 3. Optical micrographs of an ensemble of porous colloids subjected to UV irradiation (λ = 365 nm) at different intensities. (a) The micrograph represents the typical particle distribution before irradiation (t = 0 min). (b-e) Optical micrographs recorded at the time of maximum aggregation under irradiation with light of different intensities: (b) 42 µW/cm^2, (c) 128 µW/cm^2, (d) 163 µW/cm^2, (e) 573 µW/cm^2. (f) Direct separation of particles recorded after t = 30 s of irradiation at maximal intensity of I = 1.8 mW/cm^2. (g) NPD as a function of time at different

intensities. (h) Dependence of aggregation and separation time with respect to intensity (inset shows the difference of aggregation and separation time). The surfactant concentration is 1 mM for all samples. The corresponding videos are provided in **Integral Multimedia**.

The process described above is directly related to the kinetics of photo-isomerization of the surfactant molecules. **Figure 4** shows the comparison of the NPD (black line) and the isomerization kinetics (red line) at 5 different intensities of UV exposure (42 μW/cm^2, 128 μW/cm^2, 573 μW/cm^2, 1.4 mW/cm^2 and 1.8 mW/cm^2).

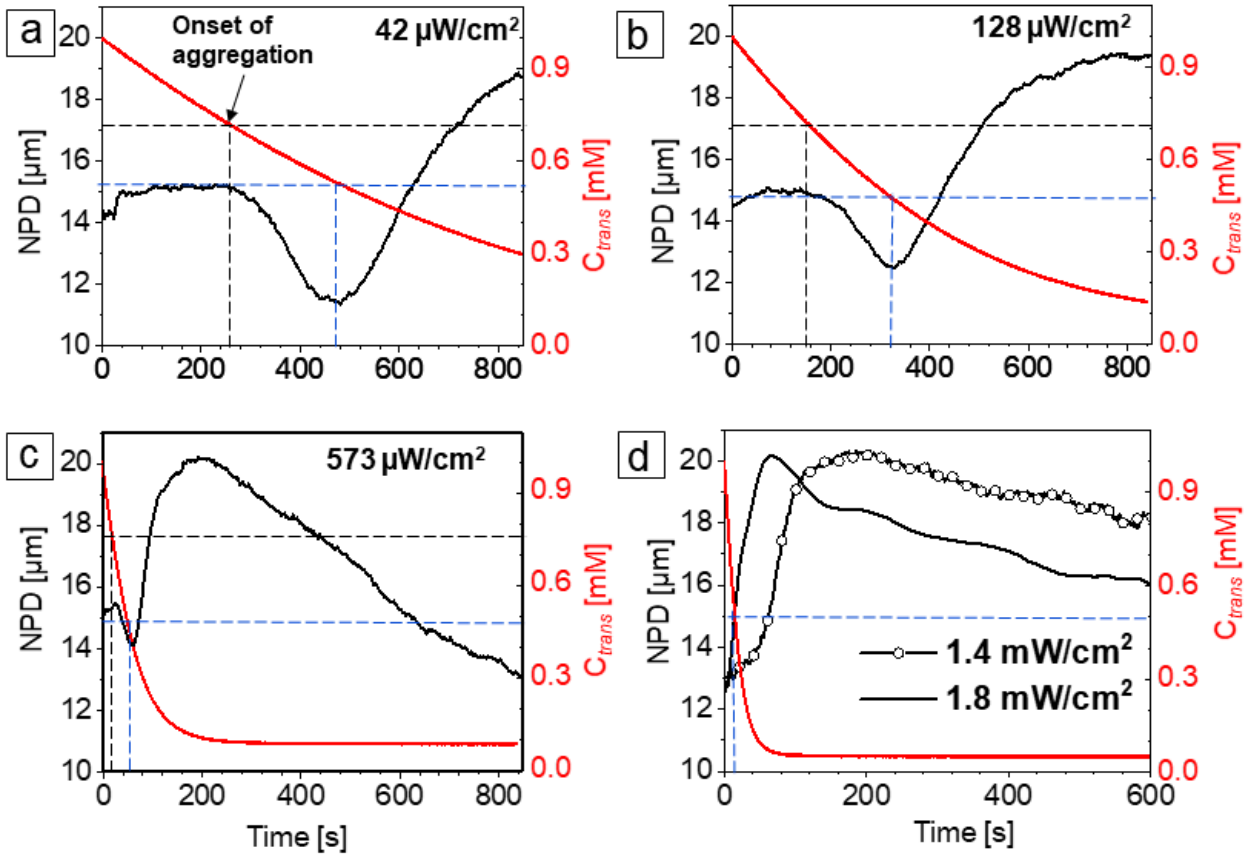

Figure 4. Nearest particle distance (NPD) (black line) and isomerization kinetic expressed as a time dependent function of *trans*-isomer concentration (red line) for different intensities of UV light: (a) 42 μW/cm^2, (b) 128 μW/cm^2, (c) 573 μW/cm^2, (d) 1.4 mW/cm^2 (black line with empty circles) and 1.8 mW/cm^2 (black line). The dashed black lines mark the onset of particle aggregation and corresponding concentration of *trans*-isomer in solution. The blue dashed lines indicate the onset of particle separation.

From the plots one may infer that particle aggregation starts when ca. 25 % of the isomerization is completed (see black dashed lines), i.e. the concentration of *trans* molecules in the bulk reduces

from 1 mM to 0.75 mM. The separation process starts when more than 50 % of isomerization is finished (blue dashed lines). At this point the bulk concentration of *trans*-isomers is smaller than 0.5 mM, which means that there are no micelles present in solution (CMC = 0.5 mM).

Mechanism of long range LDDO attraction and repulsion.

To understand the particle aggregation and separation processes under constant irradiation conditions, we should recall the mechanism of light driven diffusioosmosis (LDDO) (**Figure 5**). Here, the direction of diffusioosmotic (DO) flow is determined by the concentration gradient of *cis*-isomers, i.e. the flow points away from areas of high *cis* concentration.[20] This statement is supported by experiments where the irradiation is applied with focused UV light and the flow is generated out of the irradiated area where a majority of surfactant molecules is in the *cis*-state (**Figure 5a**).[20] On the other hand, when we invert the concentration gradient, i.e. all surfactant molecules are first converted to *cis*-state and irradiation with focused green light (generating *trans*-isomers) is applied, the flow is directed towards the laser spot, where *cis*-isomers are depleted (**Figure 5b**). It means that the particles move to each other experiencing diffusioosmotic attraction, when the concentration of *cis*-isomers in the bulk, $[\mathbf{c}]_B$, is larger than near the particles (**Figure 5d**), while the DO repulsion sets on when an excess of *cis*-isomers expelled out of the particle, $[\mathbf{c}]_p$, is generated with the time (**Figure 5c**). The inversion of the *cis*-isomer gradient at other fixed parameters, i.e. irradiation intensity, wavelength, surfactant concentration, could appear when the photo-isomerization kinetics of the surfactant is slower in the particle than in the bulk, so deferring the increase in *cis*-isomer concentration in the particle vicinity. Indeed, we have recently shown that the photo-isomerization rate depends on surfactant concentration above the CMC being slower at larger concentrations due to steric hindrances, and thus in micelles it is ca. 80% slower than in the case of single molecules.[24] Since the surfactant molecules readily adsorb in and on the particles, one can consider the particles' surface area as being enriched with surfactant. Therefore, one can postulate that the photo-isomerization kinetics of surfactant in the particles is slower than in the bulk. It means, when we apply irradiation with UV light, at a certain initial time of irradiation the amount of *cis*-isomers converted from *trans*-state in the bulk is larger than near the particle ($[\mathbf{c}]_B > [\mathbf{c}]_p$). This generates the depletion zone of *cis*-isomers near the particles and thus DO flow pointing towards the colloids establishing the DO attraction (**Figure 5d**). With increasing irradiation time, the amount of *cis*-isomers within the particle increases as well, they diffuse out

of the pores and generate an excess of *cis*-isomer concentration around each single particle, and thus, *l*-LDDO flow results pointing out of the particle (DO repulsion) ($[\mathbf{c}]_B < [\mathbf{c}]_p$) (**Figure 5c**).

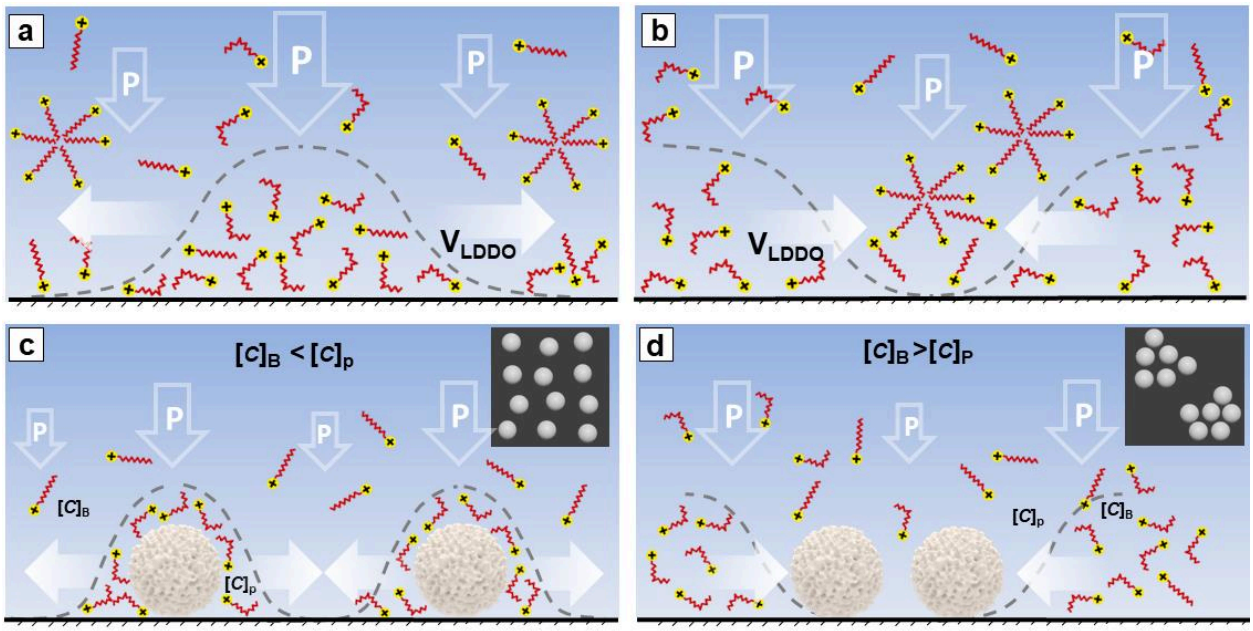

Figure 5. (a) Scheme of the *l*-LDDO flow pointing away of the largest concentration of *cis*-isomers (shown as red bent sticks). The local increase in *cis*-isomer concentration is generated under irradiation with focused UV light. Black line indicates concentration gradient of *cis*-isomers. White horizontal arrows show the direction of the diffusioosmotic flow. White vertical arrows with letter "P" mark a distribution of the osmotic pressure. (b) The LDDO flow points towards area of depleted *cis*-isomer concentration, generated during irradiation with focused green light. (c, d) Scheme of local-LDDO flow generated around porous particles under irradiation with global UV light. The inserts depict 2D distribution of colloids experiencing either (c) long range DO repulsion (the LDDO flow points out of the particles) or (d) DO attraction (the LDDO flow points towards the particles). $[\mathbf{c}]_B$ and $[\mathbf{c}]_p$ are concentration of *cis*-isomers in the bulk and in the vicinity of the particles, respectively.

We trace the direction of *l*-LDDO flow with non-active small particles, i.e. non-porous silica colloids of 1.5 μm in diameter (**Figure 6**). Non-active means that the particles do not have pores and thus cannot absorb a large amount of surfactant molecules. The particles are added to the surfactant solution containing porous active particles and their displacement is analyzed as a function of time under irradiation with UV light (**Figure 6d**).

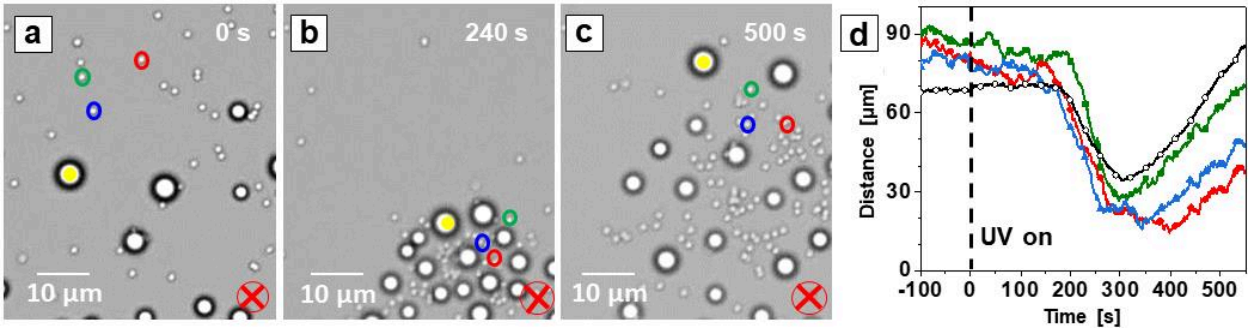

Figure 6. (a-b) Optical micrographs represent an ensemble of small non-active (1.5 µm in diameter) and active (5 µm in diameter) particles at different irradiation times under exposure to UV light (λ = 365 nm, I = 130 µW/cm^2): (a) before irradiation, (b) 240 s, (c) 500 s. The particles are immersed in surfactant solution of 1 mM concentration. (d) Analysis of position (relative to the center of coordinate marked by red cross in the lower right angle of (a, b and c)) of three non-active particles (marked in red, green and blue) and one active particle (marked in yellow) is presented as a function of time. The black line marks the displacement of active particle, while red, green and blue curves depict position corresponding non-active colloids. The corresponding video is available in **Integral Multimedia**.

As one can see from **Figure 6,** the tracer particles and the active porous particles exhibit similar motion, i.e. when UV light is switched on the particles initially undergo just simple thermal motion, but after ca. 200 s they start to aggregate, followed by separation (**Figure 6d**). In **Figure 6d** the positions of 3 non-active particles (marked by circles of different color (green, red and blue)) and one active (marked in yellow) are presented as a function of time relative to the fixed reference point (marked by red cross, lower right angle). Irrespective of size and activity, the particles move with similar velocities relative to the fixed reference point. This is supportive of the notion that the initial diffusioosmotic flow directed towards the particle is generated by the global gradient of *cis*-isomers. After aggregation, the active, porous particles start to separate due to formation of *l*-LDDO flow, while the expanding motion of the tracer particles is driven by the local radially directed flow generated around each active particle, as evidenced from the repulsion of the non-active particle displacement starting from 300 seconds of irradiation (**Figure 6d**).

Additionally, the time needed for achieving a photo-stationary state depends also on irradiation intensity and decreases as the intensity raises. For instance, for the light intensities used in this study of 42 µW/cm^2, 128 µW/cm^2, 163 µW/cm^2, and 573 µW/cm^2 the photo-isomerization time constant is 714 s, 417 s, 390 s and 56 s, respectively (**Figure S6**, **Supplementary Material**). Thus, the onset of DO attraction and repulsion shifts towards smaller irradiation times with increasing

intensity. At 1.8 mW/cm^2 the time to isomerize to 50 % of *cis*-isomers is only a few seconds, which is not enough to establish particle aggregation and only results in particles repulsion.

The system is, of course, more complex, i.e. one should take into account the different diffusion coefficients of *trans*- and *cis*-isomers in bulk and within the pores, as well as a different adsorption and desorption kinetics of the surfactant at the interface. However, the characteristic time scale for these processes is much smaller than the time needed for establishing LDDO flow. Indeed, the reported diffusion coefficients of azobenzene are ca. $2.4 \cdot 10^2$ μm^2/s and 4.2 μm^2/s in the bulk and in porous glass, respectively.[33] Although the diffusion time within pores is almost 70 times longer than in the bulk, that is, to overcome a length of 2.5μm (the radius of the porous particle) the surfactant needs 0.7s and 0.01s, respectively, it is still much faster than the characteristic time of the DO process. The same applies to the difference in adsorption/desorption time for *trans*- and *cis*- isomers, which is of the order of milliseconds as reported for the air/water interface.[34] In general, the combination of different processes such as dissimilar photo-isomerization, diffusion and adsorption/desorption kinetics of *trans*- and *cis*- isomers results in the temporal variation of the concentration gradient, which in turn is responsible for the dynamic change in the direction of DO flow and thus attractive or repulsive interactions.

Concluding, we also show that one can establish a time dependent change in concentration gradient at constant irradiation intensity by varying the surfactant concentration. For instance, we fix the intensity of UV light at 1.4 mW/cm^2 and change the surfactant concentration in a broad range starting from values as low as 0.2 mM and increase up to 2 mM (**Figure 7**). The initial (before irradiation) distribution of the particles differs with concentration, i.e. at small concentrations particles tend to aggregate (Figure 7a) due to vanishing surface charge, while at larger surfactant concentrations they are well separated as can be explained by large Z-potential and thus string electrostatic repulsion.[20] For surfactant concentrations below the CMC (0.5 mM), immediate separation between particles takes place with a maximum velocity of 1μm /s (**Figures 7a** and **7d**). Beginning with concentrations above the CMC, the delay in the separation of the particles becomes apparent, i.e. after switching on irradiation with UV light the system requires a certain time to establish a concentration gradient needed for generation of outward-directed flow (DO repulsion). With even larger surfactant concentration, one also obtains DO attraction, i.e. flow directed towards the particles (**Figures 7b, 7c, and 7e**). We should emphasize that this behavior can be

repeated indefinitely within the same experiment, apart from the behavior dictated by the initial state of the system (see **Figure S7**, **Supplementary Material**, where the dependence of the NPD on irradiation is shown for two cycles).

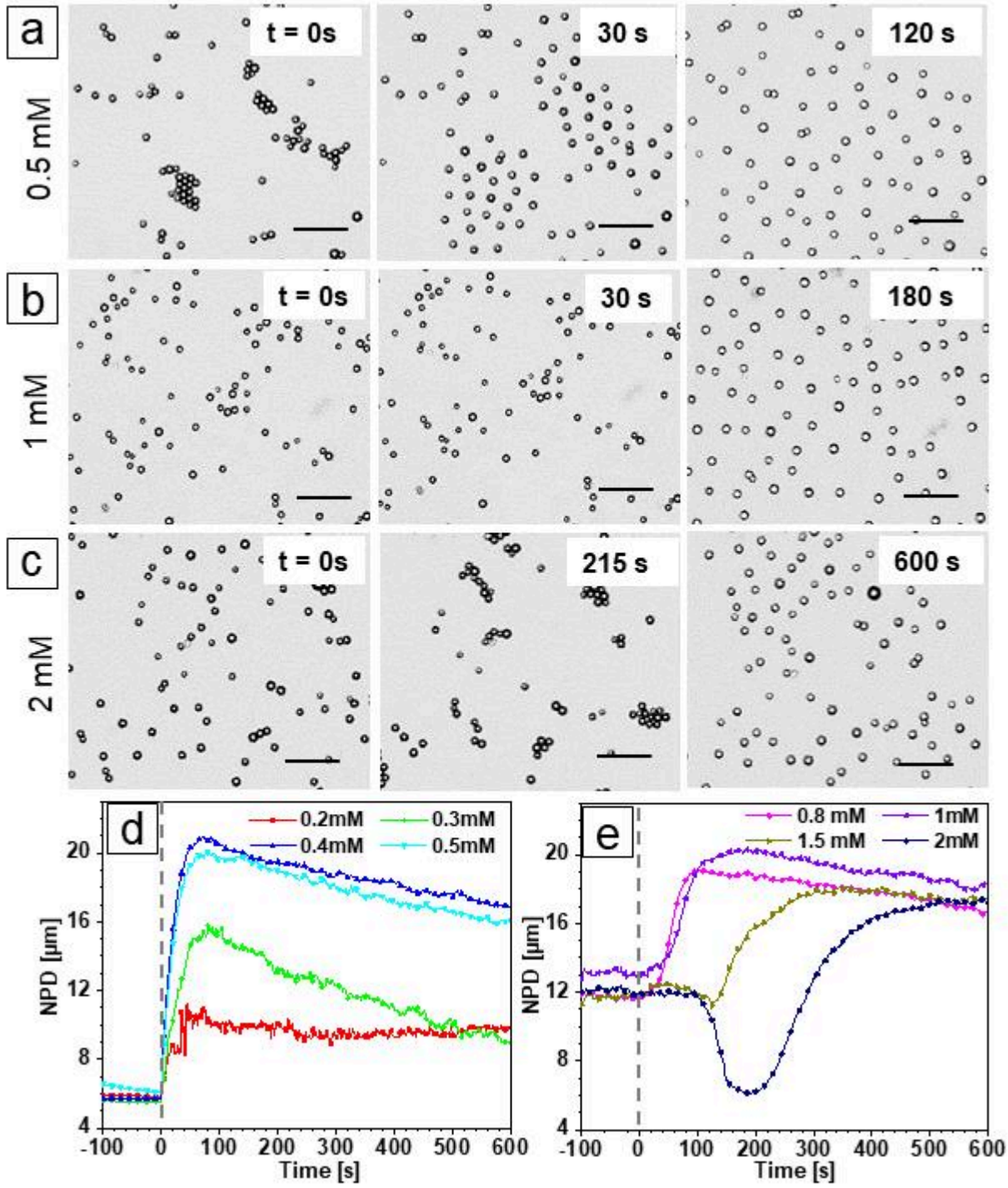

Figure 7. Optical micrographs of porous silica particles (d = 5µm) in an aqueous solution of azobenzene containing surfactant of different concentrations: (a) c_{azo} = 0.5 mM, (b) c_{azo} = 1mM, (c) c_{azo} = 2mM. The samples are exposed to irradiation with UV light of constant intensity (λ =

365 nm, I = 1.4 mW/cm^2). The snapshots at different irradiation times are shown. The scale bar is 30 μm. (d-e) Nearest particle distance (NPD) as a function of irradiation time for surfactant concentrations below the CMC (d) and above (e). The corresponding videos are presented in **Integral Multimedia**.

Conclusion

In this paper we discuss the mechanism of local light driven diffusioosmotic flow generated with porous colloids under irradiation with UV light. The particles are dispersed in aqueous solution containing photosensitive surfactant. The surfactant integrates an azobenzene group, which triggers the hydrophobicity of the whole molecule during photo-isomerization from the *trans*- to the *cis*-state. Depending on the isomer, the surfactant molecules either diffuse into the negatively charged pores (preferred by the hydrophobic *trans*-state) or out of them (the hydrophilic *cis*-state seeking the bulk). Under UV irradiation the *cis*-isomers generated within the pores diffuse out of the particles and generate an excess concentration near the colloids outer surface and develop diffusioosmotic flow pointing outside and thus causing DO repulsion. However, the direction of the flow depends strongly on the dynamic redistribution of the fraction of *trans*- and *cis*-isomers near the colloids, since the photo-isomerization kinetics in bulk as compared to within the pores is different, the latter is expected to be considerably slower. Thus just by changing the intensity of the UV light (with all other parameters fixed) one can generate either a pure repulsive effective inter-particle potential (high intensity) or at lower intensities first introduce aggregation of the mesoporous silica particles followed by strong separation; note that all phenomena occur within the same unchanged system. The range of DO interactions (repulsion/aggregation) extends over several times the particle's diameter (5 μm) being up to 18 times. The extremely long-range diffusioosmotic interaction potential can be switched on or off on demand and adjusted either for triggering aggregation or separation by convenient external stimuli such as mere changes in light intensity. The phenomenology described opens up many intriguing avenues: from manipulating particle ensembles to single colloid manipulation, fine-tuning competing inter-colloidal forces or the conception of novel types of active particles and microswimmers.[35]

Supplementary Material

Figure S1 depicts MSD plot of porous silica particles; Figure S2 shows velocity of particles as a function of irradiation time; Figure S3 and S4 show the dependence of the NPD on PSD and irradiation time, respectively; Figure S5 contains information on particle motion under irradiation with blue light; Figure S6 presents information on photo-isomerization kinetic of azobenzene as a function of light intensity and surfactant concentration; Figure S7 illustrates the dependence of the NPD on irradiation time during exposure to two different wavelengths UV and blue.

Acknowledgments

This research is supported by the Priority Program 1726 “Microswimmers-From Single Particle Motion to Collective Behaviour”, Germany; DFG (SA1657/9-2) and the International Max Planck Research School on Multiscale Bio-Systems (IMPRS), Potsdam, Germany. We thank Dr. A. Kopyshev for the support in preparation of graphical work.

Data Availability Statement

The data that support the findings of this study are available from the corresponding author upon reasonable request.

References

1. S. Marbach and L. Bocquet, Chem. Soc. Rev. 48, 3102 (2019).

2. J. C. T. Eijkel and A. van den Berg, Chem. Soc. Rev. 39, 957 (2010).

3. J. F. Brady, J. Fluid Mech. 667, 216 (2011).

4 I. Theurkauff, C. Cottin-Bizonne, J. Palacci, C. Ybert and L. Bocquet, L. Phys. Rev. Lett. 108, 268303 (2012).

5 M. Ibele, T. E. Mallouk and A. Sen, Angew. Chem., Int. Ed. 48, 3308 (2009).

6 R. Golestanian, T. Liverpool and A. Ajdari, Phys. Rev. Lett. 94, 220801 (2005).

7 I. Buttinoni, G. Volpe, F. Kümmel, G. Volpe and C. Bechinger, J. Phys.: Condens. Matter 24, 284129 (2012).

8 B. Derjaguin, G. Sidorenkov, E. Zubashchenko and E. Kiseleva, Progress in Surface Science 43, 138 (1993).

9 B. Derjaguin, S. Dukhin and A. Korotkova, Progress in Surface Science 43, 153 (1993).

10 J. L. Anderson and D. C. Prieve, Langmuir 7, 403 (1991).

11 D. Prieve, J. Anderson, J. Ebel and M. Lowell, J. Fluid Mechanics 148, 247 (1984).

12 J. L. Anderson, M. E. Lowell, D. C. Prieve, J. Fluid Mech. 117, 107 (1982).

13 D. C. Prieve, J. L. Anderson, J. P. Ebel and M. E. Lowell, J. Fluid Mech. 148, 247 (1984).

14 C. Lee, C. Cottin-Bizonne, R. Fulcrand, L. Joly and C. Ybert, J. Phys. Chem Lett. 8, 478 (2017).

15 C. Lee, C. Cottin-Bizonne, A.-L. Biance, P. Joseph, L. Bocquet and C. Ybert, Phys. Rev. Lett 112, 244501 (2014).

16 B. Abecassis, C. Cottin-Bizonne, C. Ybert, A. Ajdari and L. Bocquet, Nature Materials 7, 785 (2008).

17 B. Abecassis, C. Cottin-Bizonne, C. Ybert, A. Ajdari and L. Bocquet, New J. Phys. 11, 075022 (2009).

18 J. Palacci, B. Abecassis, C. Cottin-Bizonne, C. Ybert and L. Bocquet, Phys. Rev. Lett. 104, 138302 (2010).

19 J. S. Paustian, C. D. Angulo, R. Nery-Azevedo, N. Shi, A. I. Abdel-Fattah and T. M. Squires, Langmuir 31, 4402 (2015).

20 D. Feldmann, S.R. Maduar M. Santer, N. Lomadze, O.I. Vinogradova and S. Santer, Scient. Rep 6, 36443 (2016).

21 S. Santer, J Phys D: Appl Phys 51, 013002 (2017).

22 M. Montagna, and O. Guskova, Langmuir 34, 311 (2018).

23. Y. Zakrevskyy, J. Roxlau, G. Brezesinski, N. Lomadze and S. Santer, J. Chem. Phys. 140, 044906 (2014).

24 P. Arya, J. Jelken, N. Lomadze, S. Santer and M. Bekir, J. Chem. Phys. 152, 024904 (2020).

25 X. Liu and N. L. Abbott, J. Colloid Interface Sci. 339, 1 (2009).

26 D. Feldmann, P. Arya, T. Y. Molotilin, N. Lomadze, A. Kopyshev, O I. Vinogradova and S. Santer, Langmuir DOI: 10.1021/acs.langmuir.9b03270 (2020).

27 A. M. Rumyantsev, S. Santer and E. Y. Kramarenko, Macromolecules 47, 5388 (2014).

28 S. Schimka, N. Lomadze, M. Rabe, A. Kopyshev, M. Lehmann, R. V. Klitzing, A. M. Rumyantsev, E. Kramarenko and S. Santer, Phys. Chem. Chem. Phys. 19, 108 (2017).

29 S. Schimka, Y. D. Gordievskaya, N. Lomadze, M. Lehmann, R. V. Klitzing, A. M. Rumyantsev, E. Kramarenko and S. Santer, J Chem Phys 147, 031101 (2017).

30 P. Arya, D. Feldmann, A. Kopyshev, N. Lomadze and S. Santer, Soft Matter 16, 1148 (2020).

31 D. Dumont, T. Galstian, S. Senkow and A. Ritcey, Mol. Cryst. Liq. Cryst. 375, 341 (2002).

32 I. F. Sbalzarini and P. Koumoutsakos, J. Struct. Biol. 151, 182 (2005).

33 W. D. Dozier, J. M. Drake and J. Klafter, Phys. Rev. Lett. 56, 197 (1986).

34 E. Chevallier, A. Mamane, H. A. Stone, C. Tribet, F. Lequeuxa and C. Monteux, Soft Matter 7, 7866 (2011).

35 D. Feldmann, P. Arya, N. Lomadze, A. Kopyshev and S. Santer, Appl. Phys. Lett. 115, 263701 (2019).

Supporting Information

Light driven diffusioosmotic repulsion and attraction of colloidal particles

Pooja Arya[1], Joachim Jelken[1], David Feldmann[1,2], Nino Lomadze[1], Svetlana Santer[1*]

[1]*Institute of Physics and Astronomy, University of Potsdam, 14476 Potsdam, Germany*

[2]*School of Mechanical Engineering, Tel-Aviv University, Tel-Aviv 6997801, Israel*

AUTHOR EMAIL ADDRESS: santer@uni-potsdam.de

RECEIVED DATE

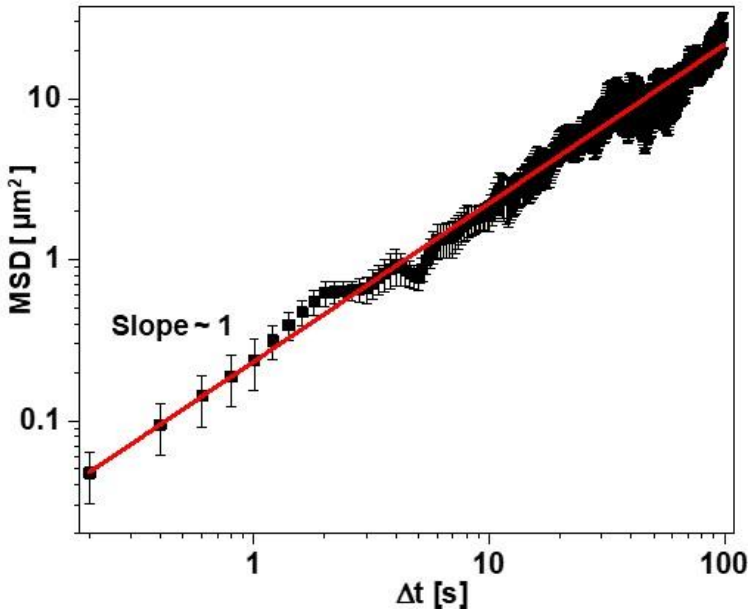

Figure S1. MSD plot of porous silica particles at a glass surface dispersed in aqueous solution containing photosensitive surfactant (c_{azo}=1mM). The slope of the MSD is ~1 showing that the particles without irradiation undergo Brwonian motion.

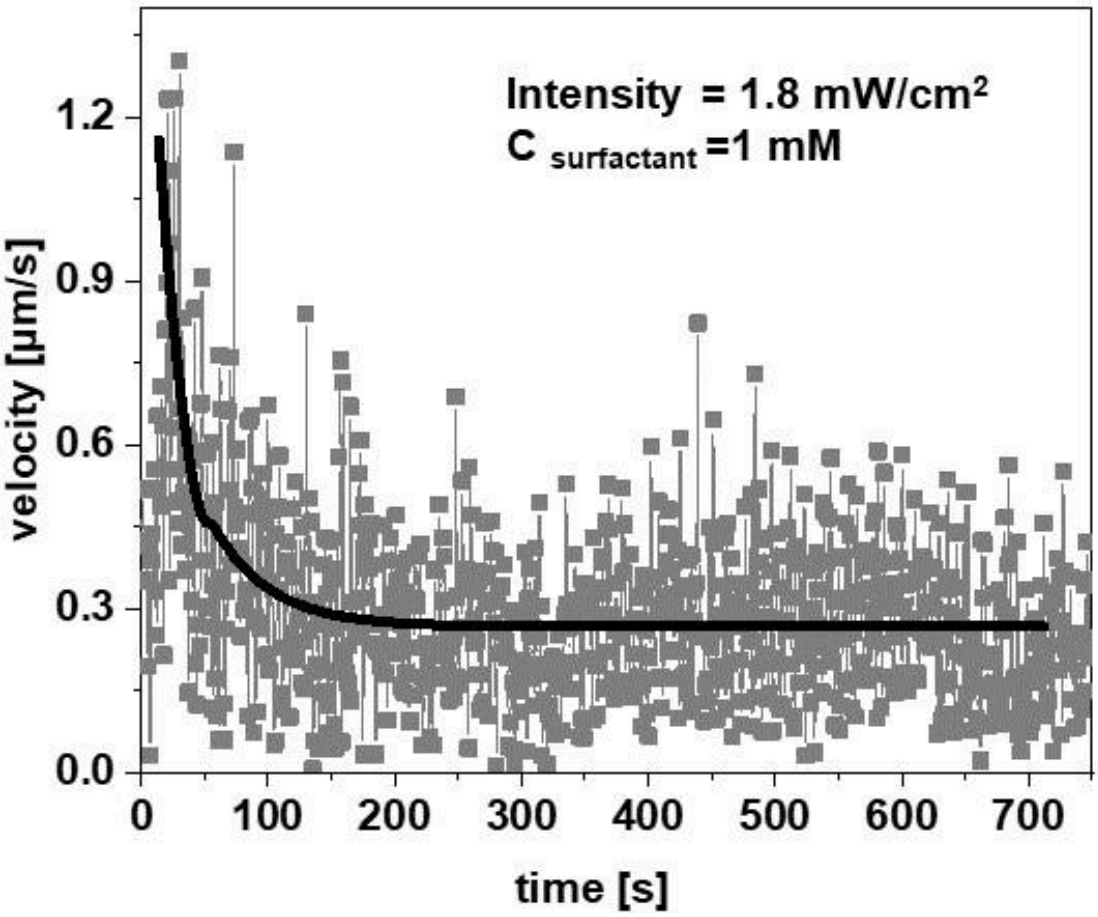

Figure S2. Velocity of particles as a function of irradiation time under exposure to UV light (λ = 365 nm, I = 1.8 mW/cm^2). The initial averaged (over particle ensemble) velocity is 1.2 µm/s.

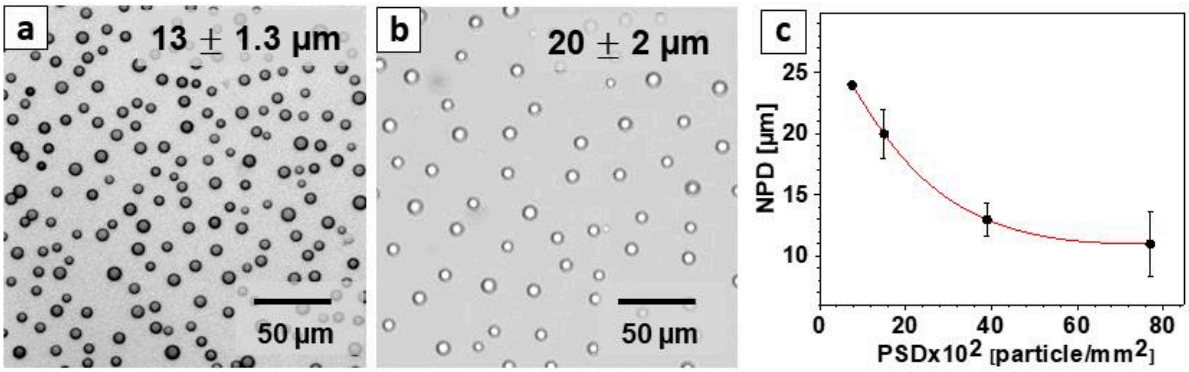

Figure S3. Optical micrographs of an ensemble of 5 µm silica porous particle at a glass surface in 1 mM surfactant solution at different particle surface density (PSD): (a) 15x10^2 mm^{-2}; (b) 39x10^2 mm^{-2}. (c) Nearest particle distance (NPD) as a function of PSD**.**

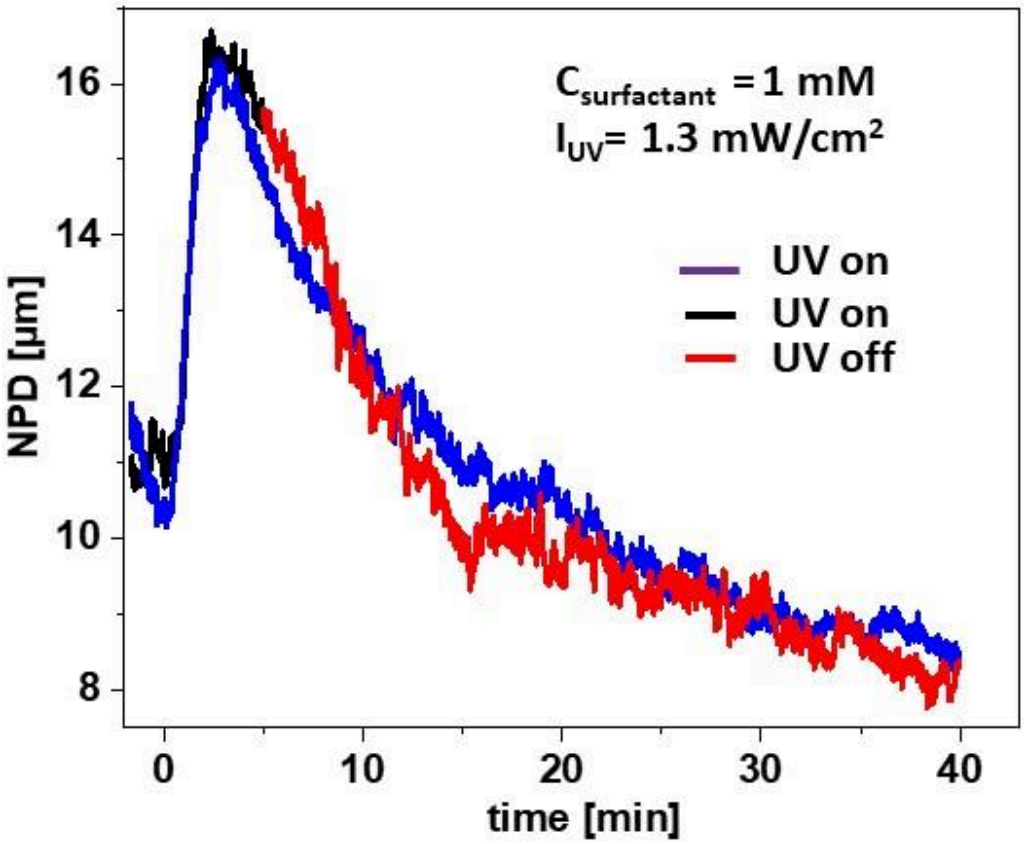

Figure S4. Dependence of NPD on irradiation time for two different irradiation scenarios: the irradiation with UV light is switched on at t = 0, the NPD increases due to DO repulsion between the particles, afterwards in one case the UV light is kept on (blue curve), while in the second scenario the UV light is switched off after 5 min (red curve). In both cases the NPD decreases with time similarly indicating the absence of diffusioosmotic flow. The colloids are depleted of *cis*-isomers and move thermally in the *cis*- enriched surfactant solution. The surfactant concentration is 1mM, the irradiation intensity is 1.3 mW/cm^2.

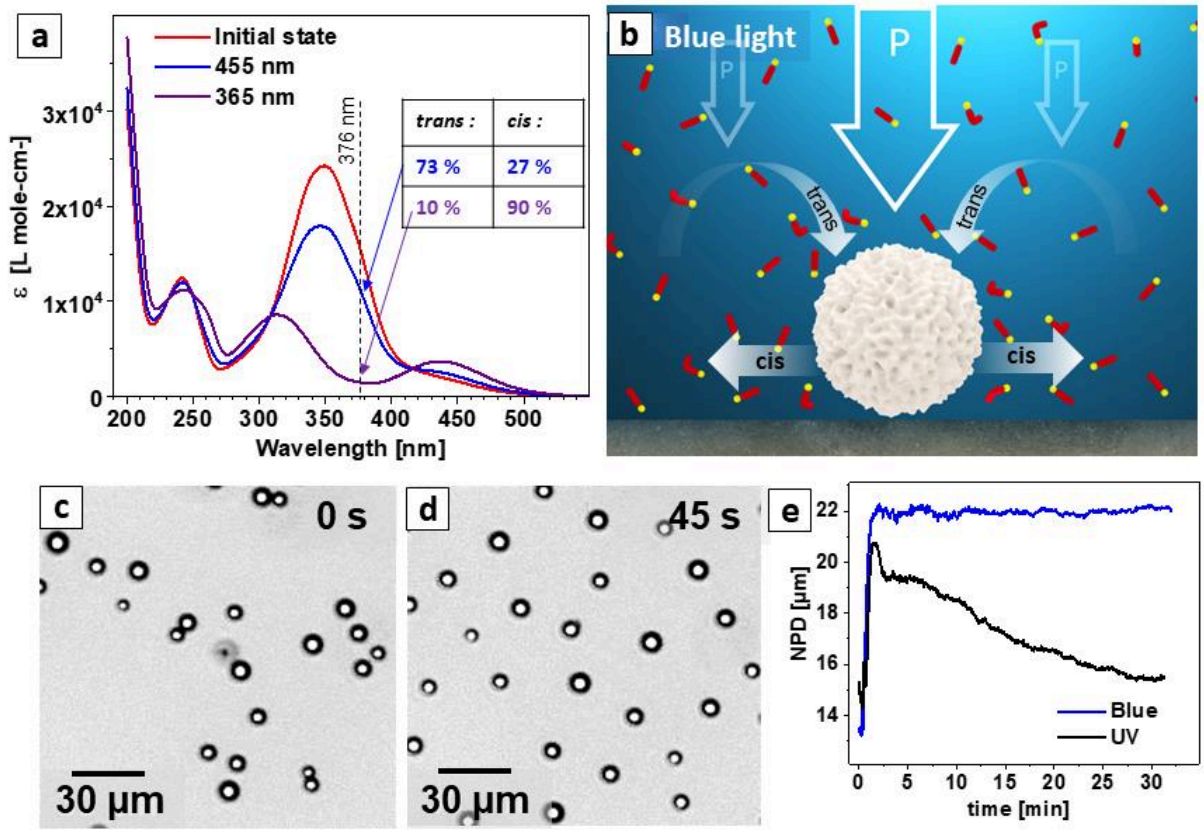

Figure S5. (a) UV-vis absorption spectra of surfactant in dark (*trans* state), under blue (λ = 455 nm) and UV (λ = 365 nm) irradiation. Inset shows the fraction of *trans* and *cis* molecules at the photo stationary states. (b) Scheme of *l*-LDDO flow generated under irradiation with blue light. (c-d) Optical micrographs of mesoporous silica particles at a glass surface under blue light before irradiation (t = 0 s) and after 45 s of light exposure. (e) Average nearest particle distance (NPD) as a function of time during irradiation with UV (black curve) and blue light (blue curve).

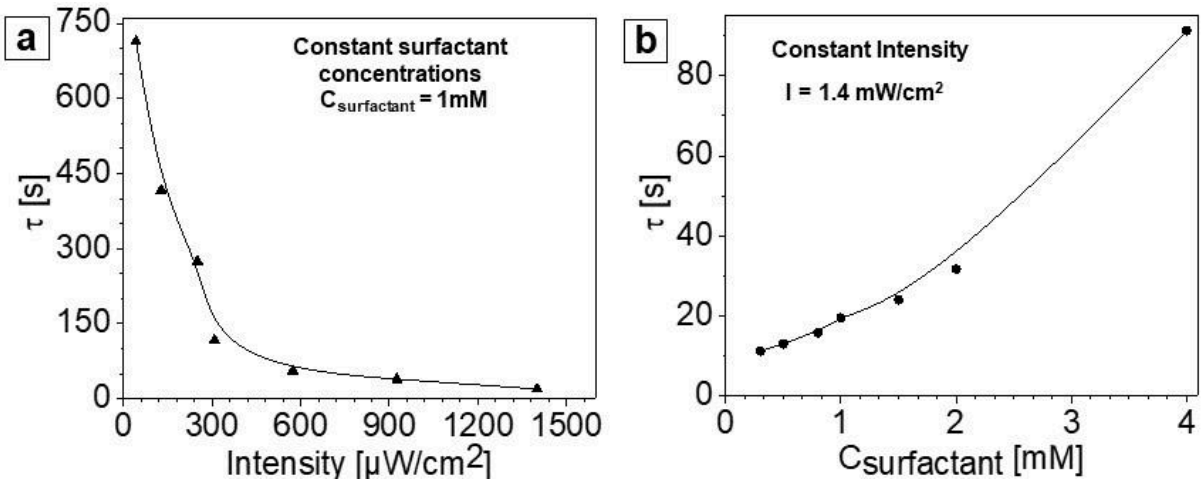

Figure S6. Time constant (τ) of photo-isomerization kinetic of surfactant molecules: (a) for different UV irradiation intensity and constant surfactant concentration of 1 mM, (b) at different surfactant concentration and fixed intensity I = 1.4 mW/cm^2. τ is the decay time of *trans-cis* photo-isomerization.

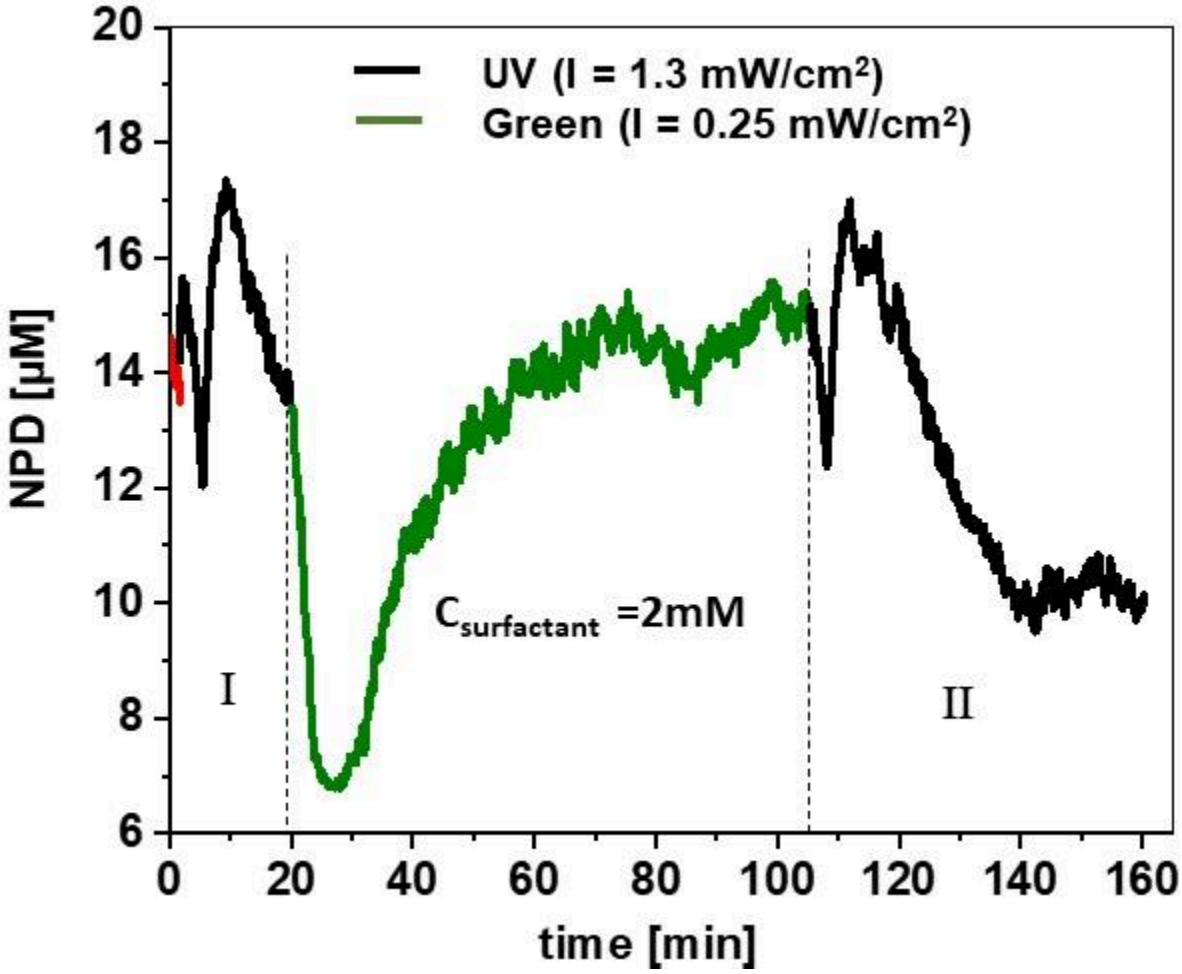

Figure S7. Dependence of NPD on irradiation time during exposure to two different wavelengths (UV, λ = 365 nm, I = 1.3 mW/cm^2, and green, λ = 532 nm, I = 0.25 mW/cm^2) recorded for two cycles. Black line indicates the NPD under UV irradiation during (I) the first cycle (time range from 0 to 20 minutes) and (II) the second cycle (time range from 107 to 160 minutes). Irradiation with green light is performed between 20 and 107 minutes. In both cycles similar behavior of the colloids is observed: when UV is switched on, at first the colloids aggregate during 3 min, which is followed by a separation in 4 min reaching the photo-stationary state, and finishes when the LDDO flow decays. The irradiation with green light is applied after the first cycle in order to convert surfactant to the *trans*-state until equilibration. The intensity of the green light is chosen smaller to assure a slower photo-isomerization and, thus, to allow for *trans*-isomers diffuse into the colloids, ruling out fast micelle formation at the colloidal surface and thus blocking of *trans*-isomer penetration.

Volume 16
Number 5
7 February 2020
Pages 1127–1378

Publication 4

Soft Matter

rsc.li/soft-matter-journal

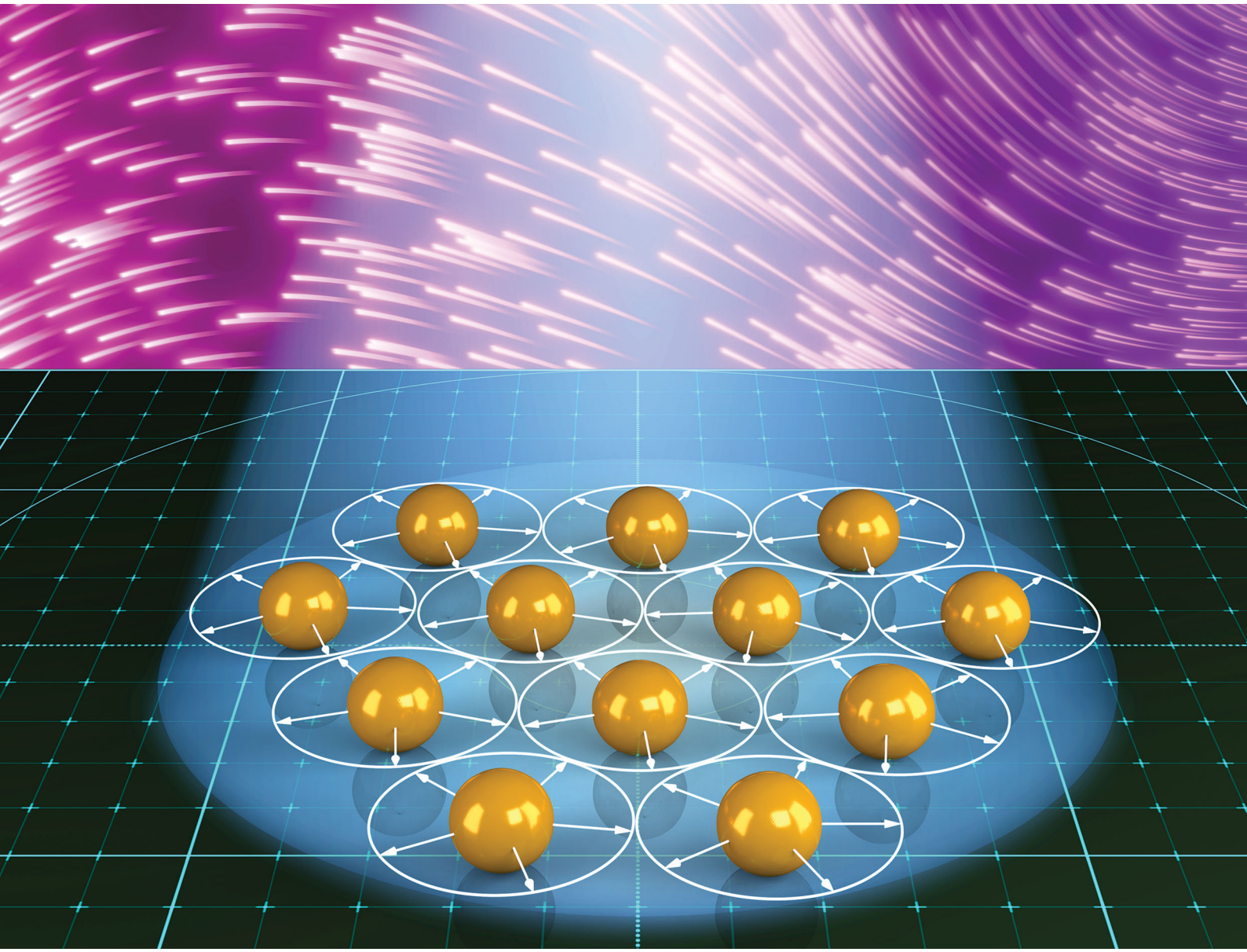

ISSN 1744-6848

ROYAL SOCIETY OF CHEMISTRY

PAPER
Svetlana Santer *et al.*
Light driven guided and self-organized motion of mesoporous colloidal particles

Soft Matter

ROYAL SOCIETY OF CHEMISTRY

PAPER

View Article Online
View Journal | View Issue

Cite this: *Soft Matter*, 2020, **16**, 1148

Light driven guided and self-organized motion of mesoporous colloidal particles†

Pooja Arya,[a] David Feldmann,[ab] Alexey Kopyshev,[a] Nino Lomadze[a] and Svetlana Santer *[a]

Received 17th October 2019,
Accepted 4th December 2019

DOI: 10.1039/c9sm02068c

rsc.li/soft-matter-journal

We report on guided and self-organized motion of ensembles of mesoporous colloidal particles that can undergo dynamic aggregation or separation upon exposure to light. The forces on particles involve the phenomenon of light-driven diffusioosmosis (LDDO) and are hydrodynamic in nature. They can be made to act passively on the ensemble as a whole but also used to establish a mutual interaction between particles. The latter scenario requires a porous colloid morphology such that the particle can act as a source or sink of a photosensitive surfactant, which drives the LDDO process. The interplay between the two modes of operation leads to fascinating possibilities of dynamical organization and manipulation of colloidal ensembles adsorbed at solid–liquid interfaces. While the passive mode can be thought of to allow for a coarse structuring of a cloud of colloids, the inter-particle mode may be used to impose a fine structure on a 2D particle grid. Local flow is used to impose and tailor interparticle interactions allowing for much larger interaction distances that can be achieved with, *e.g.*, DLVO type of forces, and is much more versatile.

Introduction

Understanding and controlling the pattern formation of large groups of artificial micro-swimmers is currently an active topic in various fields of science.[1–8] The interest comes from questions in both fundamental and applied research. On the one hand, it could help to understand the mechanisms directing the consistent motion of active micro-swimmers as observed in different biological systems.[9–16] On the other hand, some interesting applications of self-propelled particles have been reported where different functional tasks are performed such as micro-pumps or micro-motors.[17–19] This could help to tackle many challenges in biology and medicine, such as the use of micro-motors in drug delivery aiming at controlled and localized release of biochemicals that colloids are loaded with.[20–23]

Collective behavior in ensembles of artificial swimmers has been reported by different researchers who used electric fields,[24] magnetic fields[25] or light[26–28] as external stimuli in order to generate particle propulsion. In most cases, the driven swimmers are asymmetric particles commonly known as Janus particles, which show self-propulsion due to generation of chemical or thermal gradients around the particles.[29] Recently our group has introduced the mechanism of light driven diffusioosmosis (LDDO) where motion of micro-particles is established in the presence of a photo-responsive surfactant that is sensitive to light of different wavelengths.[30] The photosensitive surfactant consists of a charged head group and a hydrophobic tail into which the azobenzene moiety is incorporated.[31] The azobenzene undergoes reversible photoisomerization from a *trans* to a *cis* state upon irradiation accompanied by a significant change in molecular properties. For instance, the *cis*-isomer typically possesses a larger dipole moment as compared to the *trans* state.[32] Azobenzene incorporated into the hydrophobic tail of a cationic surfactant thus toggles the hydrophobicity of the whole surfactant as it switches between both isomers upon illumination with UV or blue light, respectively (more hydrophobic (*trans*-) and rather hydrophilic (*cis*-) isomer).[31] When the solution containing such a surfactant is irradiated with focused light an osmotic pressure gradient is created at the solid/liquid interface near the laser spot resulting in a so-called diffusioosmotic flow along the solid surface in response to the lateral pressure gradient. The flow pattern is radial and points outwards when UV light is used, and inwards upon illumination with blue light.

Utilizing the same photo-responsive surfactant it has been reported that the size of mesoporous microgels can be controlled remotely by irradiation with blue light.[33,34] The mechanism is based on a reversible accumulation within and expulsion of surfactant out of the pores of the particles depending on the state of (photo-) isomerization.[35–37] Recently it has been demonstrated that when a rigid porous particle such as porous silica

[a] *Institute of Physics and Astronomy, University of Potsdam, 14476 Potsdam, Germany. E-mail: santer@uni-potsdam.de*
[b] *Tel-Aviv University, School of Mechanical Engineering, Faculty of Engineering, Tel-Aviv, Israel*

† Electronic supplementary information (ESI) available. See DOI: 10.1039/c9sm02068c

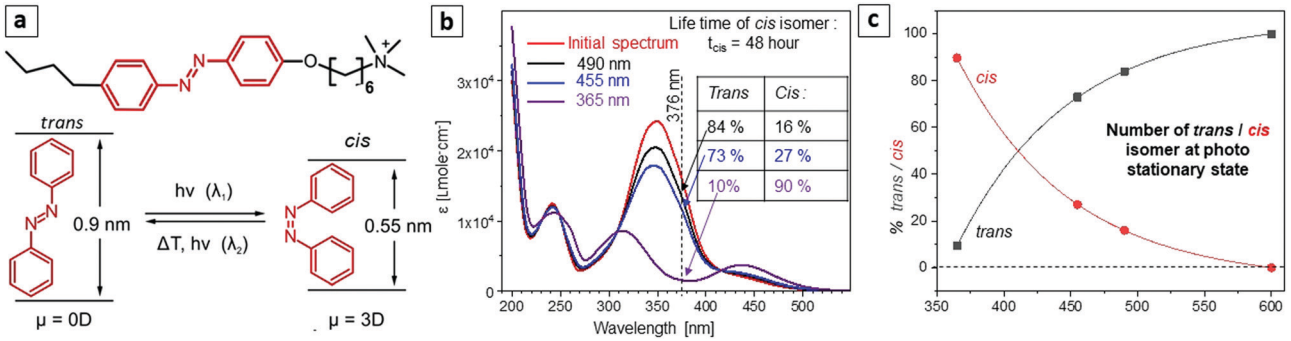

Fig. 1 (a) Chemical structure of azobenzene containing cationic surfactant (C4-azo-OC6TMAB), shown below is a scheme of azobenzene photo-isomerization. (b) UV-Vis absorption spectra of the surfactant at different photo-stationary states during irradiation with UV light (λ = 365 nm) (violet curve), blue light (λ = 455 nm) (blue curve) and 490 nm (black curve). Red curve depicts the initial state after several days of equilibration in dark. The inserted table shows the percentage of *trans* and *cis* isomers in the photo-stationary state. (c) Percentage of *trans* and *cis* isomers as a function of irradiation wavelength at the corresponding photo-stationary state.

colloid is considered the two-way diffusion of surfactant results in the generation of a local light driven diffusioosmotic flow (l-LDDO),[38] that is, each single porous particle becomes a source of the LDDO flow that can be sustained over the whole irradiation time (so far tested for time periods up to several hours).

In this article we investigate an ensemble of mesoporous colloidal particles undergoing reversible aggregation and separation when exposed to light of different wavelengths. Particles are first trapped within a confined area by light induced global diffusio-osmotic flow generated by illumination with UV from above and blue light from below the interface. The colloidal ensemble first exhibits aggregation followed by separation and finally evolves into a grid with approximately uniform interparticle distance. The porosity of the particles and the relative fraction of *trans* and *cis* isomers under irradiation with different wavelength are the two key parameters governing this peculiar collective phenomenon.

Experimental part

Materials

Mesoporous silica microspheres of 5 μm in diameter are purchased from Micromod (Sicastar, Prod. No. 43-00-503, Germany). The particles with pore diameter of 6 nm have a specific surface area (BET) of 850 $m^2 g^{-1}$ as provided by Sicastar. The porous particles are dispersed in aqueous solution at different concentrations ranging between 0.05 mg ml^{-1} and 0.5 mg ml^{-1}.

The azobenzene containing trimethyl-ammonium bromide surfactant (C4-Azo-OC6TMAB) is synthesized as described elsewhere.[39] The surfactant molecule consists of a positively charged trimethylammonium bromide head group, the spacer of 6 methylene groups connecting to the azobenzene unit with a butyl tail attached (Fig. 1a). The surfactant is dissolved in Milli-Q water and diluted to the required concentrations ranging from 0.1 to 2 mM. The critical micelle concentration of *trans*-isomers, CMC_{trans}, is 0.5 mM.

Azobenzene surfactant undergoes photo-isomerization from *trans* to *cis* state under irradiation with UV light and back from *cis* to *trans* upon exposure to light of longer wavelength as described elsewhere.[40] The *trans* isomer has a characteristic absorption band (π–π^* transition) with a maximum at 351 nm, while the spectrum of the *cis* isomer is characterized by two absorption bands with maxima at 313 nm (π–π^* transition) and at 437 nm (n–π^* transition) (Fig. 1b). The lifetime of the *cis* isomer in dark or under illumination with red light of λ = 600 nm is 48 hours.[40] In a photo-stationary state under irradiation with different wavelengths the amount of *trans* and *cis* isomers in solution differs (Fig. 1c). Under UV (λ = 365 nm) illumination at the photo-stationary state, the surfactant molecules are predominantly in the *cis* state (90%), while under irradiation with blue light (λ = 455 nm) there are 27% of *cis* and 73% of *trans* isomers in solution.

Sample preparation. The aqueous dispersion of silica particles is mixed with surfactant solution of different concentrations and kept at least for 1 hour for equilibration. The sample is inserted in a closed chamber of height 920 μm with a sample volume of 40 μl. All samples are kept in the dark or in red light to prevent premature photo-isomerization.

Methods

An inverted Olympus IX71 microscope equipped with two different wavelength of light source is used for measurements. UV LED (M365L2-C1) and Blue LED (M490L4 and M455L3) purchased from Thorlabs Gmbh (Lübeck, Germany) are used for sample irradiation from above. A monochromatic blue laser (λ = 491 nm, LAS/491/50, Olympus) is utilized as a focused light source. The laser spot size is adjusted through external iris integrated in the microscope. The laser beam is focused through the objective of the microscope to the solid–liquid interface, where the particles are adsorbed. An inverted microscope is equipped with UV light and blue laser so that both light sources can be used simultaneously during the experiment. The illumination power is measured by an optical power meter 1918-R with sensor 918D-UV-OD3R (Newport Corporation, Irvine, CA, USA). Most of the images are acquired with a Hamamatsu Orca ER (C4742-80) at a rate of 1 frame per sec. The setup is kept in dark to prevent the uncontrolled isomerization. When required red light (M625L1-C1, Thorlabs Gmbh) is used for imaging as it does not affect the photo-stationary state of the

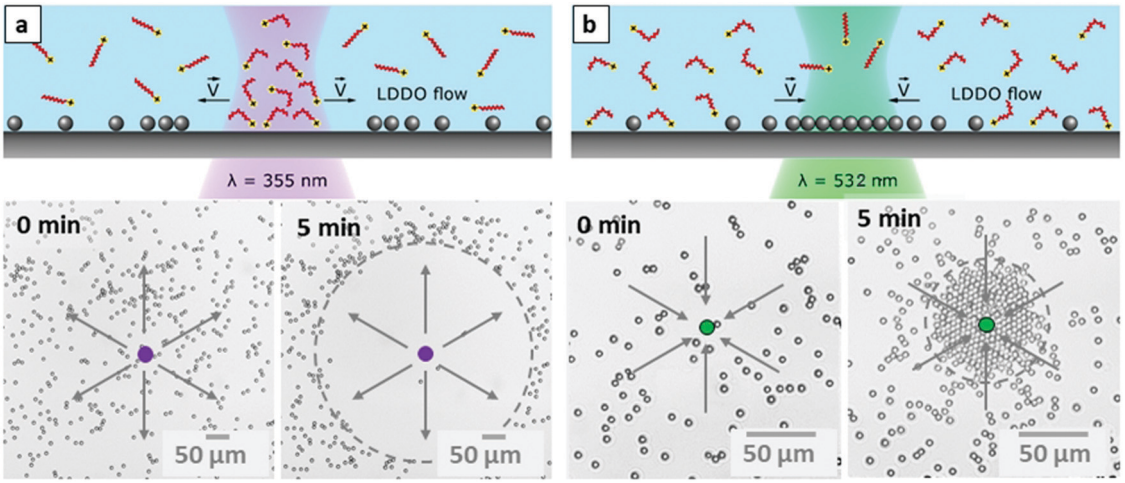

Fig. 2 Schemes (above) and optical micrographs (below) of silica non-porous particles (d = 5 μm) at a glass surface immersed into azobenzene containing surfactant solution (c_{azo} = 1 mM). (a) Under irradiation with focused UV laser light (λ = 355 nm, P = 1.5 μW), the colloids are moved out of the laser spot in radial direction (indicated by grey arrows in optical micrographs), after 5 minutes of irradiation, a circular area around the laser spot is effectively cleaned from particles. (b) The direction of particle motion is reversed under irradiation with focused green light (λ = 532 nm). The particles are gathered towards the laser spot. The sample is first irradiated with UV light for 10 minutes in order to promote the majority of surfactant molecules to the *cis*-state. Corresponding Videos of particle motion are provided in Fig. S1 (ESI†).

surfactant. The intensity of irradiation for all light source is kept constant over the whole imaging area.

Particle motion is tracked using the Mosaic Single Particle Tracking plugin for ImageJ (Rasband, W.S., ImageJ, U. S. NIH, Bethesda, Maryland, USA). The tracking algorithm is described by Koumoutsakos.[41] The analysis of the particle motion is performed using Matlab script.

UV-Vis absorption spectroscopy (Cary 5000 UV-Vis-NIR spectrophotometer, Agilent Technologies, USA) is used to measure the amount of surfactant absorb by porous colloids.

Scanning electron microscope (SEM; Ultraplus 4061, Zeiss, Germany) is utilized to characterize colloidal particles.

Results

Global LDDO flow

When aqueous solution of azobenzene containing surfactant is irradiated with a focused laser beam, there is a generation of light driven diffusioosmotic flow (LDDO) at the solid–liquid interface (see schemes in Fig. 2).[30] The direction of radially centered flow depends on the wavelength of applied irradiation: there is outward flow under UV-light, and inward flow during exposure to green light. In the latter case the sample is first irradiated with UV light in order to convert all surfactant molecules in to the *cis*-state. The particles trapped at a solid–liquid interface are moved passively within the LDDO flow as shown in Fig. 2 and Fig. S1 (ESI,† where the corresponding Videos are provided). The motion does not depend on particle shape (spherical, rod-like, *etc.*) and size (tested for particle dimensions between 500 nm and 50 μm).[30]

Local LDDO flow: long range repulsive or attractive interactions

Colloids with complex surfaces such as porous silica particles (d = 1–20 μm) follow the LDDO flow as well, *i.e.* they are removed out of the irradiated area under focused UV light, and gathered under irradiation with light of longer wavelength (blue or green). Additionally, because of the high surface to volume ratio of the porous particles, there is a generation of local light driven diffusioosmotic (l-LDDO) flow around each single colloid, even if the irradiation is not focused and rather homogeneously applied to the sample. To illustrate this point, we have studied the motion of porous particles of 5 μm in diameter under irradiation with global (non-focused) light of λ = 455 nm (blue light) and λ = 365 nm (UV light). The particles are dispersed in aqueous solution containing photosensitive surfactant at c_{azo} = 1 mM and trapped on a glass surface (Fig. 3). Before irradiation the particles undergo thermal Brownian motion and randomly distribute across the surface (see Fig. 3a and b t = 0 s). When blue light is switched on, there is a generation of local-LDDO flow around each single colloid, resulting in a long range mutual repulsion between porous particles. This repulsion is exclusively due to diffusioosmotic flow and will be referred to as diffusioosmotic repulsion in what follows. As can be inferred from the Videos in Fig. S2 (ESI†) and the time dependent series of optical micrographs in Fig. 3a (t = 45 s, 375 s, 30 min), the particles start to move, repel each other and form two-dimensional regularly spaced grids. The flow induced particle repulsion is sustained during the whole process of irradiation, verified for up to 9 hours of light exposure. The reason of such long-term stability can be explained as follows. Porous particles dispersed in surfactant solution absorb molecules in *trans*-state, such that the surfactant is stored within in the particle (for c_{azo} = 1 mM and $c_{particle}$ = 0.1 mg, 10% of surfactant is in the particles). When the light is switched on, photo-isomerization from *trans*- to *cis*-state occurs not only in solution, but also in the particles since the silica colloids are transparent in the visible range. The more hydrophilic *cis*-isomers formed within the particle are expelled from the pores resulting in generation of a local excess

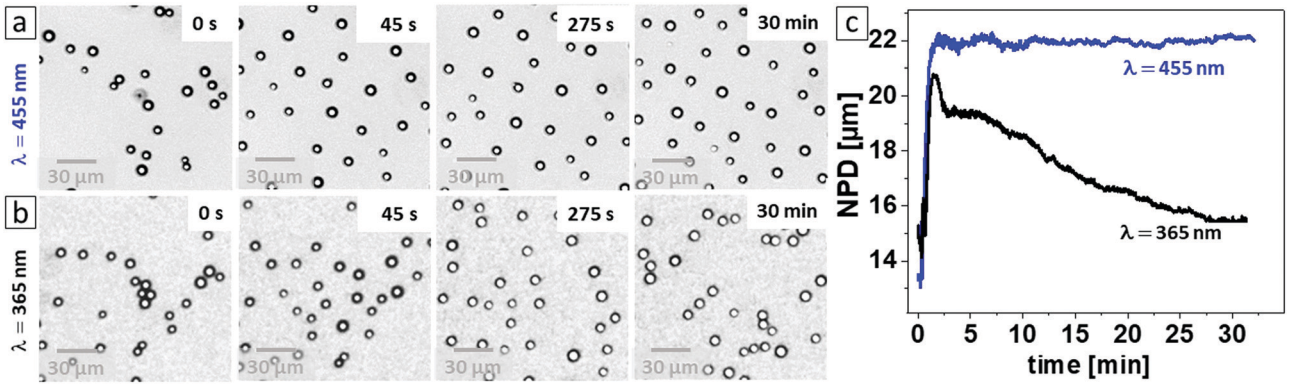

Fig. 3 Optical micrographs of porous silica particles (d = 5 μm) trapped at a glass surface and immersed in aqueous solution of photo-sensitive surfactant (c_{azo} = 1 mM). (a) Under exposure to blue light (λ = 455 nm, I = 1.3 mW cm^{-2}) for different irradiation time: t = 0 s, 45 s, 275 s and 30 min. (b) Under UV light (λ = 365 nm, I = 1.35 mW cm^{-2}) irradiation t = 0 s, 45 s, 275 s and 30 min. (c) average nearest particle distance (NPD) is shown as a function of irradiation time for blue (blue curve) and UV (black curve) light. Videos of particle motion under irradiation with blue and UV light are provided in Fig. S2 (ESI†).

concentration of *cis*-isomers in the vicinity of the colloid, inducing a local osmotic pressure gradient and corresponding local LDDO flow. The flow points radially away from the particle and extends over distances as large as several times the particle diameter and beyond. One can state that the porous particle acts as a micro pump. Its continuous operation, however, requires the irradiation wavelength to be well-chosen. Indeed, when UV light is applied, after the initially strong particle repulsion (Fig. 3b, t = 45 s), the l-LDDO flow decays as irradiation goes on and ultimately the particles start to move randomly (see Fig. 3b, t = 30 min and Fig. 3c, black curve). The particles effectively use up all of the surfactant molecules stored as "fuel" in the interior within several minutes of irradiation (Fig. 3c) and since in solution under UV irradiation there is only a small amount of *trans*-isomers left, there is no chance for a "free refill". In contrast, under blue light in a photo-stationary state, there are 73% of *trans*- and 27% of *cis*-molecules, meaning that when *cis*-isomer leaves the pore it makes room for *trans*- present in solution to enter the colloid. In this way a steady state flow of *cis*- and *trans*-isomers out of and into the particle can be maintained indefinitely under exposure to blue light. To characterize the particle ensemble, average nearest particle distance (NPD) is plotted as a function of irradiation time for both wavelengths, blue and UV (Fig. 3c). Under blue light (blue curve) the NPD is constant over the whole irradiation time, while under UV light (black curve) the NPD starts decreasing after 150 s due to exhaustion of *cis*-isomers flowing out of the particles.

An interesting question is, given suitable experimental conditions, can we also induce mutually attractive particle interactions? Indeed, we observe that when irradiation with blue light, is switched off, the particles appear to gather with initial velocity of single particles of *ca.* 0.4 μm s^{-1} (Fig. 4d) resulting in formation of tight aggregates (Fig. 4b, c and red curve in Fig. 4d showing the analysis of NPD as a function of time) (see Video in Fig. S3, ESI†). The gathering is actually due to mutual attractive interactions (and not because of a residual global flow patterns) and of diffusioosmotic nature. These interactions can be explained by the generation of depletion zones of *trans*-isomers around neighboring particles. When the blue light is switched off, the production of *trans*-isomers stops, but in the vicinity of the colloids the *trans*-molecules still diffuse into the pores decreasing the local concentration of *trans*-isomers around the colloids. This in turn results in generation of local osmotic pressure gradients and establishes local flows pointing towards the neighboring particles and small aggregates. The strength of attraction decays as soon as the pores are saturated with *trans*-isomers. On switching irradiation with blue light on again, the l-LDDO flow results in renewed particle repulsion. Summarizing this part, one can conclude that in our system we can tune the sign of the long range interaction potential

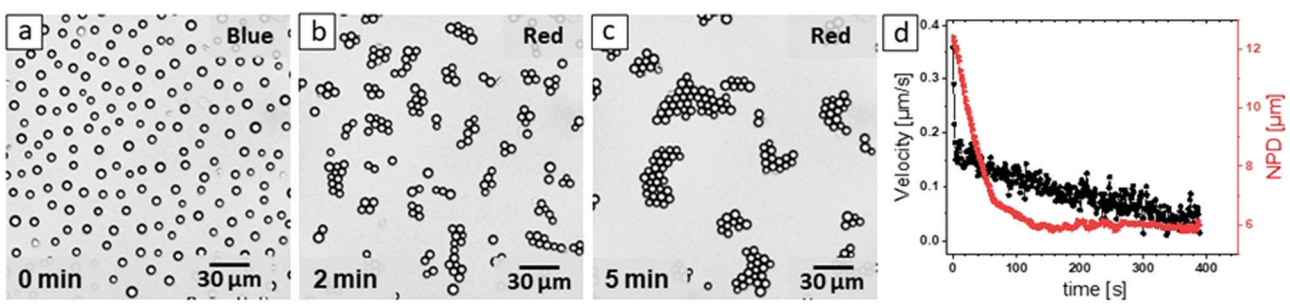

Fig. 4 Optical micrographs of the ensemble of porous colloids (a) under irradiation with blue light, and after switching off the light (*i.e.* using only red light for imaging) after: (b) t = 2 min, (c) t = 5 min. (d) Analysis of the average particle velocity (black dots) and average NPD (red curve) as a function of time after switching off the irradiation with blue light. Fig. S3 (ESI†) depicts corresponding Video.

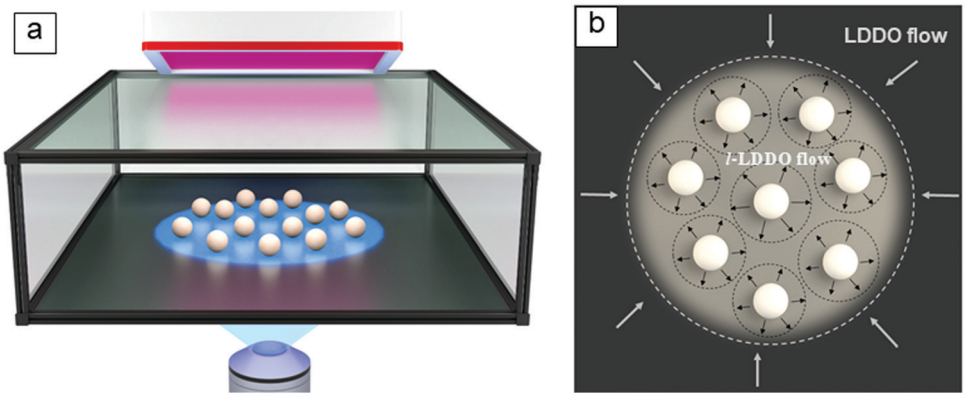

Fig. 5 Scheme of the setup equipped with UV and blue light source. Illumination with UV light (λ = 365 nm, P = 1.05 mW) is from below and covers the whole sample area, while the blue light (λ = 491 nm, P = 190 μW, laser diameter = 325 μm) is focused on a much smaller circular area of the solid-(glass) liquid (aqueous solution) interface. The colloids are shown schematically as white spheres. The sample is placed in a closed chamber preventing exposure to ambient air. (b) Top view of the process: white and black arrows show the direction of the flow due to global LDDO and local-LDDO flow, respectively.

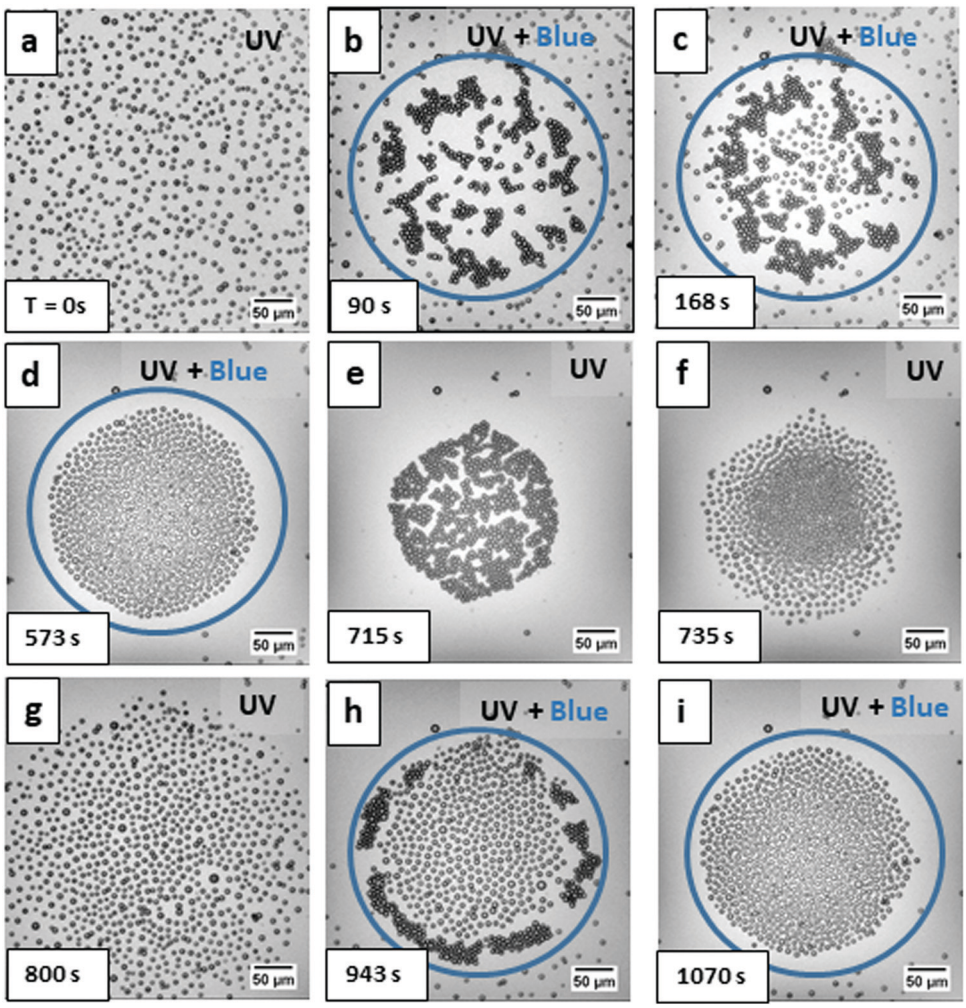

Fig. 6 Optical microscope images of porous silica particles (d = 5 μm) of concentration 0.2 mg ml^{-1} in 1 mM azobenzene containing surfactant. (a) The photo-stationary state is achieved after 10 min of global UV irradiation; (b) after switching on irradiation with focused blue laser light (λ = 491 nm, D_{laser} = 325 μm, P = 190 μW), the particles move to the light spot and aggregate; (c) aggregated particles in the center of the laser spot start separating; (d) in *ca.* 10 min particles are completely separated and stay trapped at the irradiated area; (e) 15 seconds after switching off irradiation with blue light. Particles aggregate first towards the center and subsequently are pushed out of the center within a few seconds (f and g); (h and i) the blue laser is switched on again. The corresponding Videos are provided in Fig. S4 (ESI†).

between the colloids from repulsive (under blue light) to attractive (first minutes when blue light is switched off).

Combination of global and local LDDO flow

Both processes of LDDO flow generation by irradiation with focused light and formation of local flow around each colloid can be induced simultaneously in one system by combining illumination with two different wavelength UV and blue. The scheme of the experiment is shown in Fig. 5. The setup with its solid–liquid interface is globally and homogeneously exposed to UV light allowing for continuous *trans* to *cis* photo-isomerization. The blue laser light is focused through the microscope objective and reaches the interface from below.

After initial irradiation with UV light for 10 min, the colloids undergo thermal motion in the solution with about 90% of surfactant molecules in their *cis*-state (Fig. 6a). When the blue light focused on a circular area of about 325 μm in diameter is switched on, the particles exhibit a combination of LDDO and l-LDDO motion (Fig. 6a–d), *i.e.* they move towards the irradiated area with a maximal particle velocity of 5 μm s^{-1} as shown in Fig. S4 (ESI†), but within the confined area a regular 2D particle grid emerges (Fig. 6d) gradually over time, with a uniform interparticle spacing. At the beginning of the irradiation one observes a transient state where small aggregates consisting of several colloids are formed first at the irradiated area (Fig. 6b). This is explained by the fact that the *trans*-molecules formed enter the empty pores of the particles generating a depletion zone of *trans*-isomers around each particle. Overlapping depletion zones of neighboring particles lead to their mutual attraction and aggregation, since the LDDO flow crucially depends on the spatial distribution of the *trans*- and *cis*-isomers relative to each colloid. With ongoing irradiation, however, (Fig. 6c), the particles start to repel each other because a steady state gradient of relative *trans–cis* concentration has been established, and the flow generated is now directed radially outwards and finally form a well-separated confined ensemble (Fig. 6d). At this point the terminology ''radially outward directed flow'' should be made more precise. Of course, the particle does neither act as a source or sink of liquid flow itself, only absorbs or replenishes surfactant molecules in their *cis* form. The flow is generated outside the particle through the local gradients of *cis*/*trans* concentration, leading to lateral pressure gradients. These gradients actually set in motion a three-dimensional convective flow cell with a stagnation point centered at the particle position. When we say that ''outward directed radial flow'' leads to mutual particle repulsion, we actually mean that the three dimensional, cylindrical convection zones are interacting accordingly.

The separation process sets in first within the center of irradiation spot where the illumination intensity is at maximum. After *ca.* 10 minutes of irradiation, the colloidal ensemble forms a well separated, regularly spaced grid (Fig. 6d). This phase is stable as long as the irradiation with both UV and blue light is kept constant. The NPD, as the distribution of inter-particle distances measured between colloid midpoints peaks at 7 μm, implying a separation of 2 μm from surface to surface.

The inter-particle distance is defined by the number of confined particles with all other parameters fixed. Fig. 7a shows a well separated 2D arrangement of colloidal particles confined by the laser spot (with a NPD of 10 μm implying a surface-to-surface distance of 5 μm). In this case, the concentration of colloids is two times smaller (0.1 mg ml^{-1}). In contrast, when non-porous particles are irradiated under similar conditions, they are gathered towards the center of the laser spot and form a grid with a NPD of 5 μm, *i.e.* a densely packed monolayer (Fig. 7b).

As soon as the irradiation with blue light is switched off but retaining global UV illumination, particles start to move towards the center forming a densely packed cluster within the first 15 seconds (Fig. 6e) (after irradiation with blue light has been halted) followed by subsequent strong separation (Fig. 6e–g) as in the case of irradiation with global UV light described in Fig. 3b. The aggregation of the particles (Fig. 6e) can be explained by the combination of two effects. On the one hand,

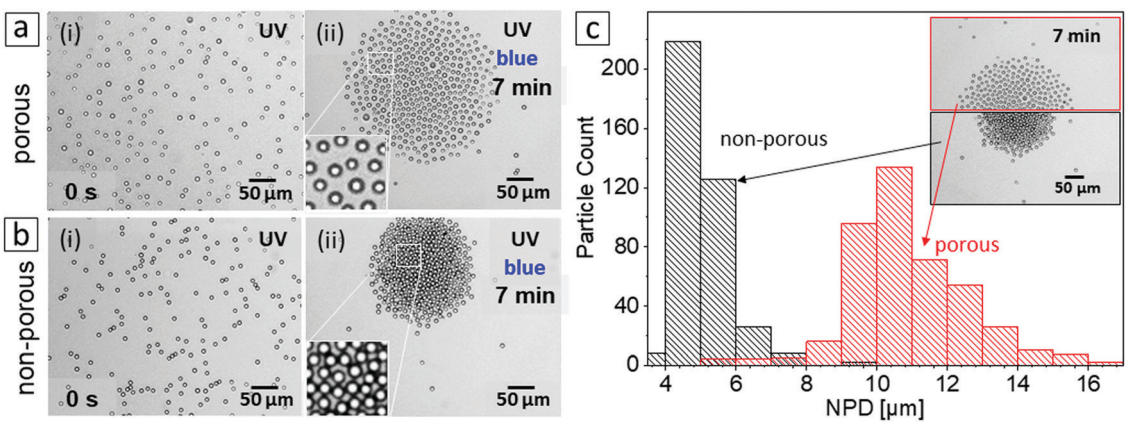

Fig. 7 Comparison of porous and non-porous particles (c_p = 0.1 mg ml^{-1}, c_{azo} = 1 mM) under simultaneous blue (λ = 491 nm, beam diameter = 325 μm) and UV (λ = 365 nm, global) irradiation. (a) Porous particles: (i) photo stationary state achieved after 10 min of global UV irradiation, (ii) 7 min after switching on irradiation with the focused blue laser. (b) Non-porous particles: (i) photo stationary state achieved after 10 min of global UV irradiation, (ii) 7 min after irradiation with the focused blue laser, (c) Nearest particle distance for porous (average: 10 μm) and non-porous (average: 5 μm) colloids. The corresponding Video is provided in Fig. S5 (ESI†).

in the absence of blue light a depletion zone of *trans* isomers around the particles is formed causing strong mutual attraction of colloids in immediate proximity, similar to situation describe in Fig. 6b. Additionally, LDDO flow gathers particles more tightly due to the decrease of repulsion, since the local flow around each colloids decays. As soon as the blue light is turned on, the process starts over (Fig. 6h and i). The aggregation/separation process can be repeated many times (see Video in Fig. S6, ESI†).

Conclusions

We demonstrate and explain guided and self-organized motion of an ensemble of mesoporous colloidal particles that undergoes dynamic aggregation or separation when exposed to light of different wavelengths. At the heart of the phenomenology described here is a photo-switchable azobenzene containing cationic surfactant which undergoes a reversible *trans–cis* photoisomerization from a more hydrophobic to a more hydrophilic state upon illumination with light of different wavelengths. The wavelength can be tuned to achieve different ratios of *cis–trans* isomers in solution at the photo-stationary state. Under exposure to UV light almost all surfactant molecules are converted to *cis*-state, while under illumination with blue light 3/4(73%) of *trans* and 1/4(27%) of *cis*-isomers are present. Using the isomerization property of photo-active surfactant molecule under illumination with focused UV or blue light, we can generate at the solid/liquid interface a light driven diffusioosmotic (LDDO) flow dragging colloidal particles passively across the surface. Additionally, porous particles may also act as a source of radially directed local LDDO (l-LDDO). With the porous particle representing a stagnation point, a cylindrical three dimensional convection zone is created that in the vicinity of the solid liquid interfaced is perceived as a radially directed outward flow that under steady-state conditions with illumination with blue light leads to an effective and persistent inter-particle repulsion. l-LDDO flow can however also cause attraction between particles. When in the stationary state the blue light source is switched off, in the following first few minutes the particles attract each other due to the generation of depletion zones of *trans*-isomers because they enter the pores poor of *trans* species until saturation is achieved. We have demonstrated especially mutual particle repulsion facilitates the creation of 2D regularly spaced grids of mesoporous particles trapped within a confined area by LDDO flow due to the simultaneous irradiation with global UV light. The processes involved are quasi-stationary and may be operated indefinitely.

Conflicts of interest

There are no conflicts to declare.

Acknowledgements

This research is supported by the Priority Program 1726 ''Microswimmers-From Single Particle Motion to Collective Behaviour'', Germany; DFG (SA1657/8-1) and by the International Max Planck Research School on Multiscale Bio-Systems (IMPRS), Potsdam, Germany. We thank Prof. C. Beta for fruitful discussions and the technical support during measurements with optical microscopy.

References

1 C. Bechinger, R. Di Leonardo, H. Löwen, Ch. Reichhardt, G. Volpe and G. Volpe, *Rev. Mod. Phys.*, 2016, **88**, 045006.
2 A. Wysocki, R. G. Winkler and G. Gompper, *Europhys. Lett.*, 2014, **105**, 48004.
3 J. Stenhammar, R. J. Allen, D. Marenduzzo and M. E. Cates, *Soft Matter*, 2014, **10**, 1489–1499.
4 T. Speck, J. Bialké, A. M. Menzel and H. Löwen, *Phys. Rev. Lett.*, 2014, **112**, 218304.
5 Y. Fily and M. C. Marchetti, *Phys. Rev. Lett.*, 2012, **108**, 235702.
6 G. S. Redner, M. F. Hagan and A. Baskaran, *Phys. Rev. Lett.*, 2013, **110**, 055701.
7 J. Stenhammar, A. Tiribocchi, R. J. Allen, D. Marenduzzo and M. E. Cates, *Phys. Rev. Lett.*, 2013, **111**, 145702.
8 R. Wittkowski, A. Tiribocchi, J. Stenhammar, R. Allen, D. Marenduzzo and M. E. Cates, *Nat. Commun.*, 2014, **5**, 4351.
9 A. Das, A. Polley and M. Rao, *Phys. Rev. Lett.*, 2016, **116**, 068306.
10 J. F. Hancock, *Nat. Rev. Mol. Cell Biol.*, 2006, **7**, 456–462.
11 T. S. Van Zanten, A. Cambi, M. Koopman, B. Joosten, C. G. Figdor and M. F. Garcia-Parajo, *Proc. Natl. Acad. Sci. U. S. A.*, 2009, **106**, 18557.
12 D. Goswami, K. Gowrishankar, S. Bilgrami, S. Ghosh, R. Raghupathy, R. Chadda, R. Vishwakarma, M. Rao and S. Mayor, *Cell*, 2008, **135**, 1085–1097.
13 K. Gowrishankar, S. Ghosh, S. Saha, C. Rumamol, S. Mayor and M. Rao, *Cell*, 2012, **149**, 1353–1367.
14 A. Chaudhuri, B. Bhattacharya, K. Gowrishankar, S. Mayor and M. Rao, *Proc. Natl. Acad. Sci. U. S. A.*, 2011, **108**, 14825–14830.
15 D. Lingwood and K. Simons, *Science*, 2010, **327**, 46–50.
16 A. Sokolov, I. S. Aranson, J. O. Kessler and R. E. Goldstein, *Phys. Rev. Lett.*, 2007, **98**, 1–4.
17 M. Ibele, T. E. Mallouk and A. Sen, *Angew. Chem., Int. Ed.*, 2009, **48**, 3308–3312.
18 R. Niu, T. Palberg and T. Speck, *Phys. Rev. Lett.*, 2017, **119**, 1–5.
19 R. Niu, E. C. Oguz, H. Müller, A. Reinmüller, D. Botin, H. Löwen and T. Palberg, *Phys. Chem. Chem. Phys.*, 2017, **19**, 3104–3114.
20 B. Khezri, S. M. B. Mousavi, L. Krejčová, Z. Heger, Z. Sofer and M. Pumera, *Adv. Funct. Mater.*, 2019, **29**, 1–10.
21 J. Lu, E. Choi, F. Tamanoi and J. I. Zink, *Small*, 2008, **4**, 421–426.
22 X. Wang, L. Baraban, A. Nguyen, J. Ge, V. R. Misko, J. Tempere, F. Nori, P. Formanek, T. Huang, G. Cuniberti, J. Fassbender and D. Makarov, *Small*, 2018, **14**, 1–11.
23 A. Aubret, M. Youssef, S. Sacanna and J. Palacci, *Nat. Phys.*, 2018, **14**, 1114–1118.
24 J. Yan, M. Han, J. Zhang, C. Xu, E. Luijten and S. Garnick, *Nat. Mater.*, 2016, **15**, 1095–1099.
25 M. Vilfan, N. Osterman and A. Vilfan, *Soft Matter*, 2018, **14**, 3415–3422.

26 J. Palacci, S. Sacanna, A. P. Steinberg, D. J. Pine and P. M. Chaikin, *Science*, 2013, **339**, 936–939.
27 D. Baigl, *Lab Chip*, 2012, **12**, 3637–3653.
28 Y. Hong, M. Diaz, U. M. Córdova-Fteueroa and A. Sen, *Adv. Funct. Mater.*, 2010, **20**, 1568–1576.
29 A. Walther and A. H. E. Müller, *Chem. Rev.*, 2013, **113**, 5194–5261.
30 D. Feldmann, S. R. Maduar, M. Santer, N. Lomadze, O. I. Vinogradova and S. Santer, *Sci. Rep.*, 2016, **6**, 36443.
31 S. Santer, *J. Phys. D: Appl. Phys.*, 2017, **51**, 013002.
32 M. Montagna and O. Guskova, *Langmuir*, 2018, **34**, 311–321.
33 Y. Zakrevskyy, M. Richter, S. Rakrevska, N. Lomadze, R. Klitzing and S. Santer, *Adv. Funct. Mater.*, 2012, **22**, 5000–5009.
34 M. Richter, Y. Zakrevskyy, M. Eiselea, N. Lomadze, S. Santer and R. Klitzing, *Polymer*, 2014, **55**, 6513–6518.
35 A. M. Rumyantsev, S. Santer and E. Y. Kramarenko, *Macromolecules*, 2014, **47**, 5388–5399.
36 S. Schimka, N. Lomadze, M. Rabe, A. Kopyshev, M. Lehmann, R. V. Klitzing, A. M. Rumyantsev, E. Kramarenko and S. Santer, *Phys. Chem. Chem. Phys.*, 2017, **19**, 108–117.
37 S. Schimka, Y. D. Gordievskaya, N. Lomadze, M. Lehmann, R. V. Klitzing, A. M. Rumyantsev, E. Kramarenko and S. Santer, *J. Chem. Phys.*, 2017, **147**, 031101.
38 D. Feldmann, P. Arya, T. Y. Molotilin, N. Lomadze, A. Kopyshev, O. I. Vinogradova and S. Santer "Extremely long-range light-driven repulsion of porous microparticles" submitted to Langmuir, 2019.
39 D. Dumont, T. Galstian, S. Senkow and A. Ritcey, *Mol. Cryst. Liq. Cryst.*, 2002, **375**, 341–352.
40 Y. Zakrevskyy, A. Kopyshev, N. Lomadze, E. Morozova, L. Lysyakova, N. Kasyanenko and S. Santer, *Phys. Rev. E: Stat., Nonlinear, Soft Matter Phys.*, 2011, **84**, 1–9.
41 I. F. Sbalzarini and P. Koumoutsakos, *J. Struct. Biol.*, 2005, **151**, 182–195.

Applied Physics Letters ARTICLE scitation.org/journal/apl

Light-driven motion of self-propelled porous Janus particles

Cite as: Appl. Phys. Lett. **115**, 263701 (2019); doi: 10.1063/1.5129238
Submitted: 27 September 2019 · Accepted: 11 December 2019 ·
Published Online: 23 December 2019

David Feldmann,[1,2] Pooja Arya,[1] Nino Lomadze,[1] Alexey Kopyshev,[1] and Svetlana Santer[1,a)]

AFFILIATIONS

[1]Institute of Physics and Astronomy, University of Potsdam, 14476 Potsdam, Germany
[2]School of Mechanical Engineering, Faculty of Engineering, Tel-Aviv University, 69978 Tel-Aviv, Israel

[a)]santer@uni-potsdam.de

ABSTRACT

We introduce a versatile mechanism of light-driven self-propelled motion applied to porous Janus-type particles. The mechanism is based on the generation of local light-driven diffusio-osmotic (l-LDDO) flow around each single porous particle subjected to suitable irradiation conditions. The photosensitivity is introduced by a cationic azobenzene containing surfactant, which undergoes a photoisomerization reaction from a more hydrophobic *trans*-state to a rather hydrophilic *cis*-state under illumination with light. The negatively charged porous silica particles are dispersed in a corresponding aqueous solution and absorb molecules in their *trans*-state but expel them in their *cis*-state. During illumination with blue light triggering both *trans-cis* and *cis-trans* isomerization at the same time, the colloids start to move due to the generation of a steady-state diffusive flow of *cis*-isomers out of and *trans*-isomers into the particle. This is because a hemi-spherical metal cap partially sealing the colloid breaks the symmetry of the otherwise radially directed local flow around the particle, leading to self-propelled motion. Janus particles exhibit superdiffusive motion with a velocity of ~0.5 μm/s and a persistence length of ca. 50 μm, confined to microchannels the direction can be maintained up to 300 μm before rotational diffusion reverts it. Particles forming dimers of different shapes can be made to travel along circular trajectories. The unique feature of this mechanism is that the strength of self-propulsion can be tuned by convenient external optical stimuli (intensity and irradiation wavelength) such that a broad variety of experimental situations can be realized in a spatiotemporal way and *in situ*.

One of the most exciting recent inventions in microfluidics and micro/nanotechnology is artificial active particles that consume energy stored in their environment in order to initiate self-propulsion.[1,2] The study of these systems, originally motivated by the modeling swarm behavior of living organisms,[3] has triggered further developments in diverse fields such as soft matter, statistical physics, or micro- and nanorobotics. The design of self-organizing microrobots or smart multifunctional materials is a crucial aspect for advanced concepts of sensing and delivering chemicals in complex environments or for environmental applications.[4–9] To date, active particles are usually fabricated as small micrometer-sized colloids rendered asymmetric, e.g., as Janus particles with two faces bearing distinct physicochemical properties.[10,11] This polar nature is employed to generate local gradients around the particle, for instance, by catalytic reactions on one side of the particle.[12–23] In most cases, there is only a start-stop control over self-propulsion, with no intermediate gears. For instance, in hydrogen peroxide solution hosting platinum or titanium dioxide based Janus particles, the catalytic activity of the noble metal produces a continuous displacement of the particle; tuning the velocity, for instance, requires changing the system altogether (composition of the solvent, size, and shape of particles). More control over active particles can be gained by utilizing external stimuli such as electrical, magnetic, or optical fields to initiate or stop self-propulsion.[24–27] Specifically interesting is light as the external means for steering and guiding of active colloids, since it is contactless, has a high spatiotemporal selectivity, and does not require modification with magnetic material. By applying light, one either induces temperature changes resulting in thermophoresis or controls the catalytic reaction of hydrogen peroxide decomposition.[28–34]

Here, we propose another mechanism of light-induced self-propelled motion of Janus particles, which involves neither heating of the environment nor catalytic reactions. The physical origin is based on the phenomenon of light driven diffusioosmosis (LDDO).[35] The LDDO flow is generated at the solid/liquid interface in a solution containing photoswitchable molecules under irradiation with focused light: a gradient of isomer concentration develops,

resulting in an osmotic pressure gradient driving a local solvent flow at the irradiated area near a solid surface. The colloids are passively moved by this LDDO flow. The photoswitchable group comprises azobenzene having two distinct states: *trans* and *cis*, which can be isomerized reversibly by applying irradiation with UV light (*trans*-to-*cis*) and blue or green light (*cis*-to-*trans*). The azobenzene group is incorporated into a hydrophobic tail of surfactant altering the physical properties of the whole molecule between more hydrophobic (*trans*-isomer) and more hydrophilic (*cis*-isomer) states [Fig. 1(a)].[36–40]

The LDDO-flow can also be utilized in order to establish active particle motion. We have recently reported on the light-induced reversible repulsion and aggregation of porous silica particles dispersed in a solution of azobenzene containing surfactant.[41] The corresponding mechanism may be coined "local" LDDO-flow (l-LDDO) because it originates from a formation of local flow around each single porous particle. The cationic surfactant molecules in their *trans*-state prefer to be absorbed by the negatively charged pore surfaces inside the colloids. Under irradiation with blue light, there is a photoisomerization from *trans* to *cis* in solution and within the particles as the silica colloids are transparent in the visible range. The hydrophilic *cis*-isomers formed within the pores are expelled from the colloids, resulting in a concentration gradient around each single particle. This leads to an osmotic pressure difference in the electrostatic diffuse layer on the substrate surface. Similar to LDDO, this osmotic pressure difference is compensated by a liquid radial flow away from the particle: local-LDDO [Fig. 1(b)]. In this way, two neighboring particles experience a repulsive interaction that may notably be felt over distances exceeding several times the particle diameter. The l-LDDO flow generated under irradiation with blue light ($\lambda = 455$ nm) is sustained over the whole irradiation time (up to several hours). The reason for this is that in the photostationary state under blue light conditions, both isomers are present in solution, roughly 73% of *trans*- and 27% of *cis*-molecules.

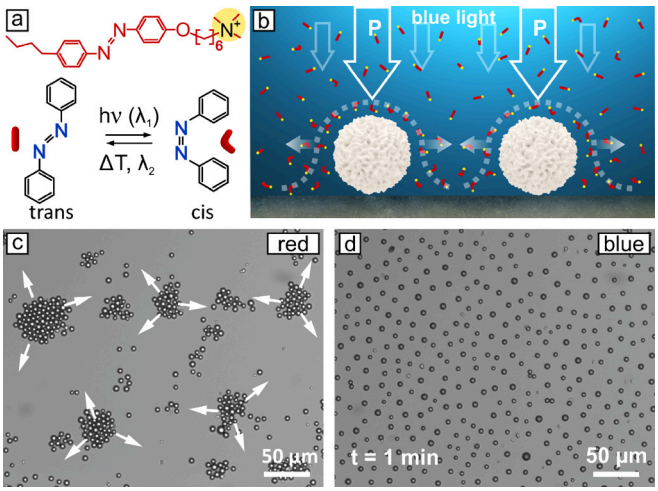

FIG. 1. (a) Chemical structure of the azobenzene containing surfactant and scheme of azobenzene photoisomerization. (b) Formation of l-LDDO flow and mutual repulsion of particles. (c) Optical micrograph of porous particles immersed in an aqueous solution containing photosensitive surfactant ($c_{azo} = 1$ mM). (d) Under irradiation with blue light ($\lambda = 455$ nm), the particles repel each other and form an ordered grid.

Thus, *cis*-isomers leaving the pores make room for *trans*-molecules to absorb. In this way, a continuous diffusion of *cis*-molecules out of and *trans*-molecules into the particle can be maintained.

In this Letter, we report on how to utilize this mechanism to establish the self-propelled motion of single porous colloids. To achieve this, we have rendered porous particles Janus-like by sealing half of the colloid with a metal cap. This breaks the radial symmetry of l-LDDO flow, thus allowing for superdiffusive motion.

When porous silica particles are immersed into an aqueous solution containing photosensitive surfactant, irradiation with blue light leads to the generation of local flow around each single particle (Fig. 1). The local flow profile is radially symmetric and extends over distances of up to several diameters of the porous particles. The interaction of flow patterns of nearby particles leads to mutual repulsion [Fig. 1(d)]. The maximal velocity of the particles undergoing mutual repulsion increases with irradiation intensity and can be adjusted between 0.2 μm/s and 1.4 μm/s by varying the intensity from 0.01mW/cm^2 to 8mW/cm^2.

When the colloid is capped with a gold layer (thickness of 40 nm; for details, see Fig. S1, supplementary material), a Janus-type particle is formed and the symmetry of the flow profile is broken: the pores across the capped side are sealed and the surfactant molecules leave and enter solely at the open hemisphere of the colloid (Fig. 2, Multimedia view). Similarly, to many other Janus-type particles, the broken symmetry initiates self-propulsion,[1] which, however, is turned on only with blue light. Under these conditions, the generated *cis*-isomers leave the pores of the particles, while *trans*-isomers enter, resulting in a steady state flow in and out of the particle (Fig. 2).

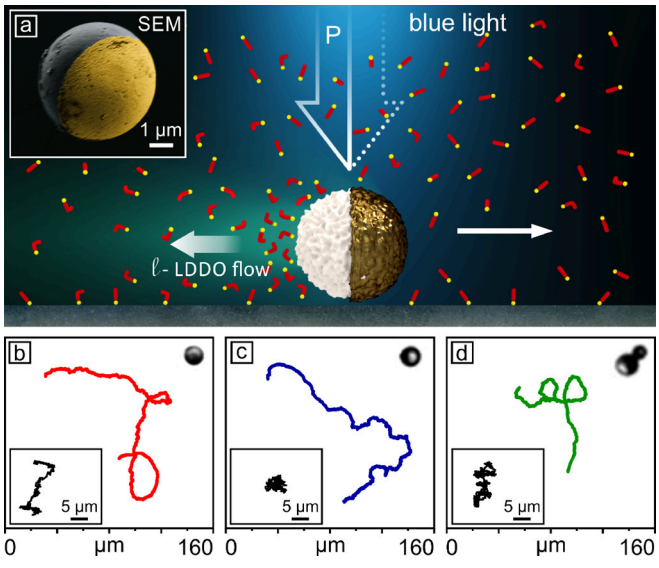

FIG. 2. (a) Scheme of light-driven self-propelled motion of a Janus-type particle. The diffusioosmotic flow near the particle is generated by a lateral gradient in osmotic pressure, P, at the open half, pushing it forward to the direction of the gold cap. The inset shows an SEM picture of the Janus particle. (b)–(d) Examples of self-propelled trajectories under irradiation with blue light t = 15 min. The insets depict thermal motion without irradiation. Multimedia view: https://doi.org/10.1063/1.5129238.1

Self-propulsion can be easily recognized by comparing trajectories recorded with and without irradiation [Figs. 2(b)–2(d)]. Before irradiation, i.e., under illumination with red light ($\lambda = 600$ nm), the motion is Brownian, governed by thermal fluctuations. Under irradiation with blue light, the majority of the single particles exhibit active motion and particles forming a dimer show rotational motion [Fig. 2(d)].

The quantitative analysis is performed utilizing the data acquired with several particles during continuous irradiation with blue light over 45 min [Fig. 3(a), Multimedia view]. The pathways are characterized by directed motion maintained over a typical time scale τ_R, after which the direction of motion is randomized by rotational diffusion leading to the well-known expression $\tau_R = 8\pi\eta R^3/k_BT$, where R is the radius of the particle, k_B is the Boltzmann constant, T is the temperature, and $\eta = 1.002$ mPa is the viscosity of water. The viscosity of the solution with 1 mM surfactant concentration is only slightly enhanced; the relative change in viscosity of a dilute surfactant solution is rather small and does not significantly impact motion of the colloids. For 5 μm sized particles, the rotational diffusion time is $\tau_R \sim 96$ s. Within this time, the particle's direction is approximately preserved, implying an equivalent persistence length $L = v\tau_R = 48\mu$m, where v is the propulsion velocity. v is calculated from the analysis of the mean square displacement (MSD) of the single particle using the following equation:[42]

$$\mathrm{MSD} = \langle(\Delta\vec{r})^2\rangle = 4D_{Trans}\Delta t + \frac{v^2\tau_R^2}{2}\left(\frac{2\Delta t}{\tau_R} + e^{-\frac{2\Delta t}{\tau_R}} - 1\right), \quad (1)$$

where $D_{Trans} = \frac{k_BT}{6\pi\eta R}$ is the translational diffusion coefficient, Δt is the time interval, v is the particle velocity, and τ_R is the rotational diffusion time. For times shorter than the rotational diffusion time, this equation reduces to

$$\mathrm{MSD} = \langle(\Delta\vec{r})^2\rangle = 4D_{Trans}\Delta t + v^2\Delta t^2. \quad (2)$$

For this time range ($\tau_R = 96$s), a propulsion speed of v = (0.5 ± 0.1) μm/s can be derived from parabolic fits of the MSD. Analyzing the plot in Fig. 3(a), one observes that Janus particles show superdiffusive behavior (slope: 1.65) under blue irradiation and slightly subdiffusive behavior under red illumination, i.e., in the dark (slope: 0.92) [Fig. 3(a) inset]. One curve is obtained from the average data from 4 independent trajectories [Fig. 3(b)]. Over longer time, the orientation and direction of motion of the particle are randomized by its rotational diffusion, and as expected, the MSD assumes a linear behavior. The persistence length of 48 micrometers is around 10 times larger than the diameter of the particle. Correspondingly, the effective diffusion coefficient, $D_{eff} = D_{Trans} + \frac{1}{4}v^2\tau_R \approx 6\,\mu\mathrm{m}^2\mathrm{s}^{-1}$, increases by a factor of nearly 70 compared to the purely Brownian value $D_{Trans} = 0.09\,\mu\mathrm{m}^2\mathrm{s}^{-1}$.

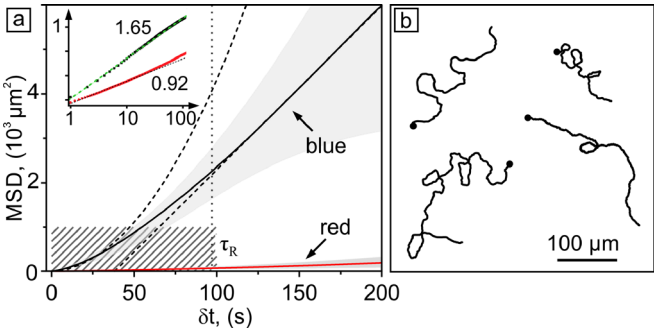

FIG. 3. (a) MSD as a function of time, comparing the motion of Janus particles under blue (black curve) and red light (red curve). Inset: log-log plot of the MSD with linear fits (of the time range marked by a dashed rectangle), at which the slope of the curve is shown. (b) Trajectories of self-propelled particles in blue light. Multimedia views: https://doi.org/10.1063/1.5129238.2; https://doi.org/10.1063/1.5129238.3; https://doi.org/10.1063/1.5129238.4

The propulsion speed depends on the surfactant concentration for a fixed irradiation intensity ($\lambda = 455$ nm, I = 1.5 mW/cm^2), although a detailed quantitative relationship still needs to be worked out. For instance, for the trajectories ($c_{azo} = 1$ mM) shown in Fig. 3, we find a maximal propulsion speed of 0.5 μm/s, while for surfactant concentrations of 0.5 and 2 mM, the velocity is 0.15 μm/s and 0.55 μm/s, respectively, summarized in Fig. S2, supplementary material. A systematic investigation of how the propulsion velocity depends on irradiation conditions (pore size, surfactant concentration, surfactant hydrophobicity, etc.) will be presented elsewhere.

The propulsion of active particles along a straight line at a distance smaller than the persistence length is only possible when the Janus particle has approximately cylinder symmetry (with respect to pore distribution and capping); asymmetric particles may lead to active net rotation around some axis. The impact of asymmetry is particularly pronounced when the colloids form dimers or other multimeric objects, e.g., formed when their metal covers are connected via necks. The resulting aggregates are usually byproducts of the preparation process of Janus particles, that is, when two or more colloids form aggregates due to imperfections in the formation of a dilute colloidal monolayer. The anisotropy leads to a total nonvanishing torque; the net motion is a superposition of translation and rotation.[43] In our case, we have also observed that particles forming dimers or trimers can spiral along circular paths during self-propelled motion (Fig. 4, Multimedia view). In fact, dimer particles can also have different types of trajectories depending on the relative alignment of constituents.[44] Direction, radius, and angular velocity are determined by the specific particle shape as illustrated in Fig. 4. In the extreme case of antiparallel alignment of single particle velocities (gold caps point to opposite directions), the trajectory of the dimer motion is almost circular with a radius of ca. 12 μm and an angular velocity of $\omega = 0.03$ rad/s (200s for one rotation), which corresponds to a linear velocity of 0.5 μm/s [Fig. 4(b)]. In the case of parallel alignment, i.e., gold caps point to the same direction, the motion is a combination of rotational ($\omega = 0.022 \pm 0.006$ rad/s) and translation displacement [Fig. 4(c)]. In the other extreme, one of the dimer particles is fixed to the surface forming a center of rotation [Fig. 4(a)]. In this case, the dimer needs roughly 145s ± 26s ($\omega = 0.041 \pm 0.006$ rad/s) for one turn, resulting in a linear velocity of 0.3 μm/s. In all cases, persistent circular orbits are observed over several hours.

Janus particles can be made to maintain their direction of motion over large distances (several hundreds of micrometers) when placed in suitably shaped microchannels (Fig. 5, Multimedia view). The direction of particle motion is rectified by the channel walls until a sufficiently large jump in particle orientation due to rotational diffusion occurs to change the direction.[45] The profile and size of the

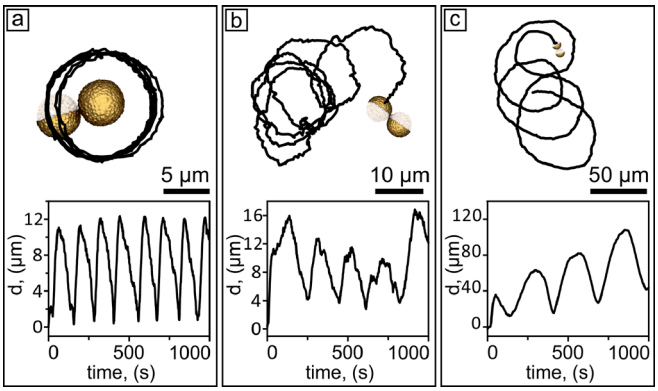

FIG. 4. Examples of circular trajectories of moving dimers of varying geometries: (a) one particle completely covered with gold and fixed on the surface, (b) gold caps of two Janus particles point to opposite directions, and (c) parallel aligned. The y-axis shows the instantaneous distance, d, of a dimer from the origin location at the start of observation. Multimedia views: https://doi.org/10.1063/1.5129238.5; https://doi.org/10.1063/1.5129238.6; https://doi.org/10.1063/1.5129238.7

microchannels are shown in Fig. 5(a), and the corresponding width and depth are 4 μm and 1 μm, respectively.

In the absence of light, thermal motion prevails and the particle barely moves into any direction along the channel [Fig. 5(b)]. Under irradiation with blue light, the particle starts moving in a "run and tumble" manner: the translational motion of active particles is superimposed with rotational diffusion. The restricted geometry only permits a quite slow reorientation of the particle because a large (and therefore rare) fluctuation in orientation must occur. For the case

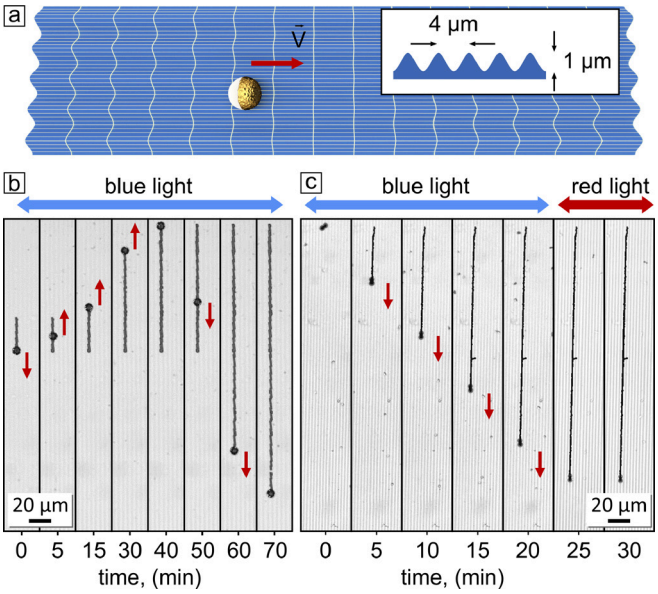

FIG. 5. (a) Scheme of a Janus particle on a surface structured with microchannels. (b) Self-propelled motion of a single and (c) a dimeric Janus particle. The trajectories are shown by the black lines. The direction of motion is depicted by red arrows. Multimedia views: https://doi.org/10.1063/1.5129238.8; https://doi.org/10.1063/1.5129238.9

shown in Fig. 5(b), during the first 35 min of irradiation, the particle moves to the top over a distance of ca. 120 μm and then turns to travel in the opposite direction for another 300 μm [Fig. 5(b)]. The average speed of the particle in both directions is $v \sim 0.15$ μm/s, which is smaller than on a flat, unstructured surface and related to the influence of the channel geometry. The dimer particle trapped within the microchannel similarly shows directed motion with an average speed of 0.3 μm/s over 400 μm. When the blue light is switched off (23 min), the dimer stops and does not change its location significantly within the next few minutes [Fig. 5(c)].

In conclusion, we have introduced a mechanism of self-propulsion of Janus-type particles based on the generation of l-LDDO flow by a single porous particle under irradiation with blue light ($\lambda =$ 455 nm). The colloids exhibit self-propulsion motion, $v \sim 0.5$ μm/s, and a persistence length of ca. 50 μm. When it is subjected to a microchannel, the particle motion can be guided along a straight line over distances exceeding up to 60 times its own diameter before the direction of motion is flipped by rotational diffusion.

See the supplementary material for detailed descriptions of azobenzene containing surfactant, Janus-particle preparation, imaging analysis, and videos of particle motion (Fig. S1); and the dependence of Janus-particle velocity on the surfactant concentration (Fig. S2).

This research is supported by the Priority Program 1726, DFG (No. SA1657/8-1).

REFERENCES

[1]C. Bechinger, R. Di Leonardo, H. Löwen, C. Reichhardt, and G. Volpe, Rev. Mod. Phys. **88**, 045006 (2016).
[2]J. Elgeti, R. G. Winkler, and G. Gompper, Rep. Prog. Phys. **78**, 056601 (2015).
[3]T. Vicsek and A. Zafeiris, Phys. Rep. **571**, 71 (2012).
[4]S. Campuzano, D. Kagan, J. Orozco, and J. Wang, Analyst **136**, 4621 (2011).
[5]J. Wang and W. Gao, ACS Nano **6**, 5745 (2012).
[6]M. Zarei and M. Zarei, Small **14**, 1800912 (2018).
[7]J. Wang, Biosens. Bioelectron. **76**, 234 (2016).
[8]B. J. Sánchez and J. Wang, Environ. Sci.: Nano **5**, 1530 (2018).
[9]J. Katuri, X. Ma, M. M. Stanton, and S. Sánchez, Acc. Chem. Res. **50**, 2 (2017).
[10]G. R. Yi, D. J. Pine, and S. Sacanna, J Phys.: Condens. Matter **25**, 193101 (2013).
[11]W. F. Paxton, K. C. Kistler, C. C. Olmeda, A. Sen, S. K. St. Angelo, Y. Cao, T. E. Mallouk, P. E. Lammert, and V. H. Crespi, J. Am. Chem. Soc. **126**, 13424 (2004).
[12]R. Soto and R. Golestanian, Phys. Rev. Lett. **112**, 068301 (2014).
[13]R. Soto and R. Golestanian, Phys. Rev. E **91**, 052304 (2015).
[14]H. R. Jiang, N. Yoshinaga, and M. Sano, Phys. Rev. Lett. **105**, 268302 (2010).
[15]S. Sanchez, A. N. Ananth, V. M. Fomin, M. Viehrig, and O. G. Schmidt, J. Am. Chem. Soc. **133**, 14860 (2011).
[16]X. Ma, K. Hahn, and S. Sanchez, J. Am. Chem. Soc. **137**, 4976 (2015).
[17]X. Ma, A. Jannasch, U.-R. Albrecht, K. Hahn, A. M. López, E. Schäffer, and S. Sánchez, Nano Lett. **15**, 7043 (2015).
[18]J. Li, V. V. Singh, S. Sattayasamitsathit, J. Orozco, K. Kaufmann, R. Dong, W. Gao, B. Jurado-Sanchez, Y. Fedorak, and J. Wang, ACS Nano **8**, 11118 (2014).
[19]R. Niu, D. Botin, J. Weber, A. Reinmüller, and Th. Palberg, Langmuir **33**(14), 3450–3457 (2017).
[20]S. J. Ebbens and J. R. Howse, Soft Matter **6**, 726 (2010).
[21]J. J. McDermott, A. Kar, M. Daher, S. Klara, G. Wang, A. Sen, and D. Velegol, Langmuir **28**, 15491 (2012).
[22]R. Niu, T. Palberg, and T. Speck, Phys. Rev. Lett. **119**, 028001 (2017).

[23]A. Reinmüller, H. J. Schöpe, and T. Palberg, Langmuir **29**, 1738 (2013).
[24]P. Tierno, R. Golestanian, I. Pagonabarraga, and F. Sagués, Phys. Rev. Lett. **101**, 218304 (2008).
[25]R. Dreyfus, J. Baudry, M. L. Roper, M. Fermigier, H. A. Stone, and J. Bibette, Nature **437**, 862 (2005).
[26]A. Ghosh and P. Fischer, Nano Lett. **9**, 2243 (2009).
[27]D. Nishiguchi and M. Sano, Phys. Rev. E **92**, 052309 (2015).
[28]Y. Hong, M. Diaz, U. M. Córdova-Figueroa, and A. Sen, Adv. Funct. Mater. **20**, 1568 (2010).
[29]G. Volpe, I. Buttinoni, D. Vogt, H.-J. Kümmerer, and C. Bechinger, Soft Matter **7**, 8810 (2011).
[30]F. Kümmel, B. T. Hagen, R. Wittkowski, I. Buttinoni, R. Eichhorn, G. Volpe, H. Löwen, and C. Bechinger, Phys. Rev. Lett. **110**, 198302 (2013).
[31]I. Buttinoni, J. Bialké, F. Kümmel, H. Löwen, C. Bechinger, and T. Speck, Phys. Rev. Lett. **110**, 238301 (2013).
[32]J. Palacci, S. Sacanna, A. P. Steinberg, D. J. Pine, and P. M. Chaikin, Science **339**, 936 (2013).
[33]S. Samin and R. van Roij, Phys. Rev. Lett. **115**, 188305 (2015).
[34]A. Würger, Phys. Rev. Lett. **115**, 188304 (2015).
[35]D. Feldmann, S. R. Maduar, M. Santer, N. Lomadze, O. I. Vinogradova, and S. Santer, Sci. Rep. **6**, 36443 (2016).
[36]H. Rau, in *Photochemistry and Photophysics*, edited by J. Rabek (CRC Press, Boca Raton, FL, USA, 1990), Vol. 119.
[37]Y. Zakrevskyy, J. Roxlau, G. Brezesinski, N. Lomadze, and S. Santer, J. Chem. Phys. **140**, 44906 (2014).
[38]X. Liu and N. L. Abbott, J. Colloid Interface Sci. **339**(1), 1 (2009).
[39]M. Montagna and O. Guskova, Langmuir **34**, 311 (2018).
[40]S. Santer, J. Phys. D: Appl. Phys. **51**, 013002 (2017).
[41]D. Feldmann, A. Pooja, Y. T. Molotilin, N. Lomadze, A. Kopyshev, O. I. Vinogradova, and S. Santer, "Extremely long-range light-driven repulsion of porous microparticles," Langmuir (to be published).
[42]J. R. Howse, R. A. L. Jones, A. J. Ryan, T. Gough, R. Vafabakhsh, and R. Golestanian, Phys. Rev. Lett. **99**, 048102 (2007).
[43]D. J. Kraft, R. Wittkowski, B. ten Hagen, K. V. Edmond, D. J. Pine, and H. Löwen, Phys. Rev. E **88**, 050301 (2013).
[44]A. Kaiser, K. Popowa, and H. Löwen, Phys. Rev. E **92**, 012301 (2015).
[45]X. Ao, P. K. Ghosh, Y. Li, G. Schmid, P. Hänggi, and F. Marchesoni, Eur. Phys. J. Spec. Top. **223**, 3227 (2014).

Supplementary Materials

Light-driven motion of self-propelled porous Janus particles

*David Feldmann[1,2], Pooja Arya[1], Nino Lomadze[1], Alexey Kopyshev[1], Svetlana Santer[1]**

[1]Institute of Physics and Astronomy, University of Potsdam, 14476 Potsdam, Germany

[2]School of Mechanical Engineering, Faculty of Engineering, Tel-Aviv University,

69978 Tel-Aviv, Israel

AUTHOR EMAIL ADDRESS: santer@uni-potsdam.de

RECEIVED DATE

TITLE RUNNING HEAD: Light driven motion of self-propelled particles, azobenzene containing cationic surfactants

KEYWORDS: azobenzene containing cationic surfactant, self-propelled colloids, micro-swimmers

Materials and Methods.

Materials

Azobenzene containing cationic surfactant with a spacer of six methylene groups between the positively charged trimethylammonium bromide head group and the azobenzene unit is synthesized as described elsewhere.[1] The surfactant is dissolved in Milli-Q water.

The photo-isomerization behavior of the surfactant has been described in detail in our previous publication.[2] In short, the *trans*- state of the surfactant is characterized by an absorption band with a maximum at 353 nm, the *cis*-isomer by two absorption bands with maxima at 313 nm and at 437 nm. The band with a maximum at ~240 nm present in both isomers corresponds to the absorption of π-conjugated benzene rings. The lifetime of the *cis* isomer in dark is 48 hours, while the photo-isomerization from *cis*- to *trans*-state under irradiation with blue light (λ=455nm, P=30μW) takes place within a few seconds, approaching a photo-stationary state (with 73% of *trans* and 27% of *cis*-isomers) after 10 minutes of irradiation.

The dispersion of Janus particles of 5μm in diameter in a surfactant solution of 1mM concentration (c_{CMC}=0.5mM) is introduced into a closed chamber of height 920 μm with a volume of 40 μl. Before measurement, the samples are kept in the dark for several minutes until the particles sediment to the bottom of the substrate.

Janus particle preparation. A dilute monolayer of silica porous particles (mean diameter: 5μm, Micromod GmbH, Germany) is prepared by spin coating of an aqueous particle dispersion (5mg/ml, 200μl) on a 2cm x 2cm glass substrate. The glass surface is cleaned prior to deposition during 15 minutes of sonication in a 2% Hellmanex solution followed by rinsing and 15 min sonication in Milli-Q water. Using an evaporation chamber (Leybold Oerlikon Univex 350), a 2nm chromium and a 40nm gold layer are deposited on the colloidal monolayer. The resulting Janus particles are taken off the substrate by carefully sliding a water-soaked lens -cleaning tissue acting as a blade over the surface.[3] During exposure of the tissue to distilled water (18.2 $M\Omega cm^{-1}$, Milli-Q), single Janus particles are re-

1 D. Dumont, T. Galstian, S. Senkow and A. Ritcey, Mol. Cryst. Liq. Cryst. 375, 341 (2002).

2 Y. Zakrevskyy, P. Cywinski, M. Cywinska, J. Paasche, N. Lomadze, O. Reich, H.-G. Löhmannsröben, and S. Santer, J. Chem. Phys. 140, 044907 (2014).

3 A. Campbell, R. Archer, and S. Ebbens, J. Vis. Exp. (113), e54247, doi:10.3791/54247 (2016)

suspended. The aqueous surfactant solution is added to get the defined concentration of c_{azo}=1mM.

Methods

Optical microscopy imaging. An inverted Olympus IX71 is equipped with a tunable monochromatic light source (Polychrome V, FEI Munich GmbH) which acts as continuous illumination and lighting source at wavelengths of λ=455nm (blue, *I*=1.5mW/cm^2) and λ=600nm (red, *I*=2mW/cm^2). The illumination intensity is measured at the solid/liquid interface with an optical power meter 1918-R with the sensor 918D-UV-OD3R (Newport Corporation, Irvine, CA, USA). Additionally, the setup is kept in the dark to prevent uncontrolled isomerization.

Tracking and data analysis. Particles are tracked using the Mosaic Single Particle Tracking plugin for ImageJ (Rasband, W.S., ImageJ, U. S. National Institutes of Health, Bethesda, Maryland, USA, http://imagej.nih.gov/ij/, 1997-2015). The tracking algorithm is described by Koumoutsakos.[4] The particle trajectories are analyzed using a Matlab script developed in our laboratory.

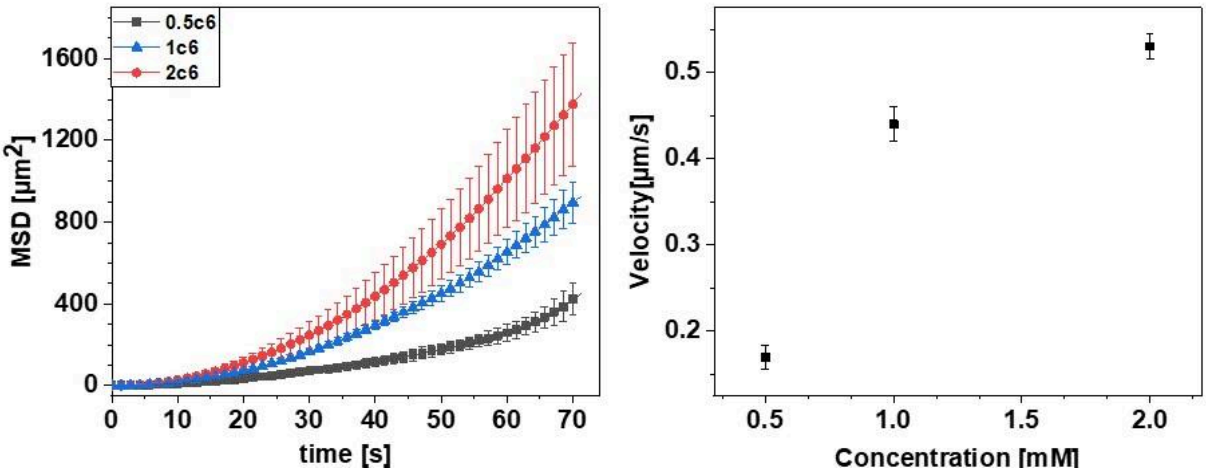

Figure S1. Left: dependence of MSD on time for 5µm Janus particle dispersed in aqueous solution of different surfactant concentrations: 0.5mM (black curve), 1mM (blue curve), 2mM (red curve). Right: the self-propelled velocity of the Janus particle a function of surfactant concentration. The self-propelled motion was induced under irradiation with blue light (λ=455nm, I=1.5mW/cm^2).

4 I. F. Sbalzarini, and P. Koumoutsakos, J. Struct. Biology 151(2), 182 (2005).

5. Discussion and conclusion

In this thesis we investigate a local light driven diffusioosmotic flow (l-LDDO), which induces active motion of porous particles when exposed to irradiation with light of appropriate wavelength. Effect of different parameters such as wavelength and intensity of light, concentration of particles and surfactant, and type of particles (porous, non-porous or Janus) on motion is discussed in detail. The effect of wavelength on collective motion of particles is significant and reported in Papers 2, 3, and 4.

The main ingredient of LDDO flow is azobenzene containing surfactant (ACS) which undergoes photo-isomerization from stable *trans* to metastable *cis* state under appropriate wavelength of light. We observed that the fraction of *trans* and *cis* molecules at photo stationary state depends upon the wavelength of light. Under UV (λ = 365 nm) irradiation, almost all *trans* molecules are isomerized to *cis* isomers. For longer wavelength, fraction of *trans* and *cis* molecules are in certain ratio, for instance, in case of 1mM surfactant concentration, at λ = 455 nm *trans* and *cis* fraction is 72 % and 28 %, respectively, and for λ = 490 nm it becomes 84 % *trans* and 16 % *cis* molecules at a photo stationary state.

To characterize the photo switching behavior of ACSs, time resolved UV-Vis absorption spectroscopy is used, where sample is irradiated with desired wavelength and intensity of light with simultaneous recording of absorbance. A kinetic model of photo isomerization is presented in **Publication 1** where isomerization reaction is assumed as pseudo first order reaction.

The effect of global blue light irradiation on a system of 5 μm silica porous particles in aqueous solution of azobenzene containing surfactant is discussed in **Publication 2**, while motion of particles under exposure to UV light is discussed in **Publication** 3. Under blue light irradiation, a continuous l-LDDO flow pointing radially outwards is induced around each particle which results in a 2D stable grid of well separated particles. It is presented that in case of UV irradiation, induced flow is not long lasting and hence the separated particles come closer due to thermal motion. Time resolved aggregation followed by separation is reported for lower intensities of UV irradiation whereas direct

separation is observed on increasing intensity to a maximum of 1.8 mW/cm^2. The induced LDDO flow by porous particle is visualized using non-porous silica particles.

In **Publication 4** we have reported the effect on collective motion of mesoporous silica particles under simultaneous irradiation with light of two wavelengths, blue and UV of different spot sizes: focused blue and global UV. Both local LDDO flow around each particle and global LDDO flow due to focused irradiation spot are induced resulting in dynamic aggregation or separation of particles in a confinement. We have clearly demonstrated that the active flow (l-LDDO flow) is absent in case of non-porous silica particles and they form a densely packed monolayer inside the confinement. We have shown that the effect is reproducible when blue light is switched on again. Many intriguing dynamic patterns can be formed by altering one of the parameters. For instance, when focused blue light is irradiated in pulse with different frequencies, a mechanical effect like heart beating is established. The detailed analysis of this process is explained in the **Appendix B.5.** This system is studied further in detail with respect to different parameters like surfactant concentration, spot size, and particle concentration and reported in **Appendix B**.

Figure 5.1 demonstrates the summary of possible combinations of blue and UV irradiation which affects the collective motion of particles on a glass surface where particles can act as either passive which moves with the flow or active, which generates the flow, depending upon the applied wavelength of irradiation.

It is also possible to induce self-propelled motion using the above system (**Publication 5**). It is shown that when pores of one side of porous particles are blocked with gold layer of thickness 50 nm (Janus particle is formed), the local LDDO flow is generated on the other half of particles which propelled it in forward direction towards the cap under global blue irradiation. The generated motion falls under the category of super diffusion which is shown using mean square displacement (MSD) curve plotted with respect to time. MSD > 1, confirms the super diffusion or self-propelled motion of porous Janus particles. We have also shown that particles forming dimers or trimers can spiral along circular path during self-propelled motion where the trajectory of circular motion depends upon the alignment of gold cap in case of dimer particles. It is reported that using substrate with micro channels (like Surface relief gratings), directed self-propelled motion can be induced.

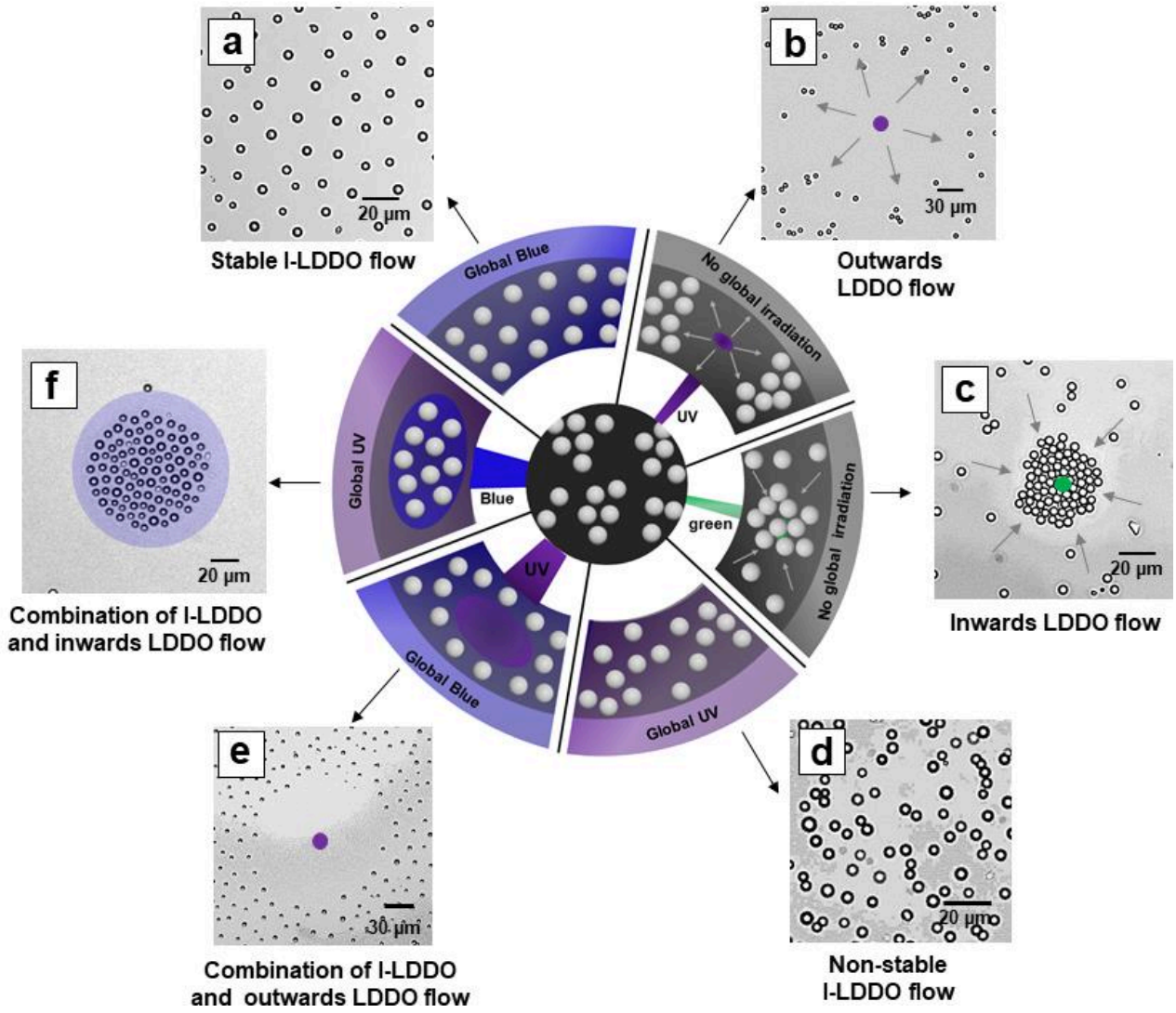

Figure 5.1. Scheme of different collective behavior of particle ensemble as a function of irradiation process. (a) Equilibrium state (stable l-LDDO flow) achieved under global blue (λ = 455 nm) light irradiation. (b) Focused UV irradiation generates outwards LDDO flow which carries particles away from the irradiation spot. (c) Focused green light irradiation resulting in inwards LDDO flow causing gathering of particles at the irradiation spot. Sample was initially exposed to global UV irradiation for 10 minutes. (d) Non stable separation under global UV irradiation. (e) collective behavior of mesoporous silica particles when two light sources (focused UV and global blue light) are applied simultaneously. (f) 2D disk of well separated particles is formed under simultaneous irradiation of focused blue and global UV light.

Appendices

Appendix A. Passive motion of colloidal particles under focused UV irradiation: dependecy upon spot size, intensity and concentration of surfactant concentartion.

When focused UV light of diameter 20 μm (too small) is applied to a monolayer of silica porous /non-porous particles, diffusioosmotic flows are generated at the liquid/solid interface. The flow direction is pointing away from the irradiation spot which carries all the particles sedimentation at the substrate and hence leaves behind particle free surface. Basic principle of LDDO flow and its dependency on other parameters like surfactant or particle concentrations and for different surfactant group is reported in previous publication and is also discussed briefly in **Section 2.4**. In this part we report on further findings of this system like range of the flow, dependency on spot diameter and intensity of irradiation.

In order to analyzed the range of LDDO flow, long term measurements under constant irradiation were performed at different surfactant concentrations keeping other parameters fixed (spot diameter = 20 μm, power = 1.5 μW)). One can say that saturation of clean area can give an estimation of the range of the LDDO. The optical image of cleaned area at t = 2 hour for different surfactant concentrations 0.5 mM, 1 mM and 2 mM is shown in **Figure A.1**. It is observed that the flow range increases upon increasing surfactant concentration and attains a maximum value of 1 mm at C_{Azo} = 1 mM within 3 hours of irradiation (red line in plot of **Figure A.1d**).

The effect of spot size on LDDO flow is further studied in detail. It has been observed that for larger spot size (more than 10 times than previous) the generated LDDO flow shows special effects inside as well as outside the irradiations spot depending upon the intensity of applied light. For lower intensities, particles which are outside the irradiation area moves immediately with the flow similar

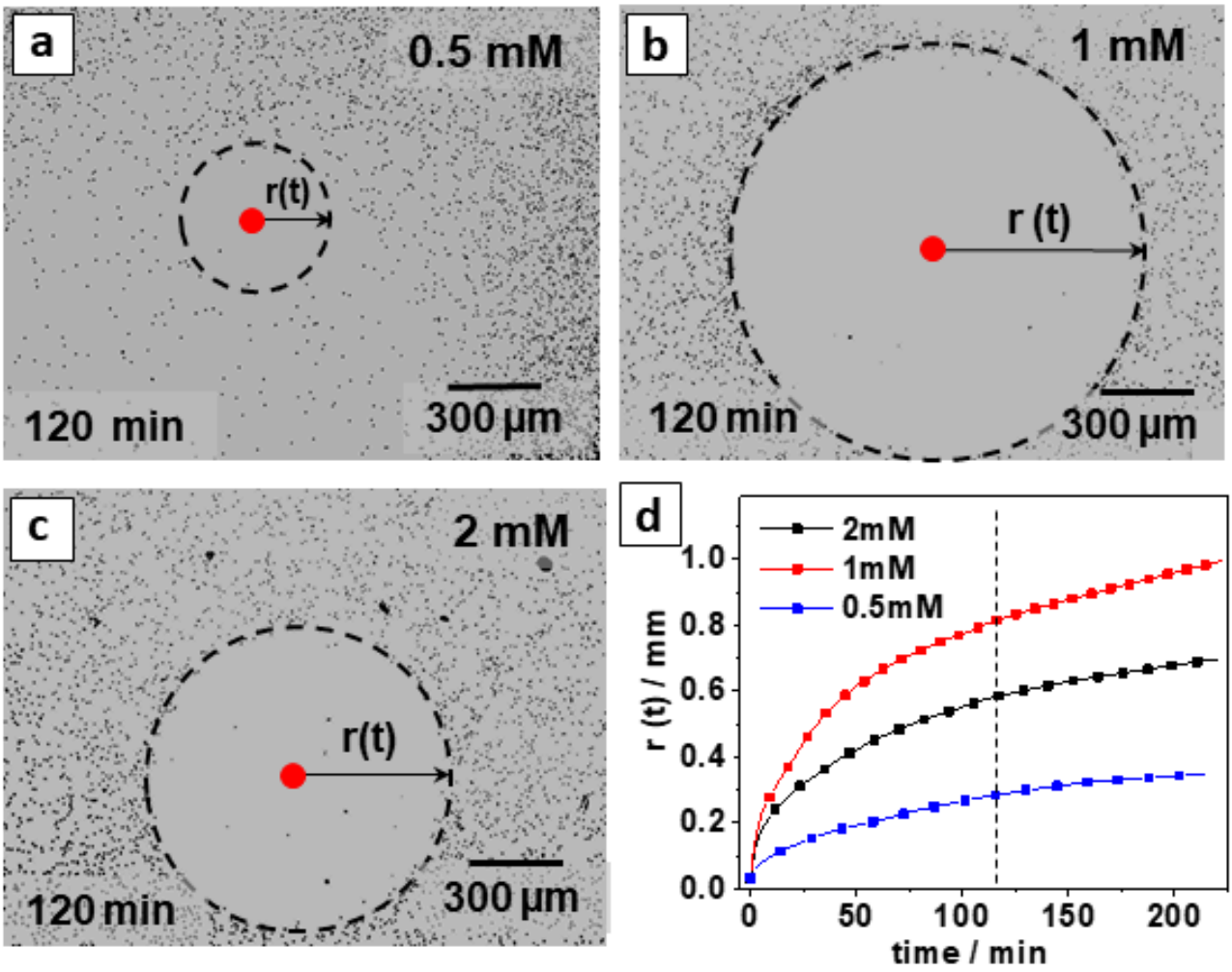

Figure A.1. Optical micrographs of monolayer of 4 µm non-porous silica particles under focused UV irradiation (red spot) for different surfactant concentration at t = 2 hours (dashed line in plot in d). (a) C_{Azo} = 0.5 mM, (b) C_{Azo} = 1 mM, and (c) C_{Azo} = 2 mM. (d) Radius of cleaned area vs time plot for different concentrations of surfactant.

to smaller spot size. The particles which were inside the laser spot moves slowly and reach to the of the laser spot. Particles achieve their maximum velocity at the boundary and the moves away from spot area. However, for intensity > 14 mW/cm^2, particles which are already inside the spot, are trapped within the irradiation area. As an illustration **Figure A.2** represents optical micrographs for two extreme cases with fixed spot diameter (d = 480 µm) and 1 mM surfactant concentration, one for lower intensity of 1.2 mW/cm^2 (**Figure A.2a-c**) and other for highest chosen intensity of 36 mW/cm^2 (**Figure A.2d-e**). This dependency upon intensities is characterized by calculating the distance traveled by the particles with respect to center of spot as a function of time. If there is no significant change is distance this means particles are trapped.

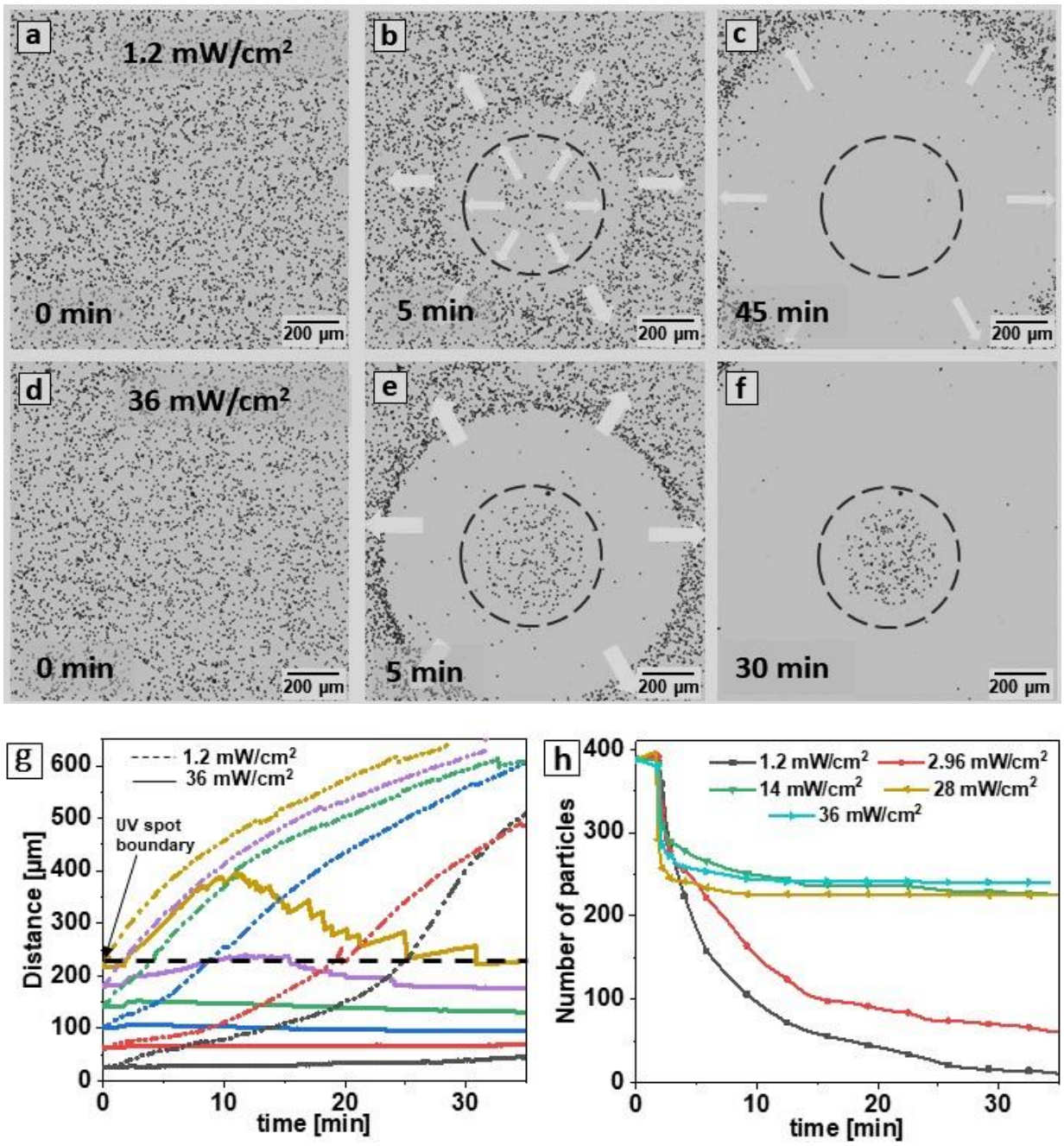

Figure A.2. Effect of intensity of focused UV irradiation (λ = 365 nm, diameter = 480 µm) upon motion of non-porous silica particles in 1 mM Azo-C6. Optical micrographs are representing the statistic images at different time zone for two different intensities; (a-c) for I = 1.2 mW/cm^2 at t= 0 min, 5 min and 45 min.; (d-f) for I = 36 mW/cm^2 at t= 0 min, 5 min and 30 min.; (g) Corresponding distance vs time plot: different colored lines (dashed and solid) represent the average distance calculated in each rings (thickness of each ring is 40 µm). For instance, black line is average distance traveled by the particles presented between 0-40 micrometer from the spot center. And furthermore, red line is the average distance for particles between 40 µm-80 µm…so on (h) Plot for particle concentration inside the irradiation spot as a function of time for different intensities ranging between 1.2 to 36 mW/cm^2. Supporting videos can be found in **Figure SA.2** in Appendix D.

Figure A.2g shows the distance vs time plot for the lowest (dashed lines) and the highest (solid line) measured intensities for spot diameter 480 µm. Different colored lines denote the average distance calculated for particles presented in each ring of thickness 40 µm. What we get from this plot is that for lower intensities (dashed lines) particles which were inside the spot also crosses the boundary (horizontal black dashed line), whereas for larger intensity particles inside the spot are trapped within the boundary and do not go outside the spot. The number of particles inside the spot as a function of time is also calculated for different intensities and shown in **Figure A.2h**. For lower intensities (red and black line) the particle number decreases to minimum indicating the movement of particle outside the area, however, for higher intensities colloids are not allowed to leave the boundary and stays within the irradiation spot. Only particles which are few micrometers nearby boundary moves out.

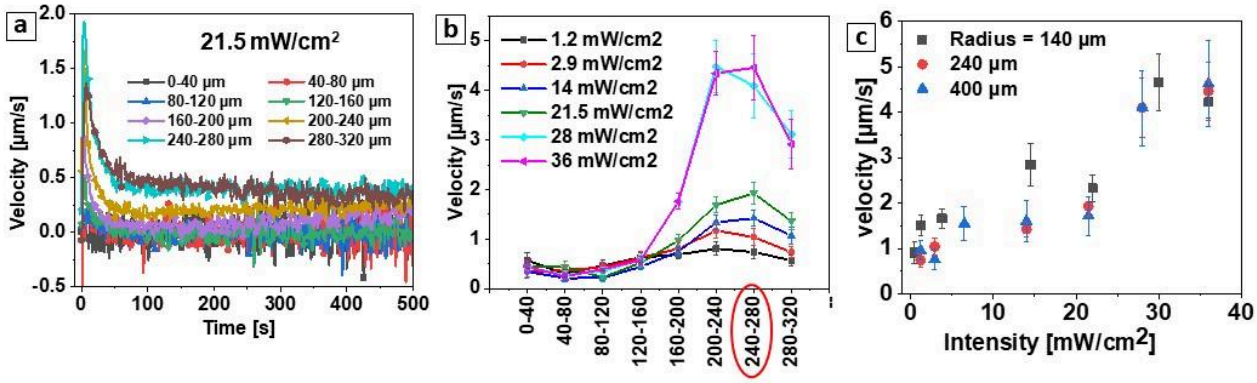

Figure A.3. (a) Velocity of particles vs time plot when monolayer of nonporous silica particles is exposed to focused UV light with intensity of 21.5 mW/cm^2 (λ=365 nm, radius = 240 nm). Each color represents average distance of the particles in each ring of 40 µm thickness. Boundary of irradiation spot is 240 micrometers away from the center. (b) Maximum velocities in each ring vs distance for different intensities of UV irradiation at fixed spot size (radius = 240 µm). (c)Maximum velocity attained at laser boundary as a function of intensity for three spot sizes (radius = 140 µm, 240 µm, and 400 µm).

The velocity profile measured in each ring (shown in different colors) at intensity of 21.5 mW/cm^2 and spot diameter of 480 µm is shown in **Figure A.3a**. Particles which are at the boundary shows maximum velocity (at 240 µm-280 µm, cyan line in the Figure A.3a). Maximum velocities in each rings as a function of distance for different intensities are shown in **Figure A.3b**. It has been observed that particle velocity is proportional to intensity of UV irradiation but is independent of spot size (**Figure A.3c**).

The mechanism behind this process is under investigation. From the basic theory of LDDO flow, it is known that concentration gradient of *cis* molecules is maximum at the boundary which also implies that pressure gradient will be maximum at the boundary which generates the LDDO flow pointing away from the spot carrying the particles passively along it. Particles inside the spot also moves away with some time lag. It is possible that for intermediate intensities forces generated due to gradient of light intensity along the light direction (i.e. in bulk as UV photons are observed by Azo-C6) also plays an important role which results in trapping of the particles in exposed region.[141] For lower intensities gradient forces is smaller as compared to osmotic forces which drives the particles slowly towards the boundary and at the boundary the flow velocity accelerates carry the particles away from the spot. The packing fraction, which is the ratio of occupied area of particles inside the irradiation area to the total area spot is shown in **Figure A.4a-c** for different intensities and spot size. When the decrease in packing fraction is less than 20% and saturated, we can say that particles are trapped inside the spot. From the plots this behavior is observed at higher intensities.

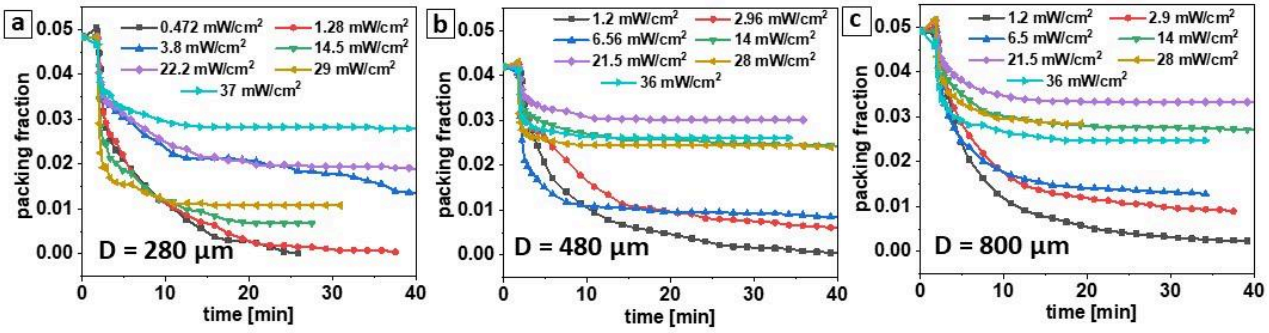

Figure A.4. Packing fraction vs time plot for various intensities and spot sizes. (a) Diameter = 280 µm, (b) D = 480 µm, (c) D = 800 µm. Packing fraction is calculated as ratio between total occupied area by particles to total area of the irradiation spot.

It has been observed that the magnitude of velocity and range of the flow depends upon the initial fraction of *trans* and *cis* molecules before applying focused UV irradiation. The flow strength is proportional to amount of *trans* molecules, which means reducing the fraction of *trans* at initial state (by applying global blue irradiation) will reduce the concentration gradient introduced by focused UV irradiation which decreases the radius/ range of the obtained maximum cleaned area. When global blue irradiation is applied simultaneously with focused UV laser, a continuous flow pointing away from the laser spot is observed. The cleaned area in this case is very small even though the intensity

of focused UV is very high (> 100 mW). This happens because global blue irradiation from the top, equilibrate the concentration gradient faster as it tries to maintain a certain fraction of *trans* and *cis* isomers. The LDDO flow generated in this case would be stable. This process is shown in **Figure A.5a-d** which represents the optical micrographs of a monolayer of porous silica particle dispersed in 1mM Azo-C6 at different irradiation time (at t = 0 s, 30 s, 12 min, and 30 min) of global blue (λ = 455 nm) and focused UV (λ = 353 nm, d = 20 µm) simultaneously. It has been

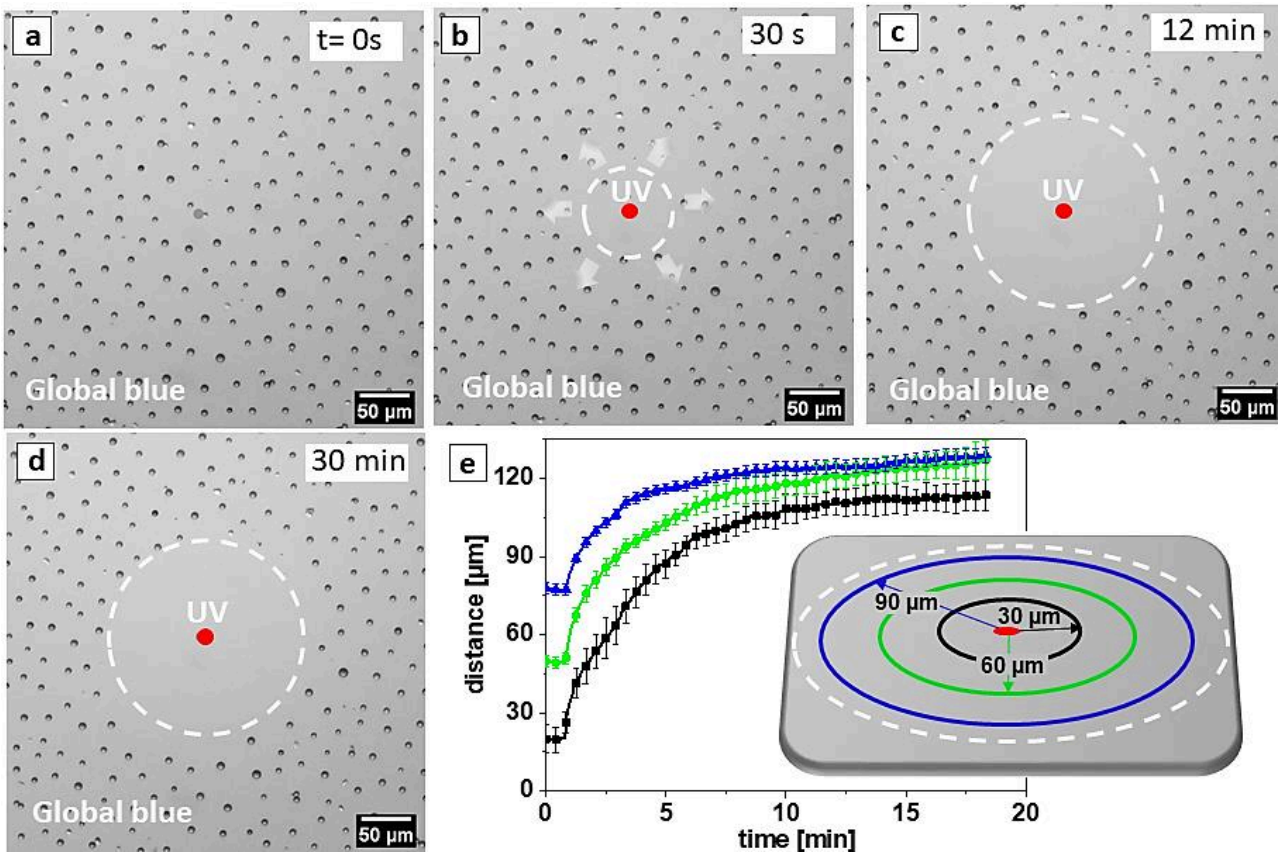

Figure A.5. Simultaneous irradiation of focused UV and global blue light. Effect is shown for mesoporous silica particles (d= 5 µm) in 1 mM surfactant concentration. (a-d) Optical micrograph of the process at t = 0s, 30s, 12 min, and 30 min. (e) Average distance vs time plot for particles in individual rings of thickness of 30 µm. It is interpreted that the equilibrium is achieved after 10 minutes of irradiation reaching the saturation of cleaning area. Video of the process is shown in **Figure SA.5** in Appendix D.

observed that Saturation of cleaning area is achieved within 10 minutes of irradiation , which is very fast as compare to previous case (see plot in **Figure A.5e**). One can say that the range of the flow for this particular case is ca 110 µm and can easily be manipulated by changing the parameters like surfactant concentration or intensities of both blue and UV irradiations. The porous particles outside

the cleaning area are well separated due to an additional flow (l-LDDO flow) introduced in this thesis. Each porous particle generated its own l-LDDO flow resulting in the state if separation. In case of non-porous particles this flow will be absent, therefore repulsion between particles will be absent and randomly distributed particles will be observed.

Appendix B. Detailed investigation of light driven collective motion of mesoporous silica particles under focused blue and global UV irradiation

In this section we would like to report on further analysis on light driven collective motion of mesoporous colloidal particles where ACS molecules interact with two light sources of different wavelength , UV (λ = 365 nm) and blue (λ = 490 nm) simultaneously. The collective behavior of particle motion is discussed in **Publication 4**. We have reported that when global UV and focused blue light is combined together, it results in a 2D disk of well separated particles trapped inside the blue irradiation spot. Complete process goes through three different mechanisms before reaching to equilibrium state : (i) passive motion of particle towards the blue irradiation area due to generation of global LDDO flow pointing in the direction of blue irradiation spot , (ii) aggregation of porous particles in side the blue spot which is followed by (iii) separation of particles due to generation of local LDDO flow around each mesoporous silica particles forming a stable 2D crystalline disk pattern. Here, we will discuss, how we can manipulate the physical variables like particle velocity, aggregation time, cluster size and separation time or total time to reach equilibrium by altering different parameters such as surfactant concentration, intensities of both global and focused irradiation, diameter of laser spot, and wavelength of light. We have observed that using appropriate parameters one can perform different tasks like transportation of 2D crystalline disk from one place to another or sweeping large number of particles in relatively lesser time than previous systems.

B.1. Dependency on surfactant concentration

We have observed that surfactant and particle concentration can strongly alter the collective behavior of particle motion. For example, the total time required for aggregation (second step) followed by separation (third step) into the area irradiated with the blue light decreases with increasing concentration. At lower concentration, tight clusters of particles are witnessed which require longer time to separate while at higher surfactant concentration, immediate separation was recorded as soon as particle enters the laser spot. **Figure B.1.1** exemplifies dependency of surfactant

concentration on the above mentioned system and represents the optical micrograph for 0.5 mM, 1mM and 1.5 mM at different irradiation time (t = 10 s, 60 s and 300 s). In case of 0.5 mM (CMC), no significant motion towards the laser spot is observed (blue circle is laser boundary). Particles which are already into the spot form clusters and initially perfom coarsening (i.e. moving from one cluster to another) which is then followed by separation with very low rate (**Figure B.1.1a**). On the other hand , in case of Cs = 1 mM, with in 5 minutes of blue irradiation all the particles inside the ring are separated with nearest particle distance of 15 µm forming 2D disk pattern **(See Figure B.1.1b)**. The step of aggregation of particle before separation disappears on increasing surfactant concentration further. This can be seen for C_{azo} = 1.5 mM (static images are shown in **Figure B.1.1c**).

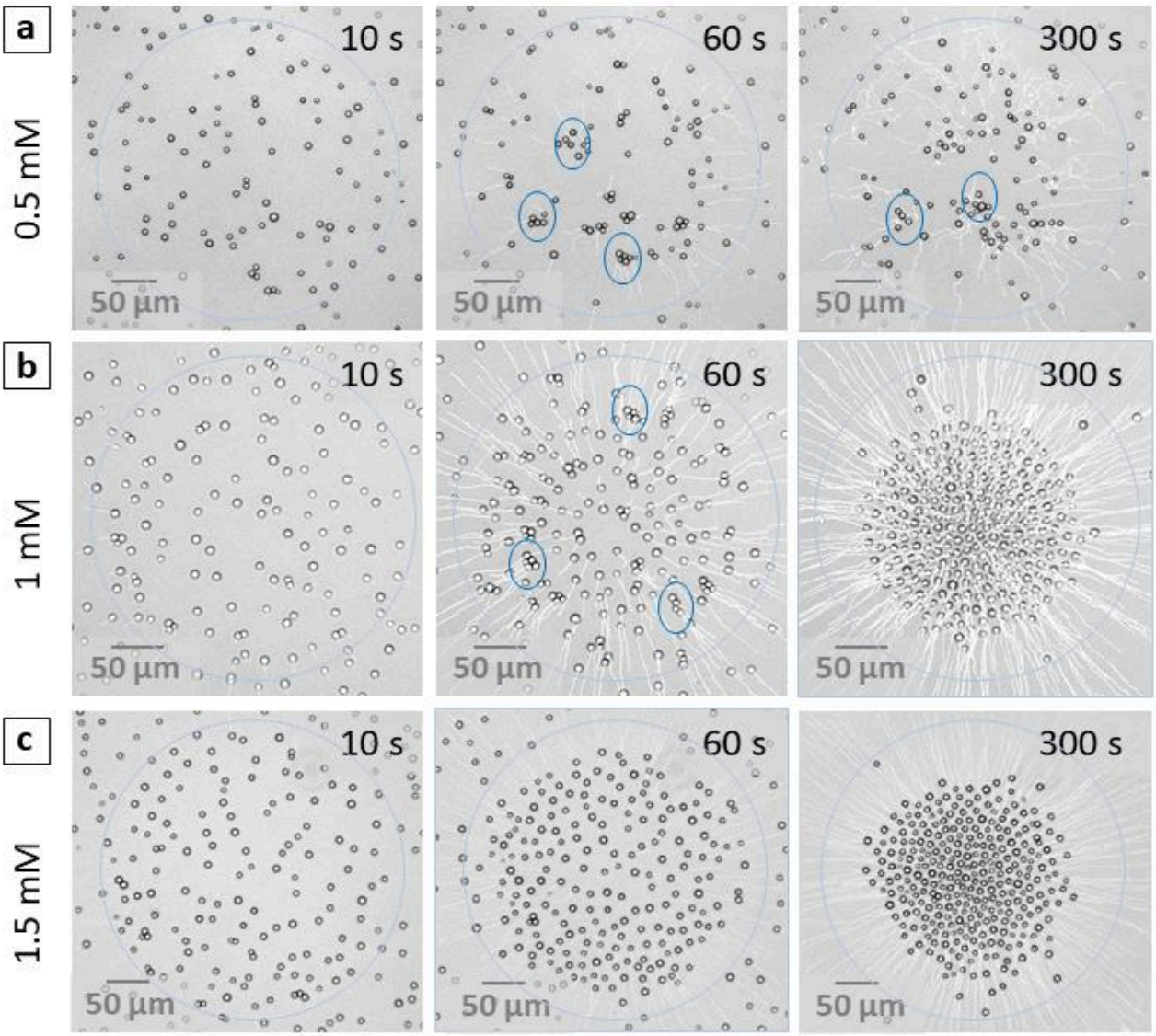

Figure B.1.1. Optical micrograph of the collective motion of mesoporous silica particles for different surfactant concentrations at time = 0s, 30s and 300s. (a) for c_{azo} =0.5 mM, (b) for c_{azo} =1 mM; (c) for c_{azo} =1.5 Mm. Supporting videos can be found in **Figure SB.1.1** in Appendix D.

To analyze the motion we traced the trajectories of each individual particles and compiled the resultant statistical data in order to calculate particle velocity and distance traveled by particles. The

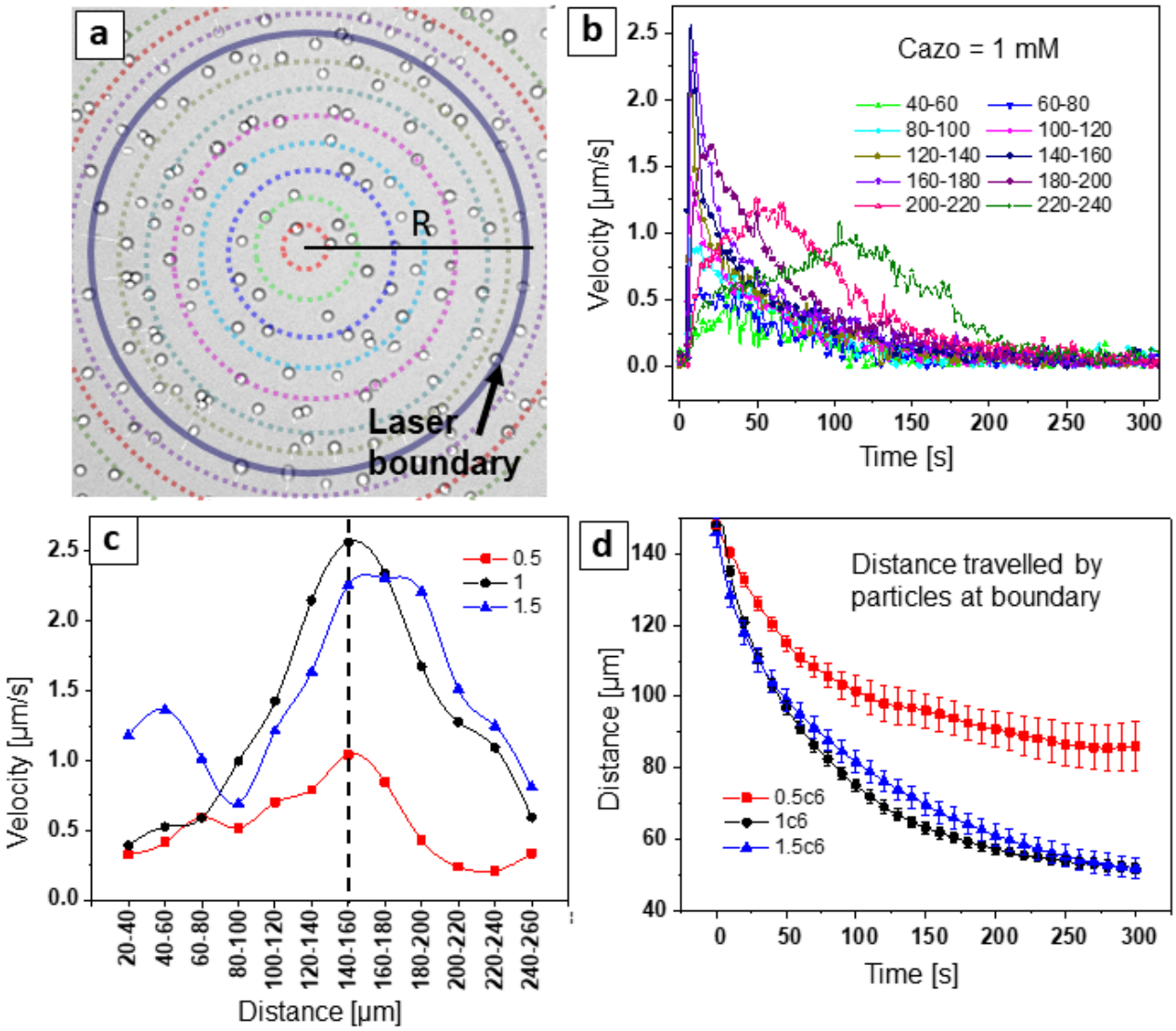

Figure B.1.2. (a) Particles distributed on the glass surface after sedimentation, 20 µm thick rings are drawn around the center of laser spot in which particles are grouped to calculate (b) average velocity with respect to distance for whole irradiation time. (c) maximum velocity in each ring plotted for different surfactant concentration. (d) Average distance travelled by particles situated at the laser boundary for $\mathbf{c_{azo}}$ = 0.5 mM, 1mM and 1.5 mM.

particles were grouped in 20 μm rings depending upon their distance from the center of the laser spot (see **Figure B.1.2a**). Average velocities and distances of all the particles in each ring is calculated as a function of time for each 20 μm thick ring which are at certain distance from the center of spot , i.e. 20 to 40 μm, 40 μm to 60 μm, and so on. **Figure B.1.2b** displays the velocity as a function of time in each ring for surfactant concentration of 1mM. Maximum velocities achieved in each ring are calculated and shown for different surfactant concentrations in **Figure B.1.2c**. Once again from the analysis we can comment that particles which were initially at the boundary achieve the maximum velocity of 2.5 μm/s, 2.25 μm/s, and 1 μm/s for 1.5 mM, 1mM, and 0.5 mM respectively. Displacement of particles at the spot boundary (i.e. : 140-160 μm) is shown in **Figure B.1.2d**. Decrease in distance is referring to the movement of particles towards the center of the spot. The lower value of distance traveled in case of 0.5 mM signifies that the strength of LDDO flow is weaker at this concentration which is not enough to drive the particles towards the irradiation area.

This dependency upon surfactant concentration can be explained as follows: In the beginning due to initial global irradiation of UV light , ca. 90% *trans*- molecules were isomerized into *cis*- *state.* This means only 10% *trans* molecules are available for particles. Using absorption spectroscopy technique we can approximate that 0.1mg particles ab/desorb total of 0.1 mM of *trans* molecules. This is shown in **Figure B.1.3a**, where absorption spectra for three samples with different particle concentration in 1 mM Azo-C6 were recorded**.** The amount of available *trans* molecules (black square) and how much is required (red line) for 0.1 mg/ml porous silica particles is shown in **Figure B.1.3b**. From the plot it is clear that the fraction of *trans* molecules for concentrations lower than 1 mM (10 % of C_s under UV light), is not sufficient to completely fill the pores of all the particles. When focused blue light irradiation is switched on (global UV is also on) , empty particles passively enter the area enriched of *trans* molecules (84% *trans* and 16 % *cis*) where *trans* molecules diffuse into the pores creating a situation of aggregation (explained in publication 4). Whereas, for concentration above 1 mM (c_{azo} > 1 mM), more than required *trans* molecules are presented in the system due to which when particles enter into the blue irradiation spot it was already full with fuel restricting the diffusion of *trans* inside the pores resulting in direct separation forming the 2D stable grid.

To support this explanation, we have performed experiments under global UV and blue light separately (In previous case both global UV and focused blue used simultaneously). Initially sample was exposed to UV irradiation which induces localized LDDO flow radially away from each particle resulting in repulsion between the colloids. After 10 min irradiation, UV light was switched

off, and global blue light was switched on. Due to shifting of wavelength the fraction of *trans* molecules at photo stationary state shifts from 10 % to 70% *trans* from UV light to blue light respectively (see **Figure B.1.3c**). Similar to the case of (combined UV and blue light), when blue light is on an immediate aggregation is observed for lower concentrations which is followed by separation later. While direct separation was witnessed for concentrations above 1 mM (see the NPD plot in **Figure B.1.3d**).

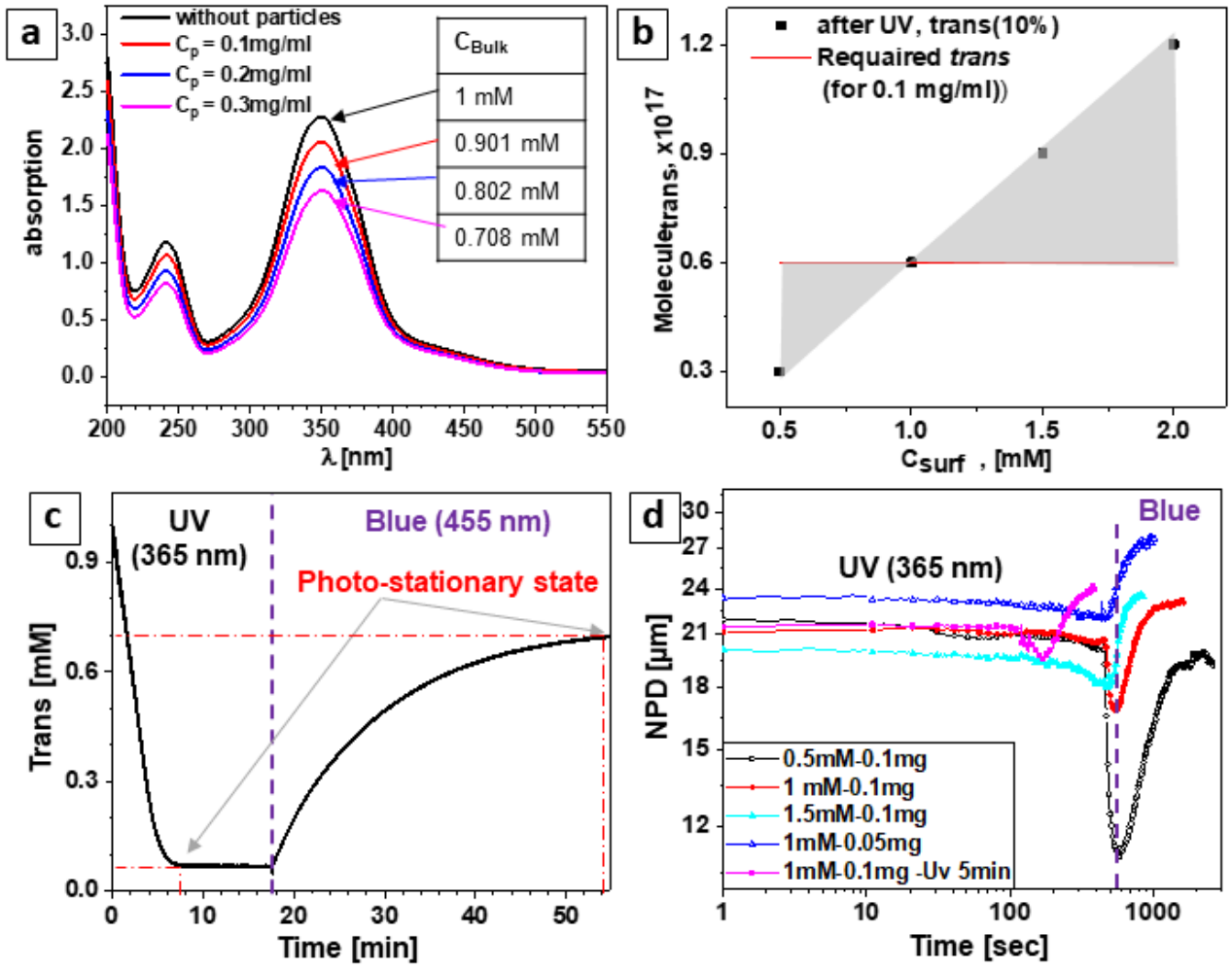

Figure B.1.3. (a) UV-Vis absorption spectra for solution containing 1mM Azo-c6 with different particle concentrations as 0.1 mg/ml, 0.2 mg/ml, and 0.3 mg/ml. Inset shows the value of concentration left in the bulk solution corresponding to each curve. (b) Fraction of *trans* molecules presented after UV irradiation and required to fill the particles with concentration of 0.1mg/ml plotted against surfactant concentrations. (c) Photo-stationary state achieved after UV and blue irradiation for Cs = 1mM. (d) Average nearest particle distance vs time for different surfactant

concentrations. Firstly sample is exposed to UV irradiation for 10 min and later only blue light is switched on.

Similar behavior is observed when particle concentration is altered keeping the surfactant concentration fix. Increasing the particle concentration means increasing the minimum amount of *trans* molecules required for particles. We can combine these dependencies in one common statement to comment that the total time of aggregation and also the size of clusters forming before separation is proportional to particle concentration and inversely proportional to surfactant concentration. A phase diagram demonstrating this dependency of concentrations is shown in **Figure B.1.4**. When parameters on the left side of black line is taken, direct separation of particle was observed, whereas for parameters on the right side aggregation followed by separation was witnessed.

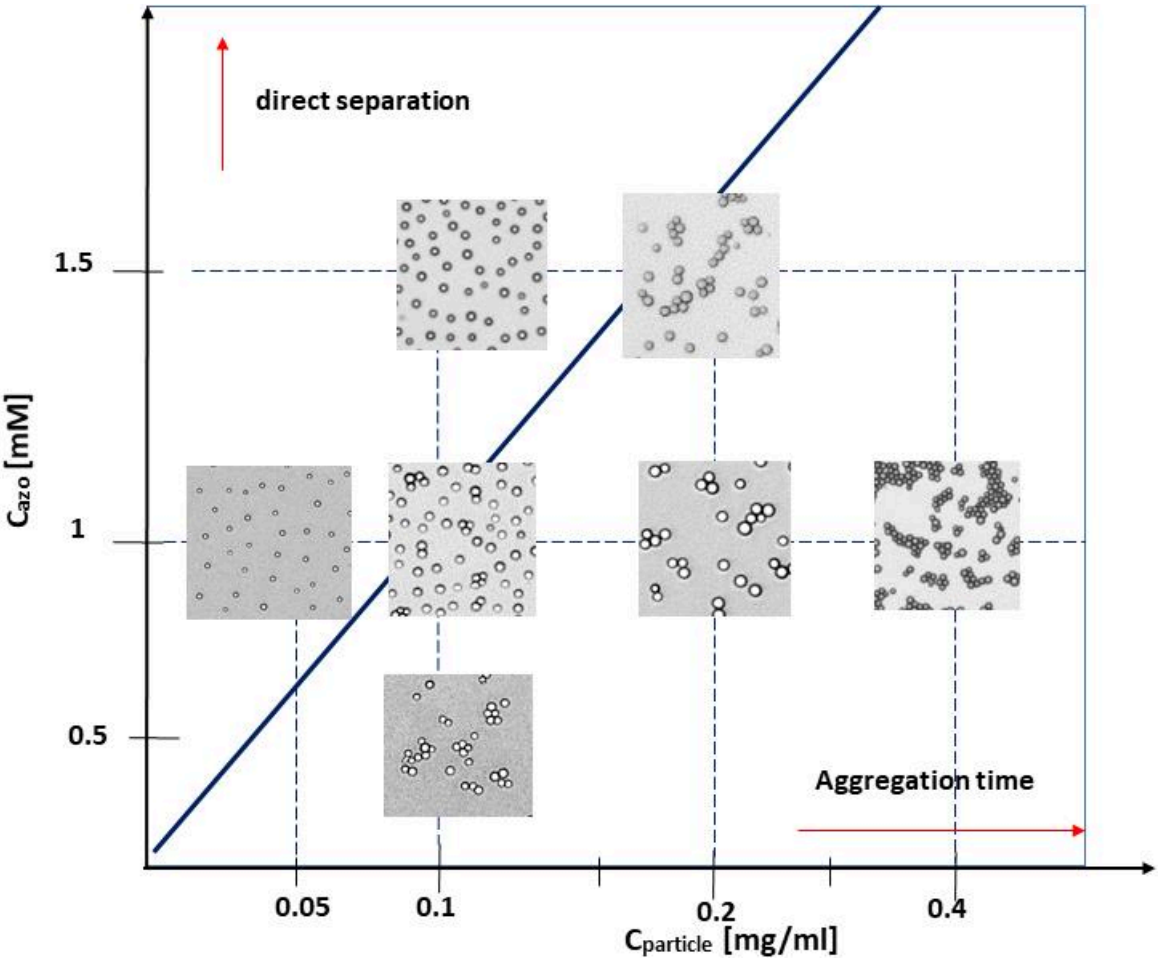

Figure B.1.4. Phase diagram depicting the dependency of particle and surfactant concentration upon particle aggregation (step 2) when Pre UV irradiated sample is exposed to focused blue laser (global UV irradiation is continuously on).

B.2. Generation of two flows of opposite directions

We have mentioned in previous section that porous silica particles move passively towards the blue irradiation area and are trapped inside the spot forming well separated 2D crystalline pattern when sample is exposed to focused blue and global UV irradiation simultaneously. However when we look the process in larger area (observing and analysis area is larger as compare to previous), certain distance from the boundary an additional flow pointing radially outwards is witnessed. **Figure B.2.1** reveals complete picture of the process at different time scale. When blue laser of (diameter = 144 µm , power = 35 µW) was added on a UV irradiated ensemble of porous silica particles, local and global light driven diffusioosmotic flow is induced due to generation of *cis* concenatrtion gradient.

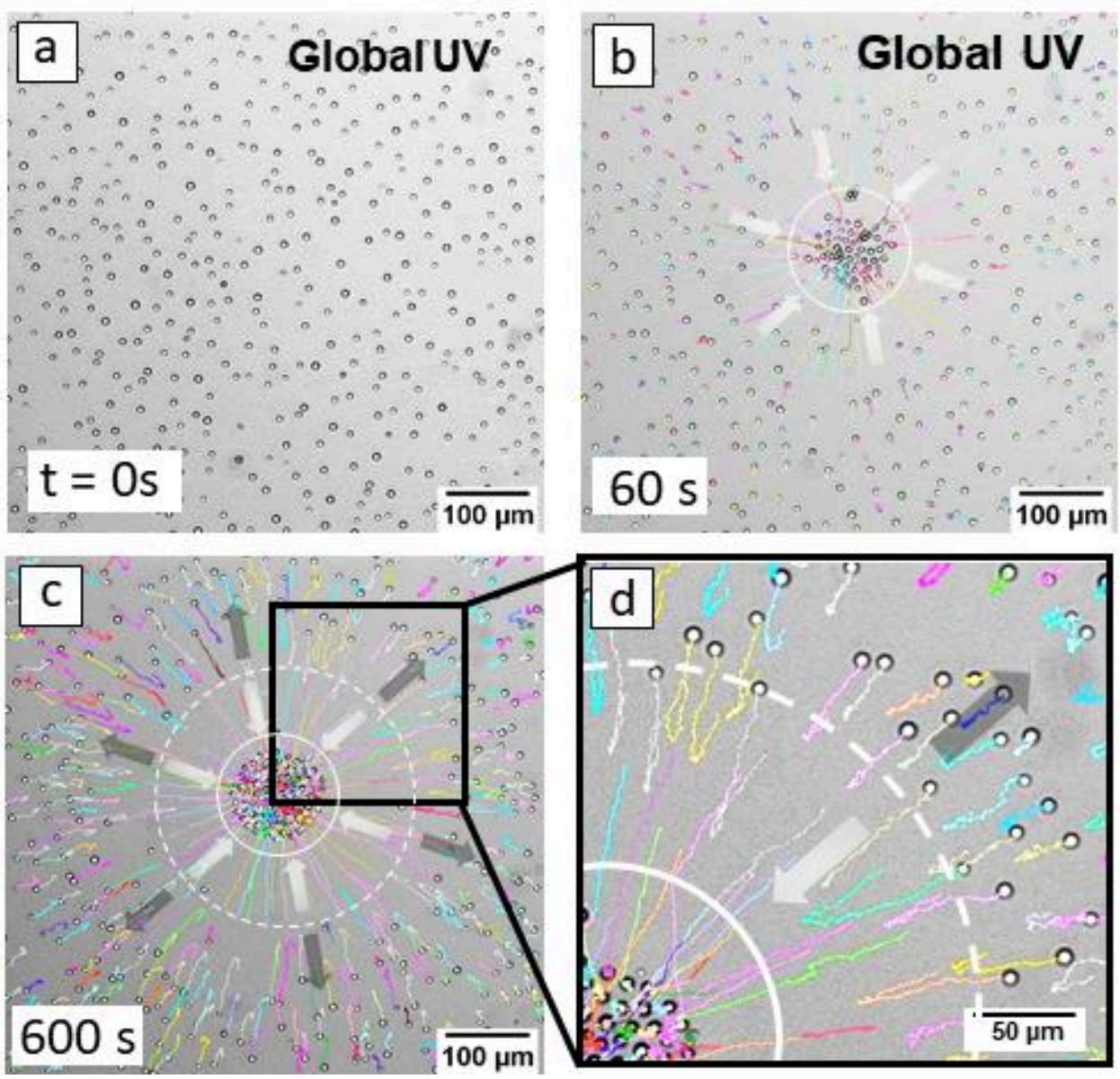

Figure B.2.1. Optical micrograph representing complete picture of the process when focused blue and global UV light is exposed to a monolayer of porous silica particle in 1 mM AzoC6. (a) at t= 0s, (b) t= 60s, (c) t = 600s (d) Enlargement of the selected area in c. The white solid line is the boundary of the irradiation spot. White dashed line denotes the imaginary boundary. Two arrow are showing the direction of the flow. Corresponding video can be found in **Figure SB.2.1** in Appendix D.

Initially the flow direction is towards the irradiated area which carries the particles (which are with in certain distance from the boundary) passively into the spot (discussed in publication 4). In few minutes an additional flow in the opposite direction from the spot is also witnessed in the experiments which drives the particles away from the spot. These observations clearly states the occurrence of two flows in opposite direction taking place at the same time: One is cleaning the surface after certain distance from blue spot boundary and other one is sweeping the particles towards the irradiated area to form a 2-D stable grid. From now on we will name the boundary where the second flow is originated as imaginary boundary which is at distance D_{Img} from the center of blue spot (marked in dashed white line in **Figure B.2.1**. According to our analysis this distance, D_{Img} is independent of surfactant concentration and blue light intensity and varies upon changing the other parameters like spot size and intensity of global UV irradiation. We will discuss about this external flow in detail in next sections.

B.3. Dependency on spot size of focused blue irradiation

To check the effect of diameter of focused blue laser upon velocity or separation distance of the particles in the irradiation spot, we varied the diameter of focus blue laser ranging between 140 µm to 470 µm. The monolayer of particles were divided in to 20 µm rings and the maximum velocities of particles calculated in each rings is plotted as a function of distance from the center of the spot. **Figure B.3.1a** shows the graph of average maximum velocity of particles in each ring plotted for 5 different laser spot size. The maximum velocity of particle calculated as ca. 3µm/s (constant intensity) and is independent of spot size and is always found at the boundary of the laser spot as shown in the plot. The distance between the particles (NPD) at the time of complete separation is independent of laser spot size (black solid line) and the number of particles (blue dashed line) in the exposed area is linearly proportional to radius of spot (see **Figure B.3.1b**). It has been observed that the particles inside the irradiated area is confined to an area which is smaller than the area of irradiation spot. Increasing the spot sizes also increases this confined area (i.e. D_c increases, black

line in Figure B.3.1d). The distance of imaginary boundary (D_{Img}) from the spot center also increase with spot size (red line in **Figure B.3.1d**). It is witnessed that time taken to induce the outer flow decreases with increase in laser diameter.

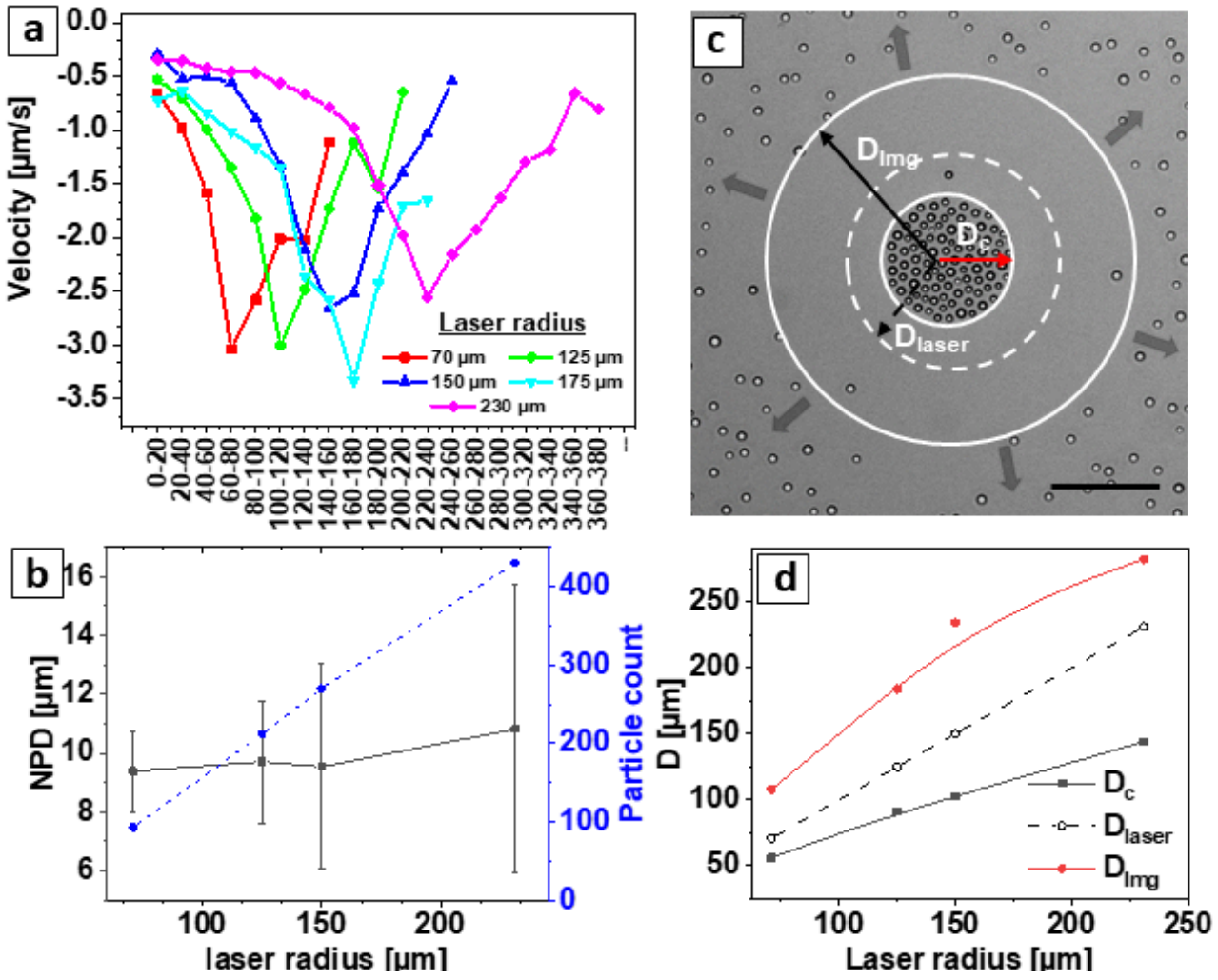

Figure B.3.1. (a) Maximum velocity of particles in each divided sections (20 µm thick rings) for different laser spot. The maximum velocity of ca. 3 µm/s is achieved at the boundary and is independent of laser spot size.(b)NPD (black line) and number of particles inside the the irradiation area plotted as a function of spot size. (c) optical micrograph representing the outer boundary where flow starts in opposite direction. D_c, D_{laser}, D_{img} are distance of the confined boundary, laser boundary and imaginary boundary respectively from the center of the spot. (d) Distance vs laser radius plot for D_c, D_{laser}, D_{img}. Supporting videos for different laser sizes can be found in **Figure SB.3.1** in Appendix D.

One of the interesting applications of combination of UV and blue light is that, the process is extremely fast to assemble large number of particles in shorter time with more precise and accurate way for desired area. It has been observed that it is approximately 10 times faster as compare to the case of

only one focused irradiation and also requires less intensity. **Figure B.3.2** exemplifies the comparison of cluster formation between two systems : (i) focused green irradiation (Diameter = 20µm) and (ii) a system with global UV and focused blue (diameter = 150 µm). The latter system is very flexible and can be used according to the requirement, changing other parameters. It is also possible to speed up the process of gathering particles even more by changing continuously the spot size from higher diameter to lowest desired diameter. If the area of spot is very small as compared to total occupied area of the particles than the additional layer of particles is formed.

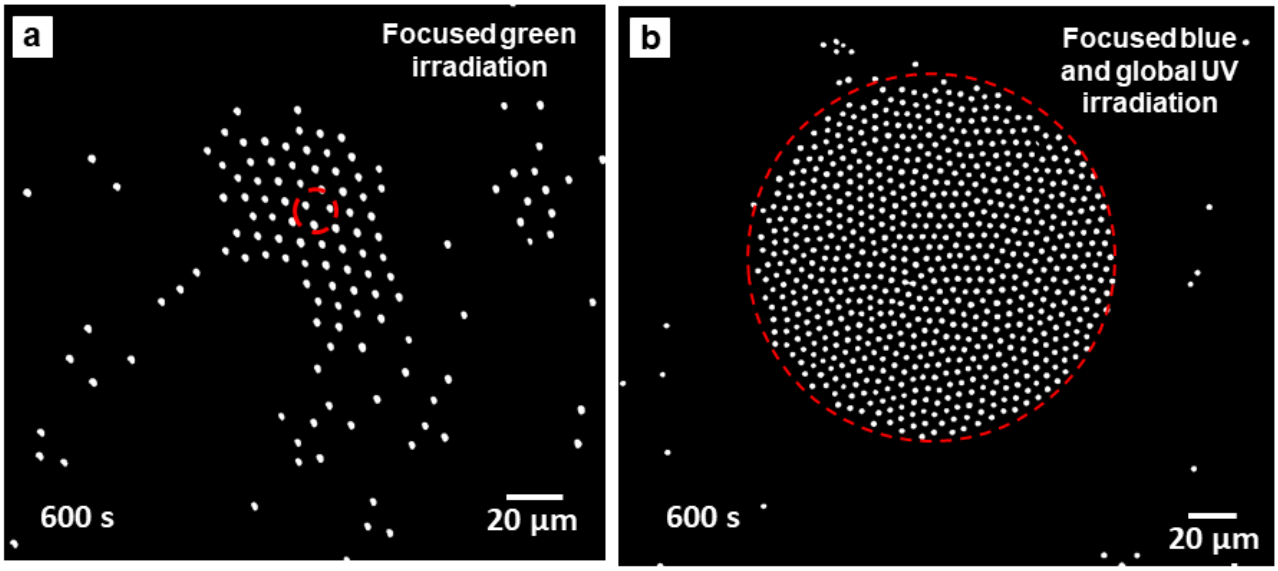

Figure B.3.2. Micrograph showing the static image after 10 minutes for ensemble of non-porous silica particle in 1mM Azo-C6 in two different systems:(a) Focused green laser with laser diameter of ca, 20 µm. (b) Focused blue light and global UV irradiation with laser spot size as 150 µm .red dashed line represent the laser boundary. Supporting video can be found in **Figure SB.3.2** in Appendix D.

B.4. Effect of intensity of irradiation wavelengths

In this section, we will discuss the effect of intensities of UV and blue irradiation on collective motion of porous silica particles in 1mM surfactant solution. The dependency is observed The motion of particles towards the irradiated area is faster for higher intensities of blue light. **Figure B.4.1a** shows maximum velocities achieved in each rings for fixed irradiation diameter (d =380 µm) and different powers of laser spot ranging from 7.5 µW, 28 µW, 57 µW, and 132 µW. The intensity of global UV irradiation is kept constant in all the experiments mentioned above as 1.4 mW/cm^2. The nearest particle distance (NPD) after the separation of particles is analyzed and is

independent of the intensities but the time to achieve the state of this separation is reducing with increasing power (see plot shown in **Figure B.4.1b**). From the above results we can conclude that the the ratio of intensities of focused blue to global UV light is an important factor for generation of LDDO flow. The flow will induce when ratio is greater than 4. For instance, when blue laser with power 7.5 µW is applied, the ratio is lower than 4 and hence LDDO flow is not that evident.

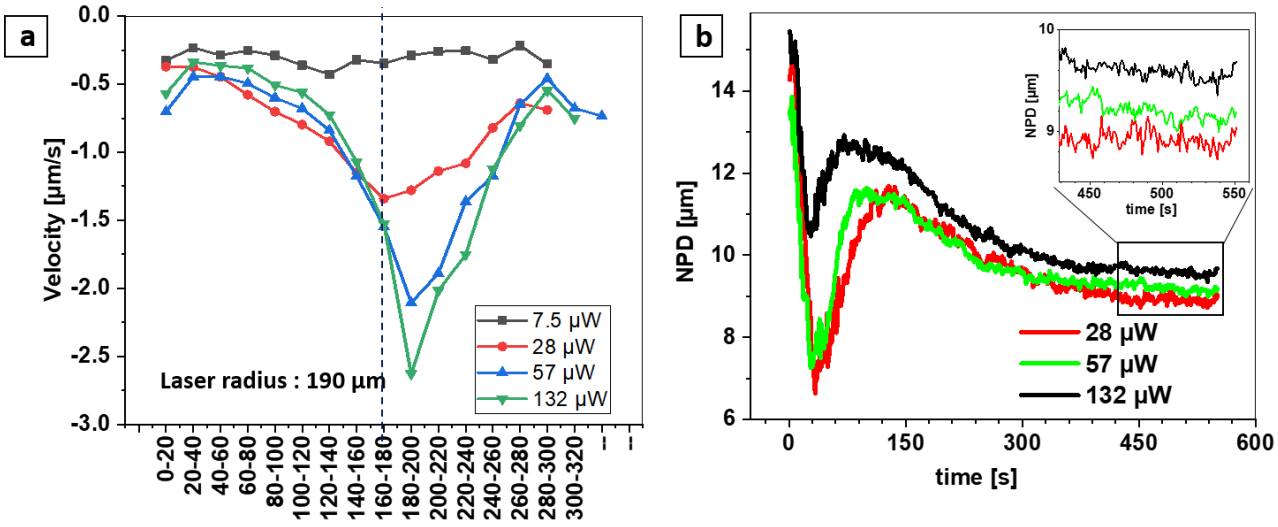

Figure B.4.1. Velocity vs distance plot for different intensities of focused blue irradiation keeping other parameter constant (c_{azo} = 1mM, laser radius = 190 µm, Intensity of UV light = 1.4 mW/cm^2). (b) NPD plot as a function of time for different intensities. Graph shows that NPD is independent of intensity of irradiation. Corresponding videos for different intensity of blue laser can be found in **Figure SB.4.1** in Appendix D.

Varying the intensities of global UV irradiation affect the system differently (keeping all other parameters fix). The major changes are observed in confined area (area of trapped particles, D_c) or in distance of imaginary boundary (D_{Img}). For lower intensities it has been observed that particles are also collected outside the laser boundary forming a ring like cover of randomly distributed particles to 2D separated disk where distance between the particle is independent of the intensity of light (**Figure B.4.2a**). This area of confined particle decreases with increase in the intensity as shown in **Figure B.4.2b**. The analysis of distance and velocity profile for I = 128µW/cm^2 (lowest) and I = 1.4 mW/cm^2 (highest) is represented in **Figure B.4.2(c-f)**.

It has been observed that the imaginary boundary (from where the additional flow starts) also changes with intensity of UV light (see red dashed line in **Figure B.4.2c and d**). It comes closer to laser

boundary for higher intensities. This means that the inward flow drives less particle towards the irradiation area which reduces the confined area in order to maintained the constant separation distance (**Figure B.4.2g**). Number of particles inside and outside the laser boundary after 20 min of irradiation is shown in **Figure B.4.2h**.

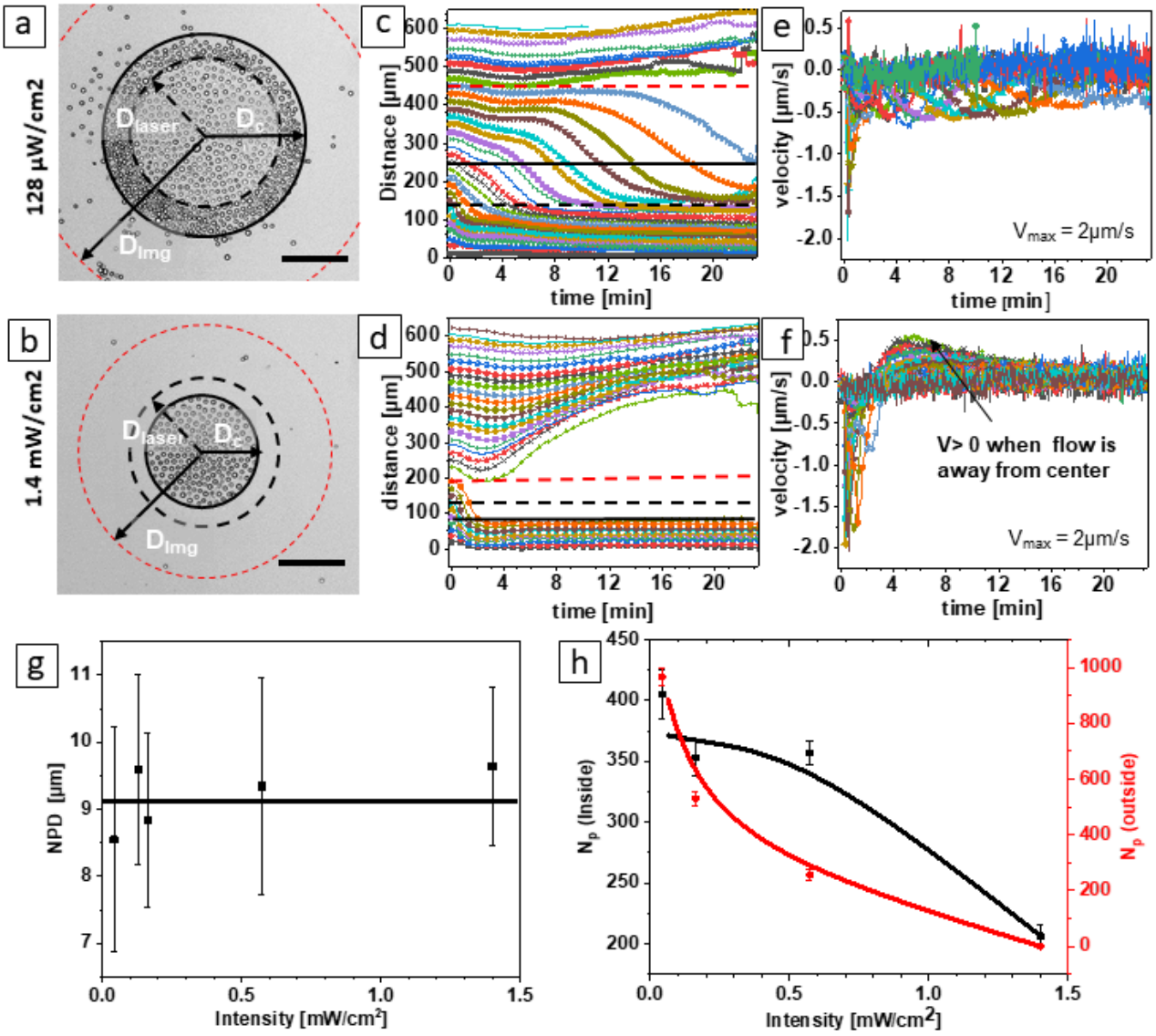

Figure B.4.2. Effect of intensity of global UV irradiation keeping other parameters fixed. Static images of the process after 20 min of irradiation for two UV intensities as (a) 128 µW/cm^2 and and (b) 1.4 mW/cm^2. (c,d) corresponding distance vs time plot for intensities mentioned in a and b. dashed black line represents the laser boundary. Solid black line and dashed red line denotes the boundary of confined area and imaginary boundary respectively. Increase in distance means the particles are going away from the spot center. (e, f) Corresponding velocity profile. Maximum velocities of particle towards the irradiation spot is similar for both the cases. However for larger Intensities the velocity of outward flow is also higher as compare to lower intensities. (g) NPD vs Intensity plot. NPD is independent of intensities. (h) Graph showing analysis of number of particles

trapped inside andoutside the irradiation spot with respect to intensities. For higher intensities, particles are only inside the spot. Videos for dependency of UV intensities can be found in **Figure SB.4.2** in Appendix D.

When global UV irradiation is switched off completely (only focused blue irradiation), two flows of opposite direction towards the laser boundary are witnessed: First, from the center of irradiation spot to the direction of its boundary and second, from outside the spot to inward direction towards the boundary. Time scale optical micrograph of this effect is shown in **Figure B.4.3** (**a-c**). When UV light is again switched on, first flow vanishes and second flow with higher strength drives the particle into the irradiation area (**Figure B.4.3d and e**). Once again switching off the UV irradiation induces two flows and particles starts gathering again at the boundary of the spot forming a ring pattern (**Figure B.4.3**(**f-h**)).

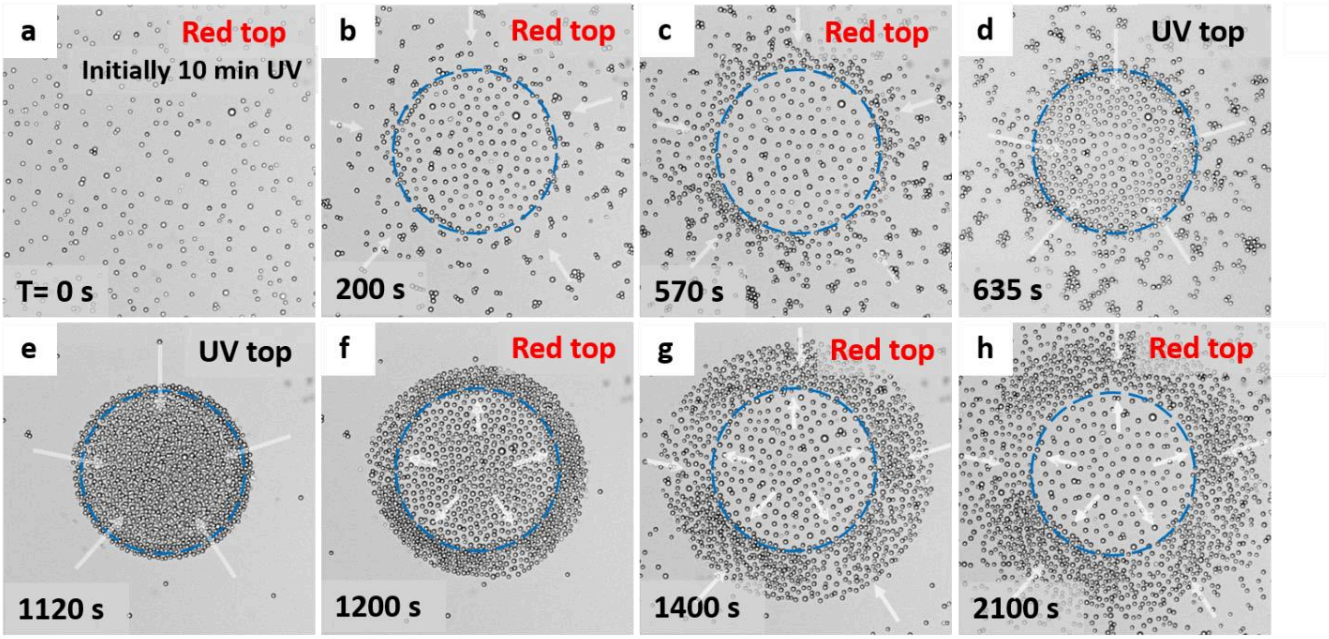

Figure B.4.3. Statistic images of the motion of mesoporous silica particles dispersed in 1mM Azo-C6 on a glass surface under continuous irradiation of focused blue light combined with momentary irradiation of global UV additionally. (a) optical micrograph after 10 minutes of UV irradiation. (b,c) Static images after 200s and 570 s when UV is switched off at t= 0, and focused blue irradiation is applied. Particles are gathering at the boundary. White arrow denotes the direction of particle motion. (d, e) Static images at 635s and 1120 s when UV light is also switched on along focused blue irradiation. Strong flow towards the center of spot is observed which carries particles into the blue irradiation spot. (f,g,h) micrograph after UV is switched off. Two flow pointing towards the boundary of the spot is witnessed and shown by white arrow in the images. Corresponding video can be found in **Figure SB.4.3** in Appendix D.

The origin of two opposite direction flows towards the boundary can be explained by the principle of light driven diffusioosmotic flow and is completely independent of porosity of particles. Initially all the molecules in the system are in *cis* state due to global UV irradiation. When global UV is turned off and focused blue is switched on, interaction potential at the interface of exposed area changes due to isomerization of *cis* to *trans* molecules. This induces the LDDO flow towards the boundary due to pressure gradient (more *cis*- to less *cis*- molecules) which moves the particle along. When spot size is very small only one flow towards the spot is visible, however, upon increasing the spot size an additional flow from center of spot to the boundary is witnessed .i.e.. particles inside the spot move towards the boundary. When particle are porous, local-light driven diffusioosmotic flow is also generated which maintained the repulsion between the particles inside the blue zone which disappears when particles go out of the boundary.

When UV light is again switched on, the *trans* molecules which were diffused out of the irradiated area, isomerizes back to *cis* state, which again generates the flow pointing in the direction of blue irradiation area.

B.5. Rveresible swarming and separation of mesoprous silica particles under focused blue irradiation: Living clusters

The mechanism of LDDO flow is unique, flexible and reproducible. It can be expanded to various different forms of collective motions of non-living as well as living organisms upon irradiation of different wavelength of light. When two wavelengths are combined together one can manipulate or change the interactions between colloids by triggering one of the wavelength.

In this section we will talk about how system interacts on pulse irradiation of focused blue light when global UV light is switched on continuously throughout the experiments. **Figure B.5.1** shows the optical micrographs recorded for one minute pulse irradiation on a system consisting of an ensemble of 0.1mg/ml particle concentration and of 1.5 mM surfactant concentration. The size and power of focused blue spot is maintained constant at 420 μm in diameter , and 300 μW in power. Initially (first time), blue light is switched on for longer time such that stable well separated 2D grid pattern in confinement forms (see **Figure B.5.1b**). After 12 min, pulse irradiation of focused blue light with frequency of 1 min^{-1} is started. Schooling behavior of micro motors is observed when blue light is off and separation between particles take place when blue light is switched on again. One

can explain it as follows: When blue light is off, strength of the LDDO flow towards the center of the spot increases for short time which results in tight cluster (see **Figure B.5.1c**). As soon as blue light is switched on particles repel each other and once again forms the crystalline pattern (**Figure**

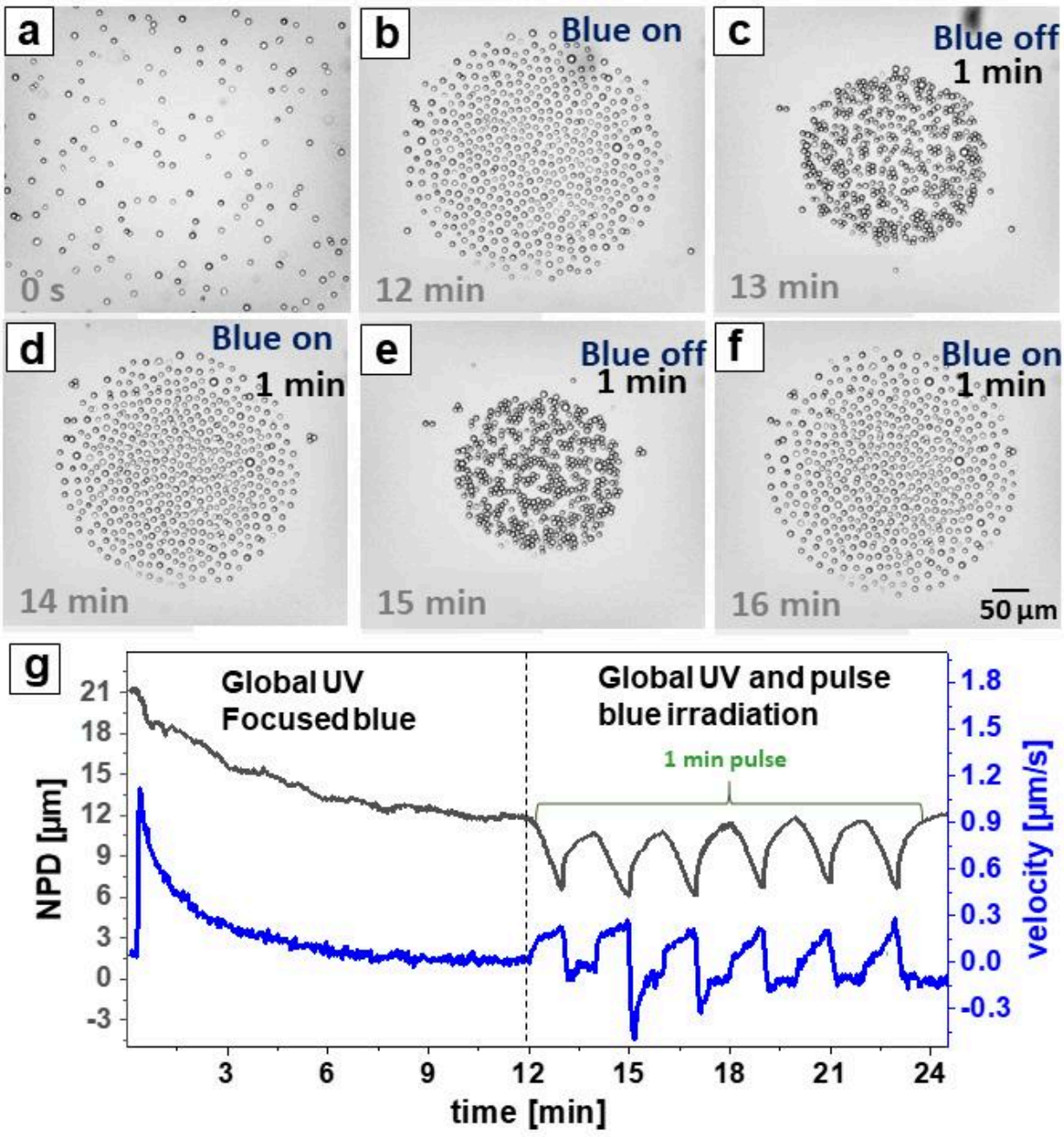

Figure B.5.1. Optical micrograph showing the static images of the process under 1 minute of pulse irradiation in 1.5 mM Azo-C6. (a) initial image at t= 0, just before blue laser is applied (b) 12 min after the focused blue light is switched (forming 2D patterned disk). (c, e) when blue light is switched off for 1 minutes. (d,f) when blue light is on. Remember global UV light is switched on through out the experiment. (g) Nearest particle distance (NPD) vs time plot under pulse irradiation. Corresponding video can be found in **Figure SB.5.1** in Appendix D.

31d). The process is repeated with each successive on and off of blue light (**Figure B.5.1d-f**). One can compare the resultant response with the beating of heart. Heartbeats because of electrical signals which results in contraction and relaxation, similarly in our case light signal is inducing a flow which result in compaction and expansion of 2D cluster or lets call it as a living cluster of particles. one can characterize the response of motion by calculating average nearest particle distance between particles. In case of compaction, NPD decrease, and when cluster is expanded NPD starts increasing to a constant value (**Figure B.5.1g**). The velocity of particle in the starting of each step is higher and decreases with time.

When frequency of pulse irradiation is reduced to 0.5 min^{-1} and 0.1 min^{-1} similar effect is observed. But decrease in NPD with each successive period is noticed for lower frequencies (NPD plots are shown in **Figure B.5.2**). we can interpret two statements here : first, the response of the particles motion is very fast in accordance with the applied irradiation and the flow induced by light exposure. This means the the reaction of *trans* and *cis* molecules to its surroundings changes spontaneously according to exposed wavelength of light. Secondly, this overall decrease in NPD could be related to reproducibility to initial state. For higher frequencies the probability of getting back to initial (coming to same fraction of *trans* and *cis* molecules after each cycle) state is less, may be due to few seconds delay in response of particle motion. More detailed studies and experiments to support and to understand the observations are still undergoing.

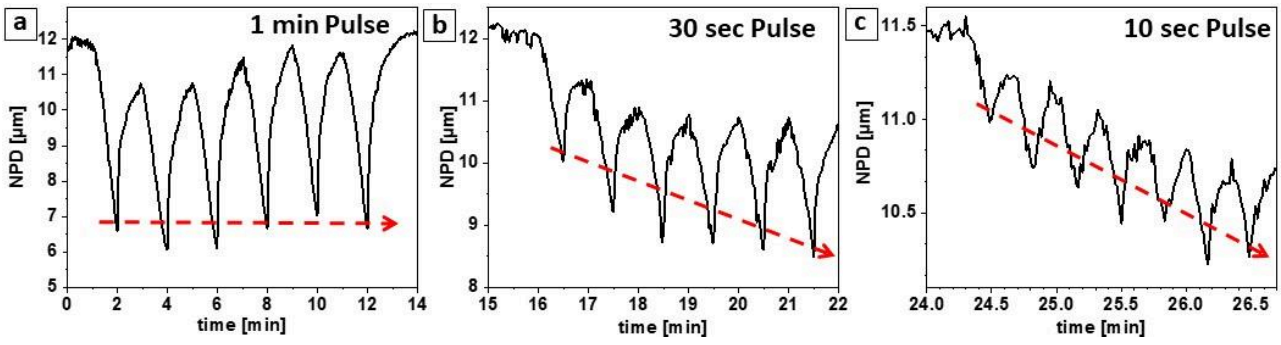

Figure B.5.2. NPD vs time plot for particle motion in 1.5 mM in Azo-C6 under focused blue light irradiation with different frequencies. (a) 1 min^{-1} , (b) 0.5 min^{-1} and (c) 0.1min^{-1}.

When 10 s pulse irradiation was applied from the beginning of the process only (in the previous case first particles were trapped in to the confinement and then pulse irradiation was applied) we have observed value of NPD is drifted to lower value with fluctuations due to pulse irradiation

(Figure B.5.3a). Also when the sample is exposed for 10 sec only in starting, particle aggregates till 100 seconds before repulsion due to continuous global UV irradiation from the top (**Figure B.5.3b**).

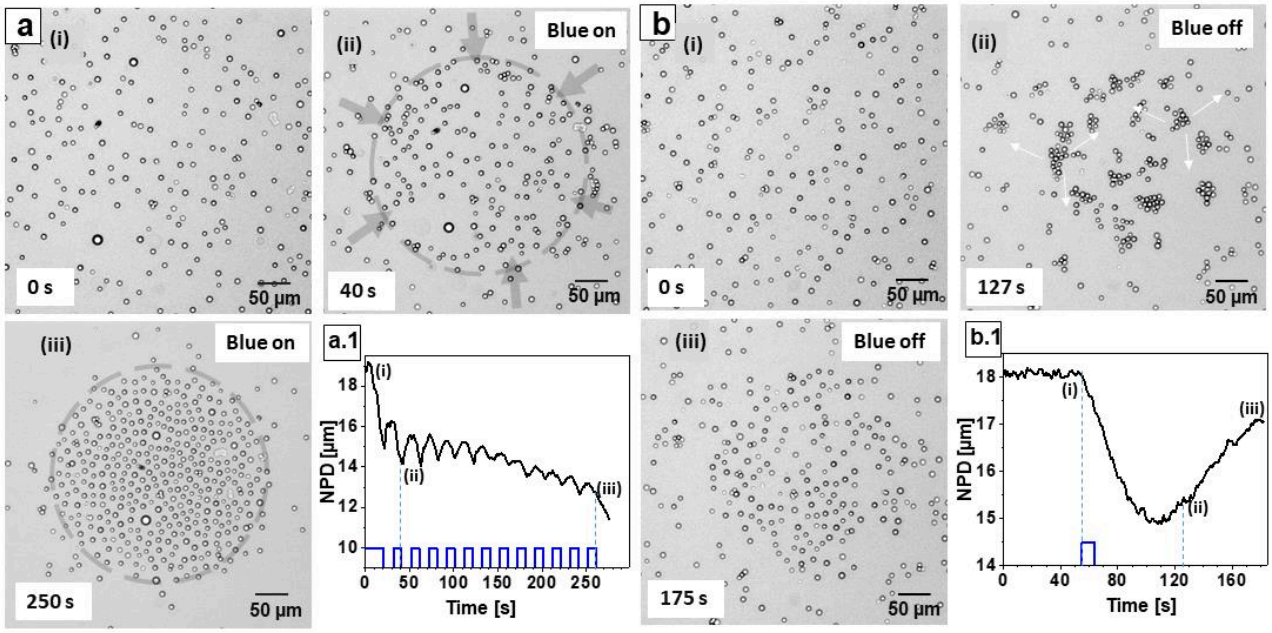

Figure B.5.3. (a) Optical micrographs at when pulse irradiation of 10 s is applied from the initial stage until the particles are trapped into the spot. (b) Optical micro-graphs representing the motion when focused blue light is applied once in the starting for 10s. Initial aggregation followed by separation is witnessed. (time of i,ii,iii are denoted in respective plots of a and b). Corresponding video can be found in **Figure SB.5.3** in Appendix D.

For a surfactant concentration of 0.5 mM, under blue irradiation, particle undergoes coarsening i.e. one particle moves from one cluster to another (also shown in **Section B.1**). Upon switching off the blue light, instead of aggregation, the repulsion between particle is observed which was not similar to the the case of 1mM and 1.5 mM AZO-C6. Switching on the blue irradiation, brings the particle more closer than before and with each successive period of irradiation, particles come more closer to form tight clusters **(**the effect is shown in **Figure B.5.4).** The reason for this could be that under UV light particles are not completely filled with *trans* molecules (only 0.05 mM *trans* molecules are present), so whenever blue light is applied more *trans* molecules are created which diffuses into the particle to form aggregates. With each successive irradiation the particle comes closer resulting in a further decrease in NPD.

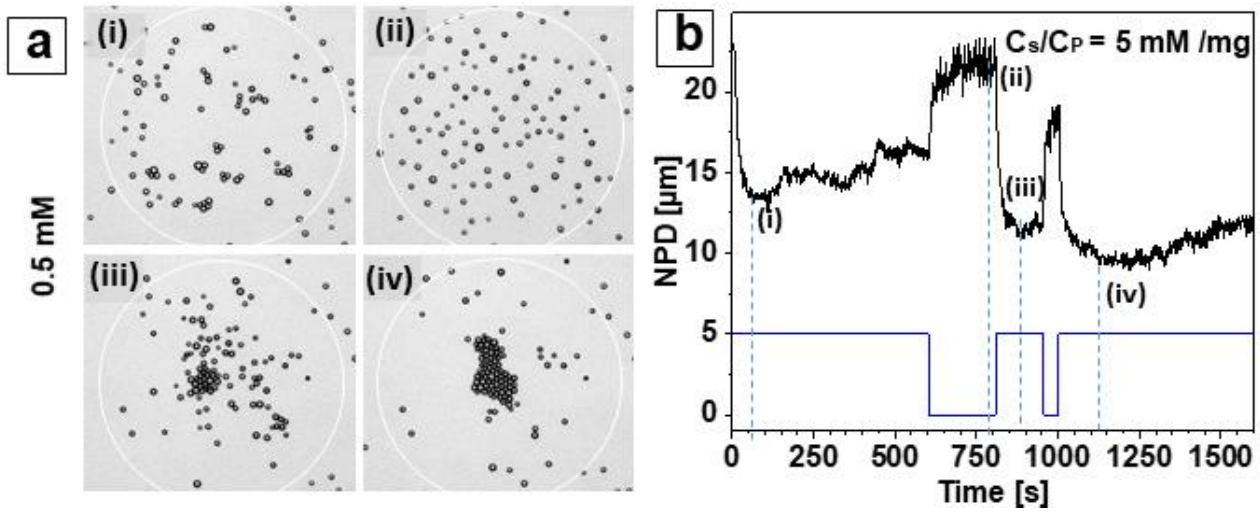

Figure B.5.4. (a) Optical micrograph representing the static images of mesoporous silica particles in 0.5 mM-Azo-C6 on glass substrate under pulse irradiation of focused UV irradiation (position of i, ii, iii and iv is shown in plot of b). (b) corresponding NPD vs time plot. Corresponding video can be found in **Figure SB.5.4** in Appendix D.

B.6. Tranportation of 2D crystalline disk

Once the particles are trapped into confined geometry induced by light driven diffusioosmotic flow using global UV and focused blue irradiation, The resulting pattern of so called micromotors can be moved in a controlled manner by moving the applied focused laser or microscope table. Shifting laser spot induces a new LDDO flow at a new position which drives the particles towards it and creating a similar 2D separated crystal pattern around the center of irradiation spot without losing its originality.

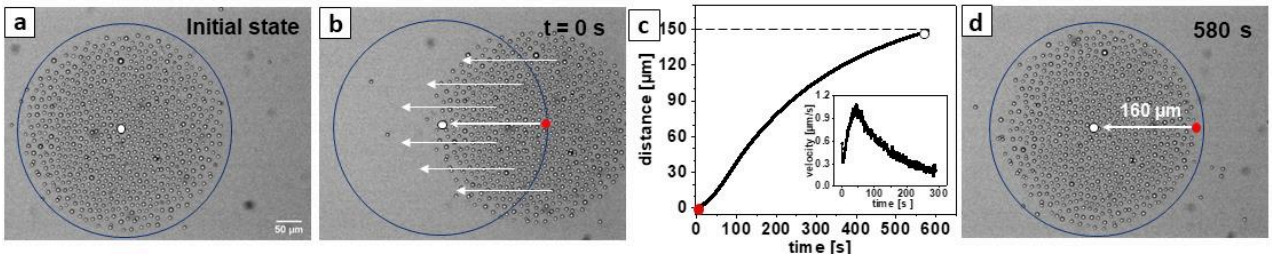

Figure B.6.1. Transportation of well separated cluster of mesoporous silica particles presented in 1 mM-Azo-C6 on glass surface. (a) initial state (b) t = 0, when microscope table is moved 150 µm away from the laser center(white spot). Blue outline is laser boundary.(c) average displacement of the particles with respect to time. Inset shows the velocity profile. (d) final state at t= 580s. Corresponding video can be found in **Figure SB.6.1** in Appendix D.

Figure B.6.1 illustrates such a controlled and reversible movement of mesoporous swarms between two positions by shifting the microscope table to 150 µm (red mark) away from its initial position (white mark). The laser spot is still at the same place represented as a blue circle in the figure. Notice that the separation between the particle after shifting does not change. The new LDDO flow corresponding to irradiated area carries all the particles towards the spot. It has been analyzed that each particles travel approx. Similar distance which is equal to applied shift. The average distance of the particles with respect to time is shown in **Figure B.6.1c**. This capability to switch the swarm location without losing its original form could be an important feature for multiple applications in medicine or cargo transport. For instance, firstly collecting the required micro-motors from the desired area using global UV and focused irradiation and then translocating them to the targeted region by moving the focused blue light and finally releasing the particles by applying global blue light to perform the desire function.

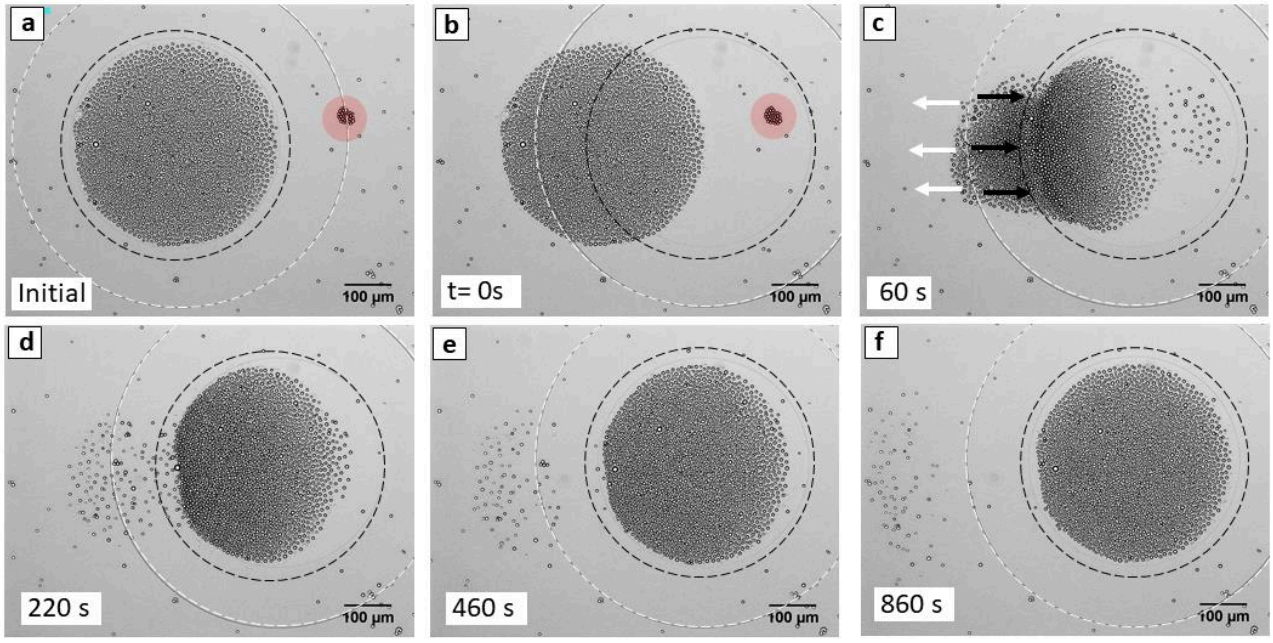

Figure B.6.2. Optical micrograph representing the static images of the process of transportation of cluster of mesoporous silica particles in 1 mM –Azo-C6 on glass surface at different time scale. (a) initial state, (b) at t=0, when microscope stable is moved to left. dashed circular lines denotes the laser boundary (in black) and so called imaginary boundary (in white).(c) at t = 60s, (d) 220s, (e) 460s, and (f) 860s. Particle outside imaginary boundary moves away where as which are inside the boundary moves towards the irradiation center. Black arrow and white arrow shows the direction of the motion. Corresponding video can be found in **Figure SB.6.2** in Appendix D.

Upon shifting the laser spot, the second flow, which moves the particle away from the imaginary boundary also shifts but the distance between laser boundary and imaginary boundary remains constant. This means the maximum shifting distance of laser spot is equal to distance between imaginary boundary and laser boundary. Moving laser spot to larger distance (i.e. larger than D_{Img} - D_{laser}) will result in loosing particle which are outside D_{Img}. To exemplifying it optical micrograph showing motion of 2D pattern cluster at different time is presented in **Figure B.6.2** where distance moved is greater than D_{Img} - D_{laser}. Initially pattern is formed applying simultaneous irradiation of global UV and focused blue light. Laser boundary and Imaginary boundary is marked in black dashed line and white dashed line respectively. Small cluster marked in red got trapped at origin (at imaginary boundary) of two opposite flows. In the **video provided** its very nicely visible that particles inside the boundary are going towards the irradiated area and particles on the other side of it are moving away from it. Now when laser spot is moved with distance d > D_{Img} - D_{laser}, particle which are with in the approach or which are inside the imaginary boundary are again trapped in to laser spot where as particles which were outside moves in other direction away from it leaving behind the cluster. The understanding of these two outer flows is still under investigation but one can say already that the above mentioned feature of the process could show many practical applications. For instance, the whole system acts like a giant ball which allows only certain things to enter and cleans away all the unwanted region which is outside the boundary. All the required videos representing this application is provided in **Figure SB.6.2** in Appendix D**.**

B.7. Effect of spacer height

In previous experiments, we have always used a closed chamber with a spacer height of 920 µm. In this section, we will discuss about the dependency of chamber thickness on the generated LDDO flow. So far we know that when we apply global UV light and focused blue irradiation simultaneously, two flows in opposite direction generates. One flow drives the particle towards the irradiated area and the other moves particles away from it and originates from the imaginary boundary stated in previous sections.

We have observed that decreasing the spacer height to 500 µm, or to 320 µm, or to 250 µm strongly alters the range of outer flow (flow away from the boundary). In case of lower spacer height, the outer flow will stop after a certain distance of the imaginary boundary. Whereas in case of larger

height of 920 µm, this saturation of the flow is not observed (atleast with in our filed of view). **Figure B.7.1a-c** show the optical micrographs for three samples consist of mesoporous silica particles and 1mM Azo-C6 on a glass surface with different spacer height after 47 min of exposure.

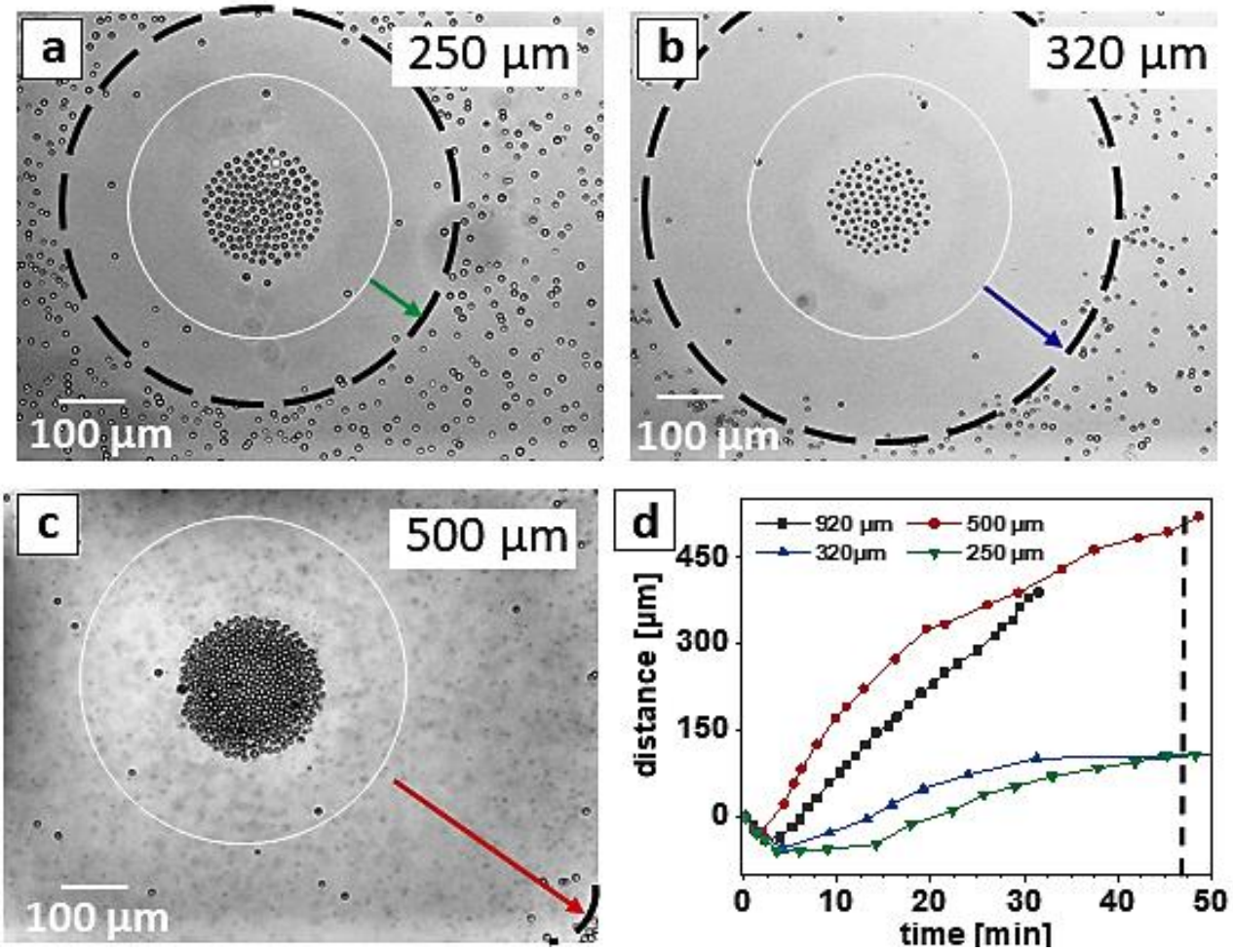

Figure B.7.1. Static images after 48 minutes irradiation of global UV light and focused blue light for different spacer height. (a) h= 250 µm, (b) h= 320 µm, (c) h= 500 µm. The white circular line is representing the so called imaginary boundary formed in the process. Black dashed circle is denoting the boundary of the saturation area. Arrow is the distance between two boundaries. (d) distance is shown against time for different spacer height. Corresponding videos can be found in **Figure SB.7.1** in Appendix D.

(250 µm, 320 µm, and 500 µm). Each static image is correspondence to t = 48 min of irradiation. White circle represents the so-called imaginary boundary from where particles start moving away. Black dashed circle represents boundary of the saturation area. Cleaning area increases with increasing spacer height. Distance of boundary of saturation area to imaginary boundary is plotted

against time and shown in **Figure B.7.1d**. The inner flow where particles move towards the spot shows no significant change. Corresponding videos are provided in **Figure SB.7.1**.

The understanding of this effect is still under consideration. One possibility for this dependence could be that the flow introduced on the top slide (coverslip) also interacts with the flow induced at the bottom surface and this becomes stronger when spacer height is less.

B.8. Visualization of LDDO flow

One of the possibilities to visualize the local light driven diffusioosmotic flow is to see the flow using an appropriate dye. An anionic dye which can form complexes with our cationic surfactant molecules is the most promising candidate for our system. Using such dyes can help us in understanding the diffusion of surfactant molecules (*trans* conformers) inside or outside the pores.

In first go, we tried to perform some measurements using fluorescein dye as it is very commonly used and easily available dye in laboratories. It has an absorption maximum at 494 nm and an emission maximum of 512 nm in water. It also has a small capacity to absorb UV light. The structure of fluorescein and its absorption spectra is shown in **Figure B.8.1**.

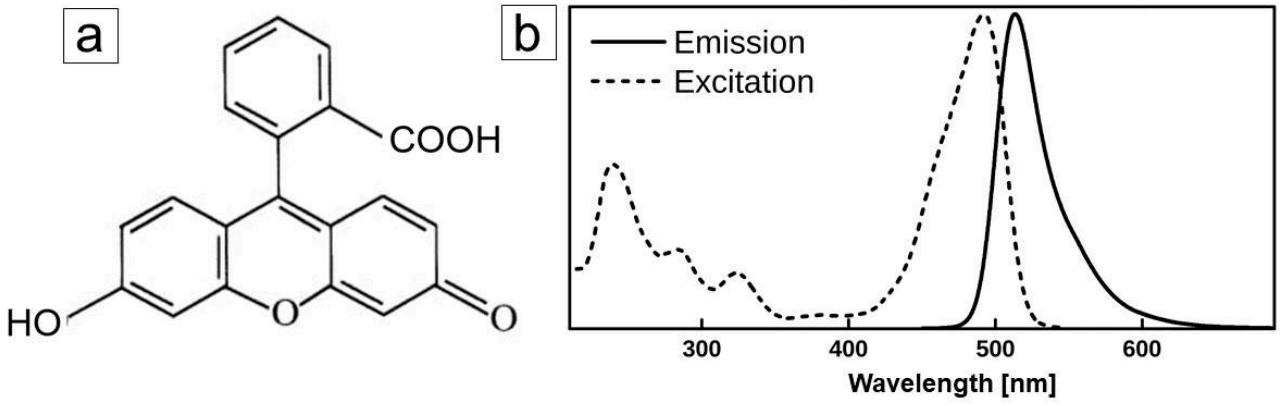

Figure B.8.1. (a) Chemical **s**tructure of fluorescein molecule. (b) Emission and excitation spectra of fluorescein in water. The excitation peak is at $\lambda = 491$ nm and the emission peak is at $\lambda = 512$ nm.

When fluorescein is added to the cationic surfactant solution, it forms a complex with the surfactant molecules. A bathochromic shift (red shift) of absorption maximum was observed with increase in the concentration of surfactant molecules which becomes constant after critical micelle

concentration is reached (0.5mM). Absorption spectra of Azo-C6 solution for different surfactant concentration with 0.05 mM concentration of fluorescein is represented in **Figure B.8.2**.

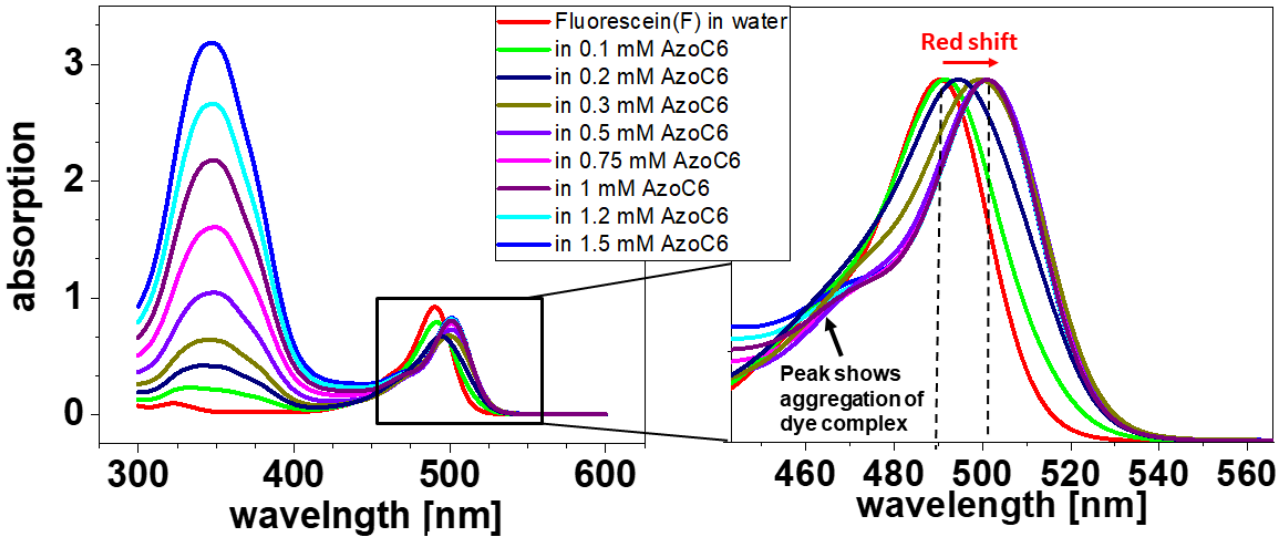

Figure B.8.2. UV-Vis absorption spectra of surfactant-dye solution at different concentration of Azo-C6 and fixed concentration of fluorescein. Inset shows the zoom in plot in the wavelength range of 440 nm to 560 nm. Maximum peak shifts to right with an increase in surfactant concentration.

According to our model of local LDDO flow, we know that when surfactant molecules are in *trans* states it diffuses into the pores of mesoporous silica particles, while in the *cis* state, it is expelled out of the particles. This means when porous particles are dispersed into a solution of surfactant and fluorescein, one can assume that the complex of *trans* molecules with fluorescein dye can also diffuses into the pores of the particle which when exposed to blue light show emission in green range and particle will glow due to presence of dye into it (see **Figure B.8.3b**). We have checked it that porous particle will not show any such emission without surfactant molecules (**Figure B.8.3a**). We tried to measure the diffusion time of *trans* molecules going into the particle by correlating it to an increase in the intensity of shiny particle. To do so, at first, porous particle was sticked on the glass surface. Then, a fresh solution containing 1 mM surfactant and 0.2 µM of fluorescein was added to the sample. Once added immediately the blue light was switched on. At t=0, the particle was not glowing, but with time the intensity inside the particle increases, indicating that the dye complex is slowly entering into the pores. Static images at t= 0 s, 5 min, 15 min, 30 min, and 40 min are shown in **Figure B.8.3c**.

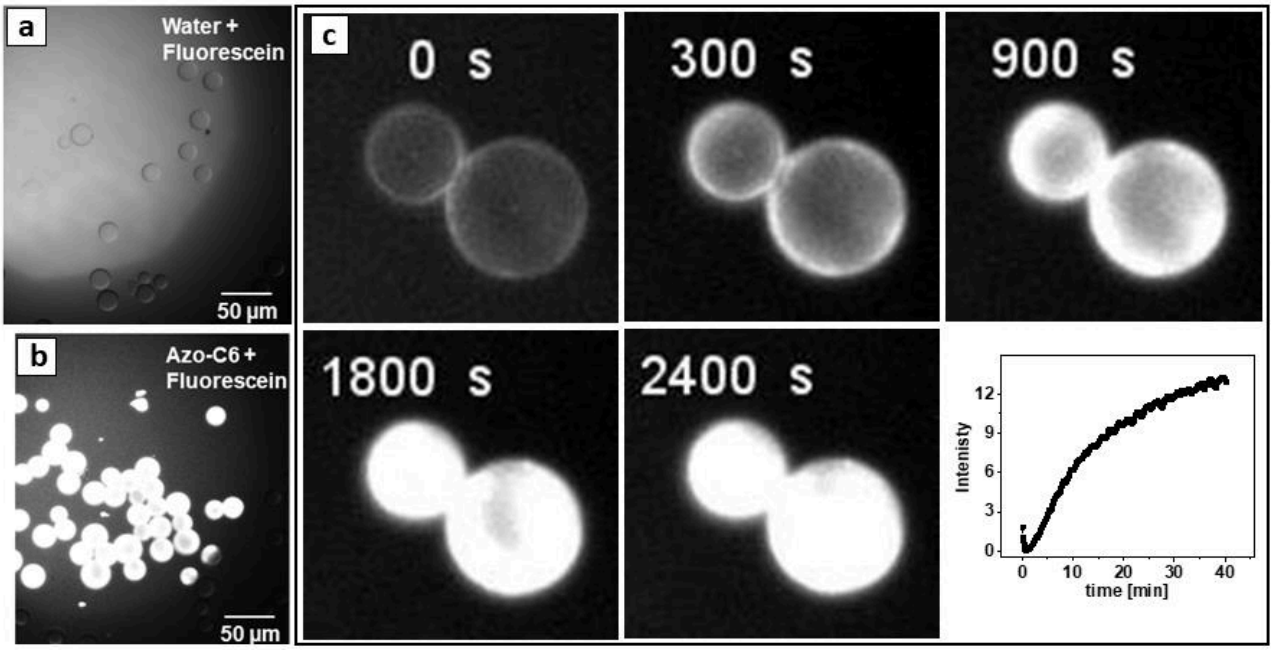

Figure B.8.3. (a) Porous silica particle (d = 5 µm) in fluorescein solution. (b) in solution of 1mM Azo-C6 and 0.2 µM of fluorescein. Particle glows in the latter case. (c) optical images of porous silica particles in a solution of 1mM Azo-C6 and fluorescein under blue (λ = 491 nm) irradiation at different time scale: 0 s, 300 s, 900 s, 1800 s, and 2400 s. The plot represents the change in intensity with respect to time under blue light irradiation. Corresponding video can be found in **Figure SB.8.3** in Appendix D.

When the colloidal particles are non-porous, it is not possible for surfactant molecules to enter inside its volume and hence non-porous particles do not glow. This means, adding dye molecules also helps in studying the system consisting of porous and non-porous silica particles together. Upon blue irradiation, porous particles will glow whereas non-porous particles appear darker. One example of such a system is shown in **Figure B.8.4**, where a mixture of 5 µm porous silica particles and 5 µm non-porous silica particles were dispersed in 1 mM Azo-c6 and 0.2 µM fluorescein solution. The sample was exposed to global UV irradiation from the top and with a focused blue laser (491 nm) from the objective. The optical micrograph of the process at different time scale is shown in **Figure B.8.4**. Porous particles which are already inside the irradiation spot and which are entering into this area glow immediately upon switching on blue light. And there is no change in the appearance of non-porous particles. It has been observed that the intensity of porous particles reduces with time (see **Figure B.8.4c**). One reason of reducing intensity is bleaching of fluorescein dye. This is well known that fluorescein bleaches faster than other dyes [refer]. In addition to bleaching, we should also consider the effect of induced LDDO flow.

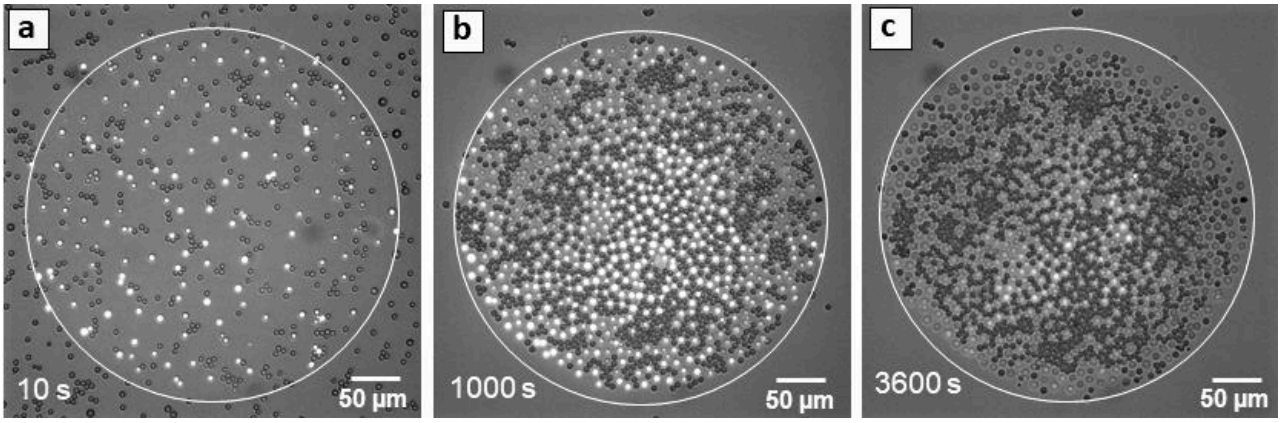

Figure B.8.4. Optical micrograph representing the monolayer of mixture of porous and non-porous silica particles dispersed in a solution of 1mM Azo-C6 and fluorescein dye. The sample is exposed to focused blue and global UV light. Static images of the motion is shown at different time scale, (a) at t= 0 s, (b) at t= 1000 s and (c) at t= 3600 s. Inside the irradiation spot, porous particle appears brighter whereas non-porous particles are in dark colour. Intensity of porous particle is fading down with time. Corresponding video can be found in **Figure SB.8.4** in Appendix D.

To understand this effect, we have studied the variation in intensity profile for different surfactant concentrations on a glass substrate without dispersing any particles. A Fixed amount of fluorescein was added in to different surfactant concentrations ranging from 0.1 mM to 1.5 mM. The Sample was irradiated to focused blue light of diameter 350 µm from the objective (shape of the laser beam is hexagon (see **Figure B.8.5i**). Without surfactant, the intensity of emitted wavelength decreases due to photobleaching behaviour of fluorescein[142,143] (See **Figure B.8.5a**). For concentrations of 0.1 mM and 0.2 mM, initial increase in intensity is observed for few seconds, after that intensity drops to 60 percent for 0.1 mM. Whereas for 0.3 mM and 0.5 mM (CMC), it increases with time with different rates. On the other hand, for concentrations above CMC like 0.75 mM, 1mM, and 1.2 mM initial decrease and later increase in intensity is witnessed. The intensity vs time plot for different concentrations are shown in **Figure B.8.5(b-h)**.

Before analysing the data, it is very much important to remember few points in addition to photo bleaching: firstly, here we used blue light, under which surfactant molecules undergoes continuous reversible isomerization of *trans* and *cis* isomers. At the same time, we are using this to excite fluorescein. which emits photon of green light. Secondly, emitted green light can also be absorbed by *cis*-isomers which could be responsible for decrease in intensity. Thirdly, due to LDDO flow *cis* molecules diffuses outside and *trans* molecules enter into the irradiation spot which makes

the interpretation of the results more difficult. All these three points are important to understand the calculated data which makes the analysis very much complex and is under investigations.

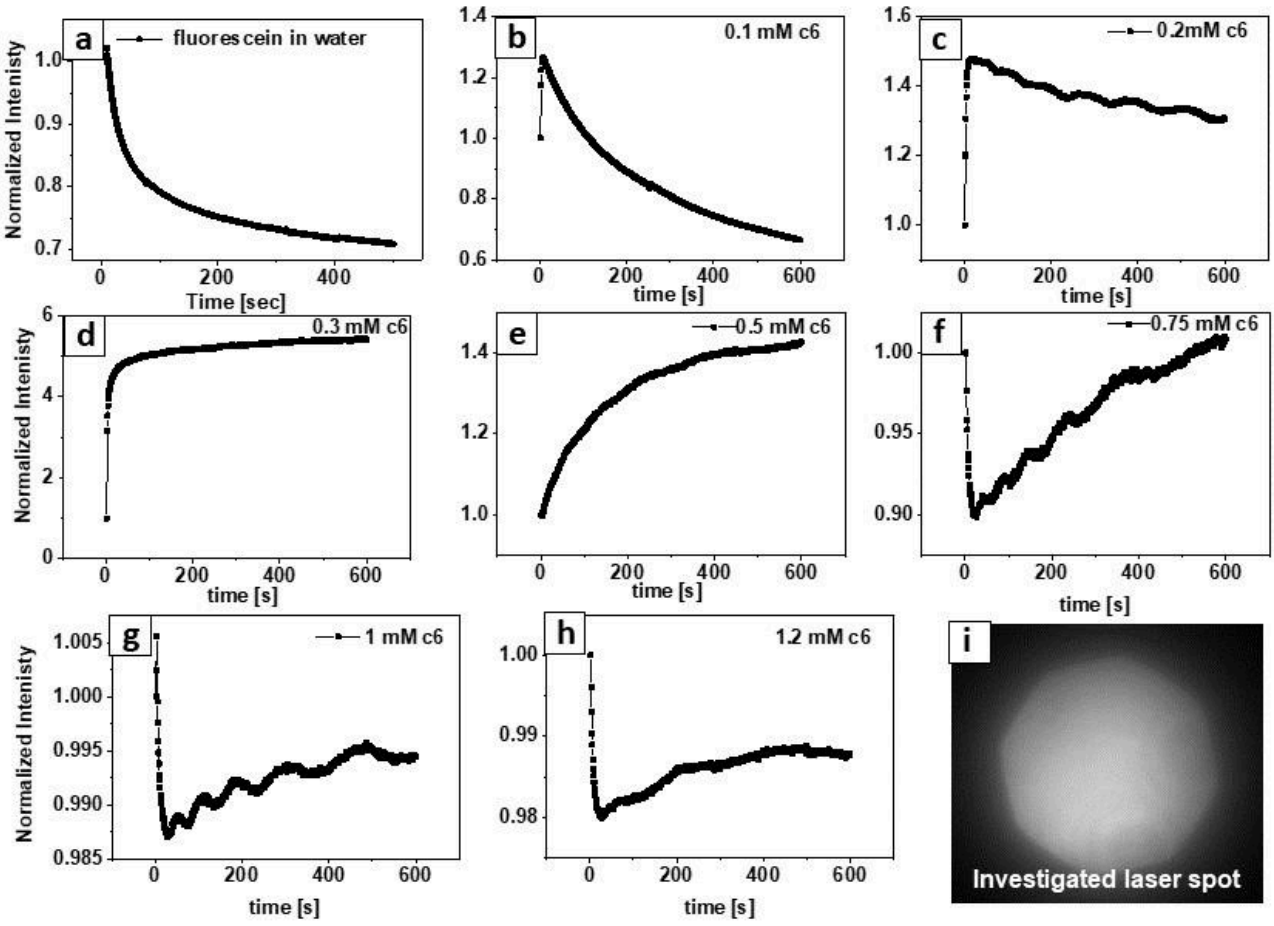

Figure B.8.5. Normalized intensity vs time plot for a fluorescein-surfactant solution with different surfactant concentration under the irradiation of focused blue light (λ= 491nm). (a) in water (b) C_s = 0.1 mM, (c) c_{azo}= 0.2 mM, (d) c_{azo} = 0.3mM, (e) c_{azo}= 0.5 mM, (f) c_{azo} = 0.75 mM, (g) c_{azo} = 1 mM, (h) c_{azo} = 1.2 mM. (i) image of irradiation spot.

In order to avoid the effect of photo isomerization we started working with another dye, (purchased from dyomic gmbh, Germany as Dy-731) which contains two sulphuric group and CN bonds. These dyes are common substituent for various systems.[144,145] For us, the positive point of this particular dye is that it excites and emit in the range of 625 nm to 680 nm. In this range our surfactant molecules are not affected which makes it best suitable dye for our visualization experiments. The chemical structure and corresponding absorption and emission spectra of the dye is shown in **Figure B.8.6**. The absorption and emission peak of the dye is in red range, where our surfactant molecules are

not affected. This means, with this dye only the effect of diffusion of *trans* and *cis* molecules will be recorded.

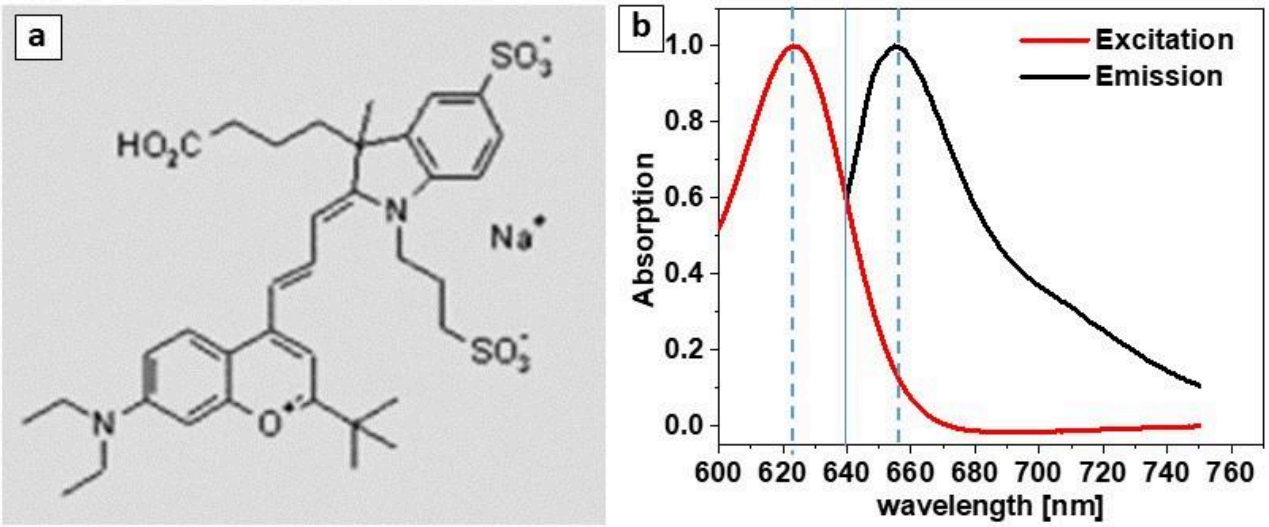

Figure B.8.6. (a) Chemical structure of sulphuric dye. (b) Excitation and emission spectra of the dye. Excitation peak is at λ = 623 nm and emission peak is at λ = 656 nm. (The figure a is taken from the Dyomics GmbH)

Appendix C. Self-propelled Motion: Transportation of cargo

We have recently reported the self-propelled motion of Porous-Janus particles under global blue light irradiation (**Publication 5**). The principle mechanism of LDDO flow was utilized in order to drive gold-capped porous particle. l-LDDO flow induced at the naked side of the particle, when particle is dispersed in the solution of azo-C6, and exposed to blue light pushes the particle in the forward direction.

In this section, we will present some preliminary results on transportation of non-porous rods (acting as a cargo) in the presence of porous silica particle on solid/liquid interface. Equal ratio of 5 µm porous silica particles and non-porous silica rods (length = 10 to 30 µm, width = 3 µm) are mixed into 1 mM surfactant solution. The sample is exposed to the global soft irradiation of blue light. Porous particles which are attached to rods perform self-propelled translational or rotational motion depending upon the position of the spherical particle to the rod particle. **Figure C.1a** shows the static images of one such sample which is exposed to blue light. Motion of three spherod (porous sphere attached to non-porous rod) particles (marked in red, green and blue) is recorded after blue light is switched on. It is observed that motion is highly dependent upon the position of the sphere with respect to the rod particle. The trajectories of the motion of particles after 30 min of irradiation is shown in **Figure C.1b**. The corresponding displacement vs time plot is shown in **Figure C.1c**. In this system of spherod particles, porous particle plays the role of a driver who utilized the fuel of photoactive surfactant molecule in order to generate l-LDDO flow radially outwards. The symmetry of the flow breaks due to the presence of rod particles itself which pushes the non-porous rods forward.

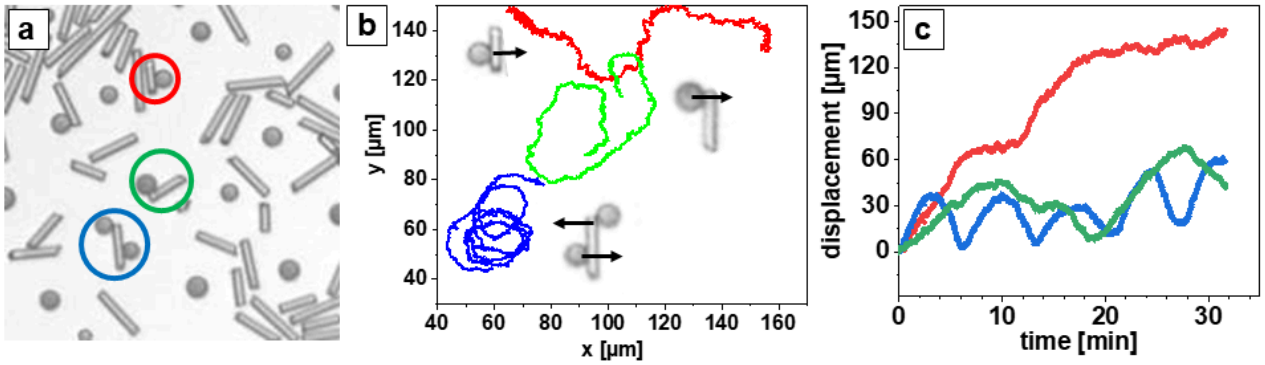

Figure C.1. (a) Optical image of the sample consist of porous and non-porous particles in 1 mM surfactant concentration. Some non-porous and porous particle fused together to form single entity (marked in red, green and blue circles). (b) Trajectories of the motion of marked particles after 30

minutes of global blue irradiation. (c) displacement vs time plot of marked particles. T=0 is considered as initial position of particle. Corresponding video can be found in **Figure SC.1** in Appendix D

When the porous sphere is attached at the extreme end of rod particle (as shown in **Figure C.2a**), motion is super diffusive in the direction of the loose end of the rod. The trajectory of the motion after 20 minutes of irradiation is shown in **Figure C.2b.** MSD plot indicates the super diffusive nature of the motion shown in **Figure C.2c**. The motion of spherod particle is similar to the motion of Porous-Janus particle reported in **Publication 5**. Before we covered the half hemisphere from gold metal layer to block the pores, whereas now non-porous particle attached to porous colloid is doing this job of blocking the pores from one side.

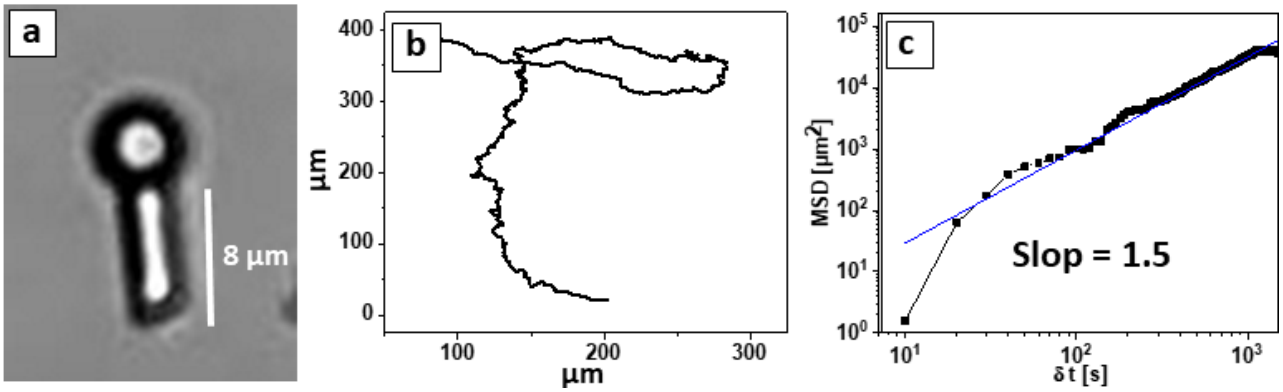

Figure C.2. (a) Optical image of spherod (porous sphere +non-porous rod) particle. (b) trajectory of particle under 20 minutes of blue light irradiation. (c) Corresponding mean square displacement (MSD) plot of the motion. Corresponding video can be found in **Figure SC.2** in Appendix D.

In the case where, sphere is connected almost at the middle of the rod (see **Figure C.3a**), l-LDDO flow is induced at one side of the sphere which exerts a net force at the center of mass of the rod driving it forward (scheme in **Figure C.3b**). The optical micrographs of one such motion at different time scale: t = 0 min, 4 min, 10 min, and 16 min is shown in **Figure C.3c**. It is noticed that another sphere marked in red and our spherod particle follows the same trajectory until t = 10 min. Afterwards, red sphere stays behind and another similar sphere join the race (shown in green circles). It is possible that two individual flows produced by two spheres (sphere on the rod, and red marked sphere) couples together in order to move together but get disturbed due to rotation and induces again when another sphere ties up a similar condition like at t=0.

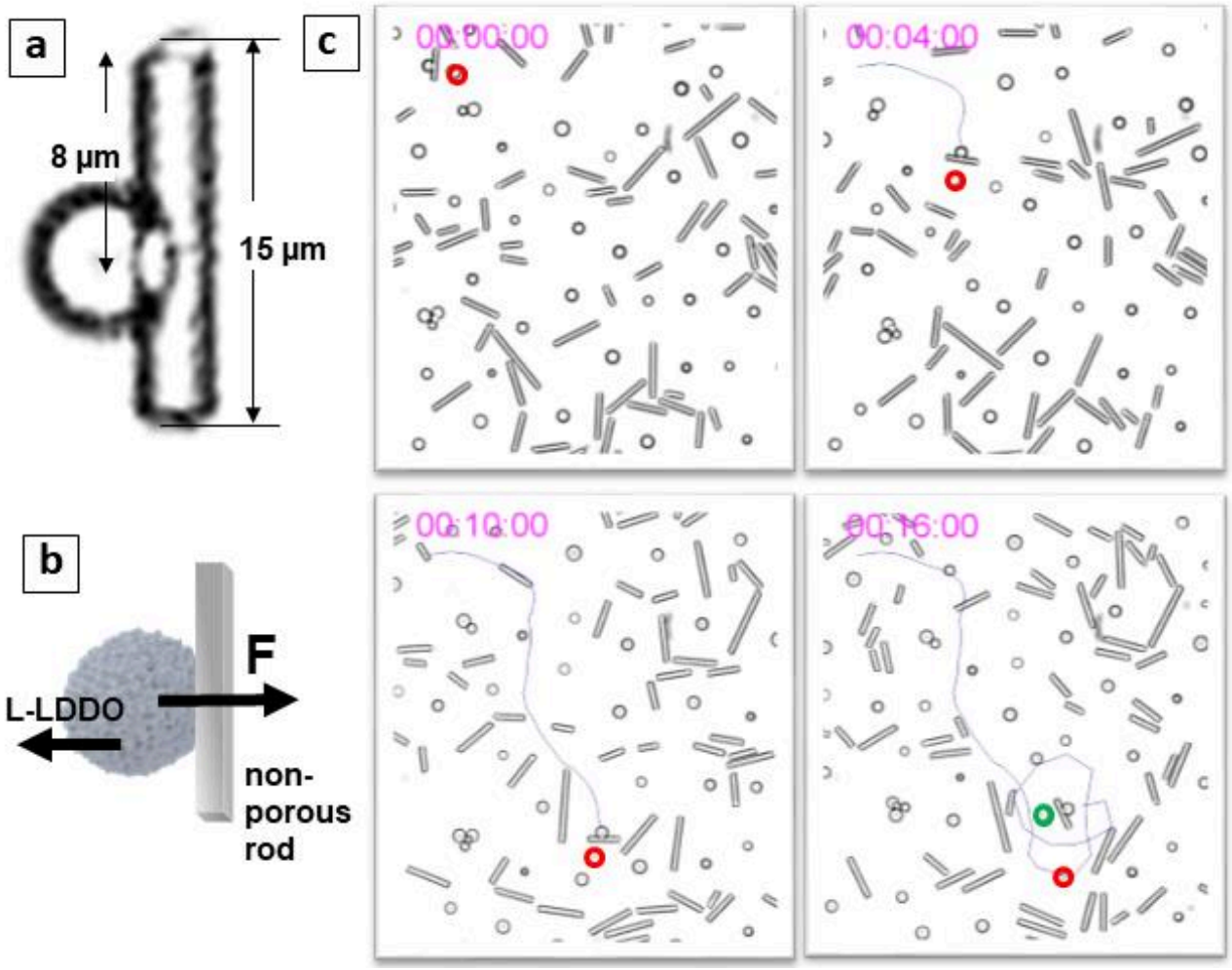

Figure C.3. (a) Optical image of Spherod particle. Porous sphere is attached at the centre of the rod. (b) Scheme of the porous-rod particle. Under blue irradiation l-LDDO flow is generated at the open side of particle which pushes the particle in the direction of rod. (c) Optical images of the motion of particle under soft blue irradiation at different time scale: o min, 4min, 10 min, and 16 min. Corresponding video can be found in **Figure SC.3** in Appendix D.

Both rotational and translational motion have been witnessed when the position of the sphere is shifted from the center of the rod particle. The translational and rotational velocity depends upon the distance of the position of net force from the center of mass. For instance, in **Figure C.4a**, sphere is joined 6 µm way from the center of mass of the rod, this exert a force which applies torque resulting in a rotational motion with an angular velocity of 0.5 rounds per minute. The corresponding displacement and MSD plot of the motion with respect to the initial position is also shown in **Figure C.4ii and iii**.

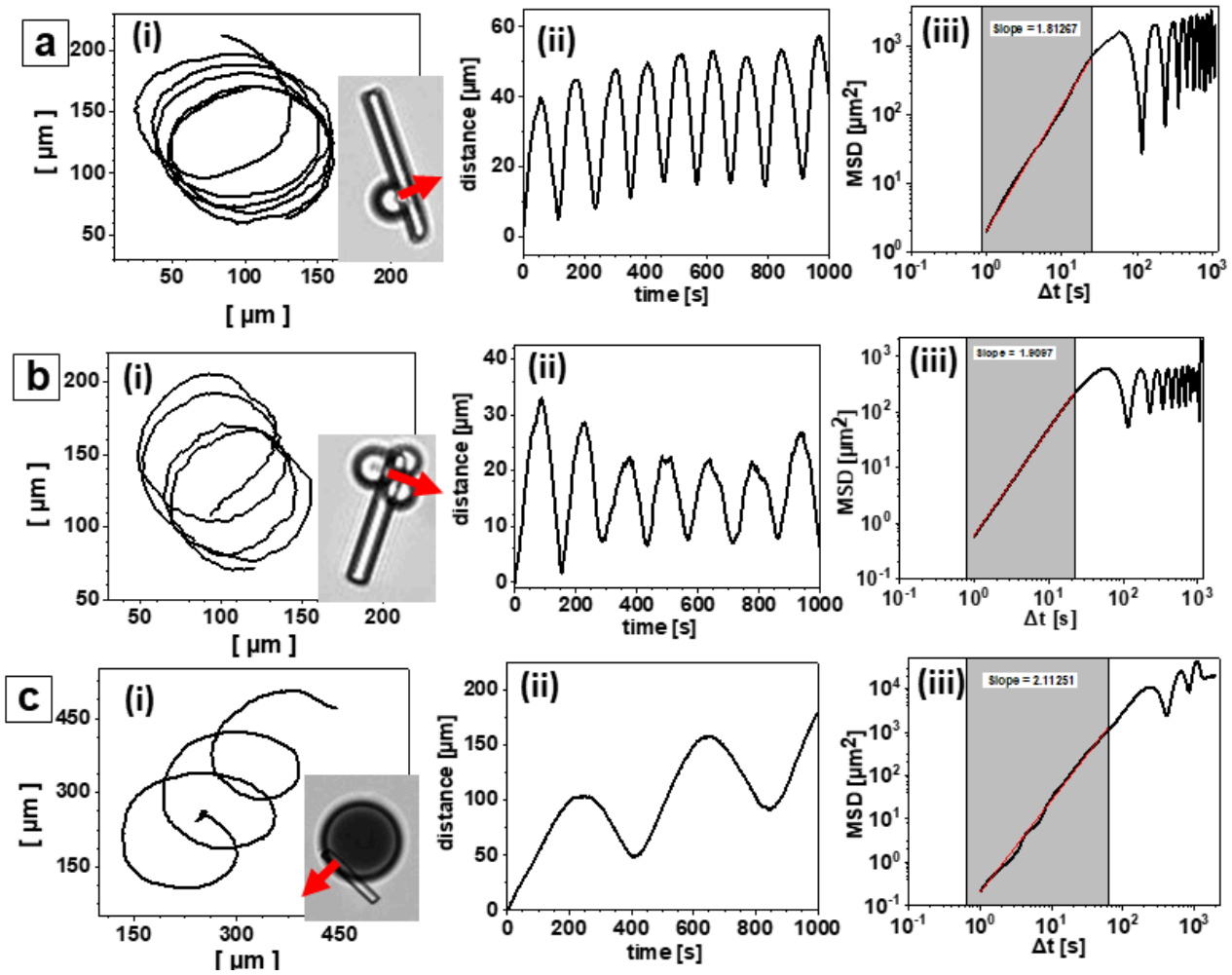

Figure C.4. Trajectory of motion, displacement and MSD plot of different type of spherod particle. (a) when porous particle attached towards the end of the rod. (b) When three particles attached at the end. (c) when ratio of particle size and length of rod is smaller (20 µm porous particle is taken). Corresponding video can be found in **Figure SC.4** in Appendix D.

When two or more particles are attached to the rod, the net total force from spheres will decide the direction of the motion. One such illustration is shown in **Figure C.4b;** where two more spheres are attached to the rod. In this case, the spheres attached to the top of the rod, therefore, do not contribute to the net force acting on the rod. It means only the force excreted by a single sphere on the surface moves the rod forwards. We can see this from figure **Figure C.4b**, that even though the number of particles attached to the rod is different there is no significant difference in the motion, only the angular frequency reduces to 0.4 rpm. In case of the smaller aspect ratio of the rod as compared to the particle, the translational motion becomes stronger and 2 dimensional helical trajectories with the time period of 400 s is witnessed (**Figure C.4c**).

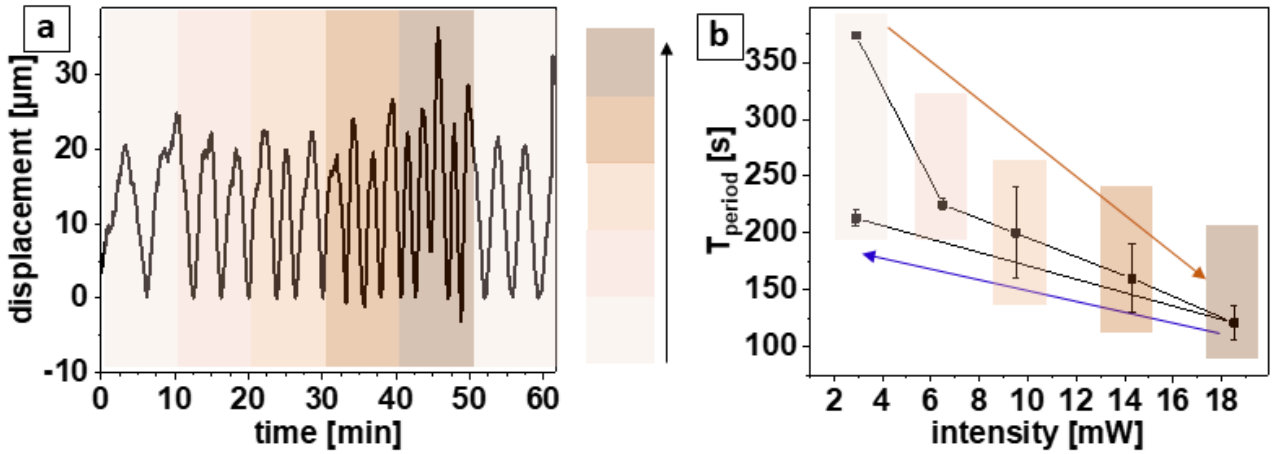

Figure C.5. (a) Displacement vs time plot. Intensity of blue light irradiation is increased in every 10 min. larger intensity has darker color. (b) The time period against of motion against intensity. Time period is time taken to complete one rotation.

The time period of circular motion as a function of intensity is calculated and shown in **Figure C.5b** for spherod particle of 5 µm sphere attached to the end of the rod of length 10 µm. It is observed that the time time required for one complete rotation decreases with increasing intensity. Displacement vs time plot is shown in **Figure C.5a**. for different intensities of blue light , which is increasing after every 10 min to larger. When intensity of blue light is reduced back to initial (from 18 mW to 2.9 mW), the time period for one rotation increases. This time period is smaller as compared to the one at the starting of the experiment. We have to keep in mind that the intensities are varied in the same experiments. This means that the previous history of the system plays an important part in the motion of particle. Further investigations are under process in order to understand the above mentioned behavior.

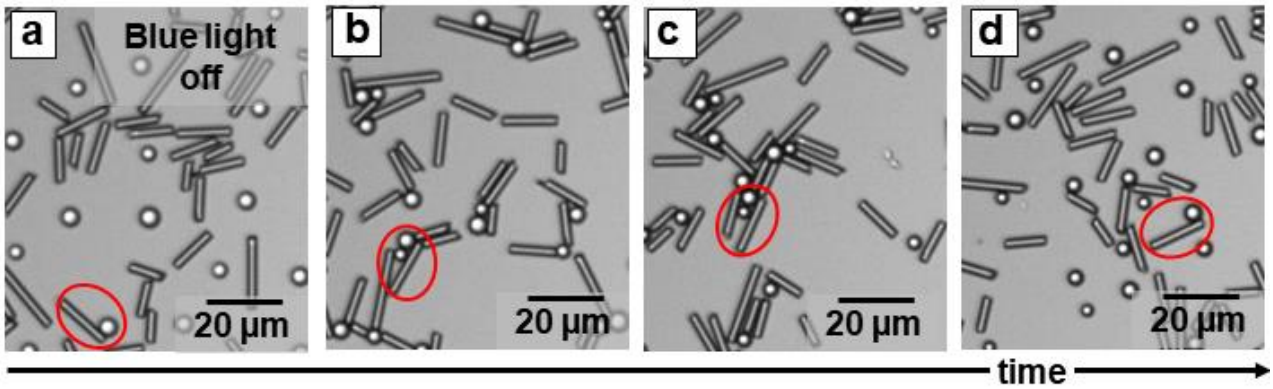

Figure C.6. Ensemble of porous and non-porous particles just after blue light is switched off. (a) at t= 0s. (b-d) optical image in different times. Particle marked in red is spherod particle. The orresponding video can be found in **Figure SC.6** in Appendix D.

When the blue light is switched off, porous particle tends to aggregate. The inward flow also carries non-porous rods in the aggregates. These clusters disaggregate with time and all particles continue doing random Brownian motion. **Figure C.6** represents static images of this effect for different times when blue light is switched off at t = 0 in **Figure C.6a**.

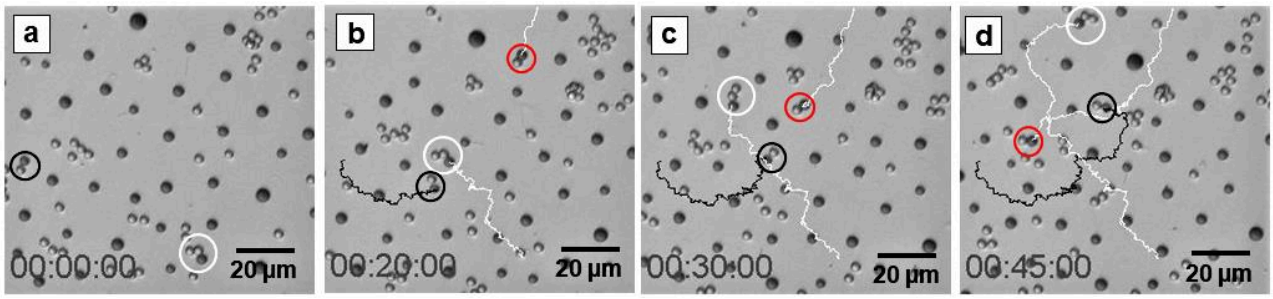

Figure C.7. Ensemble of porous and non-porous silica particles in 1 mM Azo-C6. Trajectories of motion of Porous-non-porous particles (marked in red, black and white circles) are shown through white and black lines at different time scale: (a) t= 0min, (b) 20 min, (c) 30 min, and (d) 45 min. Corresponding video can be found in **Figure SC.7** in Appendix D.

When a non-porous sphere is used instead of a rod particle, similar behavior i.e. self-propelled motion of the particle is witnessed. **Figure C.7** shows the static images of the motion at different times (0 min, 20 min, 30 min, and 45 min) of global blue irradiation. Porous particles appear darker than non-porous particles due to the presence of surfactant molecules into the pores. Porous particles which are not attached to non-porous spheres are well separated in the system due to generation of l-LDDO flow in each particle. Whereas non-porous particles (lighter one) are randomly distributed. Particle marked in white has two non-porous particles attached to one porous particle. Two sphere are flexible in movement and look as if it is a flagellum of a bacteria (video is provided in supporting information).

Fluorescein dyes are used in order to differentiate between porous and non-porous particles. Only porous particle will glow under blue laser. One such illustration with fluorescein dye is shown in **Figure C.8**. Due to focused blue irradiation, global LDDO flow generates which moves the particles which are inside the spot to outside its boundary (flow direction is marked by grey arrow). Indeed, this is the case for all the particles shown in **Figure C.8** except the particles marked in white, black and red circles (porous-non-porous particle). The marked particles in fact stay in the blue irradiated area and perform self-propelled motion against the flow. The trajectories of the

motion of these three particles are shown by black and white for the different time scale of blue light irradiation (0min, 10 min, 20 min and 30min).

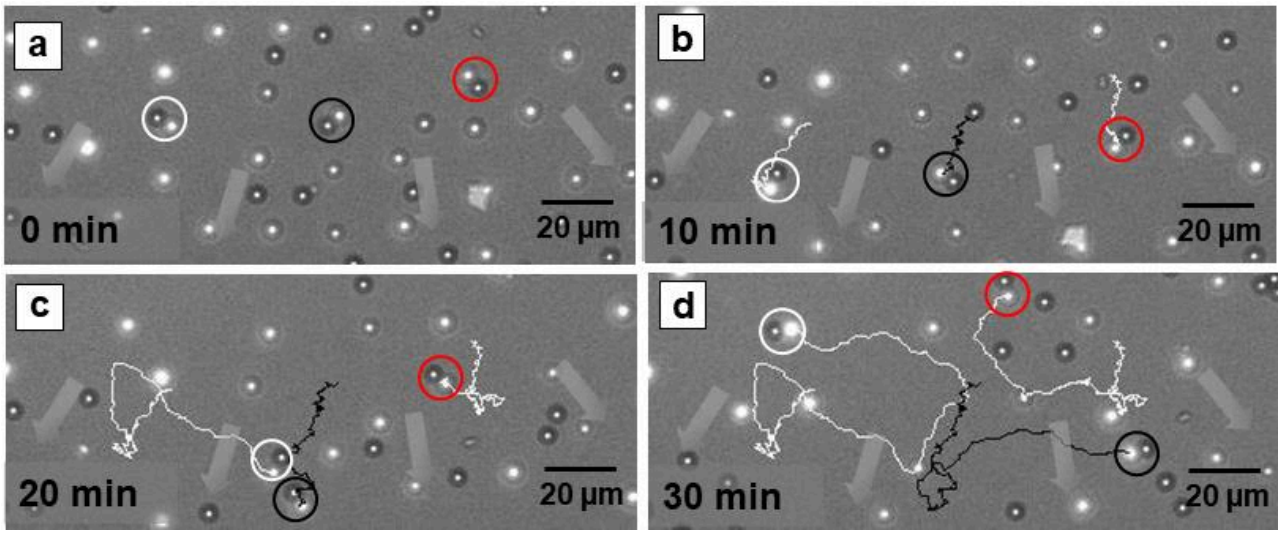

Figure C.8. Ensemble of porous and non-porous silica particles in 1 mM Azo-C6 and 0.2 µM fluorescein solution under focused irradiation of blue laser. Trajectories of motion of Porous-non-porous particles (marked in red, black and white circles) are shown through white and black lines at different time scale: (a) t= 0min, (b) 10 min, (c) 20 min, and (d) 30 min. The gray arrow shows the direction of LDDO flow which drives particle along except the marked particle. Corresponding video can be found in **Figure SC.8** in Appendix D.

Appendix D. Supporting Videos

(All the videos are presented in Appendix D-Supporting videos. pptx)

Chapter 2: Theoretical and experimental basis

Figure S2.9. Videos representing the motion of 5 μm non porous silica particles under focused irradiation of: (a) focused UV laser (diameter = 20 μm), (b) focused green laser (diameter = 20 μm), sample was initially exposed to global UV irradiation for 5 min.

Publication 2

Figure S1. Motion of mesoporous silica particles under global blue and red irradiation. Red light is used to see the effect in dark.

Figure S2. Aggregation and separation of 5 μm porous silica particles. When blue light is on, particles separate. Whereas upon switching of irradiation particles tend to aggregate.

Figure S3. Video representing the motion of mesoporous silica particles (d = 5 μm) in 1mM surfactant concentration under blue light irradiation for different particle concentration. (a) 0.005 mg/ml, (b) 0.01 mg/ml, (c) 0.05 mg/ml, (d) 0.1mg/ml (e) 0.5 mg/ml

Figure S4. Effect of ionic strength upon l-LDDO flow. Video representing the motion of mesoporous silica particles (d = 5 μm) in 1 mM surfactant concentration under irradiation of blue light for different salt (NaBr) concentration. (a) 0.1 mM NaBr, (b) 0.5 mM NaBr, (c) 1 mM NaBr, (d) 2 mM NaBr (e) 5 mM NaBr (f) 10 mM NaBr

Figure S5. Video showing the binary mixture of porous (5 μm) and non-porous (500 nm) silica particles under blue and red light irradiation. Non-porous particles were used as a tracer particle representing the generated l-LDDO flow when blue light is switched on.

Figure S6. Effect of wavelength of light. Video showing the motion of mesoporous silica particles under exposure to UV light. In UV light l-LDDO flow generated is disappearing after photo stationary state is reached. Hence the separation of particle is not stable and particles come closer due to thermal motion.

Figure S7. Range of l-LDDO flow. Video showing the binary mixture of porous silica particle surrounded by non-porous silica particles in 1mM surfactant concentration. Under blue light irradiation porous particle induces l-LDDO flow and non-porous silica particles moves passively with the flow radially away from particles. Saturation of cleaning area is the indication of the maximum range of the flow.

Publication 3

Figure S3. Videos representing the motion of mesoporous silica particles (d = 5 μm) in 1mM surfactant concentration under different intensities of UV light irradiation (fixed particle concentration). (b) 42 $\mu W/cm^2$, (c) 128 $\mu W/cm^2$, (d) 163 $\mu W/cm^2$, (e) 573 $\mu W/cm^2$ (f) 1.8 mW/cm^2

Figure S6. Video representing the motion of an ensemble of non-active (d= 1.5 μm) and active particles (d = 5 μm) in 1mM surfactant concentration under global UV light irradiation (I = 130 $\mu W/cm^2$).

Figure S7. Dependence on surfactant concentration. Video representing the motion of an ensemble of porous colloids (d = 5 μm) under global UV light irradiation (I = 1.4 mW/cm^2) for different surfactant concentrations: (a) 0.5 mM, (b) 1mM, (c) 2mM

Publication 4

Figure S2. Videos representing the motion of 5 μm non porous silica particles under focused irradiation of: (a) UV laser (diameter = 20 μm), (b) green laser (diameter = 20 μm), sample was initially exposed to global UV irradiation.

Figure S3. Videos representing the motion of 5 μm porous silica particles in 1mM surfactant concentration under continuous exposure of two different wavelengths: (a) global blue irradiation, Separation between particle is stable (b) global UV irradiation, separation between particles is unstable.

Figure S4. Videos representing aggregation of porous silica particle after blue irradiation is switched off.

Figure S6. (a-d) Motion of mesoporous silica particles under simultaneous irradiation of global UV irradiation and focused blue irradiation. (e-i) Focused blue light is switched off (UV is continuously on) and switched on after 115 s.

Figure S6 (cont.). Video representing oscillations of collective motions under pulse irradiation of focused blue light and continuous irradiation of global UV light.

Figure S7. Video representing the difference in collective motion for porous (active) and non-porous (non-active) particles: (a) Motion of "mesoporous" silica particles under simultaneous irradiation of global UV irradiation and focused blue irradiation. (b) Motion of "non-porous" silica particles under simultaneous irradiation of global UV irradiation and focused blue irradiation

Publication 5

Figure S2. Video representing the motion of Porous-Janus particles under red light irradiation (left side) and under blue light irradiation (right side)

Figure S3. Videos represent the motion of different Porous Janus particles whose trajectories are mentioned in *Figure 3* in the paper.

Figure S4. Videos show the motion of dimer Porous-Janus particles with different orientation of metal layer. (a) one particle completely covered with gold and other is half covered (particle is fixed on the surface), (b) Gold cap of two Janus particles are pointing in opposite directions, (c) gold cap of two particles are in parallel alignment

Figure S5. Video of self-propelled motion of single Porous-Janus particle on surface relief grating of height 1 μm and periodicity of 4 μm (b) Motion of dimer particle

Appendix A

Figure SA.2. Motion of non-porous silica particle under focused UV irradiation with fixed spot size (radius = 240 μm) and different intensities; for I = 1.2 mW/cm^2 (left video) and I = 36mW/cm^2 (right video)

Figure SA.5. Effect of continuous irradiation of focused UV (diameter = 20 μm) and global blue light upon an ensemble of porous silica particle in 1 mM Azo-C6.

Appendix B

Figure SB.1.1. Video representing motion of mesoporous silica particles under simultaneous irradiation of global UV and focused blue irradiation for different surfactant concentrations: (a) for 0.5 mM, (b) 1 mM, (c) 1.5 mM.

Figure SB.2.1. Video showing complete picture of particle motion under simultaneous irradiation of global UV and focused blue light. Two flows in opposite direction is witnessed. Thin white line represent the laser boundary and thick white line represents the imaginary boundary.

Figure SB.3.1. Video showing motion of mesoporous silica particles under simultaneous irradiation of global UV and focused blue light for different laser size. (a) for laser radius: 70 μm, (b) for 125 μm, (c) for 150 μm, and (d) for 230 μm. The intensities of both UV and blue irradiation is kept constant for all the measurements.

Figure SB.3.2. Videos showing difference between two systems. (a) focused green irradiation (b) simultaneous irradiation between global UV and focused blue light. Latter system is approx. 4 time faster and selective as compare to first one.

Figure SB.4.1. Videos representing motion of porous silica particles on glass surface in 1mM Azo-C6 under simultaneous irradiation of global UV (intensity = 1.4 mW/cm^2) and different intensities of focused blue (radius = 190 μm) irradiation: (a) for power = 7.5 μW, (b) 28 μW, (c) 57 μW and, (d) 132 μW

Figure SB.4.2. Effect of intensity of UV light. Videos representing motion of porous silica particles on glass surface in 1mM Azo-C6 under simultaneous irradiation of focused blue (radius = 110 μm and power = 80 μW) and global UV with varying intensities: (a) 42 μW/cm^2, (b) 128 μW/cm^2, (c) 163 μW/cm^2 and, (d) 1.8 μW/cm^2

Figure SB.4.3. Video shows the motion of mesoporous silica particles presented in 1mM Azo-C6 on a glass surface under continuous irradiation of focused blue light combined with momentary irradiation of global UV additionally. Initially sample was exposed to global UV light for 10 min. Afterward at t= 0, focused blue light is switched on resulting in a formation of ring of particles around the boundary. When global UV is again switched on at approx. 5min, all particle moves into the blue irradiation spot. Once again switching off the UV light generate motion towards laser boundary forming ring structure.

Figure SB.5.1. Reversible swarming and separation of porous colloids. Video represents the motion of mesoporous silica particles presented in 1.5 mM Azo-C6 on a glass surface under 1 min pulse irradiation focused blue light. Global UV irradiation is continuously switched on.

Figure SB.5.3b. Video showing effect of short term irradiation of focused blue light. Blue laser is switched on for initial 10 secs later switched off.

Figure SB.5.4. Video showing effect of 1 min pulse irradiation of focused blue light for mesoporous silica particles dispersed in 0.5 mM surfactant concentration.

Figure SB.6.1. Videos showing an example of translocation of well separated cluster of mesoporous silica particles presented in 1 mM-Azo-C6 on glass surface without losing its originality.

Figure SB.6.2. Videos representing the significance of imaginary boundary. Particle cluster trapped at the imaginary boundary shows very clearly that within this cluster particle which are at the boundary moves inside the spot and rest which are outside are moving away from the boundary. Moving the laser spot or table greater than the difference between laser boundary and imaginary boundary tends to lose the particles.

Figure SB.6.3. Videos showing motion of a stable cluster of particle from once place to another. Particles which lying within the imaginary boundary goes into the irradiation center whereas particles which are outside it are thrown away from the surroundings.

Figure SB.7.1. Effect of spacer height. For lower spacer heights (i.e. thickness of the chamber). (a) for spacer height of 250 μm, (b) space height of 320 μm.

Figure SB.8.3. Visualization of LDDO flow using fluorescein. Video shows 20 μm porous silica particle stacked to glass surface. Surfactant solution with dye is added and recorded immediately under blue irradiation

Figure SB.8.4. video showing motion of porous and non-porous particles in 1mM Azo-C6 and 0.2 μM fluorescein solution under focused blue and global UV irradiation. Porous particle glows due to diffusion of dye complex in pores of particle, while nonporous particle appears darker.

Appendix C

Figure SC.1. Self-propelled motion of Spherod (porous sphere and non-porous rod) particles marked in red, green and blue circles

Figure SC.2. Self-propelled motion of spherod particle where sphere is attached at the one end of nonporous rod.

Figure SC.3. Self-propelled motion of spherod particle where sphere is attached at centre of nonporous rod. Another porous sphere (marked in red) couples with the spherod particle and shows directed motion also.

Figure SC.4. Self-propelled motion of different type of spherod particle (a) when porous particle attached towards the end of the rod. (b) When three particles are attached at the end. (c) when ratio of particle size and length of rod is smaller

Figure SC.6. Video showing motion just after blue light is switched off for an eensemble of porous sphere and non-porous rods

Figure SC.7. Video showing self-propelled motion of Porous-non-porous dimer particles. Trajectories of motion is shown using white and black lines

Figure SC.8. Video showing Ensemble of porous and non-porous silica particles in 1 mM Azo-C6 and 0.2 μM fluorescein solution. Only blue laser is applied through the objective. Trajectories of self-propelled motion of Porous-non-porous particles (marked in red, black and white circles) are shown through white and black lines

Bibliography

1 M. E. Purcell, *Am. J. Phys.*, 1977, **45**, 3–11.

2 C. Brennen and H. Winet, *Annu. Rev. Fluid Mech.*, 1977, **9**, 339–398.

3 M. W. Skinner, N. Mannowetz, V. P. Lishko and R. N. Roan, *Physiol. Behav.*, 2019, **176**, 139–148.

4 C. S. Renadheer, U. Roy and M. Gopalakrishnan, *J. Phys. A Math. Theor.*, 2019, **15**, 505601.

5 G. Gompper, R. G. Winkler, T. Speck, A. Solon, C. Nardini, F. Peruani, H. Löwen, R. Golestanian, U. B. Kaupp and L. Alvarez, *J. Phys. Cond. Mat., 2019*

6 S. J. Ebbens and J. R. Howse, *Soft Matter*, 2010, **6**, 726–738.

7 I. Buttinoni, G. Volpe, F. Kümmel, G. Volpe and C. Bechinger, *J. Phys. Condens. Matter*, 2012, 24, 284129

8 H. Stark, *Acc. Chem. Res.*, 2018, **51**, 2681–2688.

9 K. Drescher, K. C. Leptos, I. Tuval, T. Ishikawa, T. J. Pedley and R. E. Goldstein, *Phys. Rev. Lett.*, 2009, **102**, 1–4.

10 S. C. Takatori and J. F. Brady, *Curr. Opin. Colloid Interface Sci.*, 2016, **21**, 24–33.

11 J. Elgeti, R. G. Winkler and G. Gompper, *Reports Prog. Phys.*, 2015, **78,** 056601

12 H. P. Zhang, A. Be'er, R. S. Smith, E. L. Florin and H. L. Swinney, *Epl*, 2009, **87**, 2–7.

13 I. S. Aranson, *Nature*, 2016, **531**, 312-313.

14 T. Mirkovic, N. S. Zacharia, G. D. Scholes and G. A. Ozin, *ACS Nano*, 2010, **4**, 1782–1789.

15 S. Palagi, A. G. Mark, S. Y. Reigh, K. Melde, T. Qiu, H. Zeng, C. Parmeggiani, D. Martella, A. Sanchez-Castillo, N. Kapernaum, F. Giesselmann, D. S. Wiersma, E. Lauga and P. Fischer, *Nat. Mater.*, 2016, **15**, 647–653.

16 I. Karamouzas, B. Skinner and S. J. Guy, *Phys. Rev. Lett.*, 2014, **113**, 1–5.

17 T. Vicsek, *Proc. - 2nd IEEE Int. Conf. Self-Adaptive Self-Organizing Syst. SASO 2008*, 23, 3–11.

18 L. Isa, K. Kumar, M. Mu, J. Grolig, M. Textor and E. Reimhult, *ACS Nano*, 2010, **4**, 5665–5670.

19 E. K. Fleischmann, H. L. Liang, N. Kapernaum, F. Giesselmann, J. Lagerwall and R. Zentel, *Nat. Commun.*, 2012, **3**, 1–8.

20 M. Guix, C. C. Mayorga-Martinez and A. Merkoçi, *Chem. Rev.*, 2014, **114**, 6285–6322.

21 G. A. Ozin, I. Manners, S. Fournier-Bidoz and A. Arsenault, *Adv. Mater.*, 2005, **17**, 3011–3018.

22 L. Xu, F. Mou, H. Gong, M. Luo and J. Guan, *Chem. Soc. Rev.*, 2017, **46**, 6905–6926.

23 B. Jurado-Sánchez, S. Sattayasamitsathit, W. Gao, L. Santos, Y. Fedorak, V. V. Singh, J. Orozco, M. Galarnyk and J. Wang, *Small*, 2015, **11**, 499–506.

24 S. Sattayasamitsathit, H. Kou, W. Gao, W. Thavarajah, K. Kaufmann, L. Zhang and J. Wang, *Small*, 2014, **10**, 2830–2833.

25 M. Suzuki, T. Yasukawa, Y. Mase, D. Oyamatsu, H. Shiku and T. Matsue, *Langmuir*, 2004, **20**, 11005–11011.

26 S. Sundararajan, S. Sengupta, M. E. Ibele and A. Sen, *Small*, 2010, **6**, 1479–1482.

27 T. Tsuji, S. Saita and S. Kawano, *Phys. Rev. Appl.*, 2018, **9**, 24035.

28 S. K. Srivastava, G. Clergeaud, T. L. Andresen and A. Boisen, *Adv. Drug Deliv. Rev.*, 2019, **138**, 41–55.

29 C. Bechinger, D. R. Leonardo, H. Löwen, C. Reichhardt, G. Volpe and G. Volpe, *Rev. Mod. Phys.*, 2016, **88**, 045006.

30 H. Chen, Q. Zhao and X. Du, *Micromachines*, 2018, **9**, 41

31 J. Burelbach, *Phys. Rev. E 100*, 2019, **042612**, 1–8.

32 J. G. S. Moo and M. Pumera, *Chem. - A Eur. J.*, 2015, **21**, 58–72.

33 D. Velegol, A. Garg, R. Guha, A. Kar and M. Kumar, *Soft Matter*, 2016, **12**, 4686–4703.

34 R. Piazza, *Soft Matter*, 2008, **4**, 1740–1744.

35 H. R. Jiang, N. Yoshinaga and M. Sano, *Phys. Rev. Lett.*, 2010, **105**, 1–4.

36 J. F. Brady, *J. Fluid Mech.*, 2011, **667**, 216–259.

37 J. Kuhr, J. Blaschke, F. Ruehel and H. Stark, *Soft Matter*, 2017, **13**, 7548–7555.

38 K. Villa and M. Pumera, *Chem. Soc. Rev.*, 2019, **48**, 4966–4978.

39 T. Tsuji, Y. Matsumoto, R. Kugimiya, K. Doi and S. Kawano, *Micromachines*, 2019, **10,** 321

40 P. Fischer and A. Ghosh, *Nanoscale*, 2011, **3**, 557–563.

41 G. Loget and A. Kuhn, *Nat. Commun.*, 2011, **2**, 1–6.

42 D. Ahmed, M. Lu, A. Nourhani, P. E. Lammert, Z. Stratton, H. S. Muddana, V. H. Crespi and T. J. Huang, *Sci. Rep.*, 2015, **5**, 1–8.

43 A. V. Straube, J. M. Pagès, A. Ortiz-Ambriz, P. Tierno, J. Ignés-Mullol and F. Sagués, *New J. Phys.*, 2018, **20**, 075006.

44 M. Paven, H. Mayama, T. Sekido, H. J. Butt, Y. Nakamura and S. Fujii, *Adv. Funct. Mater.*, 2016, **26**, 3199–3206.

45 A. Kausar, H. Nagano, T. Ogata, T. Nonaka and S. Kurihara, *Angew. Chemie - Int. Ed.*, 2009, **48**, 2144–2147.

46 F. Mou, Y. Li, C. Chen, W. Li, Y. Yin, H. Ma and J. Guan, *Small*, 2015, **11**, 2564–2570.

47 S. Wang and N. Wu, *Langmuir*, 2014, **30**, 3477–3486.

48 W. Duan, R. Liu and A. Sen, *J. Am. Chem. Soc.*, 2013, **135**, 1280–1283.

49 D. Feldmann, S. R. Maduar, M. Santer, N. Lomadze, O. I. Vinogradova and S. Santer, *Sci. Rep.*, 2016, **6**, 1–10.

50 A. A. Solovev, S. Sanchez and O. G. Schmidt, *Nanoscale*, 2013, **5**, 1284–1293.

51 J. Palacci, S. Sacanna, S. Kim, G. Yi, D. J. Pine and P. M. Chaikin, *Trans. R. Soc. A*, 2014, **372**, 20130372.

52 A. Ashkin, J. M. Dziedzic, J. E. Bjorkholm and S. Chu, *Opt. Lett.*, 1986, **11**, 288–290.

53 A. Ashkin, *Phys. Rev. Lett.*, 1970, **24**, 24–27.

54 B. Roy, N. Ghosh, S. Dutta Gupta, P. K. Panigrahi, S. Roy and A. Banerjee, *Phys. Rev. A -At. Mol. Opt. Phys.*, 2013, **87**, 1-9

55 Y. Zhang, J. Lei, Y. Zhang, Z. Liu, J. Zhang, X. Yang, J. Yang and L. Yuan, *Sci. Rep.*, 2017, **7,** 1–8.

56 M. Ibele, T. E. Mallouk and A. Sen, *Angew. Chemie - Int. Ed.*, 2009, **48**, 3308–3312.

57 H. Ke, S. Ye, R. L. Carroll and K. Showalter, *J. Phys. Chem. A*, 2010, **114**, 5462–5467.

58 F. Mou, L. Kong, C. Chen, Z. Chen, L. Xu and J. Guan, *Nanoscale*, 2016, **8**, 4976–4983.

59 S. Giudicatti, S. M. Marz, L. Soler, A. Madani, M. R. Jorgensen, S. Sanchez and O. G. Schmidt, *J. Mater. Chem. C*, 2014, **2**, 5892–5901.

60 A. Aubret, M. Youssef, S. Sacanna and J. Palacci, *Nat. Phys.*, 2018, **14**, 1114–1118.

61 D. V. Rao, N. Reddy, J. Fransaer and C. Clasen, *J. Phys. D. Appl. Phys.*, 2019, **52**, 014002.

62 L. Wang, M. N. Popescu, F. Stavale, A. Ali, T. Gemming and J. Simmchen, *Soft Matter*, 2018, **14**, 6969–6973.

63 S. Schimka, Y. D. Gordievskaya, N. Lomadze, M. Lehmann, R. Von Klitzing, A. M. Rumyantsev, E. Y. Kramarenko and S. Santer, *J. Chem. Phys.*, 2017, **147,** 031101

64 A. Diguet, R. M. Guillermic, N. Magome, A. Saint-Jalmes, Y. Chen, K. Yoshikawa and D. Baigl, *Angew. Chemie - Int. Ed.*, 2009, **48**, 9281–9284.

65 D. Baigl, *Lab Chip*, 2012, **12**, 3637–3653.

66 E. Merino and M. Ribagorda, *Beilstein J. Org. Chem.*, 2012, **8**, 1071–1090.

67 M. Montagna and O. Guskova, *Langmuir*, 2018, **34**, 311–321.

68 T. Shang, K. A. Smith and T. A. Hatton, *Langmuir*, 2003, **19**, 10764–10773.

69 B. A. Cicciarelli, T. A. Hatton and K. A. Smith, *Langmuir*, 2007, **23**, 4753–4764.

70 S. Schimka, N. Lomadze, M. Rabe, A. Kopyshev, M. Lehmann, R. Von Klitzing, A. M. Rumyantsev, E. Y. Kramarenko and S. Santer, *Phys. Chem. Chem. Phys.*, 2017, **19**, 108–117.

71 S. Schimka, S. Santer, N. M. Mujkić-Ninnemann, D. Bléger, L. Hartmann, M. Wehle, R. Lipowsky and M. Santer, *Biomacromolecules*, 2016, **17**, 1959–1968.

72 Y. Zakrevskyy, A. Kopyshev, N. Lomadze, E. Morozova, L. Lysyakova, N. Kasyanenko and S. Santer, *Phys. Rev. E - Stat. Nonlinear, Soft Matter Phys.*, 2011, **84**, 1–9.

73 N. S. Yadavalli, T. König and S. Santer, *J. Soc. Inf. Disp.*, 2015, **23**, 154–162.

74 J. Jelken and S. Santer, *RSC Adv.*, 2019, **9**, 20295–20305.

75 A. Kopyshev, C. J. Galvin, R. R. Patil, J. Genzer, N. Lomadze, D. Feldmann, J. Zakrevski and S. Santer, *ACS Appl. Mater. Interfaces*, 2016, **8**, 19175–19184.

76 P. Arya, J. Jelken, N. Lomadze, S. Santer and M. Bekir, *J. Chem. Phys.*, 2020, **152**, 024904.

77 D. Feldmann, P. Arya, T. Y. Molotilin, N. Lomadze, A. Kopyshev and O. I. Vinogradova, *Langmuir*, 2020, DOI:10.1021/acs.langmuir.9b03270.

78 P. Arya, J. Jelken, D. Feldmann, N. Lomadze and S. Santer, *J. Chem. Phys.,2020 (printing)*

79 P. Arya, D. Feldmann, A. Kopyshev, N. Lomadze and S. Santer, *Soft Matter*, 2020, **16**, 1148–1155.

80 D. Feldmann, P. Arya, N. Lomadze, A. Kopyshev and S. Santer, *Appl. Phys. Lett.*, 2019, **155**, 263701, 1-5

81 G. Hartley, *Z. physiol. C.*, 1933, **216**, 1073.

82 H. Song, C. Jing, W. Ma, T. Xie and Y. T. Long, *Chem. Commun.*, 2016, **52**, 2984–2987.

83 T. Fujino and T. Tahara, *J. Phys. Chem. A*, 2000, **104**, 4203–4210.

84 S. Bandara, H. M. D. Bandara and S. C. Burdette, *Chem. Soc. Rev.*, 2012, **41**, 1809–1825.

85 C. Ciminelli, G. Granucci and M. Persico, *Chem. - A Eur. J.*, 2004, **10**, 2327–2341.

86 X. Yu, Z. Wang, M. Buchholz, N. Füllgrabe, S. Grosjean, F. Bebensee, S. Bräse, C. Wöll and L. Heinke, *Phys. Chem. Chem. Phys.*, 2015, **17**, 22721–22725.

87 H. M. D. Bandara and S. C. Burdette, *Chem. Soc. Rev.*, 2012, **41**, 1809–1825.

88 W. R. Browne and B. L. Feringa, *Nanosci. Technol. A Collect. Rev. from Nat. Journals*, 2009, 79–89.

89 R. J. Mart and R. K. Allemann, *Chem. Commun.*, 2016, **52**, 12262–12277.

90 Y. Zhang and S. C. Zimmerman, *Beilstein J. Org. Chem.*, 2012, **8**, 486–495.

91 S. Wang, Y. Song and L. Jiang, *J. Photochem. andPhotobiology C phtochemistry Rev.*, 2007, **8**, 18-29

92 D. Dumont, T. V Galstian, S. Senkow, A. M. Ritcey, T. V Galstian, S. Senkow and A. M. R. L. Crystal, *J. Mol. Cryst. Liq. Cryst.*, 2010, **1406**, 341–352.

93 K. Harada, M. Itoh, T. Yatagai and S. I. Kamemaru, *Opt. Rev.*, 2005, **12**, 130–134.

94 D. W. Kalina and S. G. Grubb, *Thin Solid Films*, 1988, **160**, 363–371.

95 X. Li, W. Xiao, G. He, W. Zheng, N. Yu and M. Tan, *Colloids Surfaces A Physicochem. Eng. Asp.*, 2012, **408**, 79–86.

96 E. Chevallier, A. Mamane, H. A. Stone, C. Tribet, F. Lequeux and C. Monteux, *Soft Matter*, 2011, **7**, 7866–7874.

97 S. K. Oh, M. Nakagawa and K. Ichimura, *J. Mater. Chem.*, 2002, **12**, 2262–2269.

98 S. Santer, *J. Phys. D. Appl. Phys.*, 2018, **51**, 2237-2240.

99 H. C. Kang, B. M. Lee, J. Yoon and M. Yoon, *J. Colloid Interface Sci.*, 2000, **231**, 255–264.

100 S. Santer, *J. Phys. D. Appl. Phys.*, 2018, **51**, 013002.

101 S. Kaneko, K. Asakura and T. Banno, *Chem. Commun.*, 2017, **53**, 2237–2240.

102 M. Richter, Y. Zakrevskyy, M. Eisele, N. Lomadze and S. Santer, *Polymer (Guildf).*, 2014, **55**, 6513–6518.

103 S. Kaneko, K. Asakura and T. Banno, *Chem. Commun.*, 2017, **53**, 2237–2240.

104 Y. Kasuo, H. Kitahata, Y. Koyano, M. Takinoue, K. Asakura and T. Banno, *Langmuir*, 2019, **35**, 13351–13355.

105 J. Grawitter and H. Stark, *Soft Matter*, 2018, **14**, 1856–1869.

106 S. N. Varanakkottu, S. D. George, T. Baier, S. Hardt, M. Ewald and M. Biesalski, *Angew. Chem. Int. Ed.*, 2013, **52**, 7291–7295.

107 A. Diguet, H. Li, N. Queyriaux, Y. Chen and D. Baigl, *Lab Chip*, 2011, **11**, 0–4.

108 L. Nurdin, Venancio-M. Anna, S. Rudiuk, M. Morel and D. Baigl, *C.R. Chim.*, 2016, **19**, 199–206.

109 M. Anyfantakis and D. Baigl, *Angew. Chem. Int. Ed.*, 2014, **53**, 14077–14081.

110 K. G. Yager and C. J. Barrett, *J. Photochem. Photobiol. A Chem.*, 2006, **182**, 250–261.

111 Z. Wu, X. Li, X. Jiang, T. Xie, H. Li, G. Zhang and J. Jiang, *Phy. Chem. Chem. Phys*, 2019, **21**, 21030

112 B. A. Cicciarelli, J. A. Elia, T. A. Hatton and K. A. Smith, *Langmuir*, 2007, **23**, 8323–8330.

113 Z. Li, Y. Feng, X. Yuan, H. Wang, Y. Zhao and J. Wang, *int. J. Mol. Sci.*, 2019, **20**, 1–13.

114 J. Y. Shin and N. L. Abbott, *Langmuir*, 1999, **15**, 4404–4410.

115 B. S. Shinkai, Matsuo Katsuta, A. Harada and O. Manabe, *J. Chem. Soc. Perkin Trans*, 1982, **2**, 1261–1265.

116 E. M. Kramer and D. R. Myers, *Trends Plant Sci.*, 2013, **18**, 2012–2014.

117 T. Y. Cath, A. E. Childress and M. Elimelech, *J. Memb. Sci.*, 2006, **281**, 70–87.

118 A. V. Raghunathan and N. R. Aluru, *Phys. Rev. Lett.*, 2006, **97**, 1–4.

119 G. N. Lewis, *J. Am. Chem. Soc.*, 1908, **30**, 668–683.

120 S. Marbach and L. Bocquet, *Chem. Soc. Rev.*, 2019, **48**, 3102–3144.

121 A. V. Belyaev and O. I. Vinogradova, *Phys. Rev. Lett.*, 2011, **107**, 1–4.

122 M. Lian, N. Islam and J. Wu, *J. Phys. Conf. Ser.*, 2006, **34**, 589–594.

123 R. Niu, T. Palberg and T. Speck, *Phys. Rev. Lett.*, 2017, **119**, 1–5.

124 A. Manz, C. S. Effenhauser, N. Burggraf, D. J. Harrison, K. Seiler and K. Fluri, *J., micro-mechanics Microengineering*, 1994, **4**, 257–265.

125 V. Pretorius, B. J. Hopkins and J. D. Schieke, *J. Chromatogr. A*, 1974, **99**, 23–30.

126 B. Liebchen, R. Niu, T. Palberg and H. Löwen, *Phys. Rev. E*, 2018, **98**, 1–6.

127 A. Ajdari and L. Bocquet, *Phys. Rev. Lett.*, 2006, **96**, 1–4.

128 A. Kar, T. Y. Chiang, I. Ortiz Rivera, A. Sen and D. Velegol, *ACS Nano*, 2015, **9**, 746–753.

129 S. Shin, E. Um, B. Sabass, J. T. Ault, M. Rahimi, P. B. Warren and H. A. Stone, *Proc. Natl. Acad. Sci. U. S. A.*, 2016, **113**, 257–261.

130 J. C. T. Eijkel and A. Van den Berg, *Chem. Soc. Rev.*, 2010, **39**, 957–973.

131 S. Shin, J. T. Ault, J. Feng, P. B. Warren and H. A. Stone, *Adv. Mater.*, 2017, **29**, 1–7.

132 D. Michler, N. Shahidzadeh, R. Sprik and D. Bonn, *Epl*, 2015, **110**, 28001.

133 J. S. Paustian, C. D. Angulo, R. Nery-Azevedo, N. Shi, A. I. Abdel-Fattah and T. M. Squires, *Langmuir*, 2015, **31**, 4402–4410.

134 M. Lokesh, S. K. Youn and H. G. Park, *Nano Lett.*, 2018, **18**, 6679–6685.

135 N. V. Churaev, I. P. Sergeeva, V. D. Sobolev, H. J. Jacobasch, P. Weidenhammer and F. J. Schmitt, *Colloids Surfaces A Physicochem. Eng. Asp.*, 2000, **164**, 121–129.

136 S. Manne, J. P. Cleveland, H. E. Gaub, G. D. Stucky and P. K. Hansma, *Langmuir*, 1994, **10**, 4409–4413.

137 P. Pham, M. Howorth, A.P Chretien, and S. Tardu, *COMSOL Users Conf. 2007, Grenoble,* 2007.

138 J. L. Anderson and D. C. Prieve, *Langmuir*, 1991, **7**, 403–406.

139 D. C. Grahame, *Chem. Rev.*, 1947, **41**, 441–501.

140 Z. Tao, Y. Xie, J. Goodisman and T. Asefa, *Langmuir*, 2010, **26**, 8914–8924.

141 R. Páez, U. Ruiz and S. L. Neale, *Biomed. Opt. Express*, 2015, **6**, 7275–7282.

142 C. Eggeling, J. Widengren, R. Rigler and C. A. M. Seidel, *Anal. Chem.*, 1998, **70**, 2651–2659

143 L. Song, E. J. Hennink, T. Young and H. J. Tanke, *Biophys. J.*, 1995, **68**, 2588–2600.

144 J. Pauli, T. Vag, R. Haag, M. Spieles, M. Wenzel, W. A. Kaiser, U. Resch-genger and I. Hilger, *Eur. J. Med. Chem.*, 2009, **44**, 3496–3503.

145 J. Pauli, M. Grabolle, R. Brehm, M. Spieles, F. M. Hamann, M. Wenzel, I. Hilger and U. Resch-genger, *Bioconjugate Chem.*, 2011, **22**, 1298–1308.

List of Publications

This dissertation is partly based on the following publications

1. Arya, P.; Jelken, J.; Lomadze, N.; Santer, S.; Bekir, M; Kinetics of photo-isomerization of azobenzene containing surfactants, *Journal of Chemical Physics*, 152 024904 ,2020

2. Arya, P.; Jelken, J.; Feldmann, D.; Lomadze, N. and Santer, S., Light driven diffusioosmotic repulsion and attraction of colloidal particles, *Journal of Chemical Physics*, accepted, 2020

3. Arya, P.; Feldmann, D.; Kopyshev, A.; Lomadze, N. and Santer, S.; Light driven guided and self-organized motion of mesoporous colloidal particles, *Soft Matter*, 16, 1148 2020

4. Feldmann, D.; Arya, P.; Molotilin, TY.; Lomadze, N.; Kopyshev, A.; Vinogradova, OI.; Santer, S., Extremely Long-Range Light-Driven Repulsion of Porous Microparticles, *Langmuir*, DOI: 10.1021/acs.langmuir.9b03270 , 2020

5. Feldmann, D.; Arya, P.; Lomadze, N.; Kopyshev, A.; Santer, S.; Light-driven motion of self-propelled porous Janus particles, *Applied Physics Letters,* 115, 263701, 2019

Other Publication

6. Frenkel, M.; Arya, P.; Santer, S; and Bormachenko, E., Voronoi entropy of active light driven colloids, *Langmuir*, (In preparation)

Declaration

I hereby declare that this thesis has been composed by myself and that the work of this thesis has not been submitted for any other degree to any other university or institution. I confirm that the work submitted is my own, except where work which has formed part of jointly authored has been included. Any ideas, techniques, quotations or any other material from the work of other people included in my thesis, published or otherwise, are fully acknowledged in accordance with the standard referencing system.

Potsdam, May 2020

Pooja Arya